

Palladium-based supramolecular assemblies: from complex structures to water-soluble anion-receptors

Présentée le 28 mars 2024

Faculté des sciences de base
Laboratoire de chimie supramoléculaire
Programme doctoral en chimie et génie chimique

pour l'obtention du grade de Docteur ès Sciences

par

Sylvain Alexandre Marie SUDAN

Acceptée sur proposition du jury

Prof. S. Gerber, présidente du jury
Prof. K. Severin, directeur de thèse
Prof. J. Lewis, rapporteur
Prof. M. Rickhaus, rapporteur
Dr A.-S. Chauvin, rapporteuse

Acknowledgements

First of all, I would like to thank Prof. Kay Severin for his supervision over these past four years. Your constant availability to discuss the ongoing projects was greatly appreciated. Our constructive discussions allowed me to continuously improve as a chemist.

I thank Prof. James Lewis, Prof. Michel Rickhaus, Dr. Anne-Sophie Chauvin and Prof. Sandrine Gerber for agreeing to be part of the jury and for dedicating the time to read and provide valuable comments on my thesis.

The year spent within the LSMO group, in Sion, has an important part to play in my decision to pursue doctoral studies. Thank you, Kyriakos, for giving me the opportunity to develop my own project and supporting me all the way through it. Thank you, Andrzej, for your mentoring throughout the year and for your friendship; I learned a lot. Thank you to all my other colleagues and friends within the group for contributing to a fantastic atmosphere, not only within the lab but also outside of it.

Thank you, Nicolas, Cédric and Edouard, for the time we spent together during our bachelors and masters at EPFL, as well as throughout these last four years. Even though less frequently, we will always find time to share our stories over beers and sambuca.

Thank you, Marko, for being there since the beginning of my studies. I was far from being the most studious during our time in pharmaceutical sciences, but you taught me never to give up. Your determination guided me all the way throughout my chemistry studies to this day, and I will always be grateful for that.

Thank you to the LCS members who were present when I joined the group: Carl, Nastya, Cesare, Iris, Rujin, Cristian, Zhaowen, Erica, José, Ophélie, Alik and Pavel. I felt warmly welcome to the group and, even though the pandemic started soon after my arrival, we managed to make up for the lost time. Thank you to all following

members: Wolfram, Bastiaan, Noga, Chaolei, Christeena, Mrittika, Dicky, Jean, Atena, Damien and Alex. Since my start in the group, I cannot recall a single day in the lab without laughter. Coming to work, knowing that, immensely contributed to the successful development of my thesis. It is great to see that this joyful working atmosphere continues to endure.

During my years within the LCS, I had the chance to collaborate with two very talented students. Thank you, Geoffrey and Damien, for your dedication and your contribution to this thesis.

I have been extremely lucky be able to conduct my studies so close to the area where I grew up. Having long-time friends around was of great support during the challenging times. Thank you to all my friends of the Vevey area.

I wish to thank my parents, for supporting me from the day I was born to this moment. None of this would have been possible without you. Thank you also to my brother and sister, Aurèle and Elena, for being who you are. Sharing is not our most developed skill, but I think that you will get what I wanted to say.

Last, but certainly not least, I wish to thank you Mélanie. You probably do not realize how much you did for me. You've been part of my life for almost fourteen years now and have never given up on me, even during the hardest times. Choosing to have a child while pursuing a PhD might not seem like the easiest path, but I will never regret the decision we made. Combining the parent and doctoral student lives wouldn't have been possible without the precious support of our parents. Philippe and Christianne, thank you sincerely for everything.

I want to dedicate this work to my life companion, Mélanie, and to our wonderful daughter, Livia.

Abstract

The combination of palladium salts and bipyridyl ligands can lead to the formation of a large variety of coordination complexes, with different shapes and sizes, displaying a very versatile host-guest chemistry. Increasing their structural complexity remains a central challenge in the field and this thesis describes different approaches to address it.

Chapter 2 describes a selection approach, which allowed to identify a novel hexanuclear assembly incorporating two types of dipyriddy ligands. A virtual combinatorial library of $[\text{Pd}_n\text{L}_{2n}](\text{BF}_4)_{2n}$ complexes was prepared by mixing six different ligands with substoichiometric amounts of Pd^{2+} . Equilibrating the reaction mixture resulted in the preferential formation of a heteroleptic $[\text{Pd}_6\text{L}_6\text{L}'_6](\text{BF}_4)_{12}$ assembly which was then synthesized on a preparative scale. A related but significantly larger $[\text{Pd}_6\text{L}_6\text{L}'_6](\text{BF}_4)_{12}$ cage was obtained from a pair of metalloligands with a similar combination of bending angles.

Chapter 3 describes an investigation on the Li^+ -binding properties of Pd^{2+} -based hosts. One of the complexes underwent a significant structural rearrangement when LiBF_4 was added. Namely, the initial Pd_2L_4 species was converted to a low-symmetry Pd_4L_8 assembly, enclosing two solvated LiBF_4 ion pairs. The conversion did not occur with other alkali metal ions, indicating highly specific host-guest interactions. Structural analyses revealed the important contributions of π -stacking intramolecular interactions to maintain the highly compact structure of the Pd_4L_8 receptor.

In Chapter 4, the possibility to target the synthesis of intricate Pd-assemblies is investigated. The observations discussed in Chapter 3 were used as a basis to define key characteristics that a ligand should possess to accommodate in such structures. A set of new ligands was designed and prepared following those guidelines. In one of the cases, the complexation with Pd^{2+} resulted in the formation of a reduced-symmetry Pd_2L_3 species displaying strong π -stacking interactions between the three adjacent ligands.

Chapter 5 describes the preparation of a five-stranded heterometallic helicate incorporating two Pd²⁺ ions and one La³⁺ center. Analyses highlighted the low symmetry of the assembly, both in solution and in the solid state. The penta-stranded helicate could be dynamically interconverted with a symmetrical, four-stranded helicate by adjusting the metal-to-ligand ratio.

Important structural complexity is, however, not always necessary to achieve strong host-guest interactions. In Chapter 5, the synthesis of a water-soluble Pd₂L₄ coordination cage from Pd(NO₃)₂ and a 1,3-di(pyridin-3-yl)benzene ligand, functionalized with a solubilizing side chain, is described. The nitrate anion located in the cage's cavity can be exchanged for halide guests. An apparent association constant of $K_a = 1.8(\pm 0.1) \times 10^5 \text{ M}^{-1}$ was determined for binding chloride in buffered aqueous solution. This value is significantly higher than what has been reported for other macrocyclic chloride receptors. While heavier halides compete with binding or self-assembly, the receptor displays very good selectivity over common biological anions. The chloride binding affinity was further increased by a factor of three using a fluorinated ligand.

Keywords: Supramolecular Chemistry · Cages · Palladium · Self-Assembly · Host-guest Chemistry · Symmetry · Helicate · Chloride

Résumé

La combinaison de sels de palladium et de ligand de bipyridyl peut conduire à la formation d'une grande variété de complexes de coordinations, de tailles et de formes différentes, présentant une chimie hôte-invité très versatile. Accroître leur complexité structurale demeure un défi central dans le domaine et cette thèse décrit différentes approches pour adresser ce dernier.

Le chapitre 2 décrit une méthode de sélection qui a permis l'identification d'un nouvel assemblage hexasucléaire, incorporant deux types de ligands bipyridyl. Une bibliothèque combinatoire virtuelle de complexes de type $[Pd_nL_{2n}](BF_4)_{2n}$ a été préparée en mélangeant six ligands différents et une quantité sous-stœchiométrique de Pd^{2+} . Équilibrer le mélange réactionnel a conduit à la formation préférentielle d'un assemblage hétéroleptique $[Pd_6L_6L'_6](BF_4)_{12}$ qui a ensuite été synthétisé à l'échelle préparative. Une cage $[Pd_6L_6L'_6](BF_4)_{12}$ apparentée, mais significativement plus grande, a été obtenue à partir d'une paire de metalloligands présentant une combinaison similaire d'angles de flexion.

Le chapitre 3 décrit une étude sur la capacité de complexes basé sur le Pd^{2+} à servir d'hôtes pour des cations Li^+ . Un des complexes étudiés a subi une importante réorganisation structurale lors de l'ajout de $LiBF_4$. Plus précisément, l'espèce initiale Pd_2L_4 a été convertie en un assemblage Pd_4L_8 de basse symétrie, renfermant deux paires d'ions $LiBF_4$ solvatés. La conversion n'a pas été observée avec d'autres ions de métaux alcalins, indiquant des interactions hôte-invité très spécifiques. Les analyses structurales ont révélé la contribution importante des interactions intramoléculaires d'empilement π pour maintenir la structure hautement compacte du récepteur Pd_4L_8 .

Dans le chapitre 4, la possibilité de cibler la synthèse d'assemblages de palladium avec une structure complexe est étudiée. Les observations présentées dans le chapitre 3 ont été utilisées comme base pour définir les caractéristiques clé nécessaires à un ligand pour s'adapter dans de telles structures. Un ensemble de nouveaux ligands a été conçu et préparé suivant ces lignes directrices.

Dans l'un des cas, la complexation avec Pd²⁺ a conduit à la formation d'une espèce Pd₂L₃ de symétrie réduite et présentant des interactions d'empilement π importantes entre les trois ligands adjacents.

Le chapitre 5 décrit la préparation d'un hélicate hétérométallique à cinq brins, incorporant deux ions Pd²⁺ et un centre La³⁺. Les analyses ont mis en évidence la faible symétrie de l'assemblage, tant en solution qu'à l'état solide. De plus, l'hélicate à cinq brins a pu être dynamiquement interconverti avec un hélicate symétrique à quatre brins en ajustant le rapport métal-ligand.

Une importante complexité structurelle n'est cependant pas toujours nécessaire pour obtenir de fortes interactions hôte-invité. Dans le chapitre 5, la synthèse d'une cage de coordination Pd₂L₄ hydrosoluble, à partir de Pd(NO₃)₃ et d'un ligand à 1,3-di(pyridin-3-yl)benzene fonctionnalisé avec une chaîne latérale solubilisante, est présentée. L'anion nitrate situé dans la cavité de la cage peut être échangé avec un halogénure. Une constante d'association apparente de $K_a = 1.8(\pm 0.1) \times 10^5 \text{ M}^{-1}$ pour la fixation du chlorure en solution aqueuse tamponnée. Cette valeur est significativement plus élevée que ce qui a été reporté pour d'autres récepteurs macrocycliques de chlorure. Bien que les halogénures plus lourds entrent en compétition avec la fixation ou l'auto-assemblage, le récepteur présente une très bonne sélectivité sur les anions biologiques courants. De plus, il a été possible d'augmenter l'affinité de liaison du chlorure d'un facteur trois en utilisant un ligand fluoré.

Mots-clés: Chimie Supramoléculaire • Cages • Palladium • Auto-Assemblage • Chimie Hôte-Invité • Symétrie • Hélicate • Chlorure

Table of contents

Acknowledgements.....	i
Abstract.....	iii
1. Introduction: Pd ²⁺ -based coordination cages.....	1
1.1 Homoleptic assemblies: common structures and design rules	1
1.2 Heteroleptic assemblies	5
1.3 Homoleptic assemblies with increased structural complexity	9
1.4 Host-guest chemistry	13
2. Identification of a heteroleptic Pd ₆ L ₆ L' ₆ coordination cage by screening of a virtual combinatorial library.....	17
3. LiBF ₄ -induced rearrangement and desymmetrization of a palladium-ligand assembly	29
4. Intricate palladium complexes: a ligand design approach	39
5. A five-stranded heterometallic helicate	46
6. Synthetic receptors with micromolar affinity for chloride in water	55
7. Conclusion and outlook	68
8. Experimental section	70
9. References	133
10. Curriculum vitae.....	148

1. Introduction: Pd²⁺-based coordination cages

1.1 Homoleptic assemblies: common structures and design rules

Homoleptic palladium-based coordination cages of the general formula [Pd_nL_{2n}]X_{2n}, with $n > 1$, are generally obtained by combining Pd(II) salts, such as Pd(NO₃)₂ or [Pd(CH₃CN)₄(BF₄)₂], with bis-monodentate N-donor ligands L.^[1–9] While *cis*-protected Pd(II) complexes are also commonly used as building blocks,^[8] this introduction will focus on structures obtained from ‘naked’ Pd²⁺ ions. Following the pioneering work of McMorran and Steel, in 1998,^[10] these systems have been attracting increasing attention.

Pd(II) and bis-pyridyl ligands are convenient building blocks, mainly due to the common square-planar coordination geometry of the metal, as well as the kinetically labile character of the Pd-N bond. The latter allows for error-correction during the thermodynamically driven self-assembly process. While the number of reported structures was continuously growing, chemists started to rationalize the synthesis of assemblies with specific shapes. As the coordination environment around the Pd atom is fixed to a square planar geometry, the angle θ between the coordination vectors of the two N-donor atoms becomes a crucial parameter to control the final product’s geometry.

Fujita and co-workers synthesized a range of spherical Pd_nL_{2n} polyhedra, with $n = 6, 12, 24, 30$ and 48 , by tuning the ligand bending angle (**Figure 1**).^[11–16] While trying to approach the ‘ideal’ θ angle (based on geometric considerations), for a given target polyhedron, works well for structures with $n = 6, 12$ and 24 ($\theta \sim 90^\circ, 120^\circ$ and 135° respectively), things get more complicated for larger n values. For example, ligand **3**, could be the perfect candidate to form a Pd₃₀L₆₀ structure (‘ideal’ $\theta = 150^\circ$). However, when combined with Pd²⁺, the Pd₂₄L₄₈ species was formed preferentially: this kinetically trapped product could only be partially converted to the thermodynamic one by heating.^[14,15]

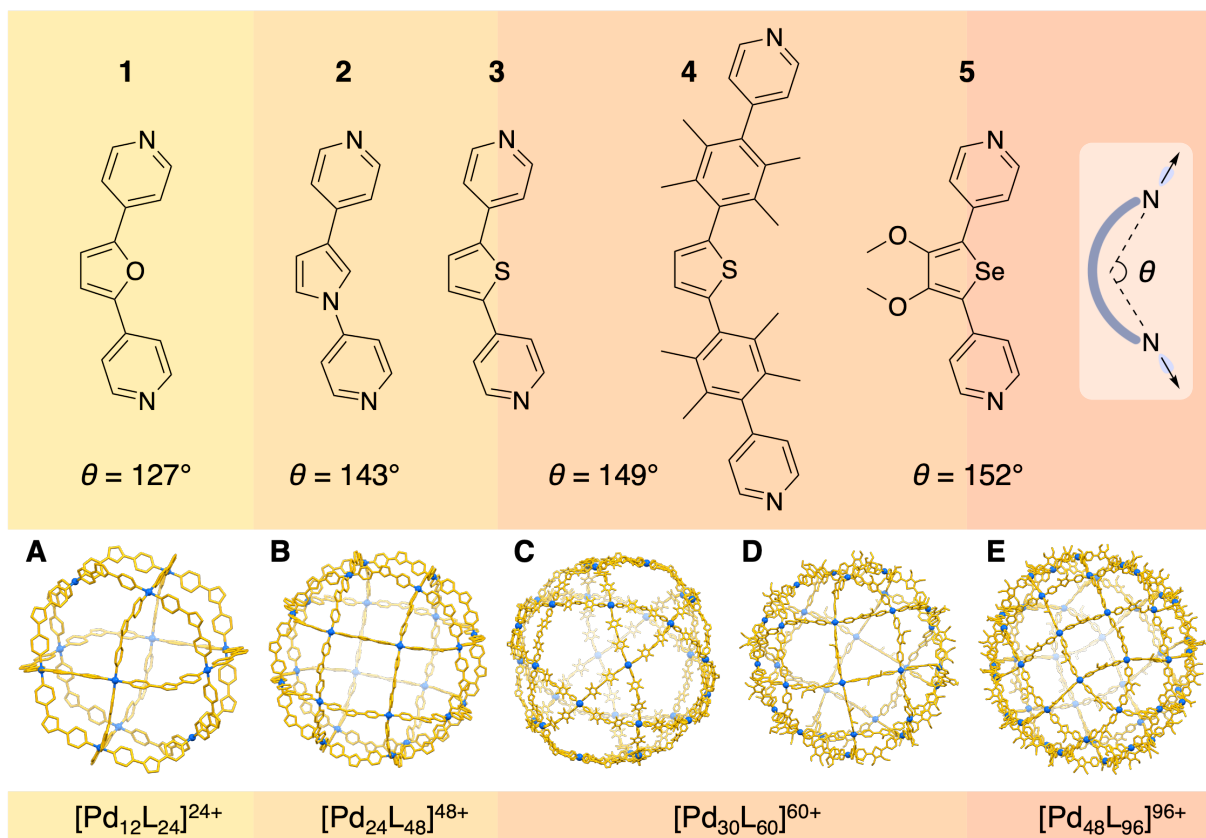


Figure 1. Structures of ligands with increasing bending angle θ and of the corresponding spherical $[\text{Pd}_n\text{L}_{2n}]^{2n+}$ complexes (with $n = 12, 24, 30$ and 48). Hydrogen atoms and counter anions are not shown for clarity.

In a later work, the same group obtained the $\text{Pd}_{30}\text{L}_{60}$ structure **C** exclusively, using ligand **4**.^[16] The latter was designed with an intermediate rigidity/flexibility, based on the hypothesis that overly flexible ligands tend to promote the formation of kinetically trapped, entropically favored species. On the contrary, ligands lacking flexibility might not efficiently adapt to the angle constraints and form a defined assembly.

A similar case was encountered with ligand **5**, which was designed with a slightly increased θ angle.^[13] The self-assembly reaction with Pd^{2+} initially led to the formation of the kinetically trapped $\text{Pd}_{30}\text{L}_{60}$ complex **D**. The thermodynamically favored $\text{Pd}_{48}\text{L}_{96}$ product **E** was then obtained by exploring different reaction conditions. Interestingly, complex **D** showed a different topology compared to what was observed for the previously reported $\text{Pd}_{30}\text{L}_{60}$ species **C**.

The borderline case of $\theta = 0$ generally leads to the formation of so-called ‘lantern shaped’ Pd_2L_4 assemblies, as one could expect from direct geometric considerations. However, in some cases, interlocked $(\text{Pd}_2\text{L}_4)_2$ dimeric complexes can preferentially form over the entropically favored product. This class of structures will be discussed in more details in section 1.3. Alternatively, numerous examples in the literature show that ligands with bending angles smaller than 0° and sufficient flexibility tend to form twisted Pd_2L_4 complexes or ‘helicates’.^[17] While the principles for ligand design have been well established to target Pd_nL_{2n} assemblies with $n = 2, 6, 12, 24, 30$ and 48 , a large structural variety has been observed for complexes obtained from ligands with $\theta \sim 60^\circ$ (**Figure 2**).

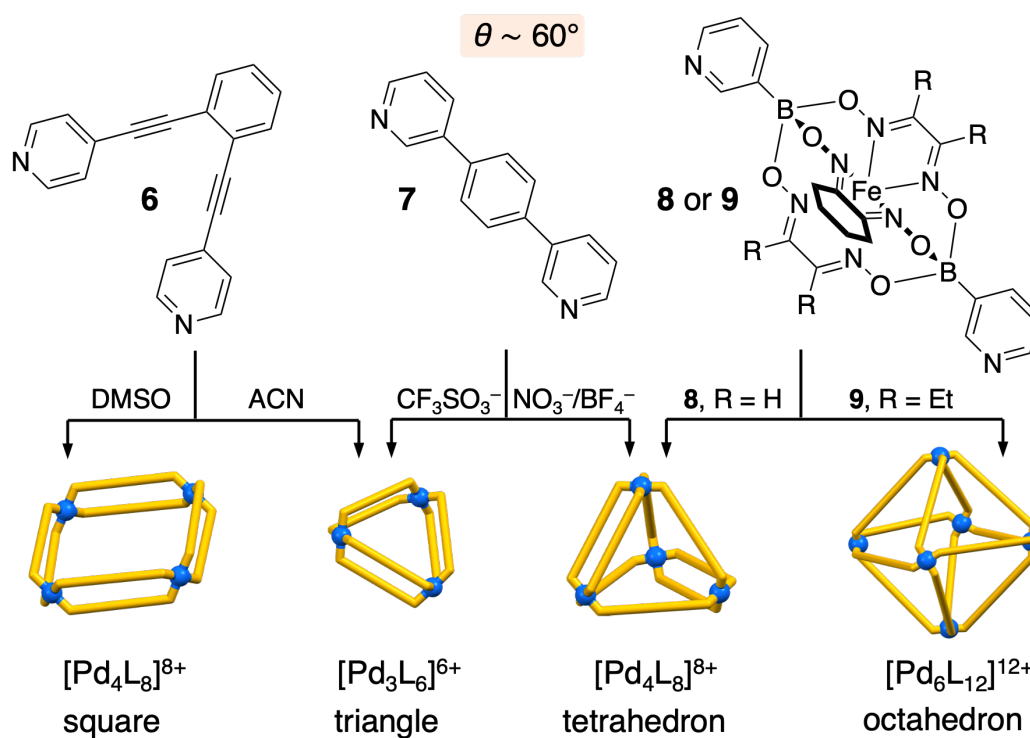


Figure 2. Structures of ligands with bending angle $\theta \sim 60^\circ$ and schematic representation of the different structural motifs observed for the corresponding $[\text{Pd}_n\text{L}_{2n}]^{2n+}$ complexes.

In the early days of the field, Fujita and co-workers reported the complexation of ligand **7** with $\text{Pd}(\text{NO}_3)_2$. Preliminary trials, using ethylenediamine *cis*-protected Pd, suggested that a Pd_3L_6 ‘double-walled’ triangle could potentially be accessed by using ‘naked’ Pd.^[18] A Pd_4L_8 tetrahedron was obtained instead of the expected product. Further investigations on the role of the counteranion revealed that the initial Pd_3L_6 target is preferentially formed with CF_3SO_3^- anions while the Pd_4L_8 tetrahedron is preferred with BF_4^- and NO_3^- .

A year later, the same group described a related, solvent-dependent, phenomenon with ligand **6**: equilibrating a mixture of $\text{Pd}(\text{NO}_3)_2$ and **6** in $\text{DMSO}-d_6$ afforded the Pd_3L_6 double-walled triangle.^[19] Alternatively, in CD_3CN , a Pd_4L_8 double-walled square was obtained. Similar to ligand **7**, the combination of the clathrochelate ligand **8** with Pd^{2+} also results in the formation of a ‘double-walled’ tetrahedron.^[20] In their study, Severin and coworkers revealed the ligand aspect ratio to be an important parameter controlling the structures of the related Pd complexes. When ligand **9** was used, featuring ethyl chains as substituents instead of hydrogen, a Pd_6L_{12} octahedron was obtained. It is interesting to note that Fujita and co-workers could target the Pd_6L_{12} octahedron by designing a ligand with a perfect 90° bending angle, but a similar structure is also obtained with ligand **9**.

Unlike ligands **1** – **6**, ligands **7** – **9** possess flexible coordination vectors due to the possible rotations around the σ -bonds. This allows them to adapt to different angle constraints, leading to a larger variety of accessible structures. However, these examples demonstrates that ligands with $\theta \sim 60^\circ$ can yield an array of diverse structures that may be close in energy to the point where the solvent and/or the counteranions start playing an important role. For smaller, more compact structures, the ligands tend to be in closer proximity and steric effects should also be considered.

1.2 Heteroleptic assemblies

1.2.1 Dinuclear assemblies

Most of the reported Pd_nL_{2n} assemblies to date feature a single type of bridging ligand L and increasing their structural complexity remains a central challenge in the field. Several groups have investigated the possibility of designing heteroleptic complexes incorporating two different ligands L and L'.^[20–41] A key challenge in this context is the controlled formation of a particular heteroleptic complex, known as 'integrative self-sorting',^[23,42] as opposed to a mixture of complexes, whether including one kind of ligand ("narcissistic self-sorting") or several following a statistical distribution. Various strategies have been developed toward this goal. In an early report, Hooley and Johnson showed that the self-assembly reaction could be controlled to favor the formation of the heteroleptic complex by endohedral functionalization of the ligands (**Figure 3a**).^[30] While the approach allowed for the preferential formation of the $\text{Pd}_2\text{L}_3\text{L}'_1$ mixed-ligands species, the homoleptic Pd_2L_4 assembly was still observed among the reaction products.

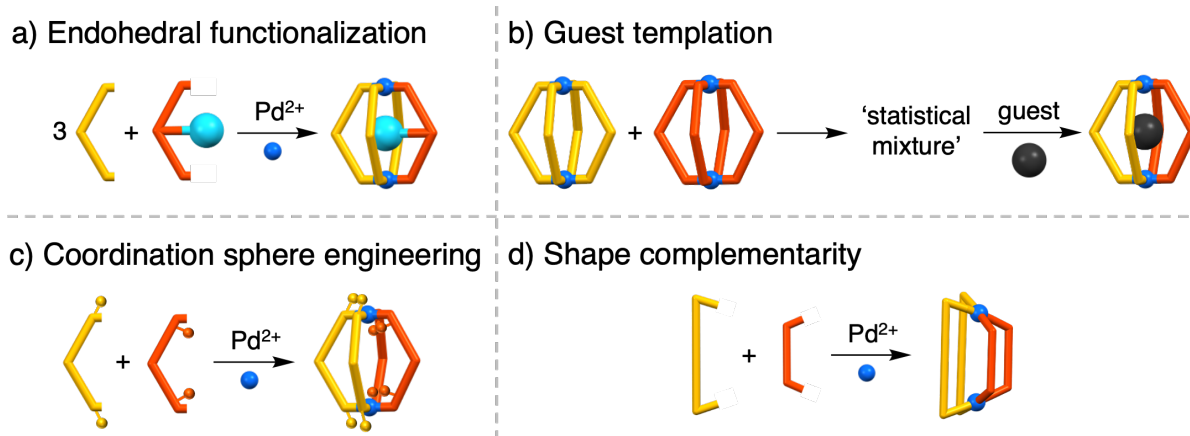


Figure 3. Schematic representation of the common strategies used to obtain heteroleptic dinuclear Pd^{2+} -based assemblies.

A few years later, Yoshizawa and co-workers reported the clean formation of a $\text{Pd}_2\text{L}_2\text{L}'_2$ species using a templating guest (**Figure 3b**).^[29] Initially, equilibrating a 1:1 mixture of the preformed Pd_2L_4 and $\text{Pd}_2\text{L}'_4$ cages led to the formation of a statistical mixture of products. However, the addition of C_{60} completely shifted the equilibrium, resulting in the exclusive formation of the $\text{Pd}_2\text{L}_2\text{L}'_2\supset\text{C}_{60}$ inclusion complex. The limitation of these two strategies lies in the formation of an occupied cavity, preventing any further host-guest chemistry.

The addition of substituent close to the N-donor atoms of the ligand, described as 'coordination sphere/donor site engineering', can also strongly influence the outcome of the self-sorting reaction via electronic and/or steric effects (**Figure 3c**). For example, Crowley and co-workers obtained a $\text{Pd}_2\text{L}_2\text{L}'_2$ cage, via ligand exchange reaction, taking advantage of inter-ligands H-bonds formation.^[27] Interestingly, the heteroleptic species could only be accessed via kinetic control and was not formed when starting from a ligand mixture.

Clever and co-worker later reported the targeted synthesis of a $\text{Pd}_2\text{L}_2\text{L}'_2$ assembly using two types of ortho-methyl-substituted bipyridyl ligands. Introducing steric bulk in the vicinity of the Pd centers allowed to direct the formation of the heteroleptic species as the thermodynamic product.^[25] The same group contributed to developing the 'shape complementarity' approach, where pairs of ligands are designed to possess complementary bending angles, with the goal of stabilizing the $\text{Pd}_2\text{L}_2\text{L}'_2$ complexes over the corresponding homoleptic assemblies (**Figure 3d**).^[26,28,43,43,44]

More recently, Zhang and co-workers reported the controlled formation of dinuclear cages from three different ligands, relying on an endo-functionalization strategy.^[45] Clever and co-workers took it a step further by accommodating four different types of ligands around the two Pd^{2+} centers under thermodynamic control.^[46]

1.2.2 Higher nuclearity assemblies

As discussed above, the self-assembly process can be controlled towards integrative self-sorting through careful ligand design. However, this rational design approach, reaches its limits when aiming for species comprising more than two palladium centers. As an early example, Fujita and co-workers reported the synthesis of a $\text{Pd}_{12}\text{L}_{23}\text{L}'_1$ coordination sphere by using an endohedral functionalization approach.^[34] A single, protein-tethered ligand L' was incorporated in the dodecanuclear product. The same group later reported the targeted synthesis of a $\text{Pd}_{12}\text{L}_{12}\text{L}'_{12}$ complex (**Figure 4a**).^[33]

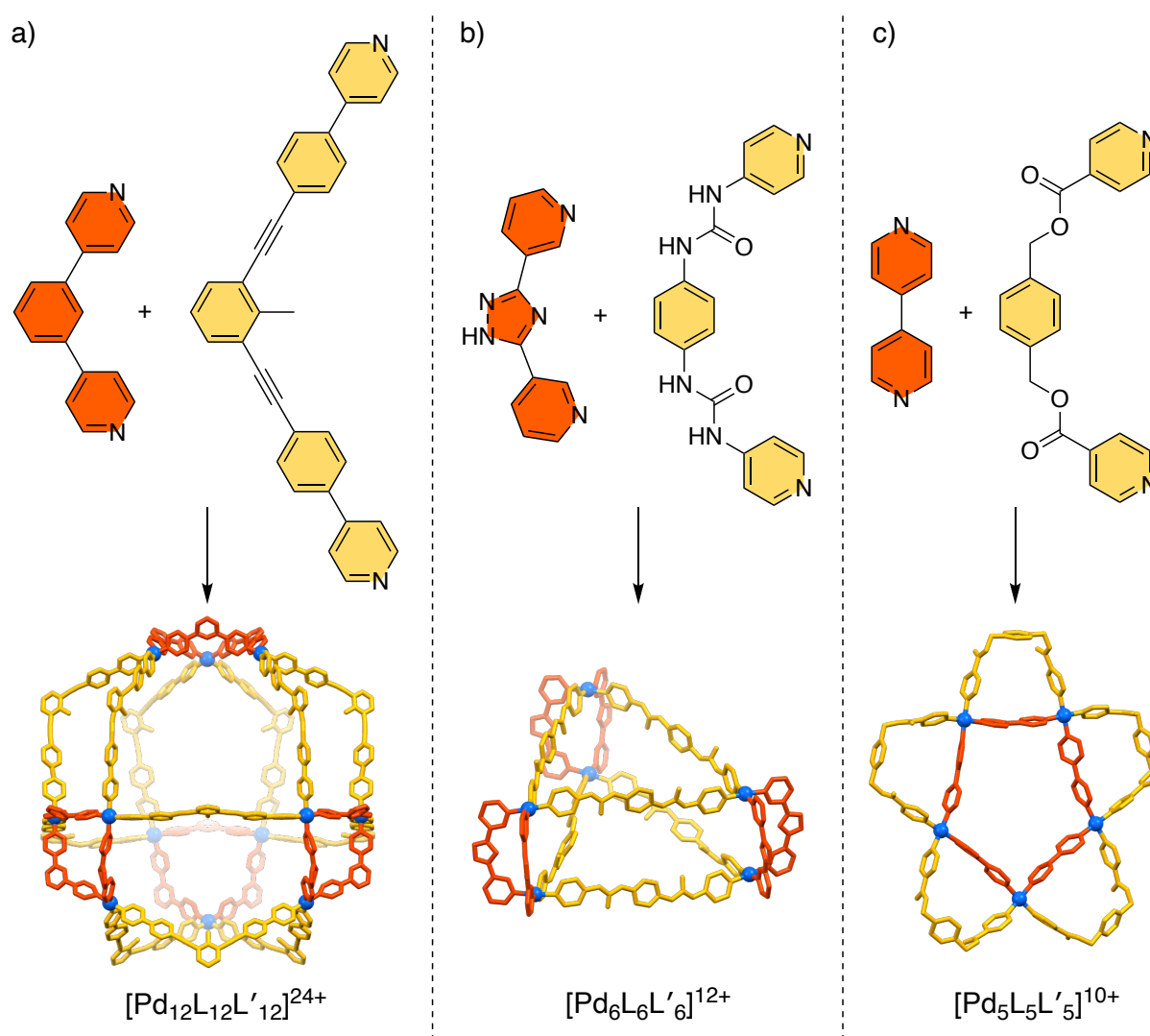


Figure 4. Structures of ligands pairs and of the corresponding heteroleptic $[\text{Pd}_n\text{L}_n\text{L}'_n]^{2n+}$ assemblies. The two different ligands are shown in red and orange. The hydrogen atoms are not shown for clarity.

The ratio r between the bridging length of L and L' was found to be a critical parameter controlling the outcome of the self-assembly process. A statistical mixture of product was observed for r values of 1–1.6, whereas combining ligands with $r \sim 2$ or larger resulted in an integrative self-sorting. Predicting the structure of potential heteroleptic structures gets increasingly difficult when aiming to incorporate two or more ligands with different bending angles. The groups of Mukherjee and Chand obtained a $\text{Pd}_6\text{L}_6\text{L}'_6$ prism and a $\text{Pd}_5\text{L}_5\text{L}'_5$ truncated star, respectively, using a rational design approach based on shape complementarity (**Figure 4b and c**).^[31,32]

Severin and co-workers later showed that a range of $\text{Pd}_n\text{L}_n\text{L}'_n$ complexes, with $n = 4, 6,$ and $8,$ could be accessed by combining ligand L ($\theta = 0$) with different ligands L' ($\theta = 120, 149$ or 180°).^[47] These results demonstrated that the nuclearity of heteroleptic complexes can also be controlled, to some extent, by the bending angle of L'. In the same year, Clever and co-workers obtained an example of a $\text{Pd}_4\text{L}_4\text{L}'_4$ tetrahedron by introducing sterically demanding substituents in the backbone of L'.^[48] This example highlights how exohedral functionalization can also efficiently promote integrative self-sorting. Unlike the commonly adopted endo-functionalization approaches discussed previously, the latter allows to access cage structures with empty cavities.

More recently, Severin and co-workers explored the possibility of forming heteroleptic structures from a mixture of three ligands with different bending angles ($0^\circ, 60^\circ$ and 120°), flexibilities and lengths. The screening experiment resulted in the formation of a $\text{Pd}_4\text{L}_4\text{L}'_2\text{L}''_2$ distorted tetrahedron as one of the major products. Interestingly, despite the variety of ligand geometries, only one of the eight combinations resulted in a complete narcissistic self-sorting. While further fine-tuning of the ligands' characteristics is required to direct the formation of a single product, these experiments provided additional examples of geometrically accessible heteroleptic structures. The development of a screening method for the identification of new heteroleptic complexes is discussed in Chapter 2 of this thesis.^[49]

1.3 Homoleptic assemblies with increased structural complexity

1.3.1 Symmetric ligands

Complexes formed from only one type of ligand can also display significant structural complexity, as seen in interlocked assemblies or when the ligand occupies chemically non-equivalent positions within the structure. These situations can result in reduced-symmetry assemblies and/or desymmetrized ligands (**Figure 5**).

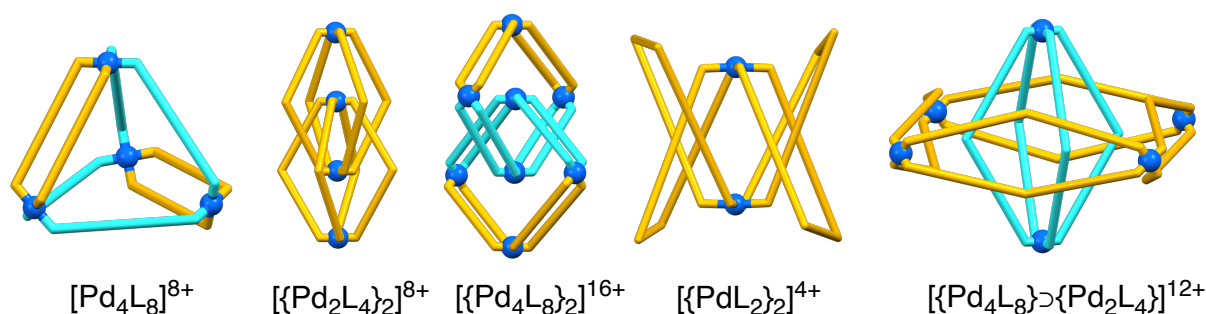


Figure 5. Schematic representations of homoleptic, Pd_nL_{2n} assemblies with increased structural complexity. Ligands belonging to chemically non-equivalent positions are shown with different colors.

The commonly encountered ‘ Pd_4L_8 tetrahedron’ structural motif is an early example of such reduced-symmetry species, where the ligands occupies two different positions.^[18,20,48,50,51] In other cases, the use of ligands with bending angles close or equal to 0° resulted in the formation of interlocked dimeric $(Pd_2L_4)_2$ structures.^[35,52–56] In addition to CH– π and π – π interactions, X-ray analyses have revealed the important role played by the anions in stabilizing these assemblies. This aspect will be further discussed in the ‘host-guest chemistry’ section of this introduction.

Recently, Clever and co-workers reported the synthesis of a unique $(Pd_4L_8)_2$ assembly composed of two interlocked Pd_4L_8 squares.^[57] In this case, additional complexity arises from both the two different ligands’ environments and the interlocking, causing the ligand’s desymmetrization. The reduced symmetry of the complex is reflected in the four-fold splitting of the signals in the 1H NMR spectrum.

The choice of solvent, as well as the nature of the anion, was found to have a crucial impact on the products' distribution. When the ligand was mixed with Pd(BF₄)₂ in DMSO-*d*₆, only the Pd₄L₈ macrocyclic monomer formed, whereas a distribution of products was observed in CD₃CN. The addition of NO₃⁻ to the mixture resulted in the complete conversion to the (Pd₄L₈)₂ dimer.

The same group later obtained a dinuclear interlocked (PdL₂)₂ species formed by two lemniscate-shaped PdL₂ monomers.^[58] Again, the dimer could be accessed in CD₃CN but not in DMSO-*d*₆.

While examples of mechanically interlocked species are regularly encountered in the literature, Lützen and co-workers reported a one-of-a-kind example of a [{Pd₄L₈}⊃{Pd₂L₄}]¹²⁺ 'cage-in-ring' assembly.^[59] Surprisingly, this rotaxane-like arrangement is held together solely by intermolecular π-stacking and attractive van der Waals interactions.

The latter case perfectly exemplifies how an increase in complexity is not necessarily accompanied by a reduced symmetry. The complexity of this structure lies in the ligands participating in the formation of two different structures, which stabilize each other to form the observed 'cage-in-ring' assembly. It is interesting to note, however, that the symmetry of the inclusion complex is the same as that of its constituting parts.

1.3.2 Low-symmetry ligands

Recently, several groups have been investigated the possibility to increase the structural complexity of Pd_{*n*}L_{2*n*}-type assemblies by using low-symmetry ligands.^[60–70] Due to the ligand's structure, these complexes exhibit cavities with a reduced symmetry and have thus been described as 'pseudo-heteroleptic'.^[68] Similar to what is observed in a mixed-ligand system, the use of low-symmetry ligands can potentially result in the formation of numerous conformational isomers. Limited to 4 for dinuclear species, this number increases to 9, 35 and 112 for Pd_{*n*}L_{2*n*} assemblies with *n* = 3, 4 and 6, respectively, and reaches 350'696 (ignoring enantiomers) for the Pd₁₂L₂₄ cuboctahedral cages.^[66,69]

Lewis and co-workers, for example, extensively studied ligand-design approaches to control the formation of Pd_2L_4 cages based on low-symmetry ligands. Shape-complementarity and coordination sphere engineering strategies allowed them to selectively form the *cis* isomers (**Figure 6a and b**).^[61,64]

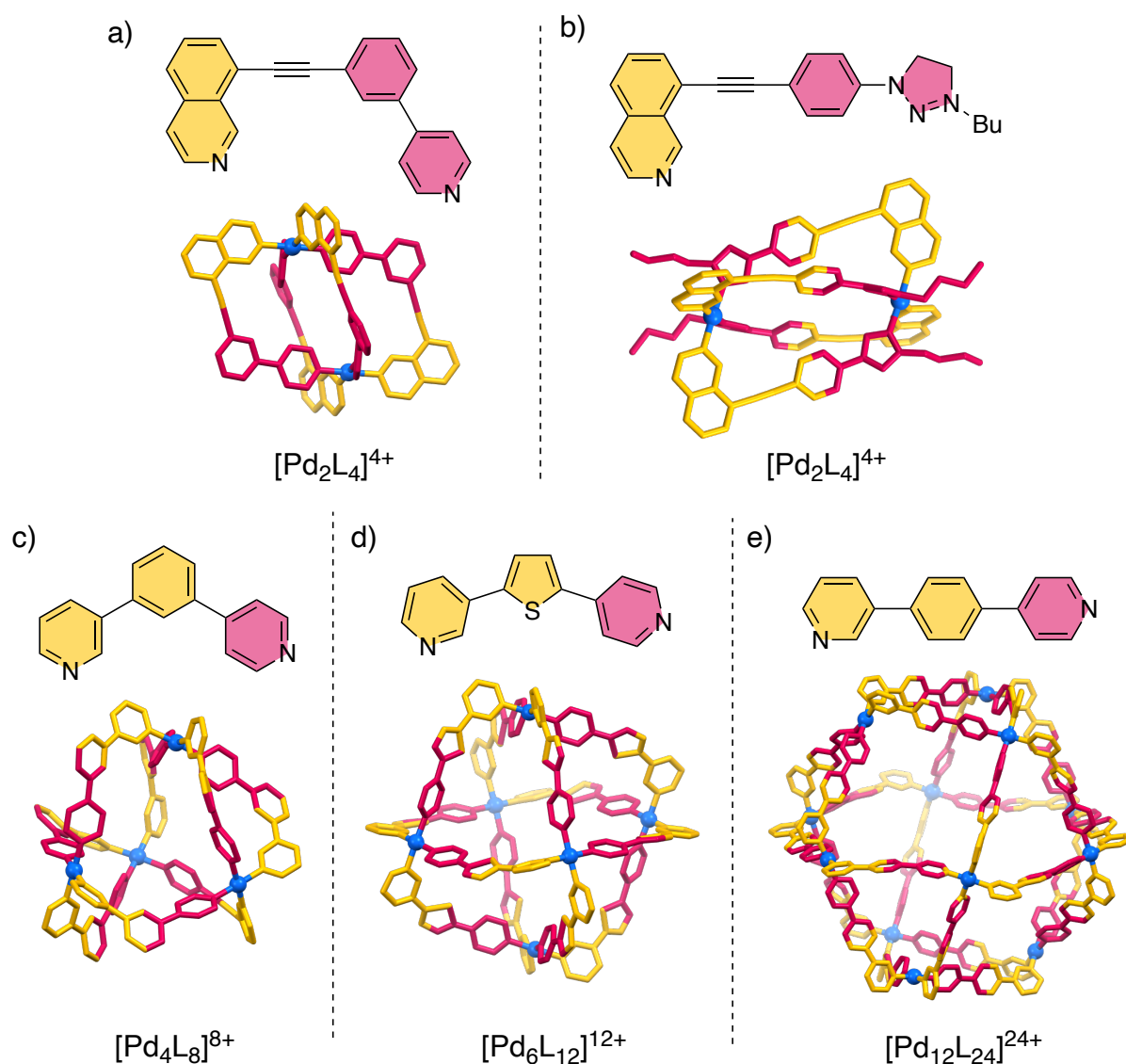


Figure 6. Structures of low-symmetry ligands and of the corresponding $[\text{Pd}_n\text{L}_{2n}]^{2n+}$ assemblies. The hydrogen atoms are not shown for clarity.

Preliminary results showed that introducing sterically demanding substituents was not as efficient in controlling the self-assembly reaction as geometric constraints. In the former case, the solvent's nature strongly influences the distribution of *cis* and *trans* isomers: the more polar *cis* isomer tended to be favored in the more polar solvent (DMSO-*d*₆) while the less-polar solvent (CD₃CN) stabilized the less polar *trans* isomer.^[61]

In addition to the solvent effect, the anions were also found to play an important role in stabilizing the different isomers, both through endo and exohedral interactions. Further investigations suggested that the observed solvent effect was likely due to its interaction with the cage's outer surface through hydrogen bonding.^[70] By refining the 'coordination sphere engineering' principles the authors successfully extended the concept to Pd₃L₆ assemblies and applied the strategy to control the formation of a heteroleptic Pd₂L₂L'₂ complex incorporating a pair of asymmetric ligands.

In parallel, Severin and co-workers reported examples of assemblies with higher nuclearity (**Figure 6c, d and e**). Early investigations demonstrated the formation of single isomers of a Pd₄L₈ tetrahedron and a Pd₆L₁₂ octahedron out of the respective 35 and 112 possible combinations.^[66] This highly unexpected outcome was described by the authors as 'orientational self-sorting'.

The same group later obtained a Pd₁₂L₂₄ cuboctahedron using a ligand with an increased bending angle (120°).^[69] Analyses indicated the formation of only one isomer out of the pool of the 350'696 possibilities. Interestingly, X-ray analyses revealed a *cis* coordination of the ligands around the Pd²⁺ centers, common to all the three structures (Pd₄L₈, Pd₆L₁₂ and Pd₁₂L₂₄). The superior thermodynamic stability of the *cis* arrangement was further supported by geometric analyses and a computational study. The scope and limitations of the '*cis* rule', as defined by the authors, was recently investigated in more details by conformational analyses of a range of octahedral Pd₆L₁₂ assemblies, obtained from different heteroditopic ligands.^[71]

1.4 Host-guest chemistry

1.4.1 Anionic guests

Owing to their cationic environment, provided by the positively charged Pd atoms, $[\text{Pd}_n\text{L}_{2n}]^{2n+}$ assemblies are ideal host for anionic guests. The first example, reported by McMorran and Steel, revealed the presence of a PF_6^- anion encapsulated within the Pd_2L_4 cage cavity.^[10] Such inclusion complexes are frequently encountered within the literature and several groups have been investigating the anion–structure relationships.^[3,17,41,51,72,73] The early example of Fujita and co-workers, discussed previously, showed that both the Pd_3L_6 triangle and P_4L_8 tetrahedron, based on the same ligand, could be accessed by selecting the adequate counteranion (**Figure 2**).^[18]

Since the first example of an interlocked $(\text{Pd}_2\text{L}_4)_2$ species, the structural motif has frequently been found in the literature.^[74] Following this seminal work, Kuroda and co-workers further investigated the role of the anion.^[52,75] The dimerization of the parent Pd_2L_4 complexes was observed with NO_3^- and BF_4^- but not with TfO^- or PF_6^- . The reaction could be reversed by the addition of 2-naphthalenesulfonate that was shown to act as a template for the Pd_2L_4 monomer. The host-guest chemistry of interlocked $(\text{Pd}_2\text{L}_4)_2$ cages was also explored by Clever and co-workers.^[3] The group reported examples of allosteric halide binding, where exchanging the BF_4^- with Cl^- in the outer pockets triggered the structure's contraction, resulting in an accessible central cavity.^[53,76–78] Examples of interpenetrated host-guest complexes are shown in **Figure 7**.

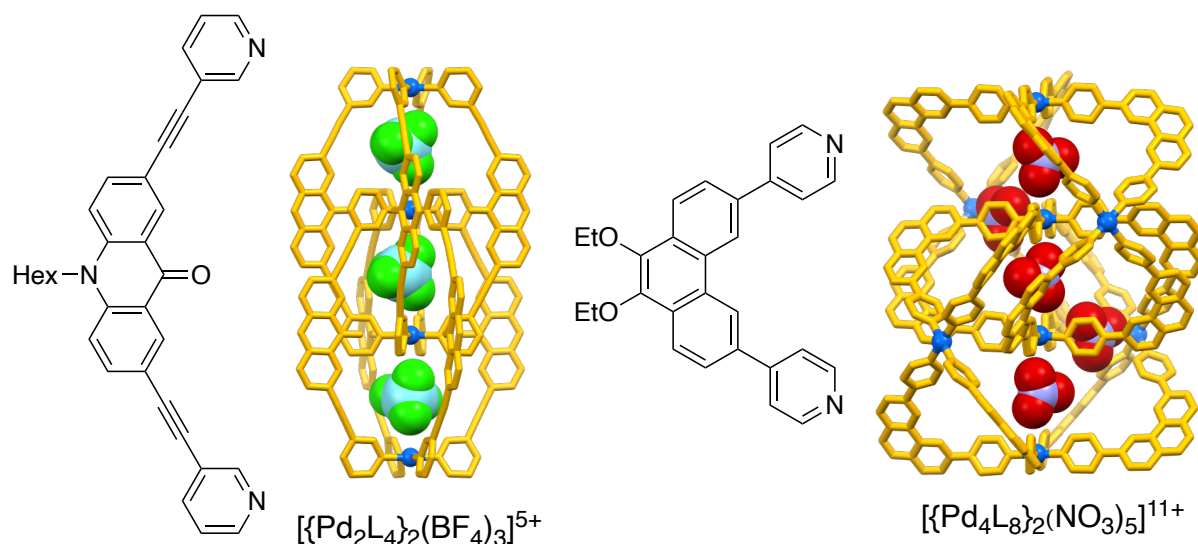


Figure 7. Structures of ligands and of the corresponding interpenetrated complex with Pd^{2+} . The side chains and hydrogen atoms are not shown for clarity. Guests color coding: B: light-cyan, F: green, N: purple, O: red.

In the case of some smaller Pd_2L_4 assemblies, the templating anion was found to significantly contribute to the overall stability. Besides mitigating the electrostatic repulsion between the two Pd centers, it balances the important structural strain caused by rigid ligands.^[39,47] Nevertheless, the reduced size of those assemblies makes them ideal candidates for halide encapsulation.^[79–83] The preparation of high-affinity Pd_2L_4 hosts for Cl^- is discussed in Chapter 6.

1.4.2 Neutral guests

Neutral molecules and complexes have been frequently investigated as potential guests for Pd_nL_{2n} -type hosts. In the early days of the field, Fujita and co-workers functionalized the interior of a $\text{Pd}_{12}\text{L}_{24}$ complex with azobenzene.^[84] The resulting structure efficiently bound pyrene guests through hydrophobic interactions and the capture could be reversed by light irradiation. The same group later employed a similar approach to bind C_{60} , using a coronene *endo*-functionalized species.^[85] Since then, the design of cages with a hydrophobic cavity has rapidly become a widely adopted strategy for encapsulating neutral guests.

Yoshizawa and co-workers reported numerous host-guest studies with a range of Pd₂L₄ assemblies based on anthracene ligands.^[86–93] A large variety of neutral molecules (coronene, fullerenes, organic dyes, sugars, hormones, ...) could bind within the hydrophobic cavity of the cages via hydrophobic interactions with the extended π surfaces of the ligands (**Figure 8**, right).

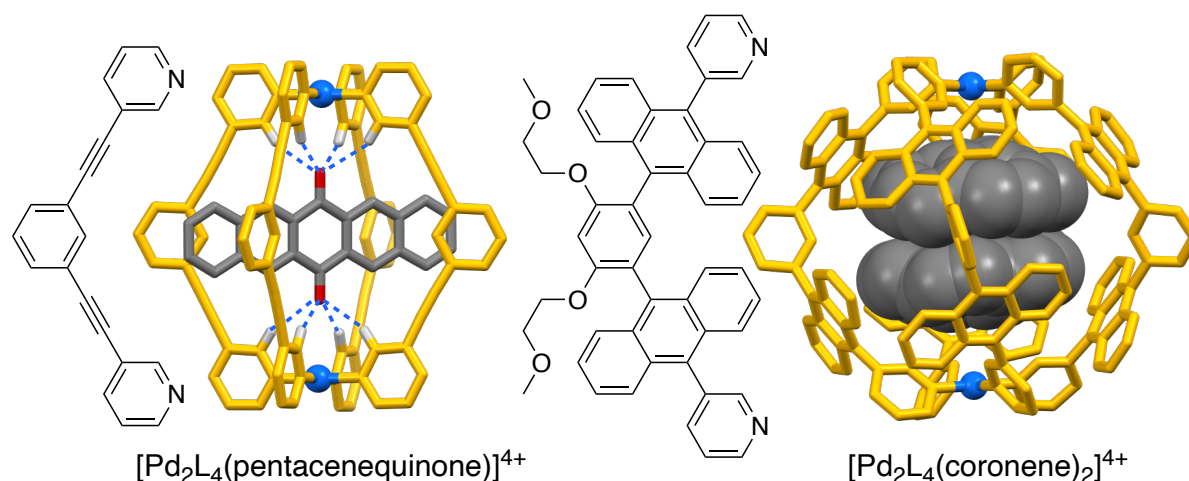


Figure 8. Structures of ligands and of the corresponding [Pd₂L₄(guest)]⁴⁺ inclusion complexes. Only the hydrogen atoms involved in H-bonding (blue dotted line) are shown. Side chains are omitted for clarity. Guests color coding: C: grey and O: red.

Binding neutral guests in the cavity of Pd₂L₄ lantern-shaped assemblies was also shown to be possible by relying on a good geometric and electronic complementarity between the host and the guest rather than hydrophobic effects.^[94] Moreover, the polarized C-H bonds in ortho position to the N-donors are efficient H-bond donors. Combined to their positively charged environment, this makes the vicinity of the Pd centers ideal sites for interactions with electron-rich functionalities such as ketones, nitriles or halides (**Figure 8**, left).^[95–97]

1.4.3 Cationic guests

Given their positively charged environment, Pd²⁺-based hosts do not appear as well-suited candidates for the encapsulation of cationic guests. There have been, however, a few examples demonstrating that it is possible to overcome the electrostatic repulsion. The groups of Liu and Fujita, for example, successfully addressed this challenge by designing endo-functionalized cages bearing cation-binding groups.^[98,99]

As a different approach, Lipke and co-workers prepared *cis*-protected Pt assemblies based on redox active porphyrin ligand. Electron transfer from the cobaltocene guests to the host was shown to compensate the positive charge of the cage and thus enabled the guest encapsulation. Interestingly, reoxidation of the ligands did not lead to the guest expulsion. Instead, the resulting inclusion complex was found to be kinetically stable over the course of several weeks.^[100]

Another possibility to mitigate the Pd²⁺-[guest]ⁿ⁺ negative interaction is the co-encapsulation of anions, which act as an 'electrostatic glue' (**Figure 9**).^[66,101–103] It was found that the ion pair encapsulation could also lead to a structural rearrangement or could be used to stabilize an unprecedented five-stranded helicate. Those examples are discussed in Chapter 3 and 4 respectively.

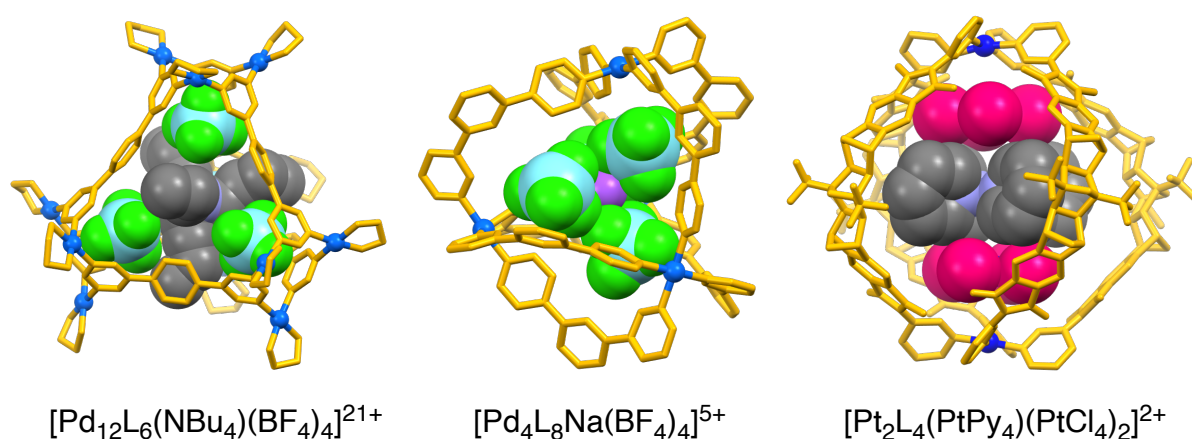


Figure 9. Structures of Pd²⁺ and Pt²⁺ based assemblies encapsulating both cationic and anionic species as guests. The hydrogen atoms are not shown for clarity. Guests color coding: B: light-cyan, F: green, C: grey, N: purple, Cl: magenta, Na: pink.

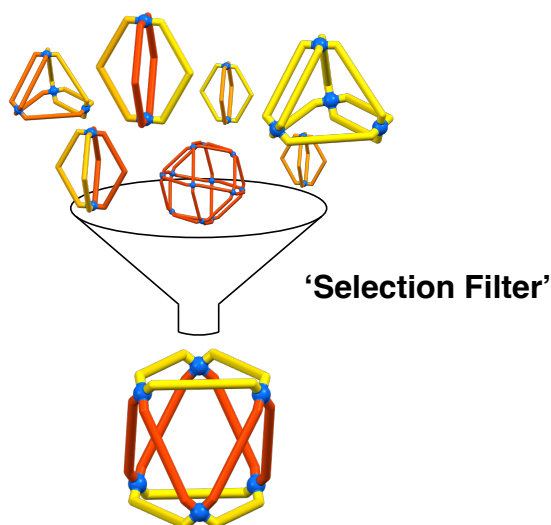
2. Identification of a heteroleptic Pd₆L₆L'₆ coordination cage by screening of a virtual combinatorial library

This chapter is based on published work:

“Identification of a Heteroleptic Pd₆L₆L'₆ Coordination Cage by Screening of a Virtual Combinatorial Library”

Adapted with permission from “S. Sudan, R.-J. Li, S. M. Jansze, A. Platzek, R. Rudolf, G. H. Clever, F. Fadaei-Tirani, R. Scopelliti, and K. Severin, *J. Am. Chem. Soc.*, **2021**, 143, 1773–1778.”. Copyright 2021 American Chemical society.

S. Sudan and K. Severin designed the experiments, S. Sudan and R.-J. Li performed the experiments and analyzed the data, S.M. Jansze, A. Platzek, R. Rudolf and K.E. provided samples of ligands **L3**, **L4** and **L6**, F. Fadaei-Tirani and R. Scopelliti collected and processed the X-ray data, and S. Sudan, K. Severin and G. H. Clever co-wrote the manuscript. The molecular modeling was performed by the group of G. Clever. All authors discussed the results and commented on the manuscript.



As discussed in Chapter 1, the rational design of defined heteroleptic complexes becomes increasingly difficult for assemblies of higher nuclearity. This chapter describes a selection approach that allowed the identification of a $[\text{Pd}_6\text{L}_6\text{L}'_6](\text{BF}_4)_{12}$ complex with an unprecedented trigonal-antiprismatic cage structure.

A molecularly defined metallosupramolecular structure needs to have a higher thermodynamic stability than competing structures. Otherwise, rearrangement reactions would occur over time. We hypothesized that screening of a virtual combinatorial library (VCL)^[104–107] of $[\text{Pd}_n\text{L}_{2n}]\text{X}_{2n}$ complexes would allow particularly stable assemblies to be identified. A VCL of Pd assemblies can be generated by using a mixture of ligands in combination with substoichiometric amounts of a Pd salt. The ligands compete for coordination to Pd^{2+} , and only highly stable assemblies will be formed. Less stable but potentially accessible complexes will not be generated to a significant extent.

We would like to note the importance of using a virtual library as opposed to a “real” library with stoichiometric amounts of Pd^{2+} . For the latter, the most stable assembly is not necessarily formed in larger amounts.^[108,109]

Results and discussion

For this study, we used six dipyridyl ligands (**L1–L6**), the structures of which are depicted in **Figure 10**. All these ligands have previously been employed to make homoleptic $[\text{Pd}_n\text{L}_{2n}]\text{X}_{2n}$ assemblies. Ligand **L1** forms a tetrahedron,^[18,20] **L2–L4** form dinuclear complexes,^[54,94,110] **L5** forms a dodecanuclear cage^[12] and **L6** forms an interlocked structure.^[111] In addition, **L4** was found to promote the formation of heteroleptic $[\text{Pd}_2\text{L}_2\text{L}'_2](\text{BF}_4)_4$ complexes.^[26]

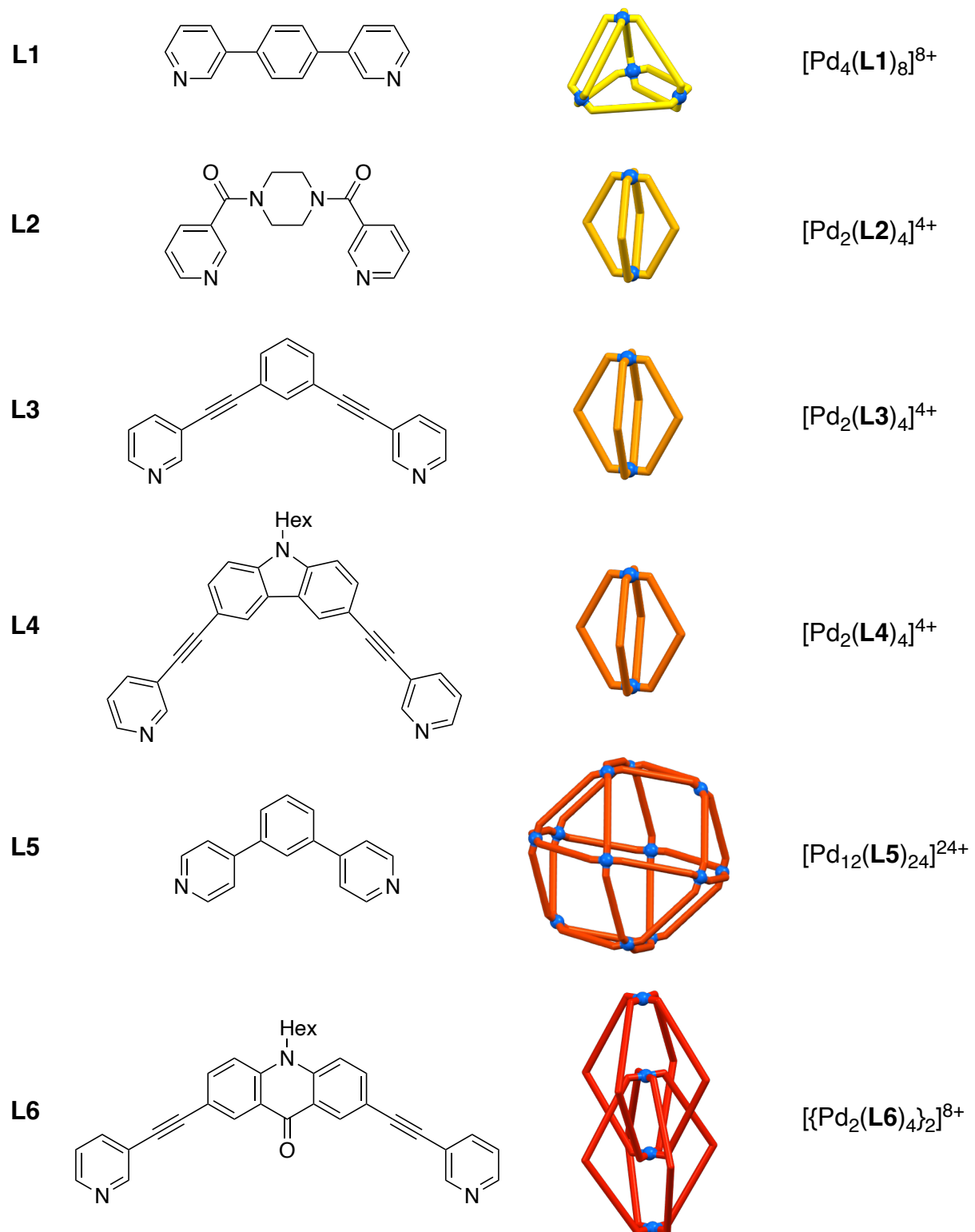
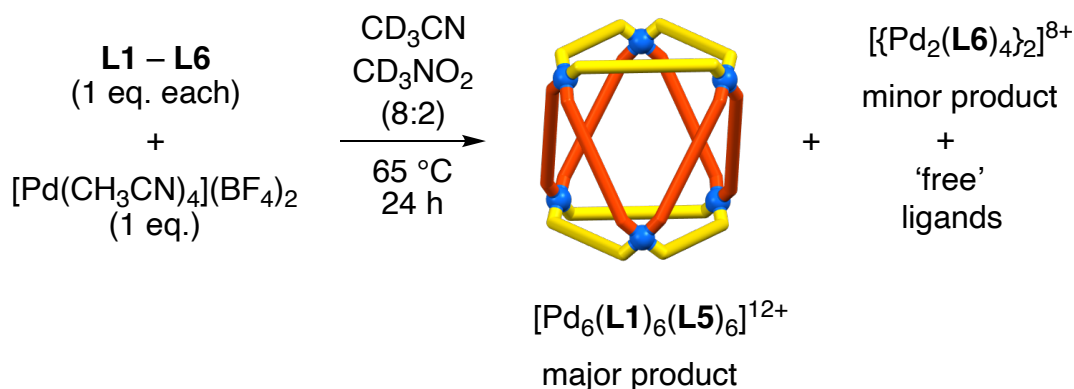


Figure 10. Structures of the N-donor ligands **L1–L6** and the corresponding homoleptic complexes with Pd^{2+} .

The competition experiment was performed as follows: equimolar amounts of the six ligands and $[\text{Pd}(\text{CH}_3\text{CN})_4](\text{BF}_4)_2$ were added to an 8:2 $\text{CD}_3\text{CN}/\text{CD}_3\text{NO}_2$ mixture,^a and the resulting suspension was heated for 17 h at 65 °C, resulting in the formation of a clear solution (**Scheme 1**).



Scheme 1. Reaction of **L1–L6** with substoichiometric amounts of Pd^{2+} .

The mixture was then analyzed by ^1H NMR spectroscopy. The region between 7.4 and 9.0 ppm is crowded by ligand signals, but the signals above 9.0 ppm can be attributed to Pd-based assemblies. When comparing these signals to those of the homoleptic complexes, we found small signals corresponding to the interlocked cage $[\{\text{Pd}_2(\mathbf{L6})_4\}_2](\text{BF}_4)_8$ (**Figure 11**). The formation of this assembly was not unexpected, as its high stability had been noted previously.^[111] In addition to the signals of $[\{\text{Pd}_2(\mathbf{L6})_4\}_2](\text{BF}_4)_8$, there were larger signals that could not be matched with any of the other homoleptic complexes.

^a This mixture provides good solubility for a range of $[\text{Pd}_n\text{L}_{2n}]\text{X}_{2n}$ complexes.

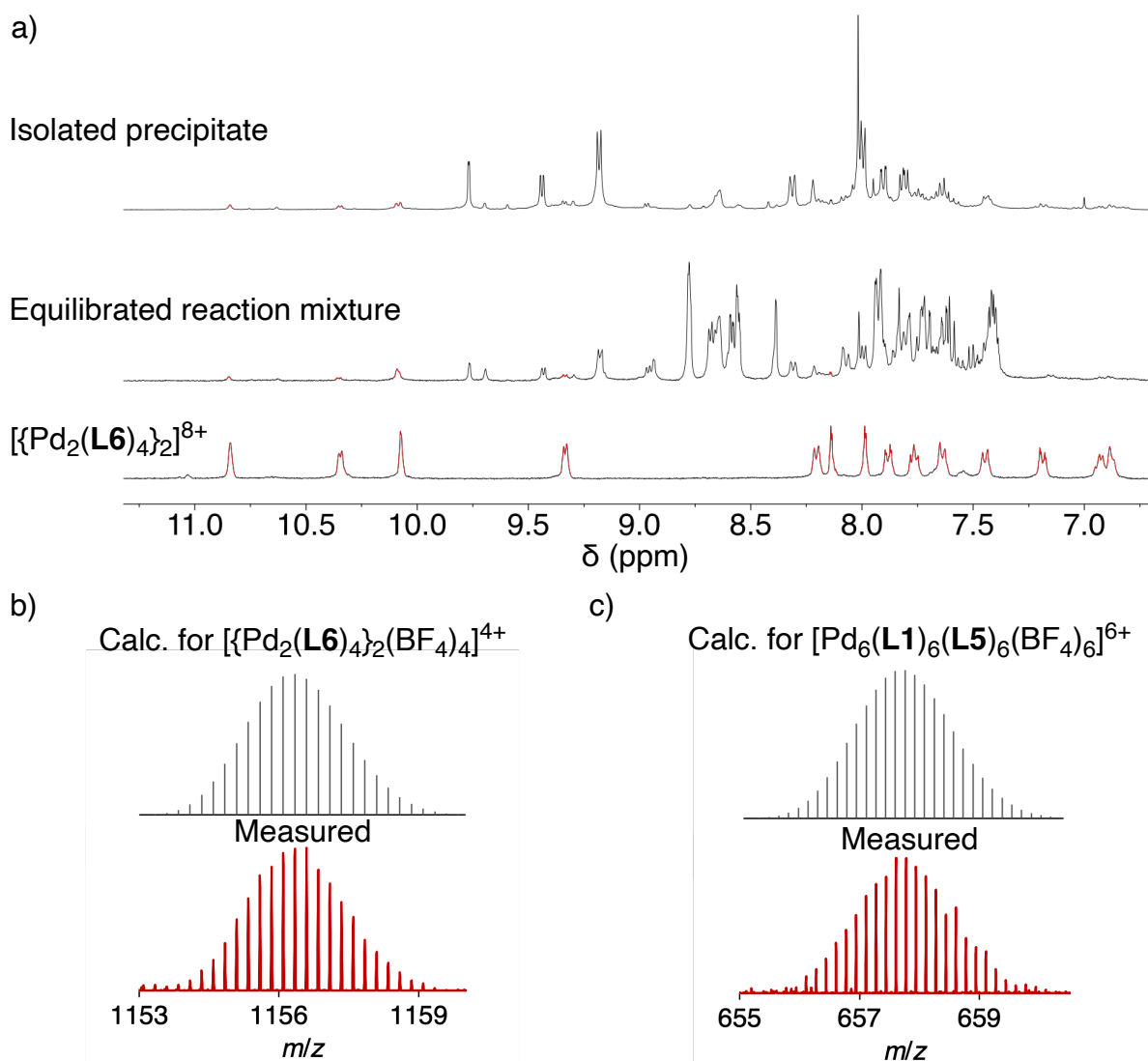


Figure 11. (a) Aromatic region of the ^1H NMR spectrum (400 MHz, $\text{CD}_3\text{CN}/\text{CD}_3\text{NO}_2$, 8:2) of the isolated precipitate (top), the reaction mixture after equilibration (center) and of $[\{\text{Pd}_2(\text{L6})_4\}_2](\text{BF}_4)_8$ (bottom). The ratio of $[\text{Pd}_6(\text{L1})_6(\text{L5})_6](\text{BF}_4)_{12}$ to $[\{\text{Pd}_2(\text{L6})_4\}_2](\text{BF}_4)_8$ in solution is approximately 3:1. In the precipitate, the corresponding ratio is $\sim 5:1$, indicating that the interlocked cage displays a better solubility. HRMS of the isolated precipitate in $\text{CD}_3\text{CN}/\text{CD}_3\text{NO}_2$ (8:2), comparing (b) the 1153 – 1160 m/z region (bottom, red) with the calculated mass spectrum for $[\{\text{Pd}_2(\text{L6})_4\}_2(\text{BF}_4)_4]^{4+}$ (top, black) and (c) the 655 – 660 m/z region (bottom, red) with the calculated mass spectrum for $[[\text{Pd}_6(\text{L1})_6(\text{L5})_6]_2](\text{BF}_4)_6]^{6+}$ (top, black).

In order to identify the main reaction product(s), we separated the ionic $[\text{Pd}_n\text{L}_{2n}]\text{X}_{2n}$ complexes from the remaining 'free' ligands by precipitation with Et_2O /pentane. Analysis of the ligand fraction by ^1H NMR spectroscopy showed a depletion of ligands **L1** and **L5** (**Figure ES7**). Analysis of the precipitate by ^1H NMR spectroscopy indicated the formation of one main product with high apparent symmetry. The multiplicities of the signals were in agreement with a complex containing equal amounts of **L1** and **L5**. Additional information was obtained by mass spectrometry (**Figure 11**). Next to signals of $\{[\text{Pd}_2(\text{L6})_4]_2\}(\text{BF}_4)_8$, we found signals corresponding to a hexanuclear complex containing **L1** and/or **L5** (these two ligands have the same mass). Taken together, the analytical data suggested that the main product of the competition experiment was an assembly of the formula $[\text{Pd}_6(\text{L1})_6(\text{L5})_6](\text{BF}_4)_{12}$.

To corroborate our findings, we synthesized $\text{Pd}_6(\text{L1})_6(\text{L5})_6(\text{BF}_4)_{12}$ on a preparative scale by mixing equimolar amounts of **L1**, **L5**, and $[\text{Pd}(\text{CH}_3\text{CN})_4](\text{BF}_4)_2$. The reaction product displayed the same NMR signals as were observed for the main product of the screening experiment (**Figure 12**). DOSY NMR spectroscopy showed that the molecular size of this new heteroleptic complex was between that of the known homoleptic complexes $[\text{Pd}_4(\text{L1})_8](\text{BF}_4)_8$ and $[\text{Pd}_{12}(\text{L5})_{24}](\text{BF}_4)_{24}$. Mass spectrometry confirmed that a hexanuclear complex had formed.

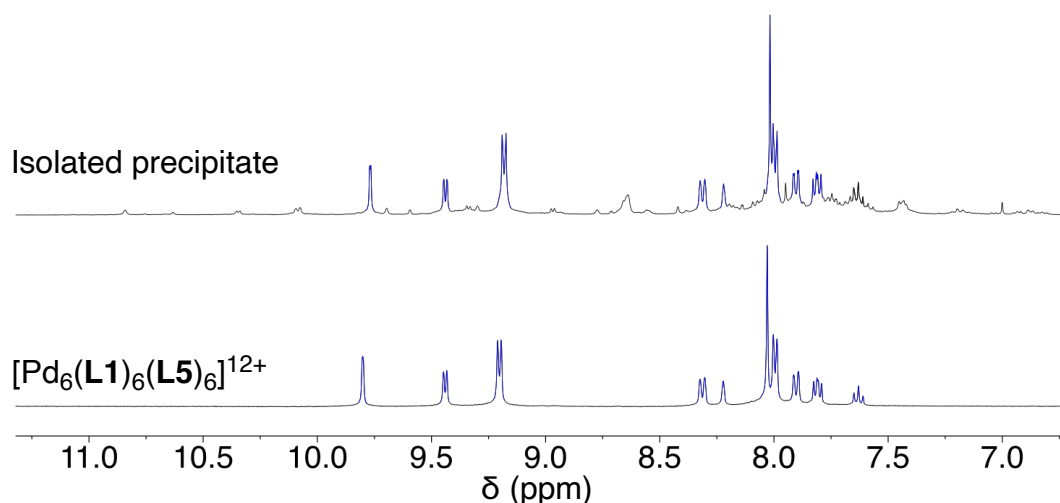
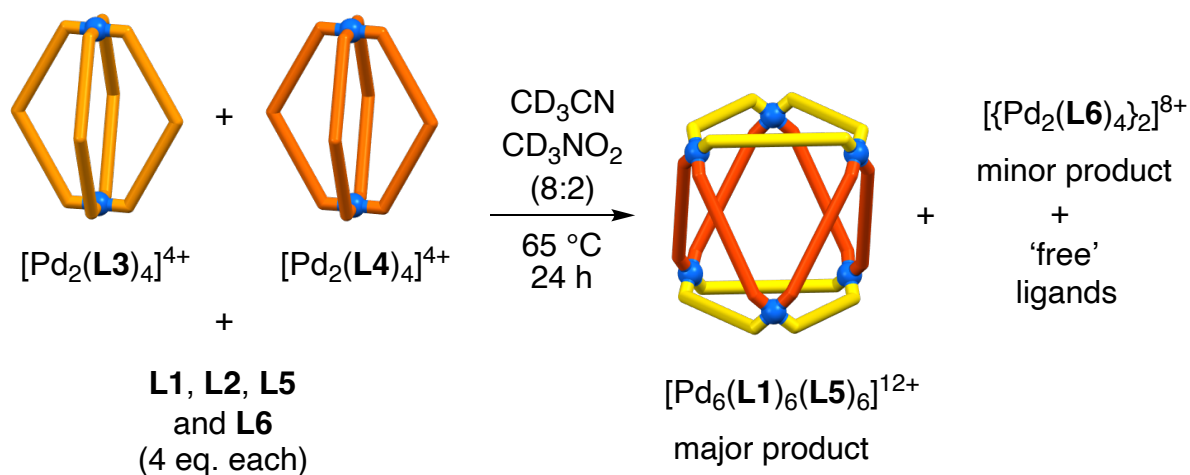


Figure 12. Aromatic region of the ^1H NMR spectrum (400 MHz, $\text{CD}_3\text{CN}/\text{CD}_3\text{NO}_2$, 8:2) of the isolated precipitate (top) and of $[\text{Pd}_6(\text{L1})_6(\text{L5})_6](\text{BF}_4)_{12}$.

To exclude the possibility that $[\text{Pd}_6(\mathbf{L1})_6(\mathbf{L5})_6](\text{BF}_4)_{12}$ was obtained under kinetic control, we repeated the competition experiment with different starting conditions. Instead of using $[\text{Pd}(\text{CH}_3\text{CN})_4](\text{BF}_4)_2$ as a source of Pd^{2+} , we employed equimolar amounts of the preformed assemblies $[\text{Pd}_2(\mathbf{L3})_4](\text{BF}_4)_4$ and $[\text{Pd}_2(\mathbf{L4})_4](\text{BF}_4)_4$. The two complexes were equilibrated with **L1**, **L2**, **L5**, and **L6** (4 eq. each) in $\text{CD}_3\text{CN}/\text{CD}_3\text{NO}_2$ (**Scheme 2**).



Scheme 2. Conversion of the homoleptic cages $[\text{Pd}_2(\mathbf{L3})_4](\text{BF}_4)_4$ and $[\text{Pd}_2(\mathbf{L4})_4](\text{BF}_4)_4$ into the heteroleptic cage $[\text{Pd}_6(\mathbf{L1})_6(\mathbf{L5})_6](\text{BF}_4)_{12}$.

The ^1H NMR spectrum of the resulting mixture was very similar to that obtained with a mixture of all six ligands (**Figure ES8**), and the heteroleptic cage $[\text{Pd}_6(\mathbf{L1})_6(\mathbf{L5})_6](\text{BF}_4)_{12}$ could be identified as the dominant Pd assembly in solution. This control experiment confirmed the superior thermodynamic stability of the heteroleptic complex. The formation of $[\text{Pd}_6(\mathbf{L1})_6(\mathbf{L5})_6](\text{BF}_4)_{12}$ starting from $[\text{Pd}_4(\mathbf{L1})_8](\text{BF}_4)_8$ (3 eq.) and $[\text{Pd}_{12}(\mathbf{L5})_{24}](\text{BF}_4)_{24}$ (1 eq.) was also examined. A rearrangement into the heteroleptic cage was observed, but the reaction was not complete after 85 days (**Figure ES9**). The reaction of **L1–L6** with stoichiometric amounts of Pd^{2+} ($[\text{ligand}]_{\text{total}}:[\text{Pd}] = 2:1$) was also performed. As anticipated, the ^1H NMR spectrum (**Figure ES10**) of the reaction mixture was very complex, indicating the formation of multiple assemblies instead of few selected compounds. Alongside signals corresponding to the homoleptic $[\text{Pd}_2(\mathbf{L2})_4(\text{BF}_4)_x]^{z+}$, $[\text{Pd}_2(\mathbf{L3})_4(\text{BF}_4)_x]^{z+}$ and $[\{\text{Pd}_2(\mathbf{L6})_4\}_2(\text{BF}_4)_x]^{z+}$ species, the mass spectrum displayed peaks that could be attributed to potential heteroleptic assemblies (**Figure 13**).

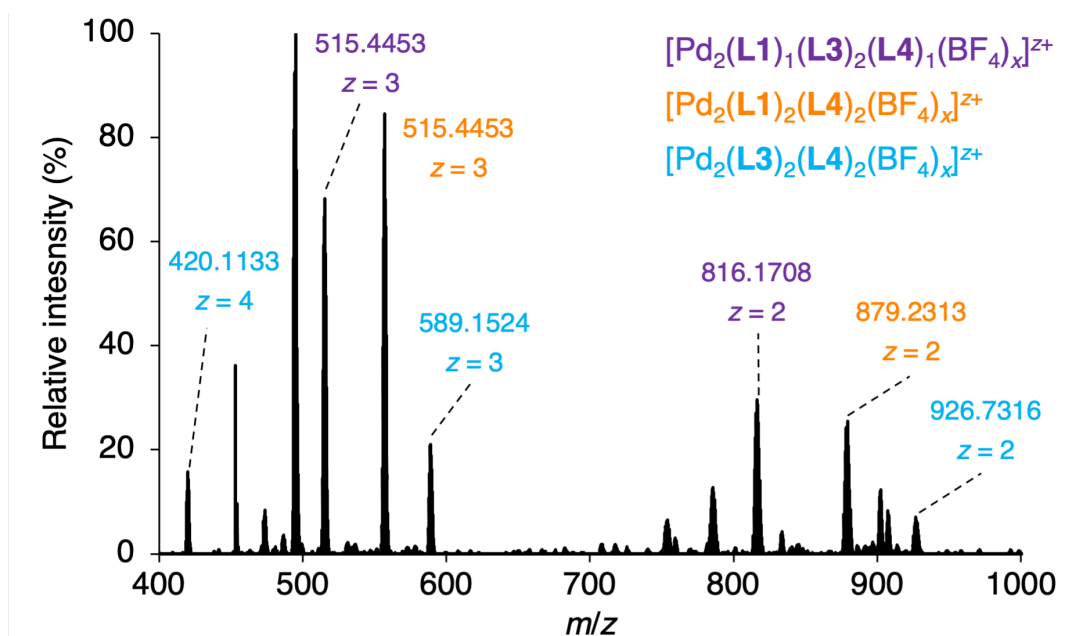


Figure 13. HRMS of an equilibrated mixture containing **L1–L6** and stoichiometric amounts of $[\text{Pd}(\text{CH}_3\text{CN})_4](\text{BF}_4)_2$ ($[\text{ligand}]_{\text{total}}:\text{[Pd]} = 2:1$) in a mixture of CD_3CN and CD_3NO_2 (8:2). The inset shows the proposed formulae of corresponding heteroleptic species.

Direct synthesis of the three proposed species was attempted. While **L1** and **L5** have the same mass, the former was used for the preliminary trials, as a good geometric complementarity is expected with **L4**.^[26] Unsurprisingly, equilibration of 1:1:1 mixture of **L1**, **L4** and Pd^{2+} resulted in the clean formation of a $[\text{Pd}_2(\text{L1})_2(\text{L4})_2]^{4+}$ species, as confirmed by HRMS and ^1H NMR analyses (**Figures ES2** and **ES3**). X-ray diffraction analysis supported the expected match between the ligands bending angle and the Pd coordination geometry (**Figure ES4**). Similarly, although less clean, the reaction of equimolar amounts of **L3** and **L4** resulted in an integrative self-sorting. ^1H NMR and HRMS analyses confirmed the presence of the $[\text{Pd}_2(\text{L3})_2(\text{L4})_2]^{4+}$ as the main product (**Figures ES5** and **ES6**). The last proposed species was of more interest to us, as it apparently consisted of three different ligands. In this case, however, equilibrating a mixture of **L1**, **L3** and **L4** with Pd^{2+} (1:2:1:1) formed a mixture of products, as deduced from the ^1H NMR spectrum (**Figure ES11**). The HRMS analysis allowed to identify $[\text{Pd}_2(\text{L1})_2(\text{L4})_2]^{4+}$ and $[\text{Pd}_2(\text{L4})_4]^{4+}$ assemblies, as major products, alongside the targeted $[\text{Pd}_2(\text{L1})_1(\text{L3})_2(\text{L4})_1]^{4+}$ species (**Figure ES12**).

Next, the molecular structure of $[\text{Pd}_6(\text{L1})_6(\text{L5})_6](\text{BF}_4)_{12}$ was analyzed by single-crystal X-ray diffraction. A graphical representation of the cationic cage is depicted in **Figure 14a**. The six Pd^{2+} ions occupy the vertices of a trigonal antiprism. The two trigonal faces of the prism are composed of $[\text{Pd}_3(\text{L1})_3]^{6+}$ macrocycles, which are bridged by six **L5** ligands. This highly symmetrical structure is in line with the NMR spectra, which show a single set of signals for the two ligands **L1** and **L5**.

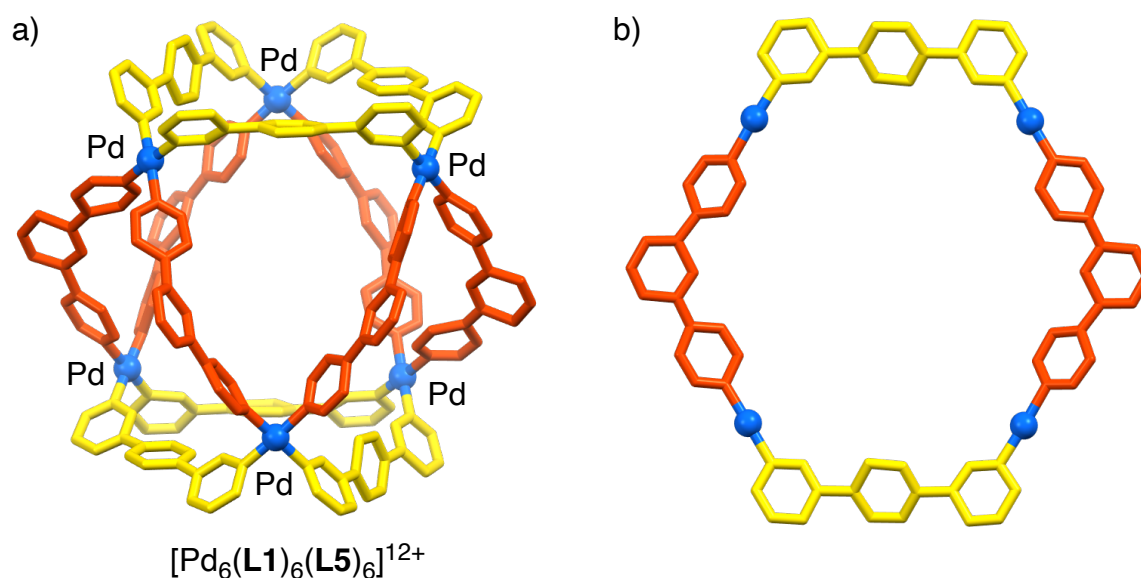


Figure 14. (a) Graphical representation of the molecular structure of $[\text{Pd}_6(\text{L1})_6(\text{L5})_6]^{12+}$ in the crystal. (b) Part of the structure showing a Pd_4 macrocyclic fragment with two ligands **L1** (yellow) and two ligands **L5** (orange). Hydrogen atoms are not depicted.

It is interesting to note that the competition experiment with **L1–L6** resulted in the preferential formation of a hexanuclear complex even though lower-nuclearity complexes are favored from an entropy point of view. Therefore, we assume that enthalpic effects are responsible for the high stability of $[\text{Pd}_6(\text{L1})_6(\text{L5})_6](\text{BF}_4)_{12}$. Inspection of the solid-state structure shows that intermolecular ligand–ligand interactions are unlikely to play a role because the 12 ligands are well-separated from each other.

However, the combination of **L1** and **L5** seems to result in a particularly favorable coordination environment for the Pd²⁺ ions. The cage can be deconstructed into [Pd₄(**L1**)₂(**L5**)₂]⁸⁺ macrocyclic fragments, one of which is shown in **Figure 14b**. It is evident that the geometry of the ligands allows for ‘perfect’ 180° coordination of the metal ions. Another possible factor for the selection of **L1** and **L5** out of a pool of six ligands is the higher basicity of the arylpyridine ligands **L1** and **L5** compared with the alkynyl and amide-based pyridine ligands **L2–L4** and **L6**.^[112] Finally, we considered the possibility that anion templating effects play a role. However, the heteroleptic cage was also formed when the hexafluorophosphate complex [Pd(CH₃CN)₄](PF₆)₂ was combined with **L1** and **L5**, suggesting that specific anion–cage interactions are not of central importance.

We then investigated whether it is possible to obtain other [Pd₆L₆L’₆]₁₂ assemblies of comparable topology by using ligands with a similar arrangement of the pyridyl donor atoms. The metalloligands **L7** and **L8** (**Figure 15a**) were used as structural analogues of the simple organic ligands **L1** and **L5**. Both ligands feature chemically inert iron clathrochelate complexes as rigid spacers between the pyridyl groups.^[113] Ligand **L7** has been described before, and it forms a hexanuclear complex with Pd²⁺.^[114] The new ligand **L8** was prepared by a multicomponent condensation reaction following a synthetic methodology developed in our laboratory.

A mixture of equimolar amounts of **L7**, **L8**, and [Pd(CH₃CN)₄](BF₄)₂ in DMSO-*d*₆ was heated overnight at 70 °C. Analysis of the resulting solution by ¹H NMR spectroscopy revealed the formation of an assembly with high apparent symmetry (a single set of signals for **L7** and **L8**). The composition of this complex could be established by high-resolution ESI-MS. Dominant peaks for a heteroleptic assembly with the formula {[Pd₆(**L7**)₆(**L8**)₆](BF₄)_{*x*}}^{*z+*} (*x* = 3–7; *z* = 9–5) could be observed (**Figure 15b**).

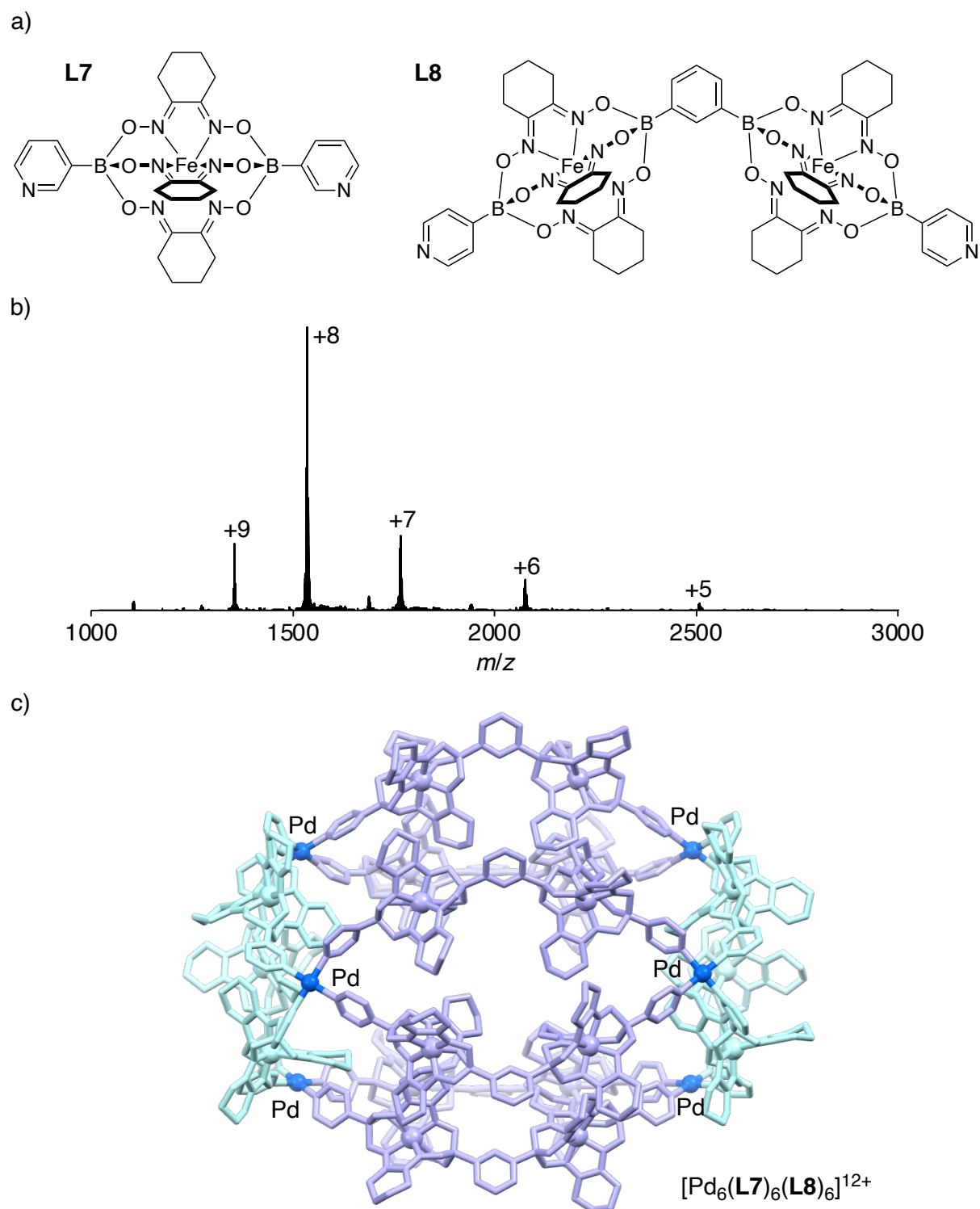


Figure 15. (a) Structures of the metalloligands **L7** and **L8**. (b) ESI mass spectrum of the assembly formed from **L7**, **L8**, and $[\text{Pd}(\text{CH}_3\text{CN})_4](\text{BF}_4)_2$. (c) Structure of $[\text{Pd}_6(\text{L7})_6(\text{L8})_6]^{12+}$ as determined by MMFF computations, with **L7** shown in cyan and **L8** shown in purple. The model is based on crystallographic data, which allowed identification of the positions of the Pd and Fe atoms and thus the connectivity of the ligands.

Single crystals of $[\text{Pd}_6(\mathbf{L7})_6(\mathbf{L8})_6](\text{BF}_4)_{12}$ were obtained from DMSO, but the quality of the diffraction data did not allow for a high-resolution structural analysis. However, we were able to locate the Pd and Fe atoms, and their positions corroborated that the complex displays a cage structure with an overall shape of a prolate spheroid. The positions of the metal ions also allowed the connectivity of the ligands to be established. The six metalloligands **L7** form two $[\text{Pd}_3(\mathbf{L7})_3]^{9+}$ macrocycles, which are positioned at the opposite ends of the spheroid. The links between the two macrocycles are established by the bent metalloligands **L8**. A structural difference between the smaller cage $[\text{Pd}_6(\mathbf{L1})_6(\mathbf{L5})_6]^{12+}$ and $[\text{Pd}_6(\mathbf{L7})_6(\mathbf{L8})_6]^{12+}$ is the connectivity of the bent ligands **L5** and **L8**. In the latter case, we observe the formation of $[\text{Pd}_2(\mathbf{L8})_2]^{4+}$ macrocycles, leading to a trigonal-prismatic arrangement of the six Pd^{2+} ions. We have used the crystallographic data as the basis for MMFF computations, and a model of $[\text{Pd}_6(\mathbf{L7})_6(\mathbf{L8})_6]^{12+}$ is depicted in **Figure 15c**.

Conclusion

We have created a virtual combinatorial library of $[\text{Pd}_n\text{L}_{2n}](\text{BF}_4)_{2n}$ complexes by mixing six different dipyriddy ligands with substoichiometric amounts of $[\text{Pd}(\text{CH}_3\text{CN})_4](\text{BF}_4)_2$. The number of potentially accessible complexes in this library is very large, but competition for a limited amount of Pd^{2+} leads to a selection process. The heteroleptic complex $[\text{Pd}_6(\mathbf{L1})_6(\mathbf{L5})_6](\text{BF}_4)_{12}$ was identified as the main Pd complex after equilibration. It is noteworthy that a hexanuclear complex was selected, even though none of the homoleptic complexes, derived from **L1–L4**, contain six Pd^{2+} ions (**Figure 10**). The preferential formation of a high-nuclearity complex with $n = 6$ is also remarkable given that low-nuclearity complexes are favored from an entropy point of view. The results obtained with metalloligands **L7** and **L8** demonstrate that complexes of the formula $[\text{Pd}_6\text{L}_6\text{L}'_6]\text{X}_{12}$ can be accessed with different types of dipyriddy ligands. It will be interesting to explore whether other “islands of stability” can be identified in the vast structural space of heteroleptic $[\text{Pd}_n\text{L}_{2n}]\text{X}_{2n}$ complexes.

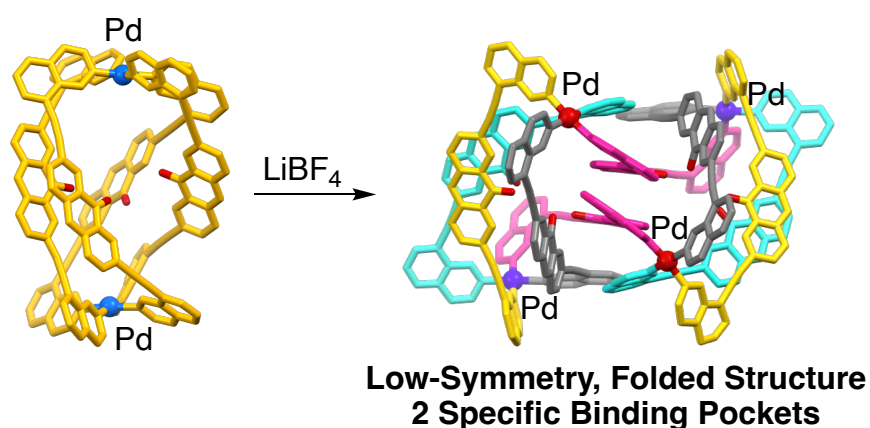
3. LiBF₄-induced rearrangement and desymmetrization of a palladium-ligand assembly

This chapter is based on published work:

“LiBF₄-Induced Rearrangement and Desymmetrization of a Palladium-Ligand Assembly”

S. Sudan, F. Fadaei-Tirani, R. Scopelliti, K. E. Ebbert, G. H. Clever and K. Severin,
Angew. Chem. Int. Ed., **2022**, *61*, e202201823.

S. Sudan and K. Severin designed the experiments, S. Sudan performed the experiments and analyzed the data, K.E. Ebbert provided samples of ligands **L4**, **L6** and **L9**, F. Fadaei-Tirani and R. Scopelliti collected and processed the X-ray data, and S. Sudan, K. Severin and G. H. Clever co-wrote the manuscript. All authors discussed the results and commented on the manuscript.



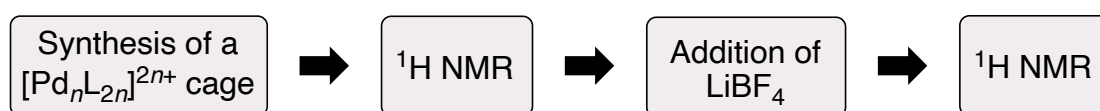
As presented in the introduction, there have been few reports of cation encapsulation in positively charged guest. One of the examples, reported by our group, showed the complexation of Na⁺ ions inside a tetrahedral [Pd₄L₈]⁸⁺ cage.^[66] The binding was enabled by co-encapsulation of four BF₄⁻ anions. Intrigued by the finding that a simple Na⁺ ion can be bound inside a [Pd₄L₈]⁸⁺ cage, we have examined if other [Pd_nL_{2n}]²ⁿ⁺ cages would also be able to bind alkali metal ions. In particular, we were interested if they could bind lithium ions. Li⁺ is a challenging guest due to its high solvation energy.

Results and discussion

For our investigations, we have prepared 13 different [Pd_nL_{2n}]²ⁿ⁺ complexes (as BF₄⁻ salts), all of which had been described in the literature (**Figure 16**). The small library contained diverse architectures including simple dinuclear [Pd₂L₄]⁴⁺ complexes, a macrocyclic [Pd₃L₆]⁶⁺ complex, cages ([Pd₄L₈]⁸⁺, [Pd₆L₁₂]¹²⁺, [Pd₁₂L₂₄]²⁴⁺), heteroleptic complexes ([Pd₂L₂L'₂]⁴⁺ and [Pd₆L₆L'₆]¹²⁺), and an interlocked {[Pd₂L₄]₂}⁸⁺ species (for details, see the Experimental Section).

The synthesis of the 13 complexes was accomplished by mixing [Pd(CH₃CN)₄](BF₄)₂ with the corresponding ditopic N-donor ligand(s) in CD₃CN and tempering for 12 h at 70 °C. The success of the self-assembly process was verified by ¹H NMR spectroscopy. Subsequently, LiBF₄ (50 eq.) was added and another ¹H NMR spectrum recorded. A potential interaction with LiBF₄ was evaluated by comparing the spectra before and after addition of the salt. The screening of 13 potential hosts gave two “hits”.

a) **Screening procedure**



b) **Library of cage complexes**

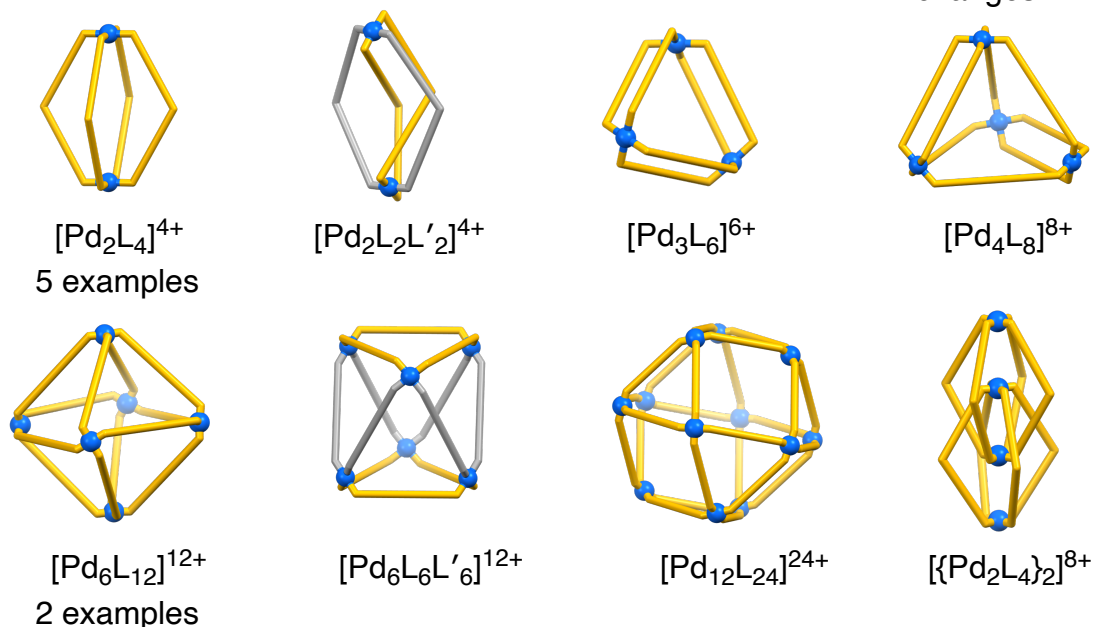
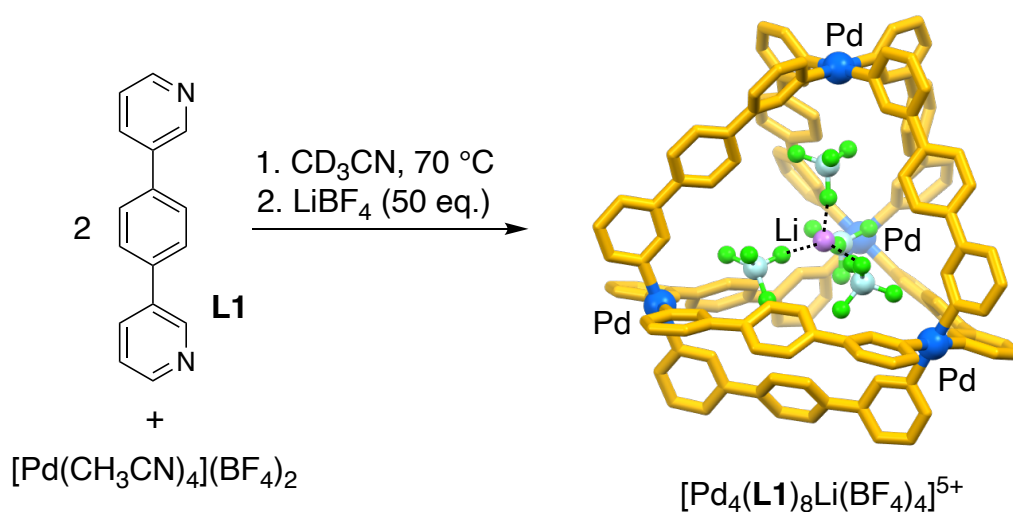


Figure 16. NMR-based screening for interaction of LiBF₄ with [Pd_nL_{2n}]²ⁿ⁺ assemblies (BF₄⁻ salts).

For a tetranuclear Pd complex based on ligand **L1** (**Scheme 3**),^[18,20] the addition of LiBF₄ (50 eq.) resulted in shifts in the ¹H NMR spectrum of up to 0.1 ppm (**Figure ES15**). A more elaborate NMR titration experiment was performed using a variable amount of LiBF₄ (10–200 eq., **Figure ES17**). The resulting isotherm was fitted to a 1:1 binding model yielding an apparent binding constant of $K_a=26(\pm 2) \text{ M}^{-1}$.^b It is important to note that the 1:1 binding model represents a simplification, as the guest is [Li(BF₄)₄]³⁻ and not just Li⁺. The cation complexation could be corroborated by a crystallographic analysis. The structural data show that binding of the cationic guest is achieved by coencapsulation of four BF₄⁻ anions, which are situated in between the Pd²⁺ ions and the Li⁺ ion. (**Scheme 3**). The larger Na⁺ could be encapsulated in a similar fashion, as evidenced by a crystallographic analysis of the host–guest complex.

^b The ¹H NMR data were fitted using the online tool provided on the following website: <http://supramolecular.org>.

A quantification of Na⁺ binding was hampered by the low solubility of NaBF₄ in acetonitrile, which prevented NMR titration experiments.



Scheme 3. Encapsulation of $[\text{Li}(\text{BF}_4)_4]^{3-}$ by the tetranuclear complex $[\text{Pd}_4(\text{L1})_8]^{8+}$. The structure of the host–guest complex is based on a crystallographic analysis. Hydrogen atoms are not shown for clarity. Color coding: Pd: blue, C and N: yellow, F: green, B: light cyan.

The second “hit” in our screening was a dinuclear cage based on ligand **L9**.^[28] Directly after the addition of LiBF₄, we observed complexation-induced chemical shifts. However, the ¹H NMR spectrum changed with time, indicating the formation of a new complex (**Figure ES16**). The rearrangement occurred with a half-life of 135 min, and it was complete within 20 h (**Figure ES18**).^[115–126] Subsequent analysis by mass spectrometry revealed the formation of a $[\text{Pd}_4\text{L}_8]^{8+}$ assembly. The tetranuclear complex could also be obtained by equilibrating a mixture of $[\text{Pd}(\text{CH}_3\text{CN})_4](\text{BF}_4)_2$, **L9**, and LiBF₄ in a 1 : 2 : 15 ratio at 70 °C for 12 h.

A striking feature of the new complex was its low apparent symmetry: the ¹H NMR signals of the aromatic CH protons were found to split eight times (**Figure 17**). This splitting was evidenced by analysis of the ¹³C and ¹H-¹³C HSQC NMR spectra (**Figure ES14**). Surprisingly, the splitting observed in the NMR spectra did not match with any of the known topologies for $[\text{Pd}_4\text{L}_8]^{8+}$ assemblies, namely: macrocyclic,^[19,127,128] distorted tetrahedral,^[18,20,66,129] and interlocked.^[52,54,55,111]

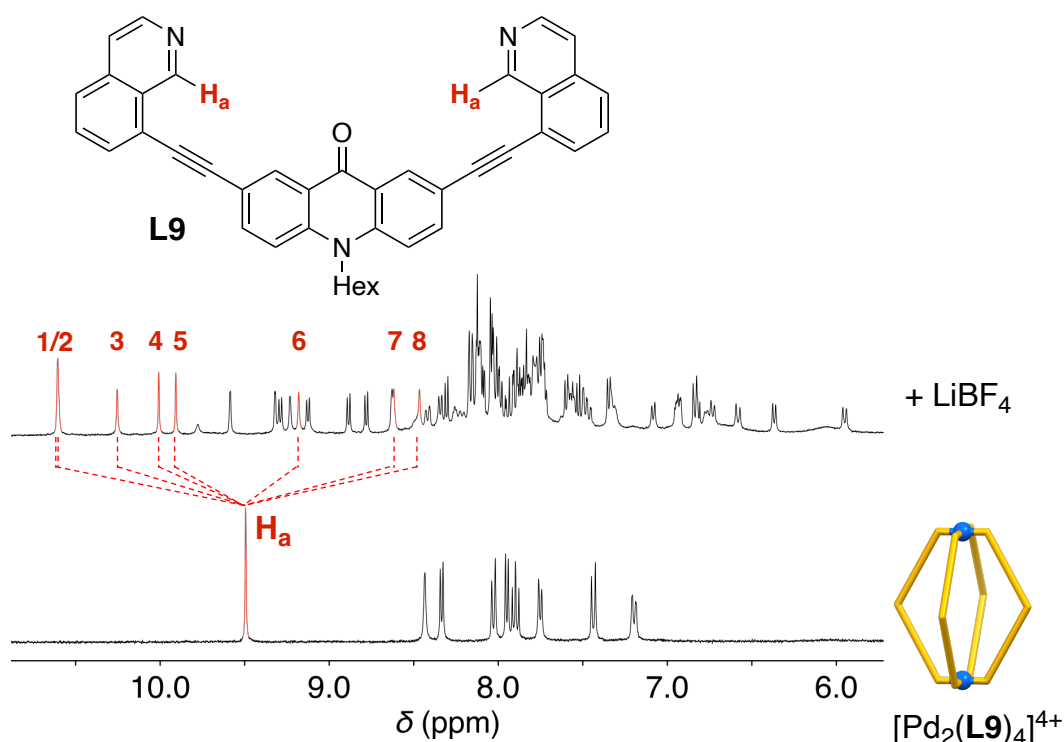


Figure 17. Aromatic region of the ^1H NMR (400 MHz, CD_3CN) spectra of a mixture of $[\text{Pd}(\text{CH}_3\text{CN})_4](\text{BF}_4)_2$ (1 eq.) and **L9** (2 eq.) after tempering at 70°C for 12 h in the absence (bottom) or in the presence of LiBF_4 (15 eq., top).

The rearrangement was only observed for lithium salts (LiBF_4 or LiOTf). The addition of NaOTf or KPF_6 to a solution of $[\text{Pd}_2(\text{L9})_4](\text{BF}_4)_4$ in CD_3CN resulted in broadening of the ligand signals, but a new species could not be detected. For CsBPh_4 , no change in the NMR spectra was observed at all (**Figure ES19**). Notably, the rearrangement was also observed for mixtures of LiOTf and NaOTf , indicating that the low-symmetry Pd complex has a very high selectivity for lithium over sodium salts (**Figure ES20**).^[130–133]

Single crystals of the new Pd assembly were obtained by slow vapor diffusion of diethyl ether into a solution of the complex in CD_3CN . The results of a crystallographic analysis showed that a tetranuclear $[\text{Pd}_4(\text{L9})_8](\text{BF}_4)_8$ complex had formed (**Figure 18a**).^c

^c As the crystallographic analysis of $[\text{Pd}_4(\text{L9})_8]^{8+}$ reveals tight encapsulation of $\text{LiBF}_4(\text{H}_2\text{O})$, the guest is also expected to be $\text{LiBF}_4(\text{H}_2\text{O})$ in experiments with LiOTf ; BF_4 coming from the Pd salt.

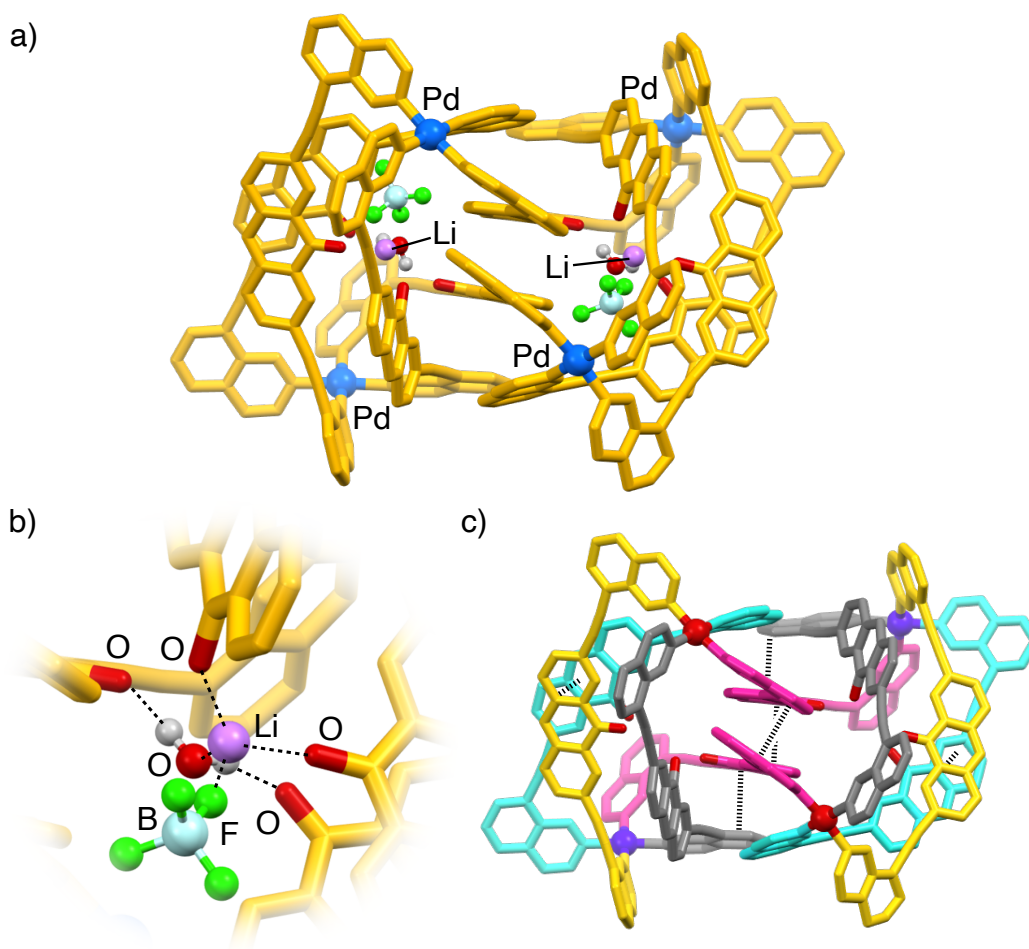


Figure 18. (a) Molecular structure of $[\text{Pd}_4(\text{L9})_8]^{8+}$ in the crystal with two $\text{LiBF}_4 \cdot \text{H}_2\text{O}$ guest molecules. Hydrogen atoms, most BF_4^- anions, and the hexyl side chains are not shown for clarity. Color coding: Pd: blue, O: red; C and N: yellow, F: green, B: light cyan. (b) Close-up view on the binding pocket. (c) Graphic representation of $[\text{Pd}_4(\text{L9})_8]^{8+}$ highlighting intra-ligand π -stacking interactions. The color coding indicates symmetry-related ligands and Pd^{2+} ions.

The assembly features two symmetry-related binding pockets (the complex has one crystallographic C_2 symmetry axis).^[2] Each pocket is occupied by a LiBF_4 ion pair and a water molecule. The Li^+ ion shows a tetrahedral coordination environment with close contacts to one BF_4^- anion ($\text{Li}-\text{F}=1.851(7)$ Å), one water molecule ($\text{Li}-\text{O}=1.902(7)$ Å), and two carbonyl groups of ligand ($\text{Li}-\text{OC}=1.895(8)$ Å, $\text{Li}-\text{O}'\text{C}'=1.907(8)$ Å) (**Figure 18b**). Two other carbonyl groups are involved in hydrogen bonding to the water molecule. The latter was found to be crucial for the rearrangement: when heat-dried LiBF_4 was added to a solution of $[\text{Pd}_2(\text{L9})_4](\text{BF}_4)_2$ in dry CD_3CN , the formation of

$[\text{Pd}_4(\text{L9})_8](\text{BF}_4)_8$ could not be detected. Instead, only broadening of the ^1H NMR signals was observed, similar as what was found for NaOTf. Quantitative conversion into $[\text{Pd}_4(\text{L9})_8](\text{BF}_4)_8$ could then be triggered by addition of small amounts of D_2O to the solution (**Figure 19**).

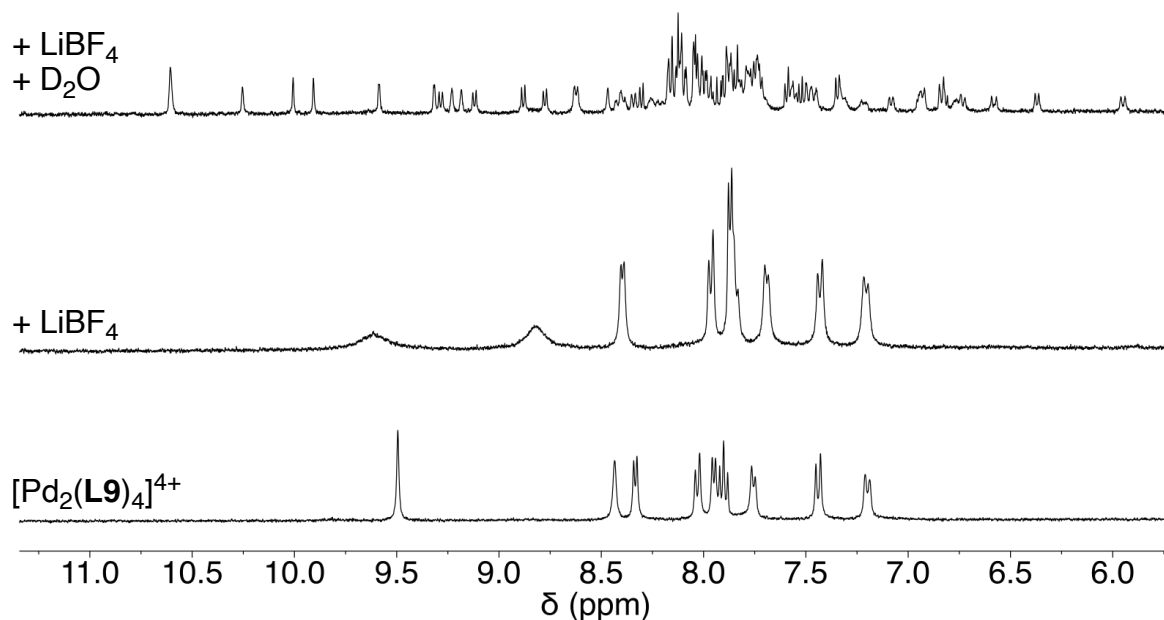


Figure 19. Aromatic region of the ^1H NMR spectra (400 MHz, CD_3CN) of the equilibrated mixture of $[\text{Pd}_2(\text{L9})_4]^{4+}$ with LiBF_4 and D_2O (top), LiBF_4 (center) and of $[\text{Pd}_2(\text{L9})_4]^{4+}$ alone (bottom). Both spectra shown at the center and bottom were recorded in absence of water.

The molecular structure of $[\text{Pd}_4(\text{L9})_8](\text{BF}_4)_8$ in the crystal is in line with the low symmetry detected by NMR spectroscopy. There are four pairs of symmetry-related ligands (**Figure 18c**). Since the ligands bridge chemically non-equivalent Pd^{2+} ions, the two isoquinoline donor groups are also no longer equivalent.^[134] The four chemically distinct ligands and the reduced internal ligand symmetry gives rise to the multiplicity of 8 for the ^1H NMR signals of the aromatic protons (**Figure 17**). The $[\text{Pd}_4(\text{L9})_8]^{8+}$ complex adopts a very compact structure, with numerous π -stacking interactions between the aromatic groups of the ligands (**Figure 18c**). Such tight intramolecular packing is reminiscent of what is found for biopolymers and for synthetic foldamers.^[135,136]

It is worth pointing out that the folding of $[\text{Pd}_4(\mathbf{L9})_8](\text{BF}_4)_8$ is essential for its low apparent symmetry. In terms of connectivity, the complex displays only three pairs of chemically distinct ligands (the ligands shown in **Figure 18c** in cyan and in grey could be interconverted by a conformational change). Attempts to unfold the assembly thermally were not successful. Even at 70 °C, the multiplicity of the NMR signals (CD_3CN) was not changed.

The prevalence of π -stacking interactions in $[\text{Pd}_4(\mathbf{L9})_8]^{8+}$ suggested that hydrophobic effects might stabilize the assembly. In order to examine if a higher solvent polarity could also lead to structures other than $[\text{Pd}_2(\mathbf{L9})_4]^{4+}$, we have carried out the reaction between $[\text{Pd}(\text{CH}_3\text{CN})_4](\text{BF}_4)_2$ and **L9** in a mixture of CD_3CN and D_2O (9:1).^d After equilibration for 5 days at 70 °C, the solution was analyzed by ^1H NMR spectroscopy and mass spectrometry.

The ^1H NMR spectrum showed several new peaks along with those of $[\text{Pd}_2(\mathbf{L9})_4](\text{BF}_4)_4$ (**Figure 20a**), and the MS spectrum showed dominant peaks corresponding to a $[\text{Pd}_2(\mathbf{L9})_5]^{4+}$ assembly (**Figure 20b**). Apparently, the increase in solvent polarity was not sufficient to promote formation of a larger tetranuclear assembly, but the results are further evidence that ligand **L9** facilitates formation of alternative structures.

^d Higher amounts of D_2O resulted in precipitation.

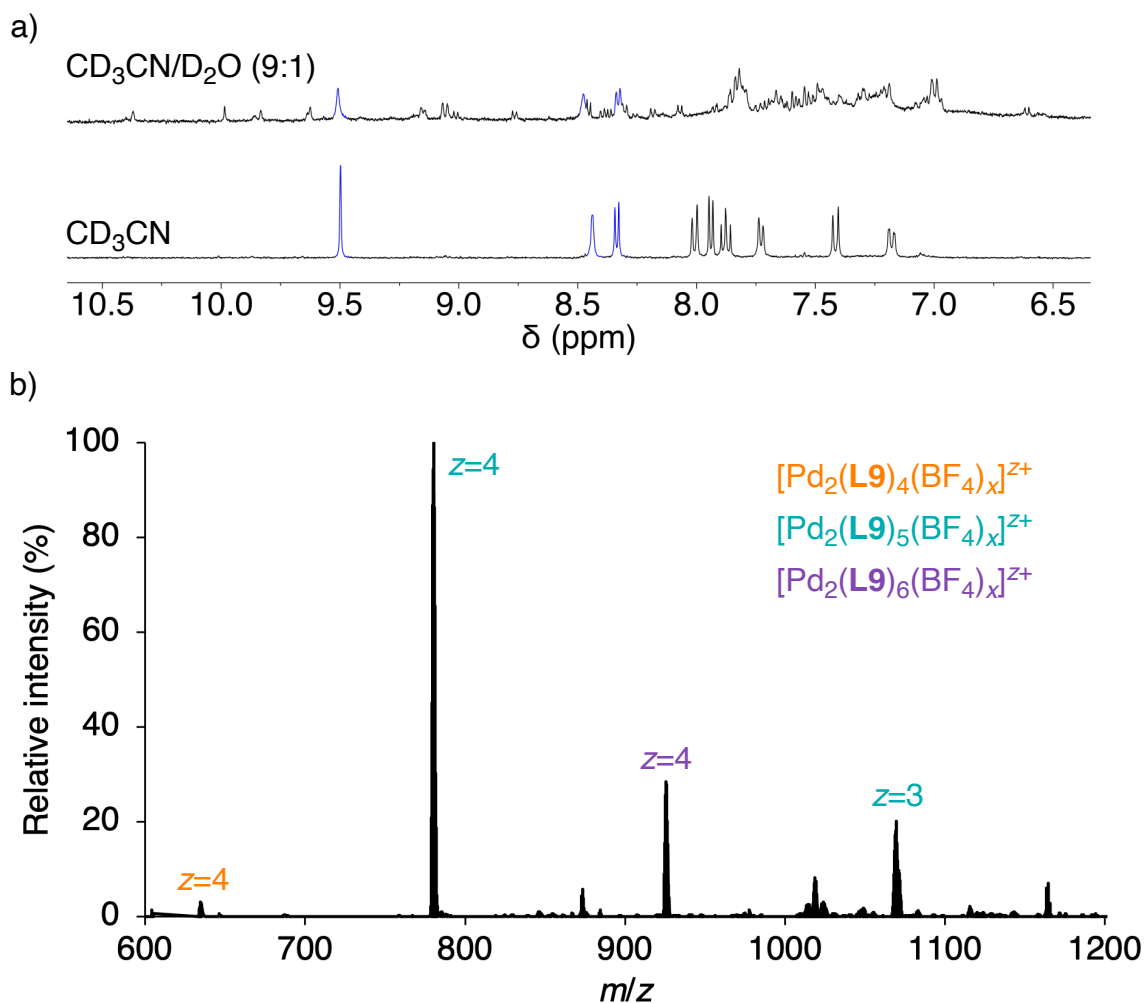


Figure 20. (a) ¹H NMR spectrum of a mixture of **L9** (2 eq.) and [Pd(CH₃CN)₄(BF₄)₂] (1 eq.) after equilibration in CD₃CN/D₂O (9:1) (top) and of [Pd₂(**L9**)₄](BF₄)₄ in CD₃CN for comparison (bottom). (b) HRMS of the equilibrated mixture in CD₃CN/D₂O (9:1). The main peaks can be attributed to a species with the formula [Pd₂(**L9**)₅](BF₄)_x²⁺.

Conclusion

Pd-based assemblies were investigated for their ability to bind lithium salts. Finding two hits within a small set of thirteen potential hosts indicates that anion-mediated binding of cations is likely a more common phenomenon for poly-cationic metal-ligand assemblies. Notably, our investigations revealed that a solvated LiBF_4 ion pair can induce the rearrangement of a $[\text{Pd}_2\text{L}_4]^{4+}$ complex into a $[\text{Pd}_4\text{L}_8]^{8+}$ assembly. The template effect is highly specific as it requires the presence of Li^+ . Other alkali metal ions were not able to promote a change in structure.

A unique feature of the $[\text{Pd}_4\text{L}_8]^{8+}$ complex is its low symmetry with four chemically distinct ligand environments. The possibility to adopt a folded, highly compact structure is a crucial factor, and ligand **L9** is well suited in that regard. It displays moderate conformational flexibility, variable coordinate vectors of the N-donor groups, and large aromatic groups, which allow for π -stacking interactions. In addition, the carbonyl groups can form additional interactions with a guest.

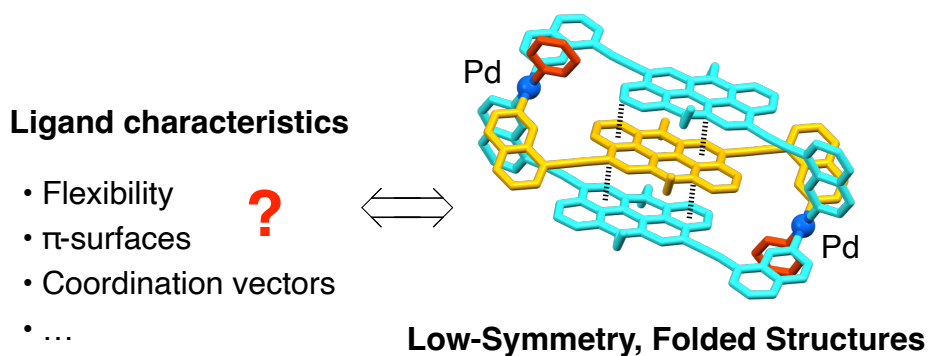
It is worth drawing a comparison with folded organic macrocycles, which were recently reported by the groups of Huc and Otto.^[137] Despite being obtained from only one type of building block, the macrocycles showed up to 12 chemically distinct subcomponents. The authors argue that folding into low-symmetry structures requires building blocks with an intermediate flexibility, and with the possibility to engage in diverse non-covalent interactions. These criteria are fulfilled for **L9**.

Interestingly, while the $[\text{Pd}_4\text{L}_8]^{8+}$ species could not be obtained relying solely on the hydrophobic effect, the results suggest that **L9** could also participate in the formation of additional structures ($[\text{Pd}_2\text{L}_5]^{4+}$ and $[\text{Pd}_2\text{L}_6]^{4+}$). This point will be discussed in Chapter 5 of this thesis. Based on the results presented in this chapter, we attempted to define more precise guidelines for the construction of homoleptic metal-ligand assemblies with folded, low-symmetry structures. A ligand-design approach will be presented in the following chapter.

4. Intricate palladium complexes: a ligand design approach

The results presented in this chapter are based on the work of **Geoffrey Gros Lambert** as part of an internship within our group.

S. Sudan and K. Severin designed the experiments, S. Sudan and G. Gros Lambert performed the experiments and analyzed the data, and F. Fadaei-Tirani collected and processed the X-ray data. The data presented in this chapter have not yet been published.



The intricate structure of the $[\text{Pd}_4(\text{L9})_8]^{8+}$ assembly (shown in **Figure 21**) described in the previous chapter, incited us to rationalize what ligand characteristics were required to obtain such complexes. Ligand **L9** showed to be an ideal candidate for its moderate flexibility, provided by the alkyne spacers, extended aromatic systems that allow for intramolecular π -stacking interactions, and the different possible orientations of the coordinating N-donor groups. These features are already responsible for the twisted helical conformation of the parent Pd_2L_4 assembly.^[28] In addition, the presence of the central ketone moiety enabled the Li^+ coordination and the subsequent rearrangement to the Pd_4L_8 complex. We envisioned the possibility to synthesize a variety of new ligands bearing similar characteristics; aiming to obtain additional examples of folded Pd-ligand complexes. Those initial trials will serve as a basis to define more accurate ligand-design principles to obtain these assemblies in a controlled fashion.

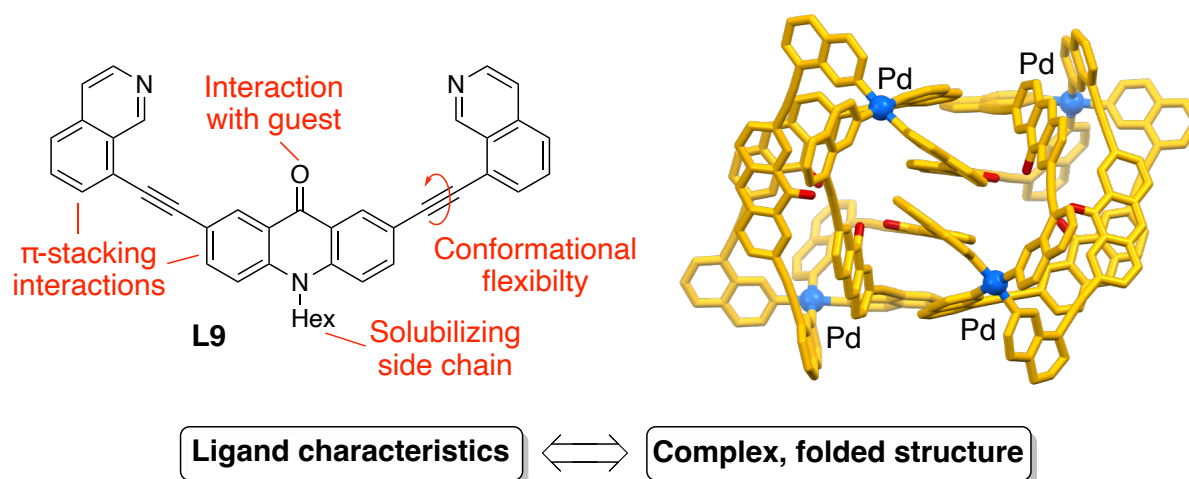


Figure 21. Ligand **L9** and its corresponding complex with Pd^{2+} in the presence of LiBF_4 .

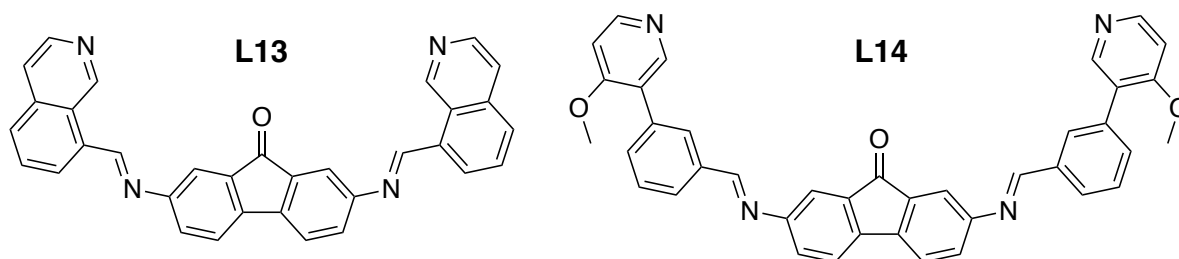
Results and discussion

The ligands showed in **Figure 22** were designed to possess the abovementioned characteristics in addition to their synthetic accessibility. **L13** and **L14** are both based on a fluorenone core linked to either isoquinoline or phenylpyridine arms via imine bonds. **L15** was designed based on dibenzothiophene to expand the scope of potential guests targets to thiophilic metals. **L16** to **L19** are built from an anthanthrene core

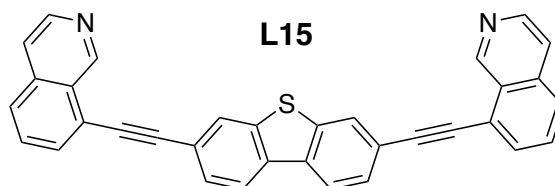
connected to isoquinoline or phenylpyridine arms providing a variety of possible orientations of the coordination vectors.

Compared to the others, these four ligands possess a much more extend aromatic surface; provided that a stable complex could form when combined with Pd²⁺, the intramolecular π -stacking interactions should promote the formation of the desired folded structures.

Fluorenone core:



Dibenzothiophene core:



Anthanthrene core:

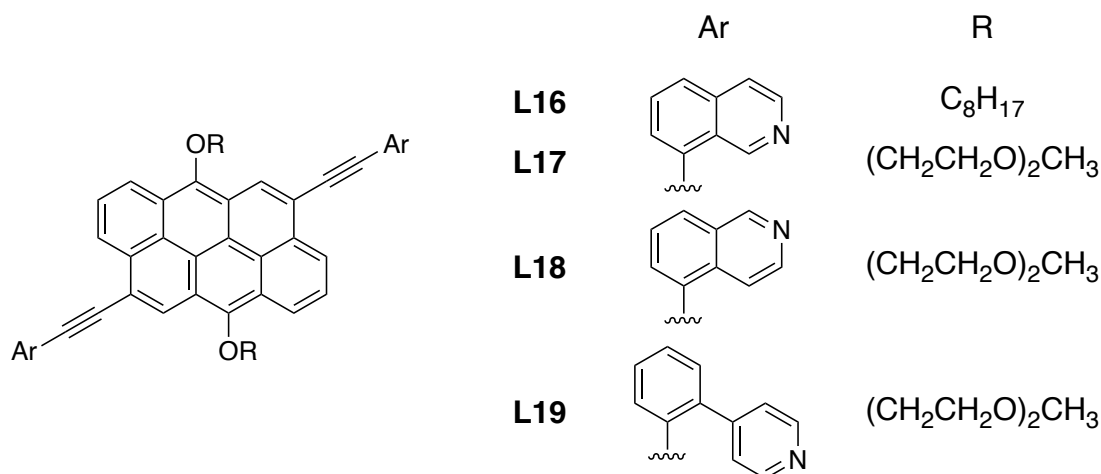


Figure 22. Structures of ligands **L13** to **L19**.

Apart from **L15**, due to the poor solubility of the mono-coupled intermediate, all the designed ligands were successfully synthesized. Next, we attempted to prepare the corresponding Pd_nL_{2n} complexes by equilibrating a 2:1 mixture of the ligand and Pd^{2+} at 70 °C for 12 h in CD_3CN or DMSO. In the case of the fluorenone based ligands, **L13** and **L14**, no assembly could be detected. Both **L13** and **L14** showed to be significantly susceptible to imine bond hydrolysis and repeating the synthesis in absence of water was not sufficient to obtain the desired Pd-ligand assemblies.

Among the four anthanthrene ligands, **L16** to **L19**, only those with the 8-ethynylisoquinoline arms gave defined species when combined with Pd^{2+} . Initial attempts to prepare the complex by equilibrating a mixture of **L16** and Pd^{2+} (2:1) in CD_3CN resulted in the formation of a precipitate. HRMS analysis of the supernatant showed the presence of a species with formula $[\text{Pd}_2(\text{L16})_3\text{F}]^{3+}$ as the main product. The combination of **L17** and Pd^{2+} in a 3:2 ratio resulted in the formation of single Pd_2L_3 assembly as supported by HRMS (**Figure 23c**). The corresponding ^1H NMR spectrum (**Figure 23b**) showed a three-fold splitting of the signal attributed to the H_a of **L17**, supporting the formation of a reduced symmetry species.

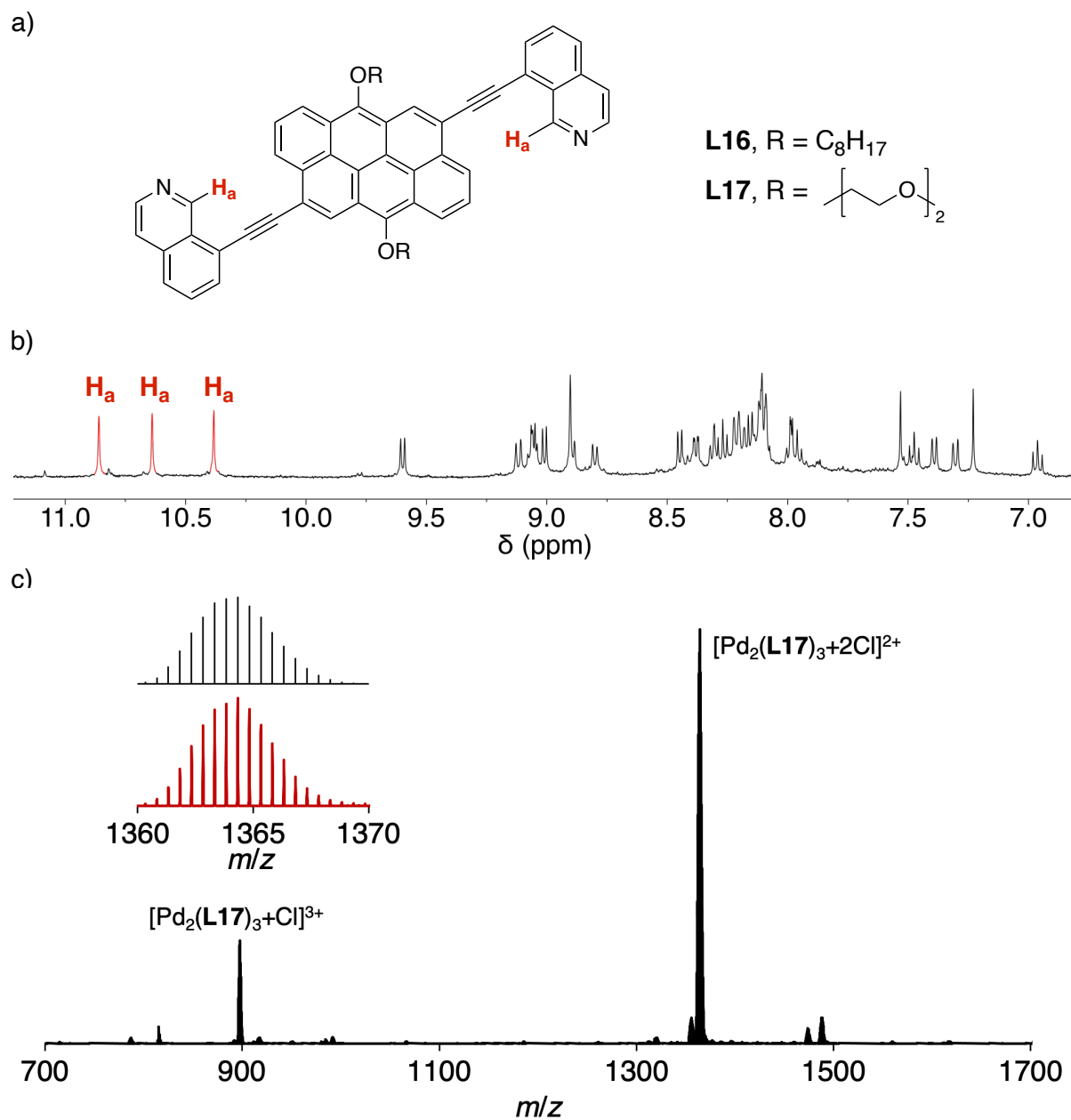


Figure 23. (a) Structures of ligands **L16** and **L17**. (b) Aromatic region of the ¹H NMR (400 MHz, CD₃CN) spectrum of a mixture of [Pd(CH₃CN)₄](PF₆)₂ (2 eq.) and **L17** (3 eq.) after tempering at 70 °C for 12 h. (c) HRMS of the equilibrated mixture. The inset shows the comparison between the 1360 – 1370 *m/z* region (bottom, red) and the calculated mass spectrum for [Pd₂(**L17**)₃Cl₂]²⁺ (top, black)

Suitable crystals for X-ray diffraction analysis were obtained by slow diffusion of diethyl ether into a mixture of $[\text{Pd}_2(\text{L16})_3]^{4+}$ (1 eq.) and pyridine (2 eq.)^e in CD_3CN .

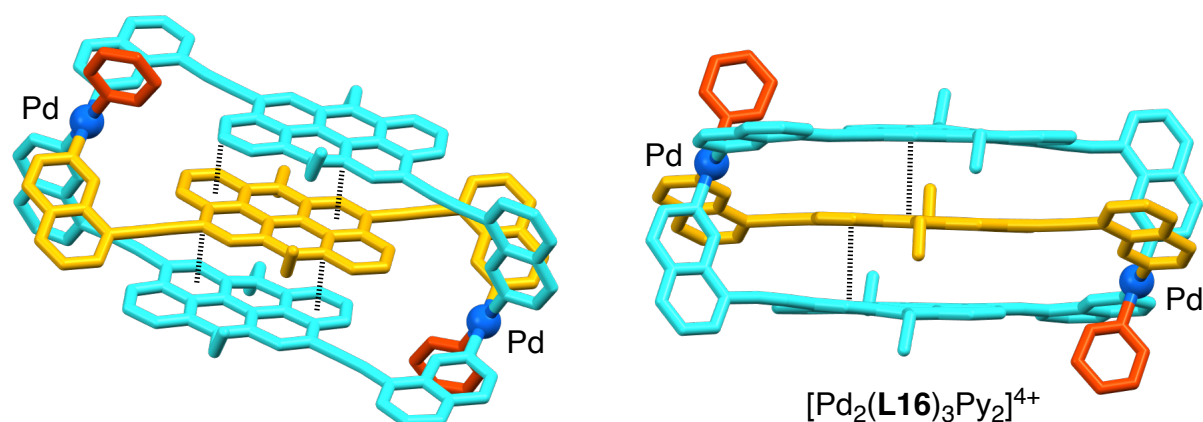


Figure 24. Graphic representation of the crystal structure of $[\text{Pd}_2(\text{L16})_3\text{Py}_2]^{4+}$, viewed from two different orientations. Intramolecular π -stacking interactions are highlighted. Hydrogen atoms, BF_4^- anions, and the side chains are not shown for clarity.

The molecular structure of $[\text{Pd}_2(\text{L16})_3\text{Py}_2]^{4+}$ aligns with the signals' multiplicity observed in the ^1H NMR spectrum; the two outer ligands (shown in light blue in **Figure 24**) possess the same chemical environment, with the two isoquinoline arms connected in *trans* and *cis* relatively to the pyridine ligand. While this gives rise to a two-fold splitting of the ^1H NMR signals, the third one stems from the central ligand (shown in yellow in **Figure 24**) sitting a symmetric environment.

The observed arrangement of the ligands in the solid-state structure explains the incapacity to obtain the initial Pd_nL_{2n} target. In addition to entropic considerations, the multiple inter-ligand π -stacking interactions are an important driving force for the formation of a compact and folded dinuclear structure. The resulting 180° angle between the two empty coordination sites does not allow a fourth **L16** coordination.

^e Pyridine was used as an auxiliary ligand to complete the Pd coordination sphere and facilitate the crystallization.

Conclusion

A set of ligands was designed with the aim of obtaining other examples of complex and folded structures. This goal was partially achieved for two ligands: the corresponding $[\text{Pd}_2\text{L}_3]^{4+}$ complexes show a highly compact and folded structure. However, the stacking of the first three sterically demanding anthanthrene cores prevented the accommodation of a fourth ligand.

Further advances in the direction will require fine-tuning of the ligand-design principles: too important π -stacking interactions appear to be detrimental to the desired adaptability of the related Pd complexes. While the fluorenone ligands, **L13** and **L14**, looked promising on paper, the incapacity to form a stable assembly with Pd^{2+} indicated an insufficient flexibility. Reduction of the imine bonds would be a potential way to remediate the issue. In addition, it would help to overcome the hydrolysis susceptibility and provide the ligands with secondary amines that could participate in inter and or intramolecular hydrogen bonding.

The attempted synthesis of **L15** highlighted the importance of solubilizing groups: the presence of extended aromatic surfaces being highly detrimental to the solubility in polar solvents such as CD_3CN . It would be interesting to investigate the solvent effect in more details. Using less polar solvents could prevent the formation of strong intramolecular π -stacking interaction and thus promote the formation of different assemblies.

The dibenzothiophene scaffold remains of interest, as it could also be easily oxidized to sulfoxide or sulfone, providing different Lewis basic sites.

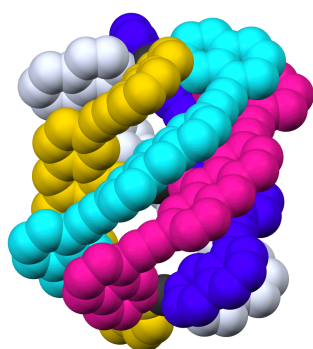
5. A five-stranded heterometallic helicate

This chapter is based on published work:

“A five-stranded heterometallic helicate”

S. Sudan, F. Fadaei-Tirani, and K. Severin, *Chem. Commun.*, **2023**, 59, 8258-8261.

S. Sudan and K. Severin designed the experiments, S. Sudan performed the experiments and analyzed the data, F. Fadaei-Tirani collected and processed the X-ray data, and S. Sudan and K. Severin co-wrote the manuscript. All authors discussed the results and commented on the manuscript.



- five stranded helicate
- 2x Pd²⁺, 1x La³⁺
- low symmetry
- dynamic

Helicates are oligonuclear coordination compounds with a helical arrangement of the bridging ligands.^[138–146] The structural diversity of this compound class is large. Variable parameters include the type of metal ions, the number of metal ions, and the arrangement of the metal ions (linear vs. cyclic helicates), as well as the structure, geometry, and relative orientation of the ligands.^[138–146] Furthermore, heteroleptic^[147–153] and heterometallic helicates^[154–158] have been reported in addition to the more common homoleptic and homometallic structures.

A key characteristic of linear helicates is the number of ligand strands, which are wrapped around the string of metal ions. Double-stranded helicates based on flexible polypyridyl ligands and two or three Cu⁺ ions were described by Lehn and co-workers in 1987 (a graphic depiction of the trinuclear complex is given in **Figure 25**, complex **A**).^[159] This publication is of special importance because the term ‘helicate’ was introduced to the scientific literature.

Early reports about triple-stranded, M₂L₃-type complexes were published by Harris and McKenzie (M = Cu),^[160] and by Scarrow, White and Raymond (M = Fe, **Figure 25**, complex **B**).^[161] In 1997, Peng and co-workers reported four-stranded, M₅L₄-type structures (M = Ni or Co).^[162] These complexes can be classified as ‘unsaturated helicates’ due to the presence of additional ligands completing the coordination sphere of the terminal metal ions.

In the following year, a fully saturated four-stranded helicate was described by McMorran and Steel (**Figure 25**, complex **C**).^[10] Albrecht *et al* reported a hexa-stranded helicate in 2001 (**Figure 25**, complex **E**).^[163] A structural analysis revealed that the ligands are arranged in a head-to-tail fashion around the Zn centers. Two additional hexa-stranded helicates have recently been described by Nitschke and co-workers.^[164]

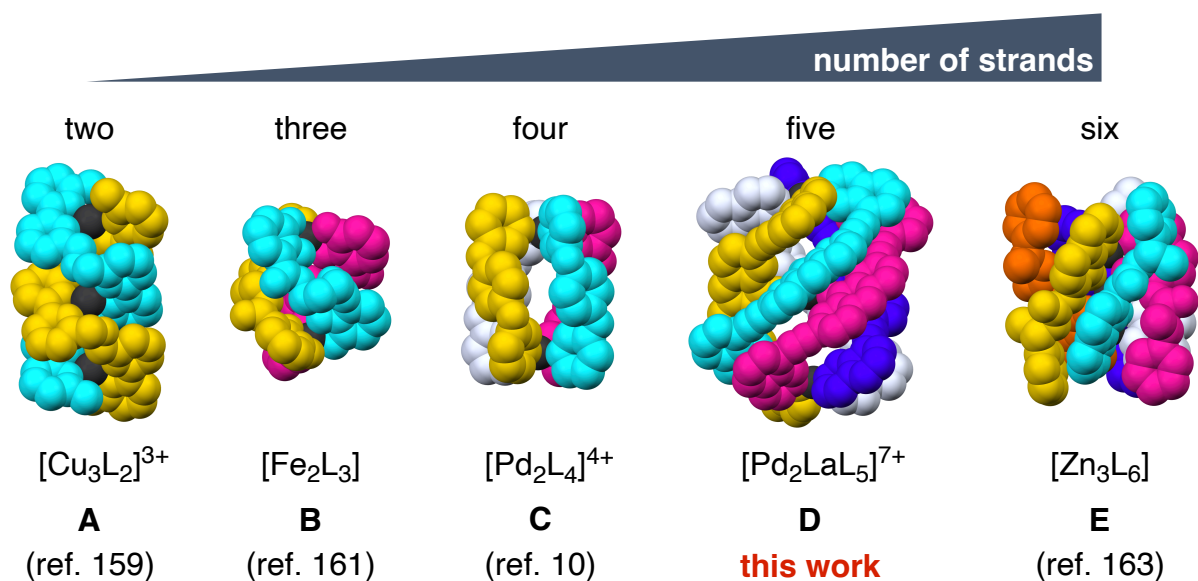


Figure 25. Representative structures of n -stranded helicates ($n = 2-6$).

This chapter describes the synthesis and the structure of a Pd-based helicate with five ligand strands (**Figure 25**, complex **D**). The assembly is stabilized by the presence of a central La^{3+} ion. Dynamic interconversion between the penta-stranded helicate and a four-stranded helicate can be achieved by adjustment of the ligand-to- Pd^{2+} ratio.

Results and discussion

Clever and co-workers have introduced ligand **L9** (**Figure 26**) as a building block in metallosupramolecular chemistry.^[28] Combined with Pd^{2+} ions, it forms a tetra-stranded $[\text{Pd}_2(\text{L9})_4]^{4+}$ helicate.^[10,17,28,52,72,110,165-169] When a solution of the helicate in DMSO was analyzed by ESI mass spectrometry, the authors observed additional peaks for an assembly of the formula $[\text{Pd}_2(\text{L9})_5]^{4+}$.^[28] However, this species could not be observed by NMR spectroscopy. While studying the host properties of $[\text{Pd}_2(\text{L9})_4]^{4+}$ in acetonitrile (see Chapter 3),^[170] we also noted MS peaks that can be attributed to a species of the formula $[\text{Pd}_2(\text{L9})_5]^{4+}$. Intrigued by these observations, we decided to pursue a targeted synthesis of this penta-stranded complex.

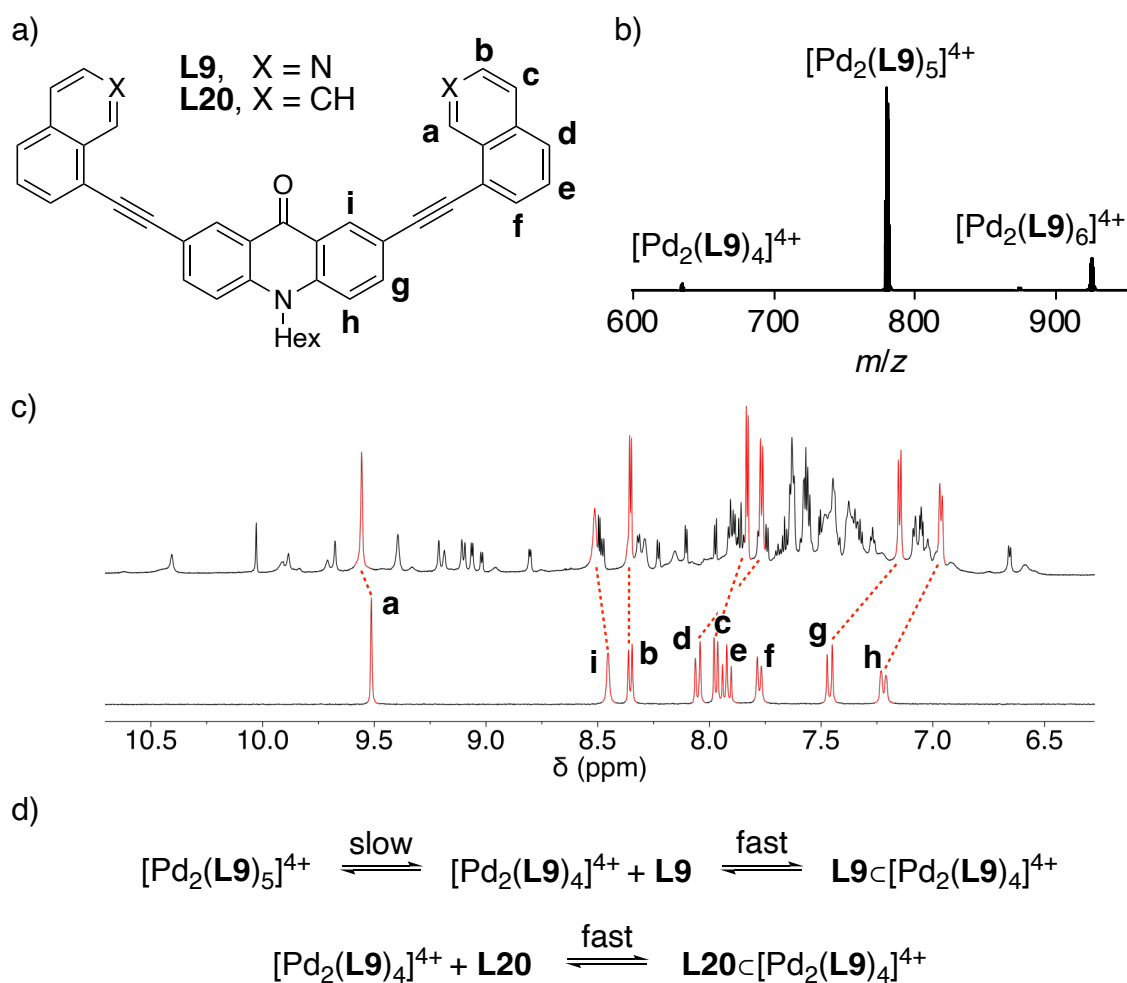


Figure 26. (a) Structures of the ligands **L9** and **L20**. (b) HRMS spectrum (600–950 m/z region) of a mixture of $[\text{Pd}(\text{CH}_3\text{CN})_4](\text{BF}_4)_2$ and **L9** (ratio: 2 : 5). (c) ^1H NMR spectrum (800 MHz, CD_3CN , 298 K) of a mixture of $[\text{Pd}(\text{CH}_3\text{CN})_4](\text{BF}_4)_2$ and **L9** (ratio: 2 : 5) (top) and of $[\text{Pd}_2(\text{L9})_4]^{4+}$ (bottom). (d) Proposed equilibria between $[\text{Pd}_2(\text{L9})_4]^{4+}$ and **L9** (top) or **L20** (bottom).

Initially, we attempted to prepare $[\text{Pd}_2(\text{L9})_5]^{4+}$ by equilibrating a mixture of **L9** and $[\text{Pd}(\text{CH}_3\text{CN})_4](\text{BF}_4)_2$ in a 5 : 2 ratio at 70 °C in CD_3CN . The ^1H NMR spectrum of the solution showed the presence of multiple species (**Figure 26c**, top). Some signals resembled those observed for $[\text{Pd}_2(\text{L9})_4]^{4+}$, but a direct comparison of the spectra revealed marked variations in the chemical shifts (**Figure 26c**, see the signals highlighted in red). The other signals in the ^1H NMR spectrum pointed to the presence of a complex of low symmetry.

The main signals in the ESI MS spectrum could be attributed to a species with the formula $[\text{Pd}_2(\text{L9})_5]^{4+}$ (**Figure 26b**). In addition, we were able to observe small signals corresponding to complexes of the formula $[\text{Pd}_2(\text{L9})_4]^{4+}$ and $[\text{Pd}_2(\text{L9})_6]^{4+}$. Unfortunately, attempts to synthesize the hexa-stranded complex by variation of the stoichiometry or by addition of templates were not successful.

To rationalize the experimental data, we hypothesized that there are two distinct assemblies with the formula $[\text{Pd}_2(\text{L9})_5]^{4+}$: a non-covalent adduct $\text{L9} \cdot [\text{Pd}_2(\text{L9})_4]^{4+}$ between ligand **L9** and the tetra-stranded helicate $[\text{Pd}_2(\text{L9})_4]^{4+}$, and a low-symmetry complex $[\text{Pd}_2(\text{L9})_5]^{4+}$ with Pd–N bonds to all five ligands (**Figure 26d**).

In order to support our hypothesis, we synthesized **L20** as a non-coordinating analogue of **L9** (**Figure 26a**). **L20** features terminal naphthyl groups instead of isoquinoline donors. We expected that **L20** would also be able to form a non-covalent adduct with the tetra-stranded helicate $[\text{Pd}_2(\text{L9})_4]^{4+}$. Unfortunately, **L20** was found to display low solubility in acetonitrile. In anticipation that an interaction with the helicate would solubilize **L20**, we equilibrated a mixture of $[\text{Pd}_2(\text{L9})_4]^{4+}$ (1 eq.) and **L20** (4 eq.) in CD_3CN at 70 °C for 12 h. After filtration, the solution was analyzed by ^1H NMR spectroscopy and ESI mass spectrometry. The ^1H NMR spectrum showed signals for ligand **L20** and for the helicate $[\text{Pd}_2(\text{L9})_4]^{4+}$ in a ratio of 1 : 1 (1 : 4 in terms of signal intensity), corroborating the presence of a 1 : 1 adduct (**Figure 27**).

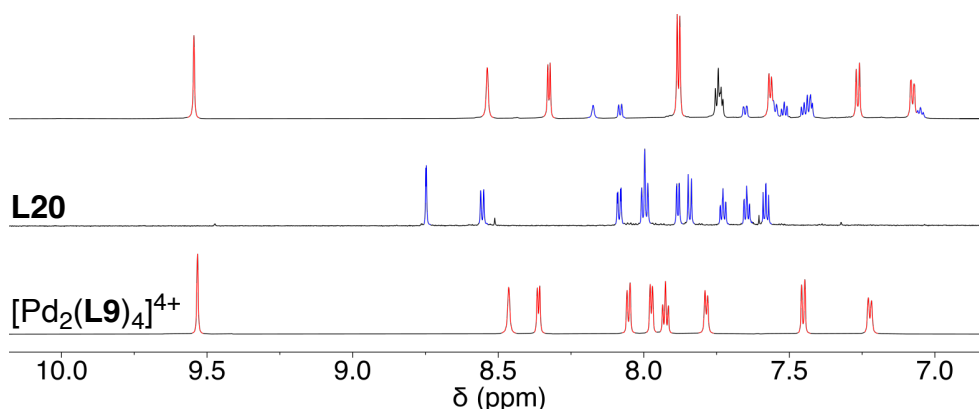


Figure 27. Comparison of the ^1H NMR spectra (800 MHz, CD_3CN , 323 K) of an equilibrated mixture of $[\text{Pd}_2(\text{L9})_4]^{4+}$ and **L20** (top), **L20** (center) and $[\text{Pd}_2(\text{L9})_4]^{4+}$ (bottom).

The signals of the helicate in $\mathbf{L20} \subset [\text{Pd}_2(\mathbf{L9})_4]^{4+}$ were shifted compared to those of the empty host $[\text{Pd}_2(\mathbf{L9})_4]^{4+}$. The magnitude and the direction of the shifts matched what we had observed for the interaction between $\mathbf{L9}$ and $[\text{Pd}_2(\mathbf{L9})_4]^{4+}$ (**Figure 26c** and **Figure 27**). In addition, important shifts of the $\mathbf{L20}$ signals were observed in presence of $[\text{Pd}_2(\mathbf{L9})_4]^{4+}$ by comparison to $\mathbf{L20}$ alone. The adduct $\mathbf{L20} \subset [\text{Pd}_2(\mathbf{L9})_4]^{4+}$ could also be detected by mass spectrometry (**Figure ES23**). Taken together, the results provide evidence that $\mathbf{L9}$ and $\mathbf{L20}$ can both form a host-guest complex with the helicate $[\text{Pd}_2(\mathbf{L9})_4]^{4+}$. A potential driving force for adduct formation are π -stacking interactions between the ligands.

Since we were not able to obtain a defined $[\text{Pd}_2(\mathbf{L9})_5]^{4+}$ complex from $\mathbf{L9}$ and $[\text{Pd}(\text{CH}_3\text{CN})_4](\text{BF}_4)_2$ directly, we investigated the possibility to stabilize the penta-stranded complex with a template. The carbonyl groups of $[\text{Pd}_2(\mathbf{L9})_4]^{4+}$ point to the center of the helicate,^[28] and they are able to interact with metal cations such as Li^+ and Na^+ .^[170] For the stabilization of an assembly with five ligands, we needed an oxophilic metal ion that would prefer high coordination numbers. La^{3+} seemed well suited in that regard. La^{3+} is also diamagnetic, facilitating NMR spectroscopy investigations.

A mixture of $[\text{Pd}(\text{CH}_3\text{CN})_4](\text{BF}_4)_2$, $\text{La}(\text{NO}_3)_3$, and $\mathbf{L9}$ in a ratio of 2 : 1 : 5 was equilibrated for 3 h at 70 °C. The ^1H NMR spectrum of the resulting solution showed the formation of a defined species with low apparent symmetry (**Figure 28a**).^[42,171,172] A five-fold splitting of the signals of the aromatic CH protons was evidenced by ^{13}C and ^1H - ^{13}C HSQC NMR analyses (**Figure ES22**). Mass spectrometry analysis showed the formation of the desired $[\text{Pd}_2\text{La}(\mathbf{L9})_5]^{7+}$ complex.

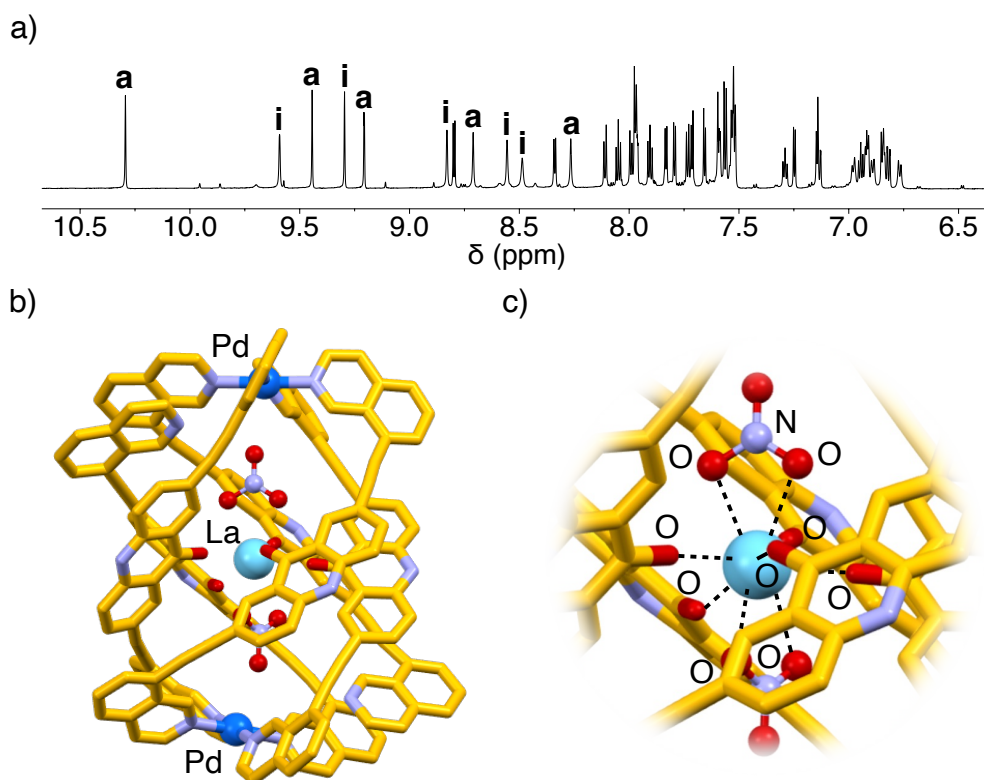
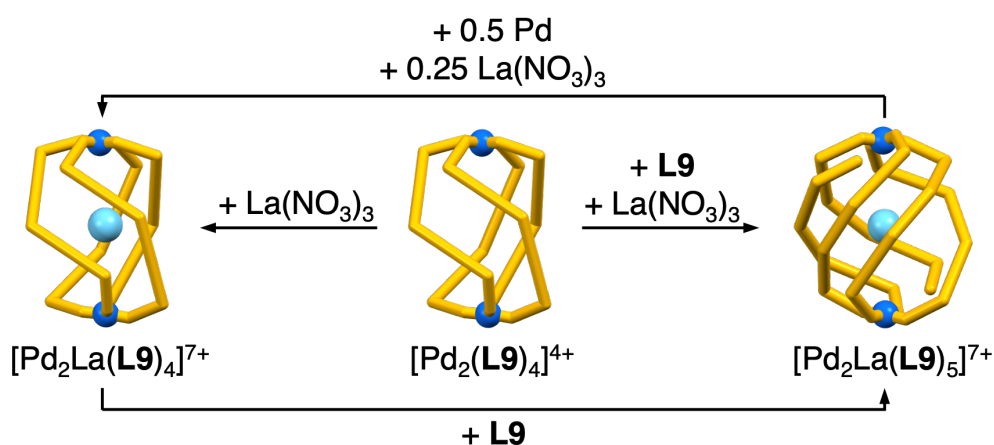


Figure 28. (a) Part of the ^1H NMR spectrum (800 MHz, CD_3CN , 323 K) of a mixture of $[\text{Pd}(\text{CH}_3\text{CN})_4](\text{BF}_4)_2$, $\text{La}(\text{NO}_3)_3$ and **L9** in a ratio of 2 : 1 : 5 . (b) Molecular structure of $[\text{Pd}_2\text{La}(\text{L9})_5(\text{NO}_3)_2]^{5+}$ as determined by X-ray crystallography. Hydrogen atoms and hexyl side chains are not shown for clarity. Color coding: Pd: blue, La: light blue, C: yellow, N: purple, O: red. (c) Close-up view on the coordination environment of La^{3+} .

Suitable single crystals for X-ray diffraction measurements were obtained by slow vapor diffusion of diethyl ether into a solution of the complex in CD_3CN . The crystallographic analysis confirmed the formation of a five-stranded helicate (**Figure 28b**). The solid-state structure provides an explanation for the low apparent symmetry, which was observed by NMR spectroscopy. Three of the five ligands bridge the two Pd^{2+} ions by coordination *via* both isoquinoline groups. The two remaining ligands show only one $\text{Pd}-\text{N}$ bond and one non-bound isoquinoline donor. The central La^{3+} ion is bound to the carbonyl O-atoms of all five ligands with $\text{La}-\text{O}$ distances ranging from 2.403(7) to 2.481(7) Å (**Figure 28c**). Two nitrate anions are found in close proximity to La^{3+} with $\text{La}-\text{ON}$ distances between 2.574(7) to 2.706(7) Å.^[66,101–103,170] The third O-atom of the nitrate points towards the Pd^{2+} ions, but a direct bond can be excluded ($\text{Pd}\cdots\text{O} = 2.88$ Å; $\text{Pd}'\cdots\text{O}' = 2.97$ Å).

In control experiments, we realized that La^{3+} is also a suited guest for the four-stranded helicate $[\text{Pd}_2(\text{L9})_4]^{4+}$ (**Scheme 4**). When $\text{La}(\text{NO}_3)_3$ (1 eq.) was added to a solution of $[\text{Pd}_2(\text{L9})_4](\text{BF}_4)_4$ in CD_3CN , a new set of NMR signals was observed (**Figure ES24**). The ESI MS spectrum of the mixture showed a main peak, which can be attributed to a species of the formula $[\text{Pd}_2\text{La}(\text{L9})_4(\text{NO}_3)_2]^{5+}$. The addition of substoichiometric amounts of $\text{La}(\text{NO}_3)_3$ gave rise to two sets of NMR signals, indicating that the complexation of La^{3+} is slow on the NMR time scale.



Scheme 4. Interconversion between the four- and the five-stranded helicate.

The four-stranded helicate with bound La^{3+} could be converted cleanly into the five-stranded helicate by the addition of one equivalent of ligand **L9** (**Scheme 4**). The inverse transformation could be achieved by the addition of $[\text{Pd}(\text{CH}_3\text{CN})_4](\text{BF}_4)_2$ (0.5 eq.) and $\text{La}(\text{NO}_3)_3$ (0.25 eq.) to a solution of the penta-stranded, La^{3+} -bound helicate (**Figure ES25**). The results demonstrate that the system comprised of $[\text{Pd}(\text{CH}_3\text{CN})_4](\text{BF}_4)_2$, $\text{La}(\text{NO}_3)_3$, and **L9** has two distinct stable states: the tetra- and the penta-stranded helicate. A reversible interconversion between the two states is possible by changing the ratio between **L9** and Pd^{2+} .^[173]

Conclusion

We have reported the synthesis and the structure of a five-stranded helicate. The assembly is formed by coordination of ligand **L9** to two Pd²⁺ ions and one La³⁺ ion. The latter was found to be of key importance for stabilizing the penta-stranded structure. The helicate is unique, not only because of the presence of five ligand strands, but also because of its low symmetry. Another noteworthy feature is the possibility to switch between a five- and a four-stranded structure by simply changing the stoichiometry of the building blocks. Preliminary studies on the role of the anion in stabilizing the [Pd₂La(**L9**)₄]⁷⁺ and [Pd₂La(**L9**)₅]⁷⁺ inclusion complexes indicated an important contribution of the coencapsulated nitrate molecules. Further host-guest investigations, with different ion pairs, could potentially reveal additional stable inclusion complexes based on **L9**.

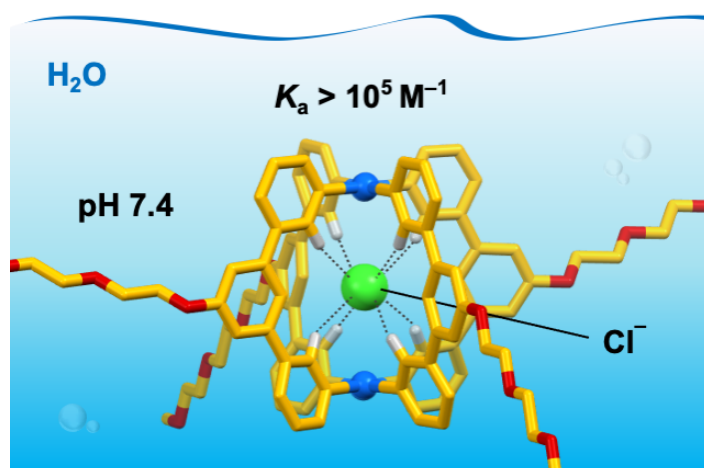
6. Synthetic receptors with micromolar affinity for chloride in water

This chapter is based on published work:

“Synthetic Receptors with Micromolar Affinity for Chloride in Water”

S. Sudan, D. W. Chen, C. Berton, F. Fadaei-Tirani, and K. Severin,
Angew. Chem. Int. Ed., **2023**, 62, e202218072.

S. Sudan and K. Severin designed the experiments, S. Sudan, D. W. Chen and C. Berton performed the experiments and analyzed the data, F. Fadaei-Tirani collected and processed the X-ray data, and S. Sudan and K. Severin co-wrote the manuscript. All authors discussed the results and commented on the manuscript.



The development of synthetic receptors for the complexation of anions in neutral aqueous solutions represents a formidable challenge. While substantial progress has been made over the years, few synthetic receptors are able to bind anions in water with high affinity and selectivity.^[174–178]

The recognition of chloride is of particular relevance because this anion is ubiquitous in biology and in the environment. Exceptionally good receptors for the binding of chloride in organic solvents have been reported,^[179–186] but as soon as water is added to the mixture, the association constants tend to drop significantly.^[187–193] Only a few receptors are able to bind chloride in pure water at neutral pH.^[174–178,194–209]

The bambusuril^[194] macrocycle **A (Figure 29)**, developed by Sindelar and co-workers, is able to bind chloride with an association constant of $K_a(\text{Cl}^-)=1.2\times 10^3 \text{ M}^{-1}$, as determined by isothermal titration calorimetry (ITC).^[195] However, receptor **A** and other bambusurils are promiscuous anion receptors, and monoanions such as NO_3^- , BF_4^- , ReO_4^- , PF_6^- , Br^- , and I^- are bound stronger than Cl^- .^[194–196] The structurally related biotin[6]juril **B** was synthesized by the group of Pittelkow.^[210] It is able to bind chloride with an association constant of $K_a(\text{Cl}^-)=63 \text{ M}^{-1}$ (D_2O , NMR), but its selectivity for chloride is also poor.^[197]

The macrobicyclic receptor **C** was developed by Li and co-workers.^[198] Its rigidity imparts good selectivity. However, the affinity of **C** for chloride is lower than what was reported for the macrocycles **A** and **B**. Kubik and co-workers have investigated extensively the anion binding properties of cyclopeptide-based receptors. The bridged dicyclopeptide **D** was found to bind chloride with an association constant of $K_a(\text{Cl}^-)=1.4\times 10^2 \text{ M}^{-1}$ (ITC).^[199] Stronger binding was observed for Br^- , I^- , and SO_4^{2-} .

The anion-binding properties of receptors relying on halogen bonding have been studied by Beer and co-workers.^[200] Rotaxane **E** was found to bind chloride in water with an association constant of $K_a(\text{Cl}^-)=55 \text{ M}^{-1}$ (D_2O , NMR).^[201] Interestingly, the replacement of the halogen-bonding C–I group with a hydrogen-bonding C–H group diminished the affinity of the receptor.^[201,202]

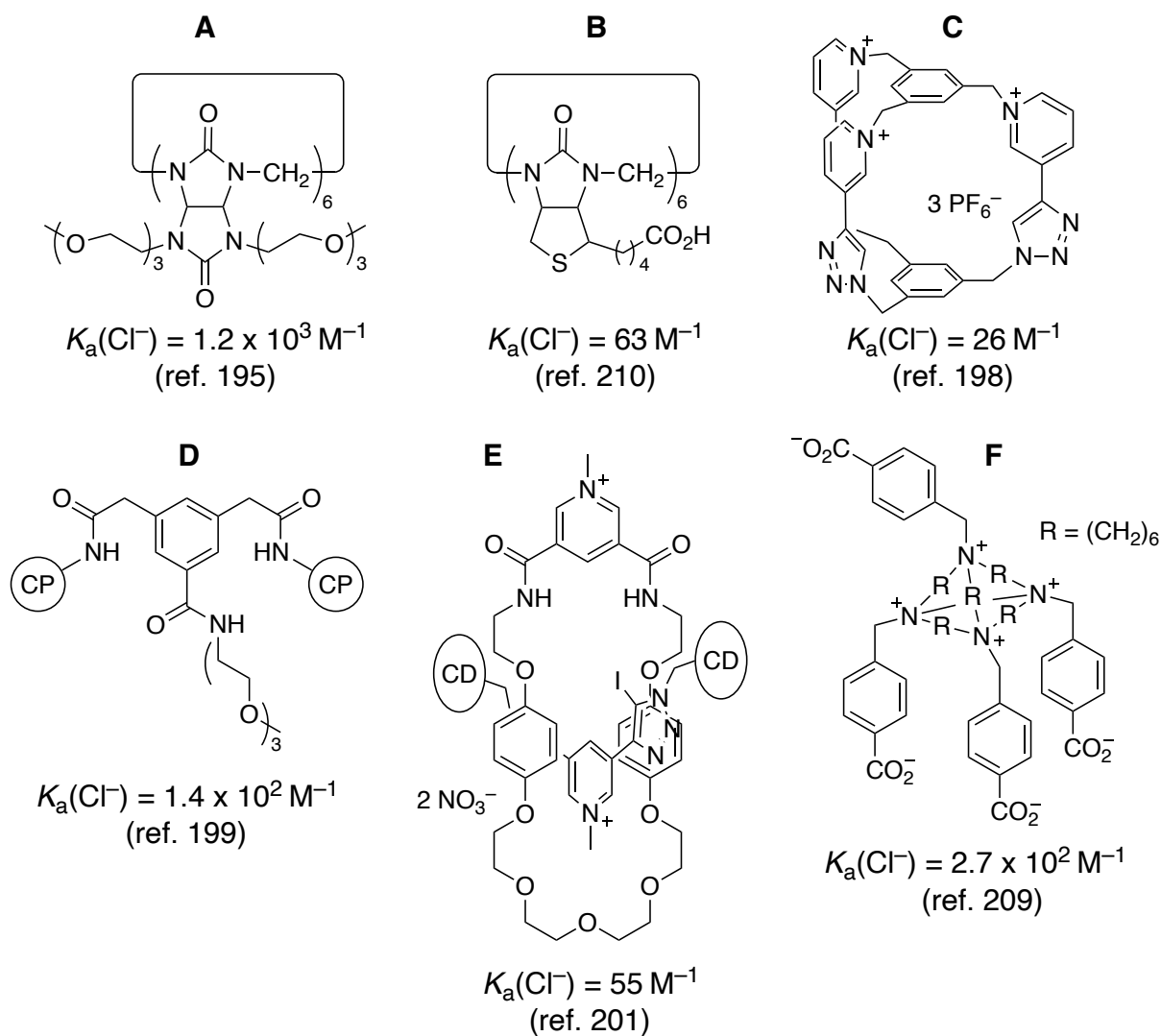


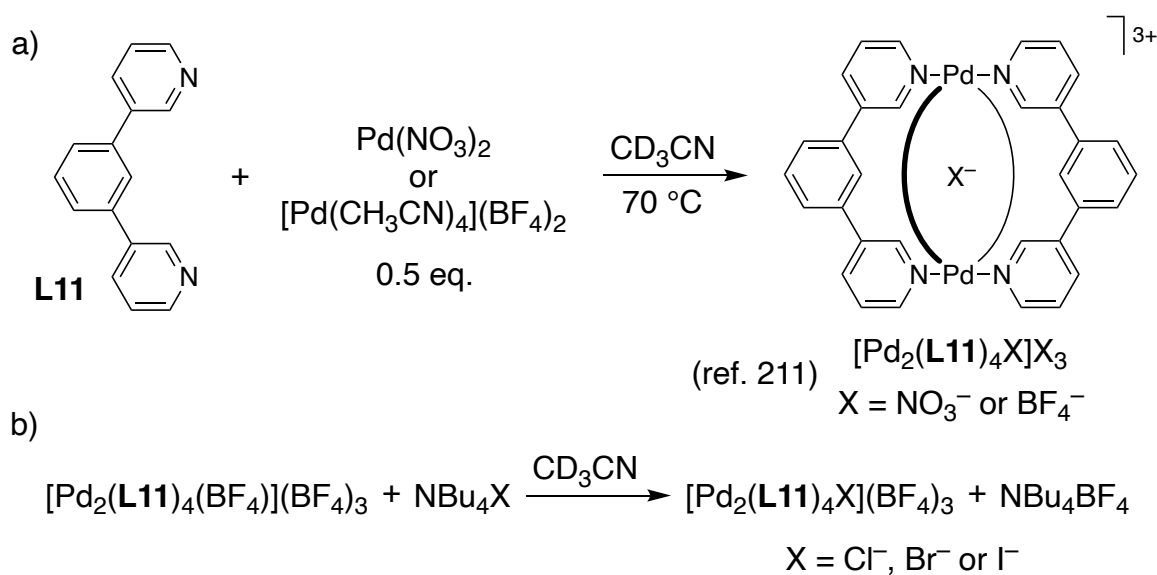
Figure 29. Macrocyclic receptors for chloride binding in water and the corresponding binding constants (CP = cyclopeptide; CD = β -cyclodextrin).

Macrocyclic polyammonium compounds were among the first halide receptors described in the literature,^[203,204] and they have been studied widely over the years.^[205–208] While receptors with tertiary ammonium groups require a low pH, the use of quaternary ammonium groups allows binding studies under neutral conditions. Worm and Schmidtchen have investigated chloride binding to the zwitterionic receptor **F**, and an association constant of $K_a(\text{Cl}^-) = 2.7 \times 10^2 \text{ M}^{-1}$ was determined (D_2O , NMR).^[209]

This chapter describes two Pd-based coordination cages, which are able to bind chloride in buffered aqueous solution. An unprecedented low micromolar affinity was observed by ITC.

Results and discussion

The syntheses of the coordination cages $[\text{Pd}_2(\mathbf{L11})_4(\text{NO}_3)](\text{NO}_3)_3$ and $[\text{Pd}_2(\mathbf{L11})_4(\text{BF}_4)](\text{BF}_4)_3$ have been recently reported by our group.^[211] The dinuclear complexes were obtained by thermal equilibration of $[\text{Pd}(\text{CH}_3\text{CN})_4](\text{BF}_4)_2$ or $\text{Pd}(\text{NO}_3)_2$ with two equivalents of 1,3-di(pyridin-3-yl)benzene (**L11**) in acetonitrile (**Scheme 5**). A crystallographic analysis of the complex formed from $\text{Pd}(\text{NO}_3)_2$ showed that the cavity of the cage is occupied by one nitrate anion.^[47] The ^{19}F NMR spectrum of the cage obtained from $[\text{Pd}(\text{CH}_3\text{CN})_4](\text{BF}_4)_2$ suggests that one BF_4^- anion is also encapsulated (**Figure ES30**). Despite the similarities, the assembly of the nitrate complex was found to be “cleaner” and less susceptible to variations in the Pd^{2+} concentration.^[211] Most likely, nitrate is better suited as a template. Intrigued by the encapsulation of NO_3^- and BF_4^- , we investigated whether $[\text{Pd}_2(\mathbf{L11})_4]^{4+}$ could encapsulate other small anions.



Scheme 5. (a) Synthesis of the coordination cages $[\text{Pd}_2(\mathbf{L11})_4(\text{BF}_4)](\text{BF}_4)_3$ and $[\text{Pd}_2(\mathbf{L11})_4(\text{NO}_3)](\text{NO}_3)_3$. (b) Formation of the halide adducts $[\text{Pd}_2(\mathbf{L11})_4\text{X}](\text{BF}_4)_3$.

When one equivalent of NBu_4Cl was added to a solution of $[\text{Pd}_2(\text{L11})_4(\text{BF}_4)](\text{BF}_4)_3$ in CD_3CN (1.0 mM), the clean formation of a new complex was observed by ^1H NMR spectroscopy (**Figure 30a**). Similar results were obtained when using NBu_4Br or NBu_4I , even though the adduct formation was accompanied by the formation of some precipitate.

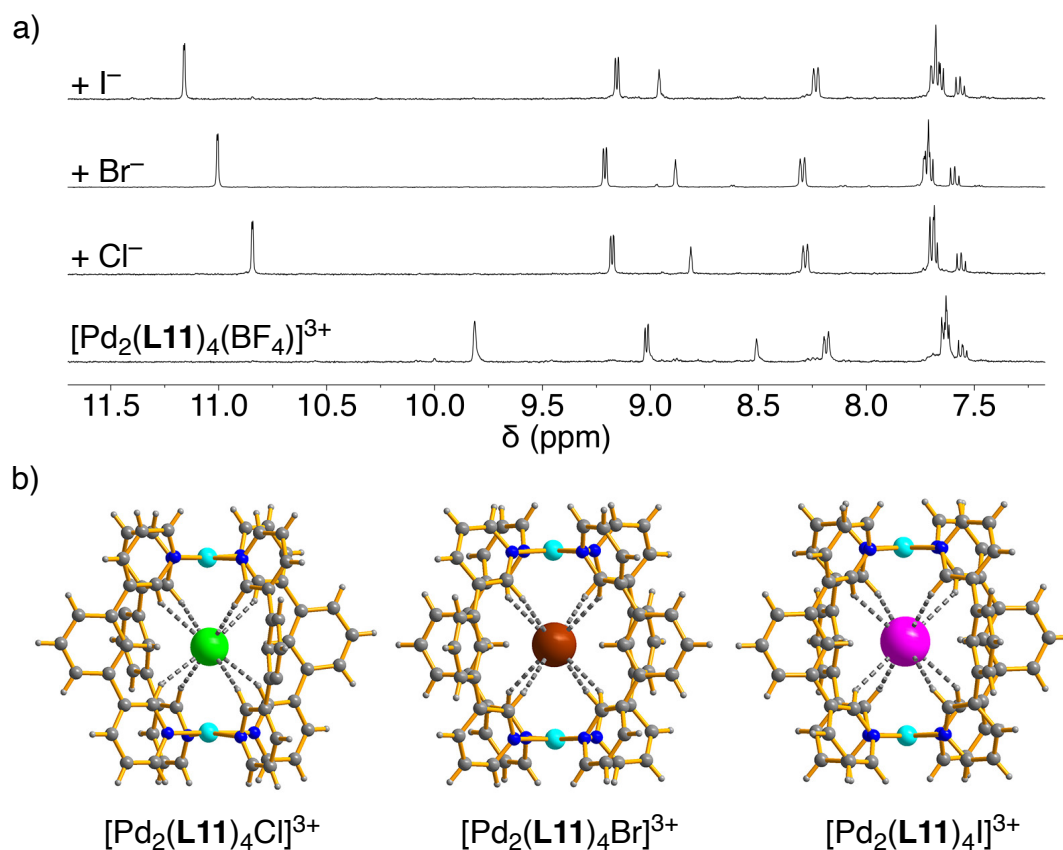


Figure 30. (a) Aromatic part of the ^1H NMR spectra (400 MHz, CD_3CN) of $[\text{Pd}_2(\text{L11})_4(\text{BF}_4)](\text{BF}_4)_3$ and of solutions containing equimolar amounts of $[\text{Pd}_2(\text{L11})_4(\text{BF}_4)](\text{BF}_4)_3$ and NBu_4X ($\text{X} = \text{Cl}, \text{Br}, \text{or I}$). (b) Molecular structures of the halide adducts $[\text{Pd}_2(\text{L11})_4\text{X}](\text{BF}_4)_3$ as determined by X-ray crystallography. The BF_4^- anions are not shown for clarity. Color coding: C: grey, H: white, N: dark blue, Pd: light blue, Cl: green, Br: brown, I: pink.

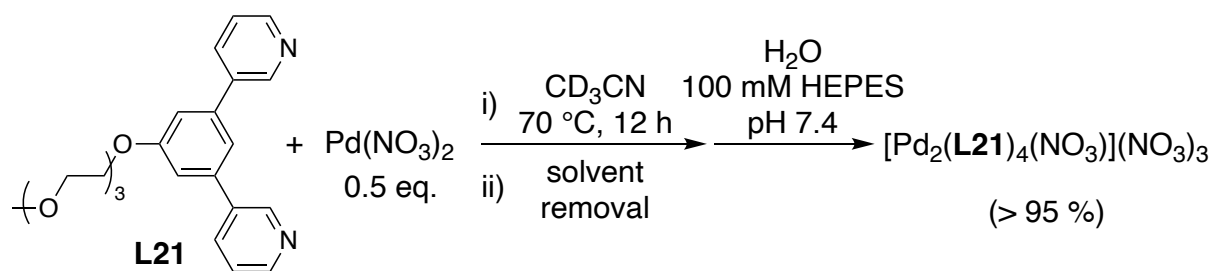
The ^1H NMR spectra of the adducts showed noticeable differences, in particular for the signals of the NCH protons pointing to the cage interior (**Figure 30a**). The addition of sub-stoichiometric amounts of NBu_4X indicated that the binding of the halides is slow on the NMR time scale (**Figure ES29**). Further confirmation for the formation of host-guest complexes was obtained by high-resolution mass spectrometry. Dominant peaks for $[\text{Pd}_2(\text{L11})_4\text{X}]^{3+}$ species were observed in all three cases.

Crystallographic analyses of the three halide adducts revealed that the anions are bound in the cavity of the lantern-shaped^[4] $[\text{Pd}_2(\text{L11})_4]^{4+}$ host (**Figure 30b**). For all three complexes, we observed eight C–H \cdots X⁻ contacts involving the pyridyl NCH protons, with $d_{\text{H}\cdots\text{X}}$ distances below 3 Å.^[212,213] The hydrogen atoms of the central phenylene spacers, on the other hand, are too far away for efficient interaction with the halide ($d_{\text{H}\cdots\text{X}} > 3.2$ Å). The Pd \cdots X⁻ distances of around 3.7 Å exclude direct coordination bonds.^[214–220] Nevertheless, the presence of two Pd²⁺ ions will promote anion binding via electrostatic interactions.

First evidence for the high chloride affinity of $[\text{Pd}_2(\text{L11})_4]^{4+}$ was provided by a failed attempt to remove chloride with a silver salt. The addition of 500 equivalents of AgBF_4 to a solution of $[\text{Pd}_2(\text{L11})_4\text{Cl}](\text{BF}_4)_3$ in CD_3CN did not result in the decomplexation of chloride, as shown by ^1H NMR spectroscopy. The high chloride affinity was further evidenced by the extraction of chloride from water using a solution of $[\text{Pd}_2(\text{L11})_4(\text{BF}_4)](\text{BF}_4)_3$ in CD_3NO_2 (**Figure ES52**).

Chloride encapsulation by palladium-ligand assemblies^[53,54,78,79,111,221–226] and by other metallasupramolecular structures^[106,107,227–234] has been described before. These studies were mostly performed in organic solvents. In view of the high apparent chloride affinity of $[\text{Pd}_2(\text{L11})_4(\text{BF}_4)](\text{BF}_4)_3$, we wanted to explore if dinuclear Pd cages could also act as chloride receptors in water.^[235,236]

Attempts to use $[\text{Pd}_2(\text{L11})_4]\text{X}_4$ complexes in water were hampered by solubility problems. Therefore, ligand **L21**, featuring a short PEG chain, was synthesized (**Scheme 6**).



Scheme 6. Synthesis of a buffered aqueous solution containing receptor $[\text{Pd}_2(\text{L21})_4(\text{NO}_3)](\text{NO}_3)_3$.

The new ligand **L21** was combined with $\text{Pd}(\text{NO}_3)_2$ in CD_3CN (**Scheme 6**). After verifying the success of the self-assembly process by ^1H NMR spectroscopy and HRMS, we removed the solvent under reduced pressure. The residue was then dissolved in H_2O containing 100 mM 4-(2-hydroxyethyl)-1-piperazineethanesulfonic acid (HEPES) buffer with a pH of 7.4 (**Scheme 6**). The ^1H NMR spectrum of the resulting solution showed the presence of $[\text{Pd}_2(\text{L21})_4(\text{NO}_3)](\text{NO}_3)_3$ in high purity (>95%; **Figure ES34**). A solution of the cage was stable over a prolonged period of time.

The template effect of the nitrate anion was found to be important. Attempts to prepare cages using $\text{Pd}(\text{OAc})_2$ or $[\text{Pd}(\text{CH}_3\text{CN})_4](\text{BF}_4)_2$ instead of $\text{Pd}(\text{NO}_3)_2$ were met with limited success. When $\text{Pd}(\text{OAc})_4$ (1 eq.) was equilibrated with **L21** (2 eq.) in CD_3CN , the ^1H NMR spectrum of the solution showed free **L21** to be the main species present. Analysis by HRMS indicated that $[\text{Pd}_2(\text{L21})_3](\text{OAc})_4$ had formed along with $[\text{Pd}_2(\text{L21})_4](\text{OAc})_4$. With $[\text{Pd}(\text{CH}_3\text{CN})_4](\text{BF}_4)_2$, on the other hand, the reaction gave $[\text{Pd}_2(\text{L21})_4](\text{BF}_4)_4$ and $[\text{Pd}_4(\text{L21})_8](\text{BF}_4)_8$ as the major products.

The binding of anions by $[\text{Pd}_2(\mathbf{L21})_4(\text{NO}_3)]^{3+}$ was first investigated by ^1H NMR spectroscopy using a water suppression pulse sequence. The addition of one equivalent of NaCl to a solution of $[\text{Pd}_2(\mathbf{L21})_4(\text{NO}_3)](\text{NO}_3)_3$ in $\text{H}_2\text{O}/\text{D}_2\text{O}$ (95:5, $[\text{cage}] = 1.0$ mM, 100 mM HEPES, pH 7.4) gave a new set of signals for the adduct $[\text{Pd}_2(\mathbf{L21})_4\text{Cl}]^{3+}$. By integration of the signals, we were able to deduce that the apparent binding constant for chloride complexation is higher than 10^4 M^{-1} (**Figure ES34**). Attempts to use UV/Vis spectroscopy for quantifying the binding affinity were not successful because only minor spectral changes were observed upon complexation of chloride (**Figure ES51**).

The utilization of NaBr gave similar results: a tight host–guest complex between the cage and the halide was formed. The addition of NaI resulted in the slow formation of a yellow precipitate. Nevertheless, the formation of the corresponding adduct could be observed by ^1H NMR spectroscopy. Likely, iodide competes with the pyridyl ligand for coordination to the Pd^{2+} ions, resulting in a partial rupture of the cage structure. Similar behavior has been observed for Pd-based cages in organic solvents.^[53,54,223,237]

The addition of one equivalent of NaF, Na_2SO_4 , NaOAc, Na_2CO_3 , or Na_3PO_4 to a solution of $[\text{Pd}_2(\mathbf{L21})_4(\text{NO}_3)](\text{NO}_3)_3$ in $\text{H}_2\text{O}/\text{D}_2\text{O}$ (95:5, $[\text{cage}] = 1.0$ mM, 100 mM HEPES, pH 7.4) did not result in changes in the ^1H NMR spectrum, indicating that the bound nitrate is not exchanged by fluoride, sulfate, acetate, carbonate, or phosphate under these conditions.

To determine the binding constants for chloride and bromide complexation, we performed ITC measurements ($T=298$ K, for details see **Figures ES36 – ES50** and **Tables ES6 – ES10**).^[238] The measurements were carried out in buffered water at pH 7.4 (10 mM HEPES). The solution of $[\text{Pd}_2(\text{L21})_4(\text{NO}_3)](\text{NO}_3)_3$ was prepared as described above. Solutions of NaCl or NaBr were titrated to a solution of the cage (0.1 mM). The data could be fitted to a 1:1 binding model resulting in apparent association constants of $K_a(\text{Cl}^-)=1.8(\pm 0.1)\times 10^5 \text{ M}^{-1}$ and $K_a(\text{Br}^-)=2.6(\pm 0.4)\times 10^6 \text{ M}^{-1}$ (**Figure 31**). For both anions, the complexation is mainly entropy-driven, with an unfavorable contribution of enthalpy in the case of chloride ($\Delta H_{\text{Cl}}=3.3 \text{ kJ mol}^{-1}$, $T\Delta S_{\text{Cl}}=33.2 \text{ kJ mol}^{-1}$; $\Delta H_{\text{Br}}=-13.1 \text{ kJ mol}^{-1}$, $T\Delta S_{\text{Br}}=23.5 \text{ kJ mol}^{-1}$).

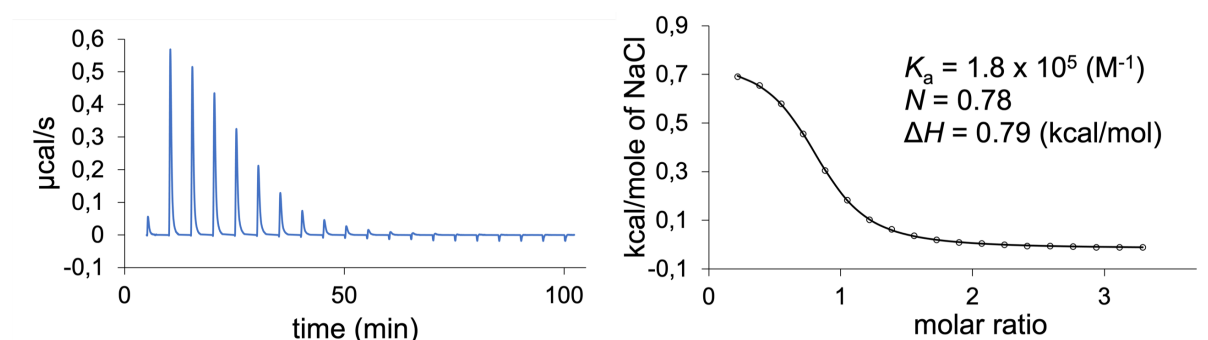


Figure 31. Representative ITC experiment (H_2O , HEPES 10 mM, pH 7.4, 298 K) for the titration of $[\text{Pd}_2(\text{L21})_4(\text{NO}_3)](\text{NO}_3)_3$ (0.1 mM) with NaCl (4 mM). Corrected thermogram for 20 injections (6 μL per injection) (left) and the corresponding integrated heat of reaction as a function of the guest/host ratio (right). The solid black line represents the best-fitting curve obtained from a 1:1 binding model.

To corroborate that nitrate ions compete with chloride for binding to $[\text{Pd}_2(\text{L21})_4]^{4+}$, we have performed ITC measurements in the presence of 0.4 mM NaNO_3 ($[\text{cage}]=0.1 \text{ mM}$, $[\text{NO}_3^-]_{\text{total}}=0.8 \text{ mM}$). The apparent binding constant for chloride complexation dropped to $K_a(\text{Cl}^-)=1.0(\pm 0.1)\times 10^5 \text{ M}^{-1}$ (**Figure 32**). The reduced affinity in the presence of NaNO_3 confirms that nitrate is a competitive guest,^[239,240] and that chloride is captured via an anion exchange mechanism, converting $[\text{Pd}_2(\text{L21})_4(\text{NO}_3)]^{3+}$ into $[\text{Pd}_2(\text{L21})_4\text{Cl}]^{3+}$.

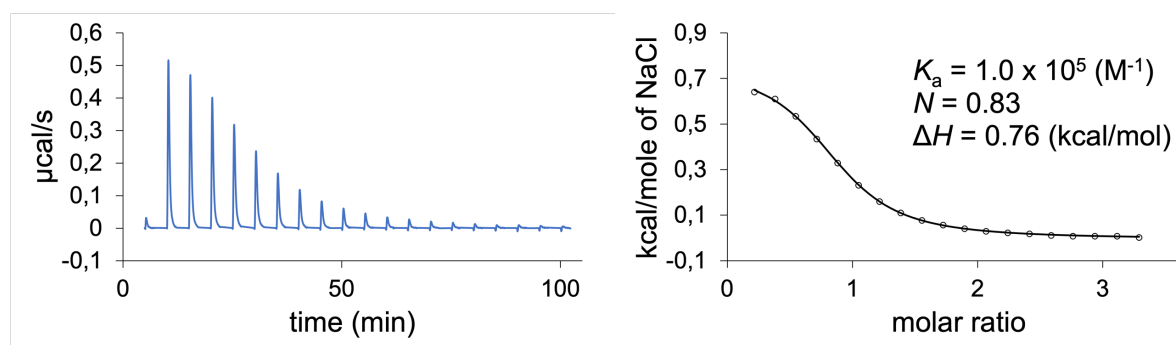


Figure 32. Representative ITC experiment (H_2O , HEPES 10 mM, pH 7.4, 298 K) for the titration of $[\text{Pd}_2(\text{L21})_4(\text{NO}_3)](\text{NO}_3)_3$ (0.1 mM) in presence of NaNO_3 (0.4 mM, $[\text{NO}_3]_{\text{tot}} = 0.8 \text{ mM}$) with NaCl (4 mM). Corrected thermogram for 20 injections ($6 \mu\text{L}$ per injection) (left) and the corresponding integrated heat of reaction as a function of the guest/host ratio (right). The solid black line represents the best-fitting curve obtained from a 1:1 binding model.

Attempts to conduct ITC binding studies with $[\text{Pd}_2(\text{L21})_4(\text{NO}_3)](\text{NO}_3)_3$ in acetonitrile were impaired by much slower anion exchange. The ^1H NMR spectra recorded directly after the addition of one equivalent of NBu_4Cl to a solution of the cage showed limited conversion to the chloride inclusion complex. Complete complexation was observed after equilibration for 5 h at room temperature and time-dependent measurements revealed a half-life of $\sim 0.2 \text{ h}$ (**Figures ES32 and ES33**). The faster anion exchange in the highly coordinating solvent water is supportive of a mechanism involving partial or full ligand dissociation of at least one ligand **L21**.

We were interested in exploring if we could alter the host–guest properties of the cage by using substituent effects. Therefore, we synthesized ligand **L22** with fluorine atoms in meta positions relative to the N-donors (**Figure 33a**). Equilibration of a mixture of **L22** and Pd(NO₃)₂ in CD₃CN gave cage [Pd₂(**L22**)₄(NO₃)](NO₃)₃ in nearly quantitative yield as shown by NMR and HRMS analyses.

ITC measurements with NaCl in buffered aqueous solution revealed an apparent association constant of $K_a(\text{Cl}^-) = 6.0(\pm 0.4) \times 10^5 \text{ M}^{-1}$ ($T = 298 \text{ K}$). This value is three times superior to the one obtained for the related [Pd₂(**L21**)₄(NO₃)](NO₃)₃ complex. The higher affinity of the fluorinated receptor is mostly due to a favorable change in binding enthalpy (fluorinated cage: $\Delta H_{\text{Cl}} = -1.9 \text{ kJ mol}^{-1}$, $T\Delta S_{\text{Cl}} = 31.1 \text{ kJ mol}^{-1}$; non-fluorinated cage: $\Delta H_{\text{Cl}} = 3.3 \text{ kJ mol}^{-1}$, $T\Delta S_{\text{Cl}} = 33.2 \text{ kJ mol}^{-1}$).

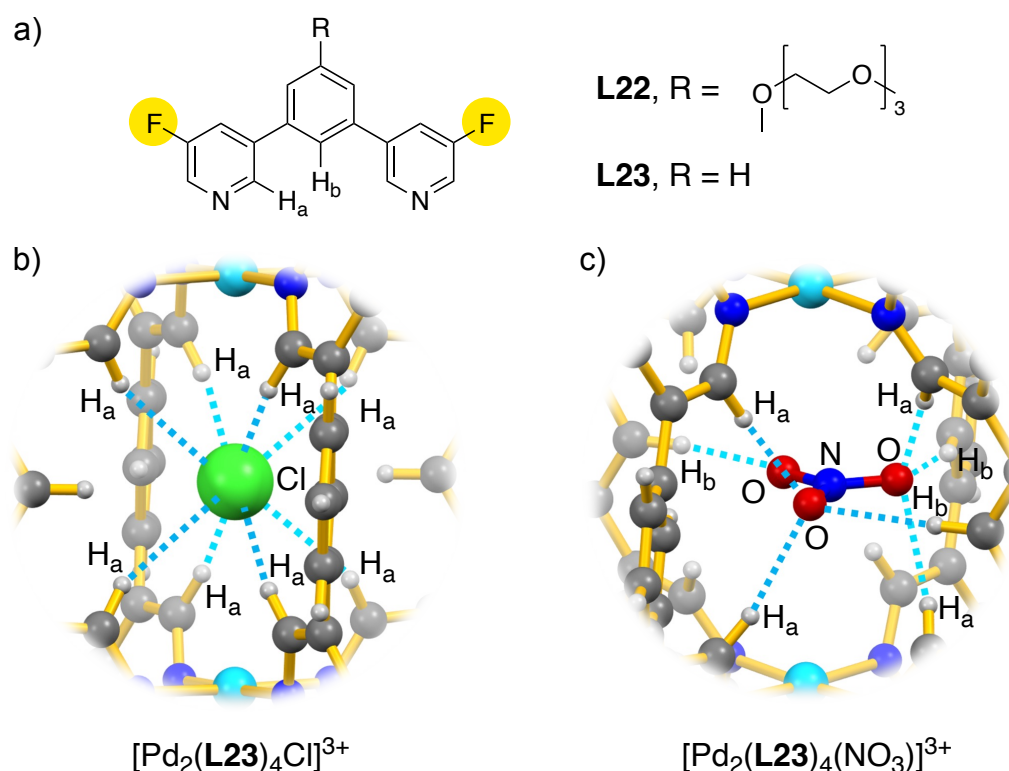


Figure 33. (a) Structures of the ligands **L22** and **L23**. (b) Close-up view of the chloride anion in [Pd₂(**L23**)₄Cl]³⁺. (c) Close-up view of the nitrate anion in [Pd₂(**L23**)₄(NO₃)]³⁺. The graphics are based on single-crystal XRD analyses.

In order to evaluate possible structural effects of the fluorine substituents, we aimed to perform a crystallographic analysis of the fluorinated cage. Unfortunately, we did not succeed in growing suitable single crystals of $[\text{Pd}_2(\mathbf{L22})_4(\text{NO}_3)](\text{NO}_3)_3$ or its chloride adduct. Therefore, we synthesized the structurally related ligand **L23** lacking an ethylene glycol side chain (**Figure 33a**). With this ligand, we managed to obtain single crystals of $[\text{Pd}_2(\mathbf{L23})_4\text{Cl}](\text{BF}_4)_3$ and $[\text{Pd}_2(\mathbf{L23})_4(\text{NO}_3)](\text{NO}_3)_3$.

XRD analysis of the chloride adduct showed that the overall structure was very similar to what was observed for the non-fluorinated ligand **L22**. The chloride anion is found in the center of the lantern-shaped cage, and one can observe eight $\text{C}-\text{H}\cdots\text{Cl}^-$ hydrogen bonds involving the pyridyl NCH protons "H_a" (**Figure 33b**).

The encapsulated nitrate in $[\text{Pd}_2(\mathbf{L23})_4(\text{NO}_3)](\text{NO}_3)_3$ is disordered over two equally populated positions. The two anions are bound in the same fashion: two of the three O-atoms are involved in hydrogen bonding to pyridyl H_a-atoms and to H_b-atoms from the central phenylene spacer (**Figure 33c**). The third O-atom, on the other hand, shows one close $\text{C}-\text{H}_b\cdots\text{ONO}_2^-$ interaction and four longer H-bonds to H_a-atoms (not depicted). The presence of the fluoride atoms in **L23** is expected to strengthen the $\text{C}-\text{H}_a\cdots\text{X}^-$ interaction.^[241] The latter appears to be more important for chloride (eight $\text{C}-\text{H}_a\cdots\text{Cl}^-$ bonds) than for nitrate (four close $\text{C}-\text{H}_a\cdots\text{ONO}_2^-$ bonds), providing a rationale for the increased chloride affinity of the fluorinated cage.

Conclusion

We have synthesized two Pd-based receptors, which are able to bind chloride in buffered aqueous solution. ITC measurements have revealed apparent binding constants of $1.8(\pm 0.1) \times 10^5 \text{ M}^{-1}$ and $6.0(\pm 0.4) \times 10^5 \text{ M}^{-1}$. These values exceed what has been reported for other synthetic receptors operating at neutral pH. Crystallographic analyses show that chloride is bound to the Pd receptors via eight C–H...Cl⁻ hydrogen bonds. The presence of Pd²⁺ promotes anion binding via electrostatic interactions. Furthermore, the coordination of Pd²⁺ to the pyridyl groups is expected to strengthen the hydrogen bonds. In terms of selectivity, the new receptors are very good. Bromide and iodide compete with binding and self-assembly, but common anions such as phosphate, acetate, carbonate, and sulfate do not interfere at all.

Chloride is bound to the receptors via an anion exchange mechanism. Consequently, the observed binding constants represent relative affinities with respect to the nitrate-bound cages. One would expect even higher binding constants for the hypothetical empty cages [Pd₂(**L21**)₄]⁴⁺ and [Pd₂(**L22**)₄]⁴⁺. However, nitrate seems to be a required template for stabilizing the dinuclear cage structures in water. Future investigations in our lab are directed toward a better understanding of structure-affinity and structure-selectivity relationships of these promising Pd-based receptors.

7. Conclusion and outlook

The investigations on Pd²⁺-based supramolecular assemblies, presented throughout this thesis, have given additional insights into the ligand-assembly structural relationships, by providing examples of unprecedented structural motifs and highly specific host-guest chemistry.

The first research chapter of this thesis described the preparation of a virtual combinatorial library of assemblies that resulted in the identification of a new hexanuclear Pd₆L₆L'₆ heteroleptic species. Using another pair of ligands with a similar combination of bending angles resulted in the formation of an additional example of hexanuclear complex. Applying the concept to different ligands combinations could allow to identify other examples of heteroleptic structures that are not easily accessible by design.

Following investigations on the Li⁺ binding properties of Pd-based assemblies revealed an unexpected complexation-induced rearrangement of a Pd₂L₄ species into a low-symmetry folded Pd₄L₈ complex with an unprecedented topology. The transformation was found to be highly specific, requiring both the presence of water and Li⁺. The key ligands' characteristics promoting the formation of such folded and compact structure were identified as its intermediate flexibility, its extended π surfaces and the variable possible orientations of the coordination vectors. It was later found that the same ligand could be used to prepare a unique five-stranded helicate, provided the presence of La³⁺ to stabilize the structure.

The aforementioned properties were then used as a basis to develop design principles for the targeted synthesis of intricate Pd-assemblies. Among the different ligands prepared following these guidelines, the combination of one of them with Pd²⁺ formed a low-symmetry Pd₂L₃ assembly, displaying important π-stacking interactions between adjacent ligands. While this work is still ongoing, these preliminary experiments allowed to further refine the design principles.

Finally, two new Pd₂L₄ receptors were shown to bind chloride in buffered aqueous solution with an unprecedented affinity. Structural analysis highlighted the contribution of H-bonding, in addition to electrostatic interactions, in stabilizing the inclusion complex. The highly symmetric and confined environment of the internal cavity provided a good selectivity of halide guests over other common biological anions. The current system required the presence of a templating nitrate guest, resulting in a measured apparent binding constant for chloride. As one could expect higher binding constants for the empty guest, further development should aim at stabilizing the complex in absence of a templating guest; it could be achieved by tuning the donor properties of the ligand with different substituents. Nevertheless, such modifications could potentially impact the H-bonding capacity of the host. Further developments would require a deeper understanding of electronic effects on the host-guest interactions.

8. Experimental section

8.1 General

NMR spectra were measured on a Bruker Avance III HD spectrometer (^1H : 400 MHz, ^{13}C : 100 MHz) equipped with a BBFO-Plus_z 5 mm probe, a Bruker Avance III spectrometer (^1H : 400 MHz) equipped with a BBFO_z 5 mm probe, a Bruker Avance III spectrometer (^1H : 400 MHz) equipped with a BBI_z 5 mm probe, a Bruker Avance III spectrometer (^1H : 400 MHz) equipped with a Prodigy BBO 5 mm cryoprobe, a Bruker Avance Neo spectrometer (^1H : 500 MHz, ^{13}C : 125 MHz) equipped with a CPTCl_{xyz} 5 mm cryoprobe and a Bruker Avance II spectrometer (^1H : 800 MHz) equipped with a 5 mm CPTCl_{xyz} cryoprobe.

Routine ESI-MS experiments were carried out on a Xevo G2-S QTOF mass spectrometer (Waters) with a positive ionization mode.

High resolution mass spectrometry experiments were carried out using a hybrid ion trap-Orbitrap Fourier transform mass spectrometer, Orbitrap Elite (Thermo Scientific) equipped with a TriVersa Nanomate (Advion) nano-electrospray ionization source. Mass spectra were acquired with a minimum resolution setting of 120,000 at 400 *m/z*. To reduce the degree of analyte gas phase reactions leading to side products unrelated to solution phase, the transfer capillary temperature was lowered to 50 °C. Experimental parameters were controlled via standard and advanced data acquisition software.

8.2 Experimental details for Chapter 2

The full experimental details can be found in the supplementary information of the related publication.^[49]

Synthesis and characterization

The ligands **L1** to **L7** were synthesized following literature procedures.^[54,94,110,111,114,242,243]

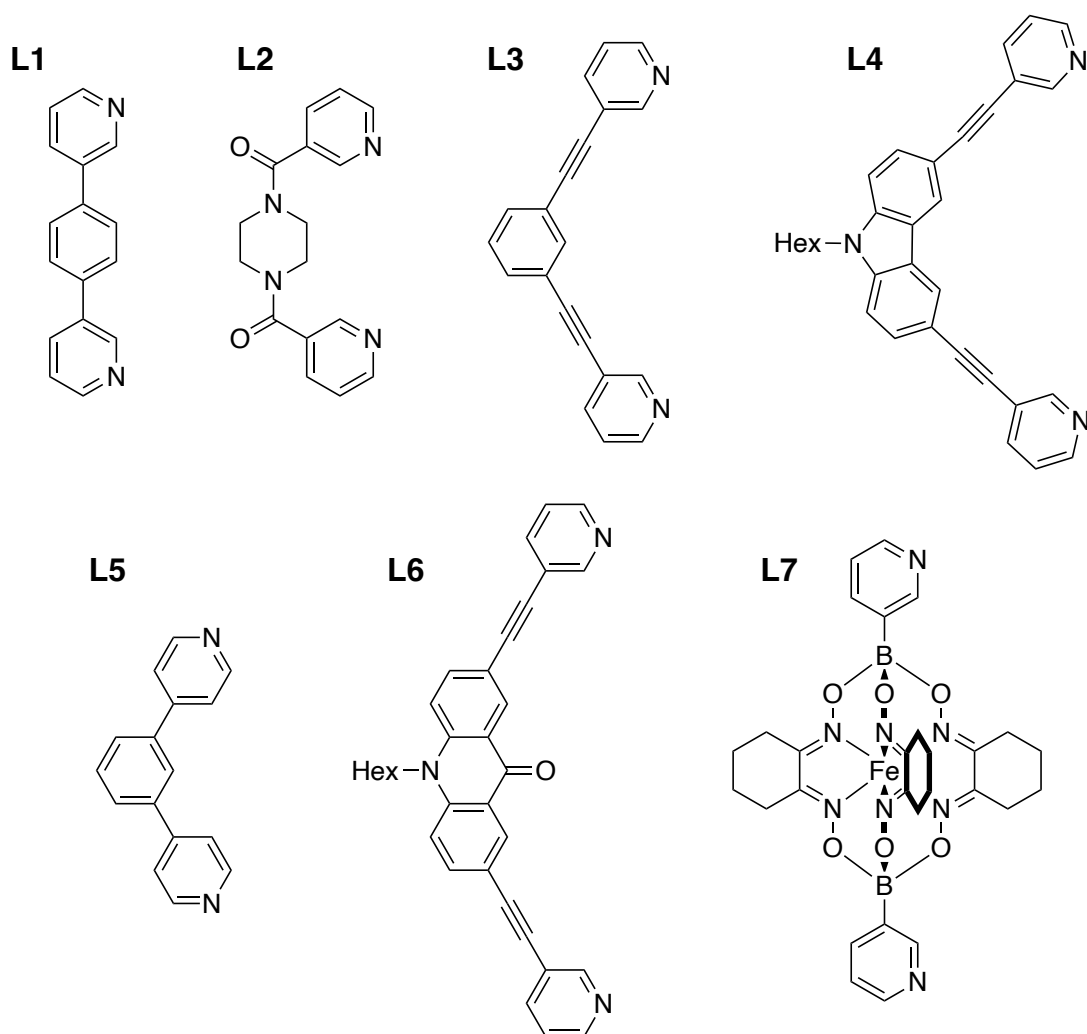
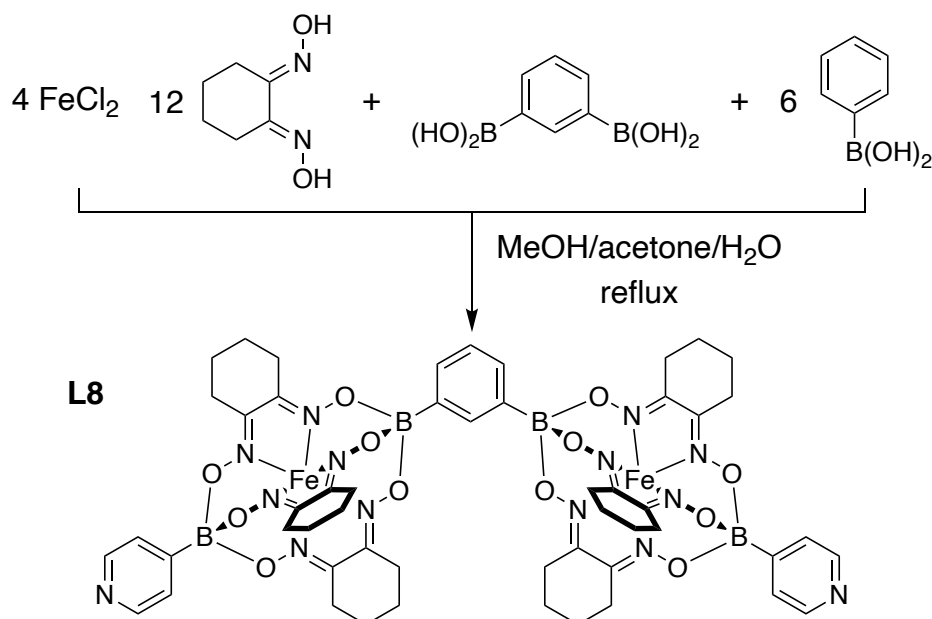


Figure ES1. Structures of ligands **L1** to **L7**.



Scheme ES1. Synthesis of **L8**

L8 was synthesized based on a published procedure.^[244] Anhydrous FeCl_2 (306 mg, 2.4 mmol, 4 equiv.) and nioxime (1.029 g, 7.2 mmol, 12 equiv.) were dissolved in MeOH (15 mL). In a separate flask, 1,3-phenyldiboronic acid (100 mg, 0.6 mmol, 1 equiv.) and 4-pyridineboronic acid (445 mg, 3.6 mmol, 6 equiv.) were dissolved in methanol (130 mL), acetone (5 mL), and water (2 mL) and heated to reflux under stirring for 30 min. The solution of nioxime and FeCl_2 was then added to the boronic acid mixture, and the mixture was heated to reflux for an additional 2 h, before the solvent was removed under reduced pressure. The remaining solid was dissolved in CHCl_3 (100 mL), filtered, and washed with a saturated aqueous solution of sodium EDTA and 5% ammonia (100 mL). The organic phase was dried over MgSO_4 , and evaporated under reduced pressure. The solid was pre-purified by a short silica column (150 g silica, 10% MeOH in DCM) to remove any polymeric material. The dark red fractions were evaporated under reduced pressure, the solid was dissolved in DCM (10 mL), filtered over H-PTFE 20/25 syringe filters, and separated on a size exclusion column (200 g, dry weight, Bio-Beads S-X3 in DCM). The pure fractions (checked by MS, pos. mode), were combined and washed with saturated NaHCO_3 solution, dried over MgSO_4 , and the solvent was removed under reduced pressure to yield ligand **L8** in form of a red powder (46%). ^1H NMR (400 MHz, $\text{DMSO}-d_6$) δ 8.49 (d, 4H), 7.93 (s, 1H), 7.50 (d, 4H), 7.46 (dd, 2H), 7.19 (t, $J = 1\text{H}$), 2.85 (broad, 24H), 1.75 (broad, 24H).

The literature-known homoleptic assemblies $[\text{Pd}_n\text{L}_{2n}](\text{BF}_4)_{2n}$ were obtained following a general procedure: A mixture of the respective ligand (**L1–L6**, 4.5 μmol , 2 eq.) and of $[\text{Pd}(\text{CH}_3\text{CN})_4](\text{BF}_4)_2$ (2.25 μmol , 1 eq.) in $\text{CD}_3\text{CN}/\text{CD}_3\text{NO}_2$ (8:2, 0.5 mL) was heated at 60 °C while stirring for 17 h. The formation of the desired products was confirmed by ^1H NMR spectroscopy. The chemical shifts were referenced to CD_3CN residual signal (δ 1.94). Stock solutions of the ligands **L1** to **L5** and of $[\text{Pd}(\text{CH}_3\text{CN})_4](\text{BF}_4)_2$ were prepared in a mixture of $\text{CD}_3\text{CN}/\text{CD}_3\text{NO}_2$ (8:2). Due to the low solubility of **L6** in this solvent mixture, **L6** was weighted as a solid.

$[\text{Pd}_4(\text{L1})_8](\text{BF}_4)_8$ – ^1H NMR (400 MHz, $\text{CD}_3\text{CN}/\text{CD}_3\text{NO}_2$ 8:2) δ 9.91 (s, 1H), 9.52 (s, 1H), 9.35 (d, 1H), 8.89 (d, 1H), 8.34 (d, 1H), 8.16 (d, 1H), 7.98 (s, 2H), 7.84 (dd, 1H), 7.72 (s, 2H), 7.53 (dd, 1H).

$[\text{Pd}_2(\text{L2})_4](\text{BF}_4)_4$ – ^1H NMR (400 MHz, $\text{CD}_3\text{CN}/\text{CD}_3\text{NO}_2$ 8:2) δ 9.27 (s, 1H), 9.16 (m, 1H), 8.01 (d, 1H), 7.71 (dd, 1H), 4.07 (d, 1H), 3.80 (t, 1H), 3.53 (t, 1H), 3.26 (d, 1H).

$[\text{Pd}_2(\text{L3})_4](\text{BF}_4)_4$ – ^1H NMR (400 MHz, $\text{CD}_3\text{CN}/\text{CD}_3\text{NO}_2$ 8:2) δ 9.42 (s, 2H), 9.09 (d, 2H), 8.09 (d, 2H), 7.94 (s, 1H), 7.69 – 7.60 (m, 4H), 7.50 (t, 1H).

$[\text{Pd}_2(\text{L4})_4](\text{BF}_4)_4$ – ^1H NMR (400 MHz, $\text{CD}_3\text{CN}/\text{CD}_3\text{NO}_2$ 8:2) δ 8.76 (s, 1H), 8.53 (d, 1H), 8.38 (s, 1H), 7.91 (d, 1H), 7.70 (d, 1H), 7.60 (d, 1H), 7.38 (dd, 1H).

$[\text{Pd}_{12}(\text{L5})_{24}](\text{BF}_4)_{24}$ – ^1H NMR (400 MHz, $\text{CD}_3\text{CN}/\text{CD}_3\text{NO}_2$ 8:2) δ 9.24 – 9.06 (broad d, 4H), 8.23 (s, 1H), 8.09 – 7.97 (broad d, 4H), 7.90 (d, 2H), 7.63 (t, 1H).

$[\{\text{Pd}_2(\text{L6})_4\}_2](\text{BF}_4)_8$ – ^1H NMR (400 MHz, $\text{CD}_3\text{CN}/\text{CD}_3\text{NO}_2$ 8:2) δ 10.81 (s, 1H), 10.32 (d, 1H), 10.04 (s, 1H), 9.31 (d, 1H), 8.18 (d, 1H), 8.11 (s, 1H), 7.96 (s, 1H), 7.86 (d, 1H), 7.74 (t, 1H), 7.61 (d, 1H), 7.42 (d, 1H), 7.16 (d, 1H), 6.94 – 6.82 (m, 2H), 1.76 (broad, 2H), 1.44 (broad, 2H), 1.29 (broad, 6H), 0.84 (t, 3H).

[Pd₆(L1)₆(L5)₆](BF₄)₁₂ – L1 (18 μmol, 4.18 mg, 1 eq.), **L5** (18 μmol, 4.18 mg, 1 eq) and [Pd(CH₃CN)₄](BF₄)₂ (18 μmol, 8.0 mg, 1 eq) were added to a mixture of CH₃CN and CH₃NO₂ (8:2, 4 mL) and heated at 65 °C for 17 h while stirring. Diethylether (6 mL) was added to the reaction mixture, the precipitate washed with diethylether, and the solvent evaporated under vacuum. The solid was redissolved in CD₃CN and a ¹H NMR spectrum recorded. The chemical shifts were referenced to CD₃CN residual signal (δ 1.94). ¹H NMR (400 MHz, CD₃CN) δ 9.75 (d, 2H), 9.39 (d, 2H), 9.15 (d, 4H), 8.29 (dt, 2H), 8.19 (s, 1H), 8.01 (s, 4H), 7.97 (d, 4H), 7.88 (dd, 2H), 7.77 (dd, 2H), 7.60 (t, 1H).

[Pd₂(L1)₂(L4)₂](BF₄)₄ – A mixture of L1 (2.5 μmol, 120.5 μL of a 21 mM stock solution in CD₃CN, 1 eq.), L4 (2.5 μmol, 376.3 μL of a 7 mM stock solution in CD₃CN, 1 eq) and [Pd(CH₃CN)₄](BF₄)₂ (2.5 μmol, 72.0 μL of a 35 mM stock solution in CD₃CN, 1 eq) was heated at 65 °C for 15 h to give [Pd₂(L1)₂(L4)₂](BF₄)₄. The chemical shifts were referenced to CD₃CN residual signal (δ 1.94). ¹H NMR (400 MHz, CD₃CN) δ 10.03 (s, 2H), 9.67 (s, 2H), 9.14 (d, 2H), 8.91 (d, 2H), 8.36 (s, 2H), 8.05 (dt, 2H), 7.92 (dt, 2H), 7.69 (dd, 2H), 7.65 – 7.60 (m, 4H), 7.53 (d, 2H), 4.31 (t, 2H), 1.74 (q, 2H), 1.29 – 1.12 (m, 6H), 0.74 (t, 3H).

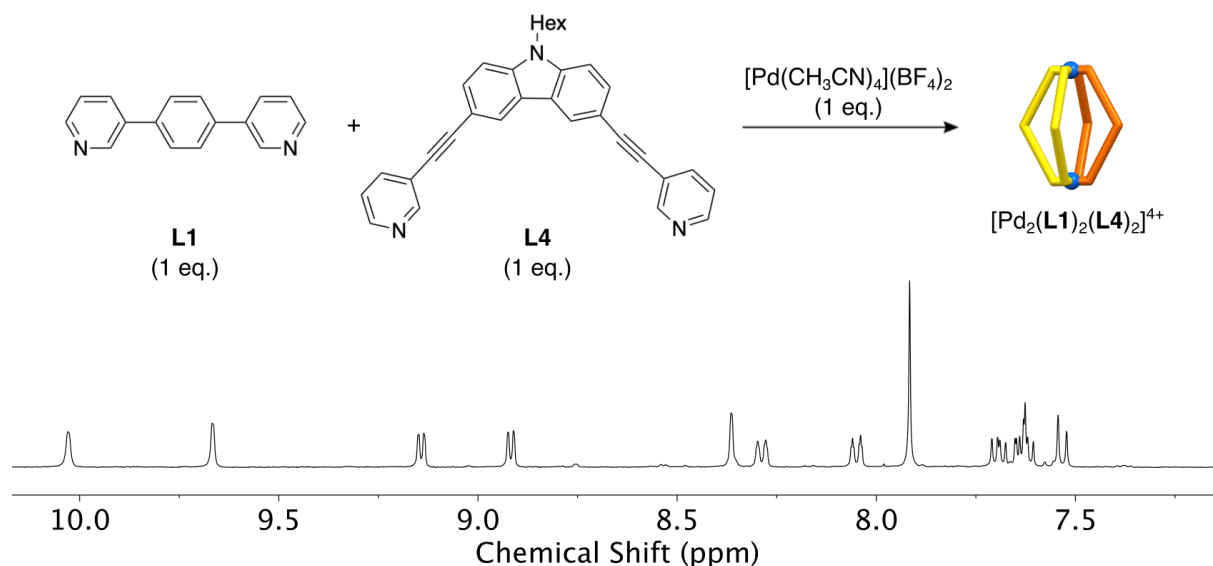


Figure ES2. Aromatic region of the ¹H NMR (400 MHz, CD₃CN) spectrum of [Pd₂(L1)₂(L4)₂](BF₄)₄.

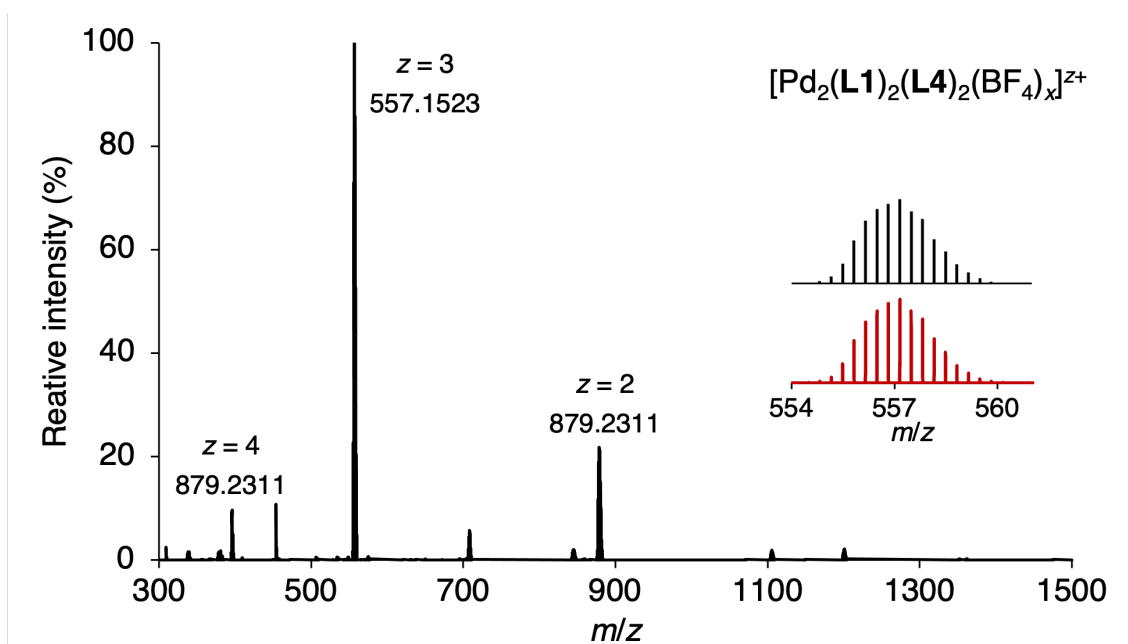


Figure ES3. HRMS of the equilibrated (1:1:1) mixture of L1, L4 and $[\text{Pd}(\text{CH}_3\text{CN})_4](\text{BF}_4)_2$. The inset shows the comparison between the 554 – 561 m/z region (bottom, red) and the calculated mass spectrum for $[\text{Pd}_2(\text{L1})_2(\text{L4})_2(\text{BF}_4)]^{z+}$ (top, black).

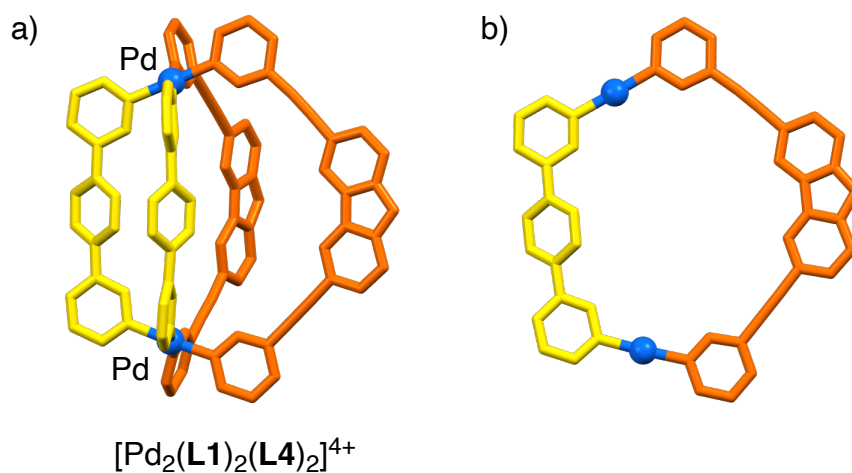


Figure ES4. (a) Graphical representation of the molecular structure of $[\text{Pd}_2(\text{L1})_2(\text{L4})_2]^{4+}$ in the crystal. (b) Part of the structure highlighting the good geometric complementarity between L1 (yellow) and L4 (orange). Hydrogen atoms are not depicted.^f

^f The graphical representation is based on a preliminary structure; further refinement of the data is still required.

[Pd₂(L3)₂(L4)₂](BF₄)₄ – A mixture of **L3** (2.5 μmol, 184.1 μL of a 14 mM stock solution in CD₃CN, 1 eq.), **L4** (2.5 μmol, 376.3 μL of a 7 mM stock solution in CD₃CN, 1 eq) and [Pd(CH₃CN)₄](BF₄)₂ (2.5 μmol, 72.0 μL of a 35 mM stock solution in CD₃CN, 1 eq) was heated at 65 °C for 15 h to give [Pd₂(L3)₂(L4)₂](BF₄)₄. The chemical shifts were referenced to CD₃CN residual signal (δ 1.94). ¹H NMR (400 MHz, CD₃CN) δ 9.34 (s, 2H), 9.21 (s, 2H), 9.01 (dd, 4H), 8.43 (s, 2H), 8.12 (dt, 4H), 7.86 (s, 1H), 7.70 (dt, 4H), 7.65 – 7.60 (m, 4H), 7.57 (d, 2H), 7.51 (t, 1H), 4.34 (t, 2H), 1.79 (q, 2H), 1.32 – 1.15 (m, 6H), 0.77 (t, 3H).

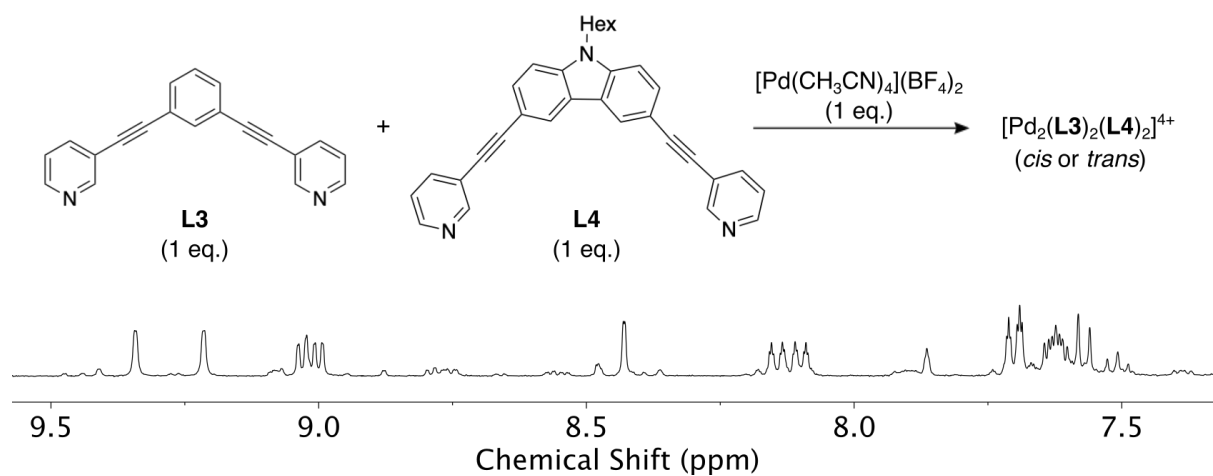


Figure ES5. Aromatic region of the ¹H NMR (400 MHz, CD₃CN) spectrum of [Pd₂(L3)₂(L4)₂](BF₄)₄.

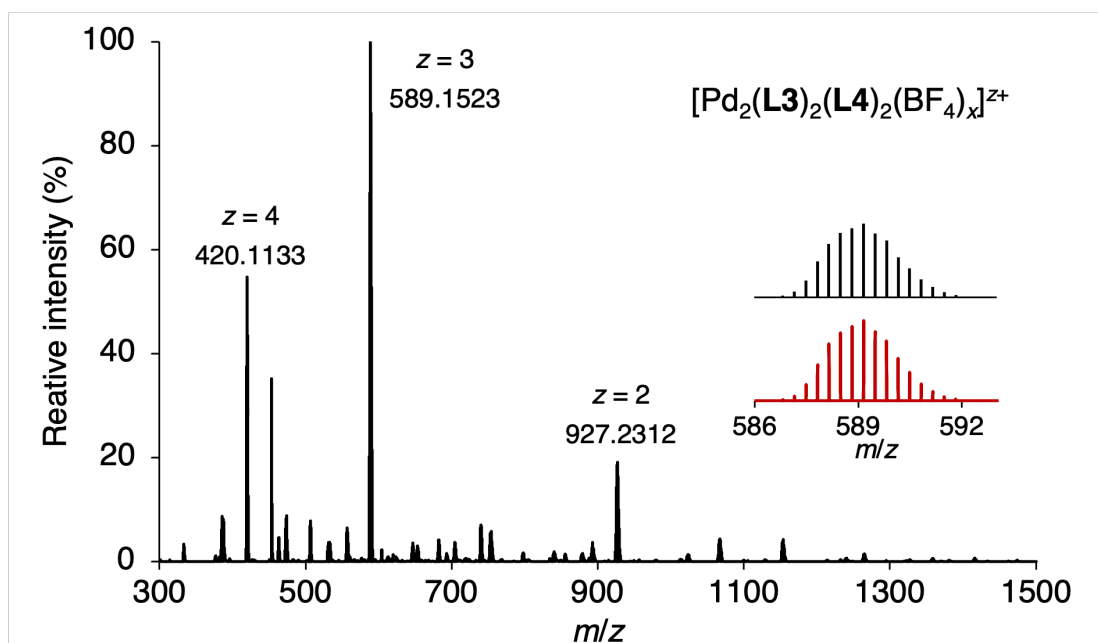


Figure ES6. HRMS of the equilibrated (1:1:1) mixture of **L3**, **L4** and $[\text{Pd}(\text{CH}_3\text{CN})_4](\text{BF}_4)_2$. The inset shows the comparison between the 586 – 593 m/z region (bottom, red) and the calculated mass spectrum for $[\text{Pd}_2(\text{L3})_2(\text{L4})_2(\text{BF}_4)]^{+3}$ (top, black).

$[\text{Pd}_6(\text{L7})_6(\text{L8})_6](\text{BF}_4)_{12}$ – A solution of $[\text{Pd}(\text{CH}_3\text{CN})_4](\text{BF}_4)_2$ (4.5 μmol , 150 μL of a 30 mM stock solution in $\text{DMSO-}d_6$) was combined with a 1:1 suspension mixture of ligands **L7** (4.5 μmol , 2.9 mg) and **L8** (4.5 μmol , 5.5 mg) in 500 μL $\text{DMSO-}d_6$ and heated at 70 $^\circ\text{C}$ overnight to give $[\text{Pd}_6(\text{L7})_6(\text{L8})_6](\text{BF}_4)_{12}$. ^1H NMR (400 MHz, $\text{DMSO-}d_6$) δ 9.61 (b, 12 H), 9.34 (b, 12 H), 9.31 (b, 24 H), 8.10 (b, 12 H), 7.80 (b, 6 H), 7.76 (b, 12 H), 7.66 (b, 24 H), 7.28 (b, 12 H), 6.94 (b, 6 H), 3.17 – 2.58 (b, 216 H), 19.1–1.31 (b, 216 H).

Competition experiment

Aliquots of stock solutions ($\text{CD}_3\text{CN}/\text{CD}_3\text{NO}_2$, 8:2) containing the ligands **L1** to **L6** ($4.5 \mu\text{mol}$ each; for details see **Table ES1**) were added to a vial. Subsequently, $[\text{Pd}(\text{CH}_3\text{CN})_4](\text{BF}_4)_2$ ($4.5 \mu\text{mol}$) was added, and the mixture was heated at $65 \text{ }^\circ\text{C}$ for 17 h while stirring, resulting in a clear yellow solution. After cooling to RT, a ^1H NMR spectrum was recorded. A mixture of pentane and diethylether (1:1; 40 mL) was added to the solution, resulting in the formation of a precipitate. The precipitate was isolated by centrifugation, washed twice with diethylether (20 mL), dried under vacuum, and dissolved in a mixture of CD_3CN and CD_3NO_2 (8:2). A ^1H NMR spectrum was recorded and a HRMS analysis was performed. After removal of the precipitate, the combined solutions were evaporated under vacuum. The resulting solid was dissolved in CD_2Cl_2 and analyzed by ^1H NMR spectroscopy (**Figure ES7**).

Table ES1. Stock solutions and amounts of **L1** to **L6** and $[\text{Pd}(\text{CH}_3\text{CN})_4](\text{BF}_4)_2$ used for the competition experiment.

Species	Stock solution concentration [mM]	Volume [μL]	Mass [mg]	Final concentration [mM]
L1	21.61	208.2	-	2.34
L2	18.07	249.1		
L3	10.96	410.5		
L4	6.69	673.0		
L5	21.47	209.6		
L6	-	-	2.17	
$[\text{Pd}(\text{CH}_3\text{CN})_4](\text{BF}_4)_2$	26.07	172.6	-	

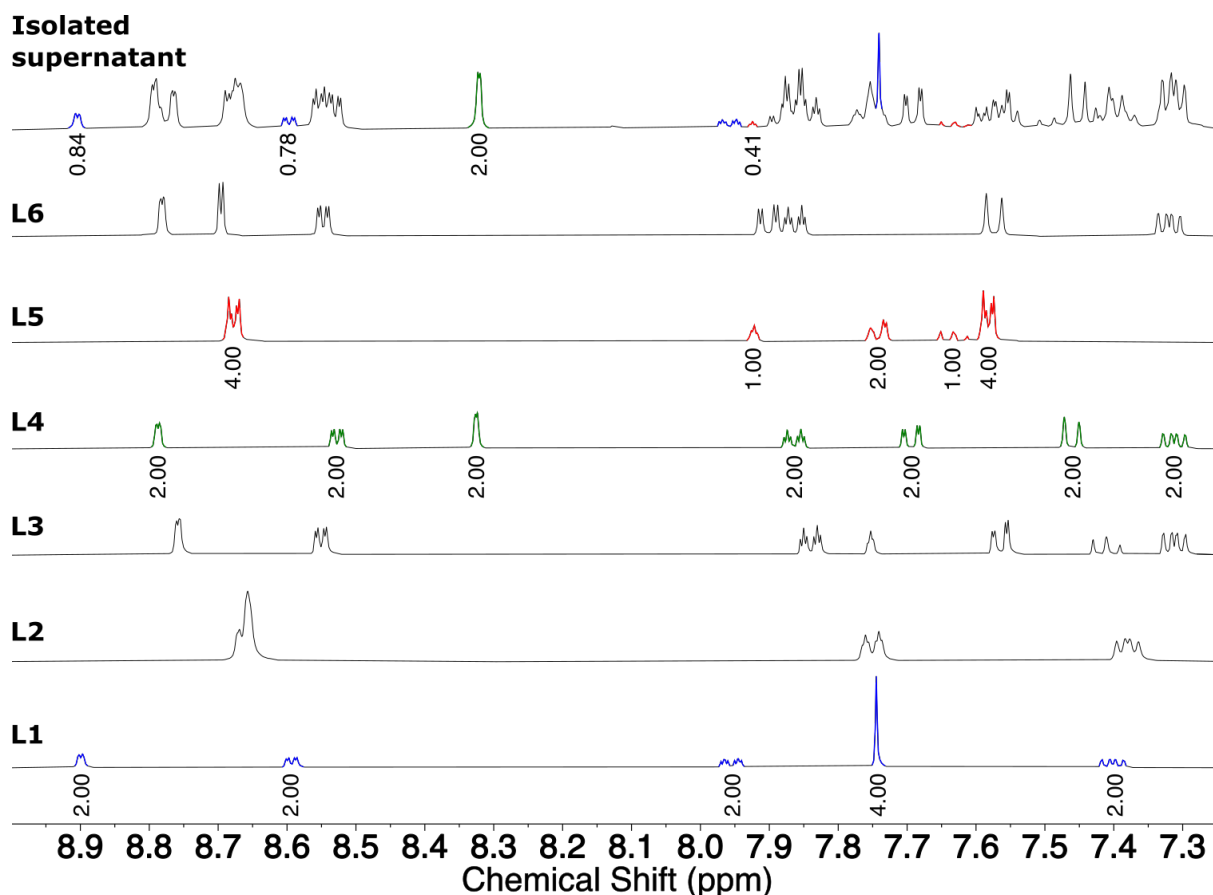


Figure ES7. Comparison of the ^1H NMR (400 MHz) spectra (CD_2Cl_2 , aromatic region) of **L1–L6**, and of the solids obtained after removal of the precipitate ('isolated supernatant'). Selected integrals are shown, highlighting the depletion of **L1** and **L5** with respect to **L4**.

Equilibration of **L1**, **L2**, **L5**, **L6**, $[\text{Pd}_2(\text{L3})_4](\text{BF}_4)_4$, $[\text{Pd}_2(\text{L4})_4](\text{BF}_4)_4$ mixture

Separate solutions of $[\text{Pd}_2(\text{L3})_4](\text{BF}_4)_4$ and $[\text{Pd}_2(\text{L4})_4](\text{BF}_4)_4$ were prepared as follow: **L3** (1.64 mg, 5.85 μmol , 1 eq.) and **L4** (2.14 mg, 4.72 μmol , 1 eq.) were dissolved in 500 μL of a mixture of CD_3CN and CD_3NO_2 (8:2). To these solutions was added 0.5 equivalent of $[\text{Pd}(\text{CH}_3\text{CN})_4](\text{BF}_4)_2$ (115.6 and 93.2 μL of a 25.3 mM stock solution respectively) and the resulting mixtures were heated at 60 $^\circ\text{C}$ while stirring for 17 h. ^1H NMR confirmed the full conversion to the expected assemblies. 3 μmol (1eq.) of **L1**, **L2**, **L5** and **L6** and 0.75 μmol (0.25 eq.) of $[\text{Pd}_2(\text{L3})_4](\text{BF}_4)_4$ and $[\text{Pd}_2(\text{L4})_4](\text{BF}_4)_4$ were mixed together and 147.5 μL of the solvent mixture added so that the final concentrations would be similar to the ones considered for the competition experiment.

The mixture was stirred for 24 h at 65 °C to allow equilibration, and a ^1H NMR spectrum was recorded afterwards.

Table ES2. Stock solutions and amounts of **L1**, **L2**, $[\text{Pd}_2(\text{L3})_4](\text{BF}_4)_4$, $[\text{Pd}_2(\text{L4})_4](\text{BF}_4)_4$, **L5**, and **L6** used for the control experiment.

Species	Concentration [mM]	Volume [μL]	Mass [mg]	Final concentration [mM]
L1	21.78	137.7	-	2.340
L2	18.07	166.1		2.340
$[\text{Pd}_2(\text{L3})_4](\text{BF}_4)_4$	2.38	315.7		0.585
$[\text{Pd}_2(\text{L4})_4](\text{BF}_4)_4$	1.99	377.0		0.585
L5	21.74	138.0		2.340
L6	-	-		1.45

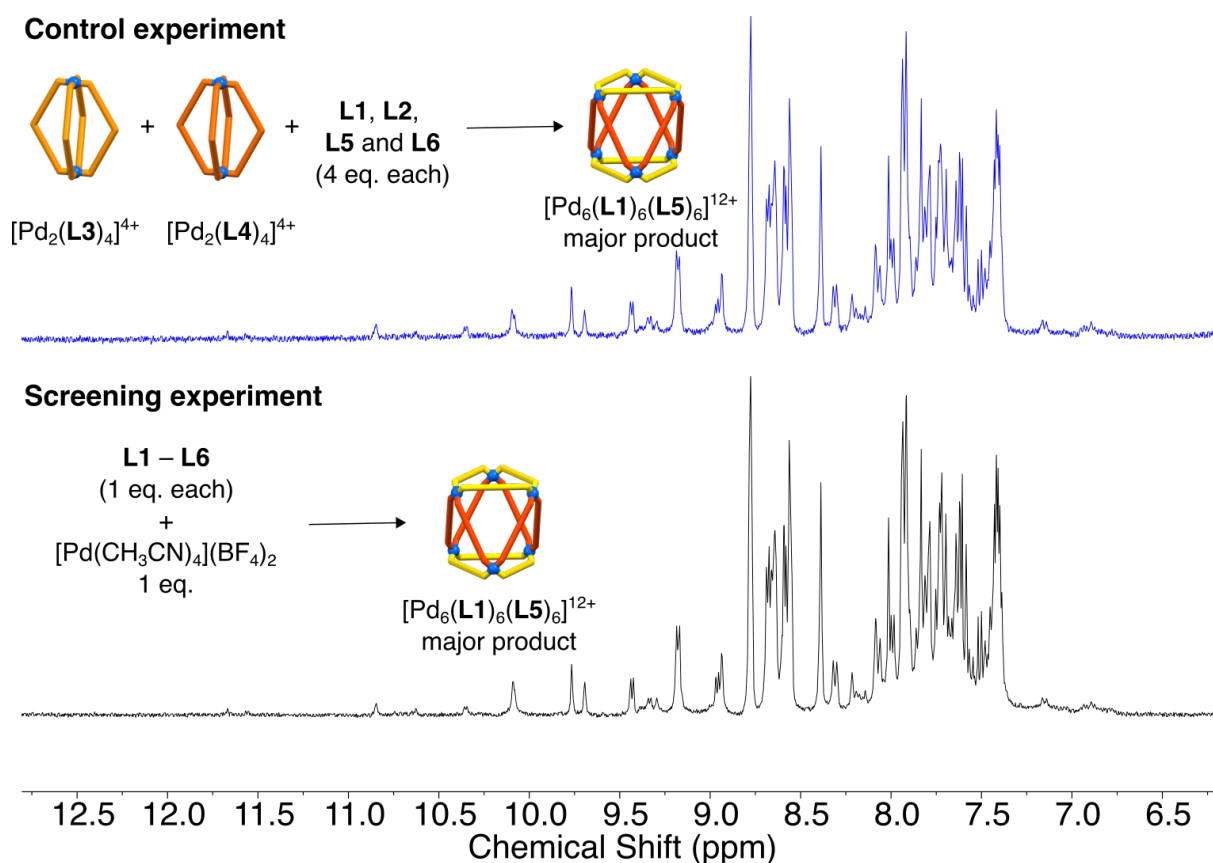


Figure ES8. Comparison of the ^1H NMR (400 MHz) spectra recorded for the screening (bottom) and control experiment (top) in a mixture of CD_3CN and CD_3NO_2 (8:2).

Equilibration of a $[\text{Pd}_4(\text{L1})_8](\text{BF}_4)_8$ and $[\text{Pd}_{12}(\text{L5})_{24}](\text{BF}_4)_{24}$ mixture

Separate solutions of $[\text{Pd}_4(\text{L1})_8](\text{BF}_4)_8$ and $[\text{Pd}_{12}(\text{L5})_{24}](\text{BF}_4)_{24}$ were prepared as follow: aliquots of stock solutions ($\text{CD}_3\text{CN}/\text{CD}_3\text{NO}_2$, 8:2) containing the ligands **L1** and **L5** ($2.70 \mu\text{mol}$ each; for details see **Table ES3**) were added to a vial. Subsequently, $[\text{Pd}(\text{CH}_3\text{CN})_4](\text{BF}_4)_2$ ($1.35 \mu\text{mol}$) and $400 \mu\text{L}$ of the solvent mixture ($\text{CD}_3\text{CN}/\text{CD}_3\text{NO}_2$, 8:2) were added, and the mixtures were heated at $60 \text{ }^\circ\text{C}$ for 17 h while stirring. ^1H NMR confirmed the full conversion to the expected assemblies. $0.144 \mu\text{mol}$ (3 eq.) of $[\text{Pd}_4(\text{L1})_8](\text{BF}_4)_8$ and $0.048 \mu\text{mol}$ (1 eq.) of $[\text{Pd}_{12}(\text{L5})_{24}](\text{BF}_4)_{24}$ were mixed together in an NMR tube and heated at $60 \text{ }^\circ\text{C}$. ^1H -NMR spectra were recorded at several time intervals over a period of 3 months.

Table ES3. Stock solutions and amounts of **L1**, **L2**, $[\text{Pd}_4(\text{L1})_8](\text{BF}_4)_8$ and $[\text{Pd}_{12}(\text{L5})_{24}](\text{BF}_4)_{24}$ used for the control experiment.

Species	Concentration [mM]	Volume [μL]	Final concentration [mM]
L1	21.53	125.4	4.61
L2	21.53	125.4	4.61
$[\text{Pd}_4(\text{L1})_8](\text{BF}_4)_8$	0.58	250.0	0.29
$[\text{Pd}_{12}(\text{L5})_{24}](\text{BF}_4)_{24}$	0.19	250.0	0.10

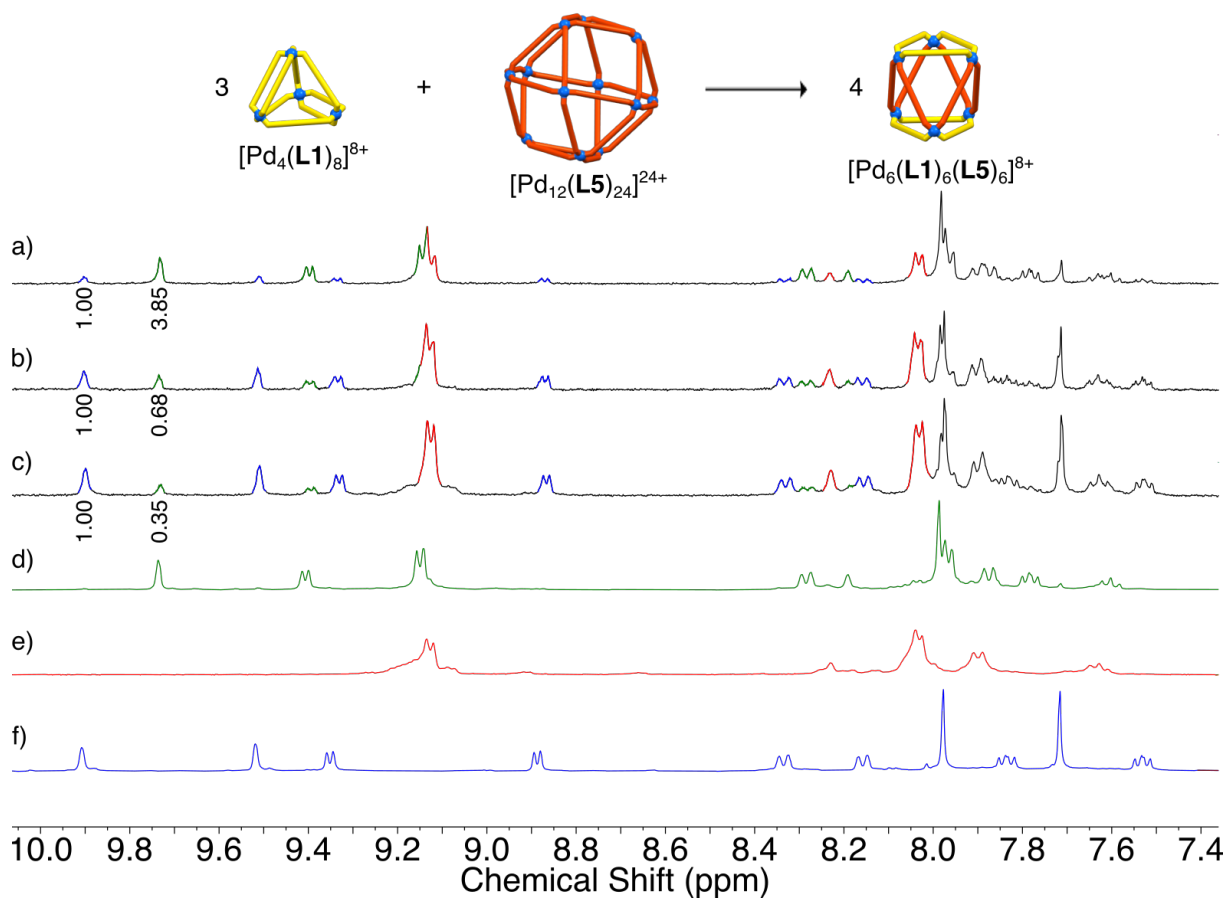


Figure ES9. (a,b,c) ^1H NMR (400 MHz) spectra of the reaction mixture after 85, 40 and 11 days respectively and of (d) $[\text{Pd}_6(\text{L1})_6(\text{L5})_6]^{12+}$, (e) $[\text{Pd}_{12}(\text{L5})_{24}]^{24+}$ and (f) $[\text{Pd}_4(\text{L1})_8]^{8+}$.

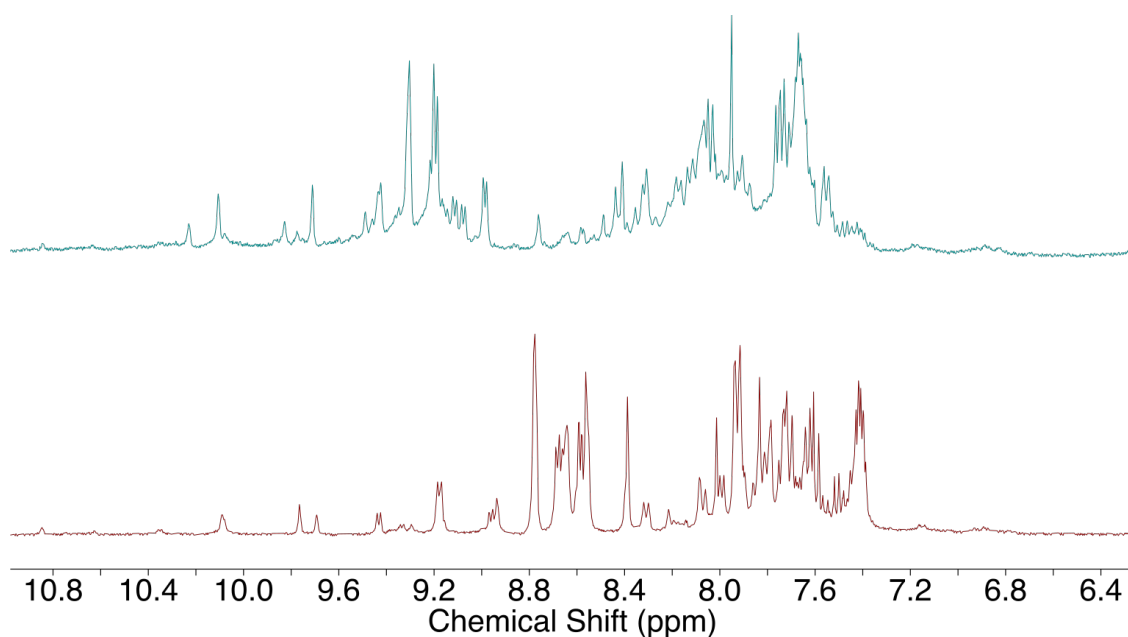


Figure ES10. Top: ^1H NMR (400 MHz) spectrum of an equilibrated mixture containing **L1–L6** and stoichiometric amounts of $[\text{Pd}(\text{CH}_3\text{CN})_4](\text{BF}_4)_2$ ($[\text{ligand}]_{\text{total}}:[\text{Pd}] = 2:1$) in a mixture of CD_3CN and CD_3NO_2 (8:2). For comparison, the spectrum of the competition experiment with substoichiometric amounts of Pd is given at the bottom.

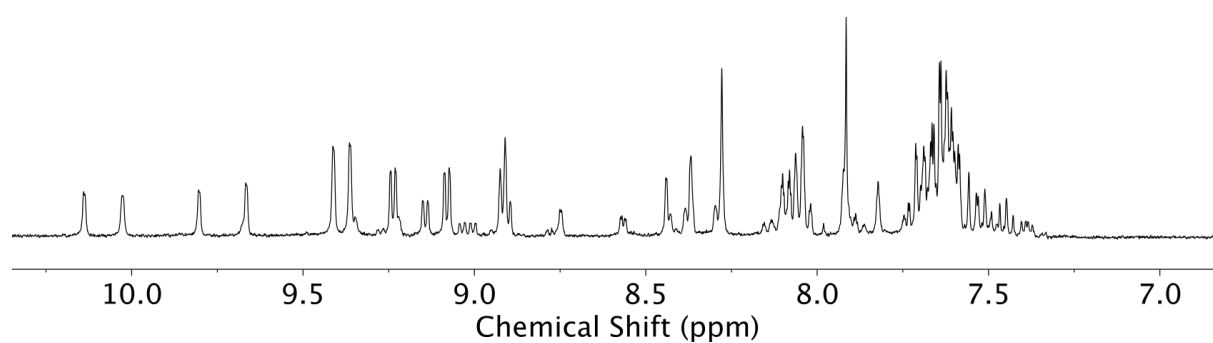


Figure ES11. Aromatic region of the ^1H NMR (400 MHz, CD_3CN) of an equilibrated (1:2:1:2) mixture of **L1**, **L3**, **L4** and $[\text{Pd}(\text{CH}_3\text{CN})_4](\text{BF}_4)_2$.

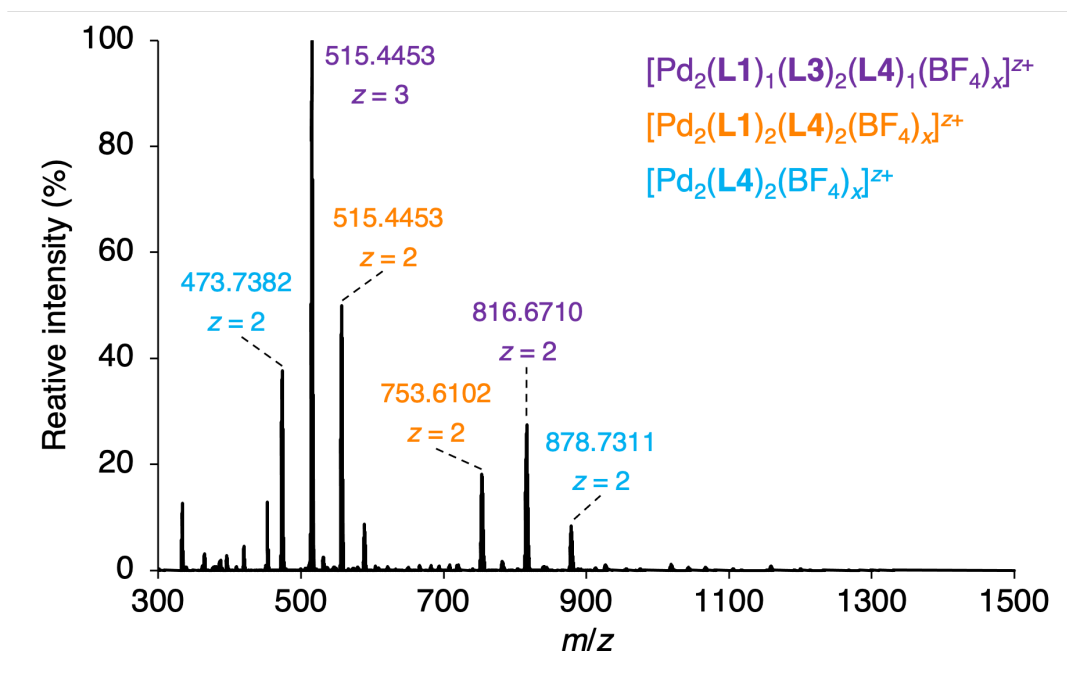


Figure ES12. HRMS of the equilibrated (1:2:1:2) mixture of **L1**, **L3**, **L4** and $[\text{Pd}(\text{CH}_3\text{CN})_4](\text{BF}_4)_2$. The color coding indicates the major products that could be identified.

8.3 Experimental details for Chapter 3

The full experimental details can be found in the supplementary information of the related publication.^[170]

Synthesis and characterization

The ligands **L9** to **L12** (**Figure ES13**) were synthesized following literature procedures.^[28,66,112,245]

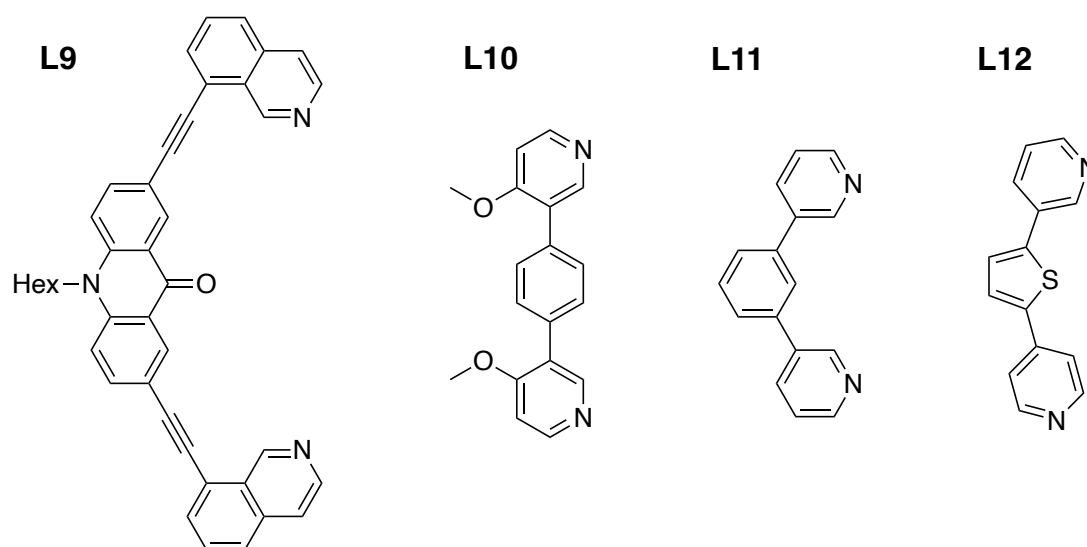


Figure ES13. Structures of ligands **L9** to **L12**.

The literature-known homoleptic assemblies, **C1** to **C11**, were obtained as follows: a mixture of the respective ligand (**L1–L7** and **L9–L12**, 2.0 eq.) and $[\text{Pd}(\text{CH}_3\text{CN})_4](\text{BF}_4)_2$ (1.0–1.1 eq.) in CD_3CN was stirred at 70 °C for 12 h. The formation of the desired product was confirmed by ^1H NMR spectroscopy. In all cases, the spectra matched what has been reported in the literature.^[26,47,49,66,112] The concentrations were adjusted according to the solubility of the ligand and/or the final assembly (**Table ES4**).

Table ES4. Amounts of ligands and $[\text{Pd}(\text{CH}_3\text{CN})_4](\text{BF}_4)_2$ used for the synthesis of the homoleptic assemblies and their final concentration.

Species	Formula	L	n_{L} [μmol]	n_{Pd} [μmol]	V_{tot} [mL]	Concentration [mM]
C1	$[\text{Pd}_4(\text{L1})_8](\text{BF}_4)_8$	L1	9.0	4.5	1.03	1.1
C2	$[\text{Pd}_2(\text{L2})_4](\text{BF}_4)_4$	L2	6.8	3.7	0.66	2.6
C3	$[\text{Pd}_2(\text{L3})_4](\text{BF}_4)_4$	L3	9.7	4.9	1.07	2.3
C4	$[\text{Pd}_2(\text{L4})_4](\text{BF}_4)_4$	L4	9.4	4.7	1.07	2.2
C5	$[\text{Pd}_{12}(\text{L5})_{24}](\text{BF}_4)_{24}$	L5	14.1	7.7	0.72	0.8
C6	$\{[\text{Pd}_2(\text{L6})_4]_2\}(\text{BF}_4)_8$	L6	3.1	1.6	0.65	0.6
C7	$[\text{Pd}_6(\text{L7})_{12}](\text{BF}_4)_{12}$	L7	14.9	7.5	1.08	1.2
C8	$[\text{Pd}_2(\text{L9})_4](\text{BF}_4)_4$	L9	4.6	2.3	1.00	1.1
C9	$[\text{Pd}_3(\text{L10})_6](\text{BF}_4)_6$	L10	5.6	3.1	0.61	1.6
C10	$[\text{Pd}_2(\text{L11})_4](\text{BF}_4)_4$	L11	5.0	2.5	0.75	1.7
C11	$[\text{Pd}_6(\text{L12})_{12}](\text{BF}_4)_{12}$	L12	5.2	2.6	1.00	0.8

The literature-known heteroleptic assemblies, **C12** and **C13**, were obtained as follows: an equimolar mixture of the two respective ligands (**L4/L9** or **L1/L5**) and $[\text{Pd}(\text{CH}_3\text{CN})_4](\text{BF}_4)_2$ in CD_3CN was stirred at 70 °C for 12 h (**Table ES5**). The formation of the desired product was confirmed by ^1H NMR spectroscopy. In both cases, the spectra matched what has been reported in the literature.^[26,49]

Table ES5. Amounts of ligands and $[\text{Pd}(\text{CH}_3\text{CN})_4](\text{BF}_4)_2$ used for the synthesis of the heteroleptic assemblies and their final concentration.

Species	Formula	L	n_{L} [μmol]	n_{Pd} [μmol]	V_{tot} [mL]	Concentration [mM]
C12	$[\text{Pd}_2(\text{L4})_2(\text{L9})_2](\text{BF}_4)_4$	L4	2.3	2.3	1.00	1.2
		L9	2.3			
C13	$[\text{Pd}_6(\text{L1})_6(\text{L5})_6](\text{BF}_4)_{12}$	L1	9.1	9.1	1.00	1.5
		L5	9.1			

[Pd₄(L9)₈(LiBF₄)₂(H₂O)₂](BF₄)₈ – [Pd(CH₃CN)₄](BF₄)₂ (7.65 μmol, 148.1 μL of a 51.7 mM stock solution in CD₃CN, 1 eq.) and LiBF₄ (114.8 μmol, 130.1 μL of a 882 mM stock solution in CD₃CN, 15 eq.) were added to a suspension of **L9** (15.30 μmol, 8.90 mg, 2 eq.) in CD₃CN (635 μL) and the mixture was heated at 70 °C for 12 h to give **[Pd₄(L9)₈(LiBF₄)₂(H₂O)₂](BF₄)₈**. ¹H NMR spectroscopy confirmed the full conversion to the expected assembly. ¹H NMR (400 MHz, CD₃CN) δ 10.61 (s, 2H), 10.25 (s, 1H), 10.01 (s, 1H), 9.91 (s, 1H), 9.59 (s, 1H), 9.32 (s, 1H), 9.29 (d, 1H), 9.23 (s, 1H), 9.18 (s, 1H), 9.13 (d, 1H), 8.89 (d, 1H), 8.78 (d, 1H), 8.63 (s, 1H), 8.62 (s, 1H), 8.47 (s, 1H), 8.42 (d, 1H), 8.34 (d, 1H), 8.31 (d, 1H), 7.08 (d, 1H), 6.58 (d, 1H), 6.37 (d, 1H), 5.95 (d, 1H). Due to important overlap, only the signals listed above could be assigned unambiguously.

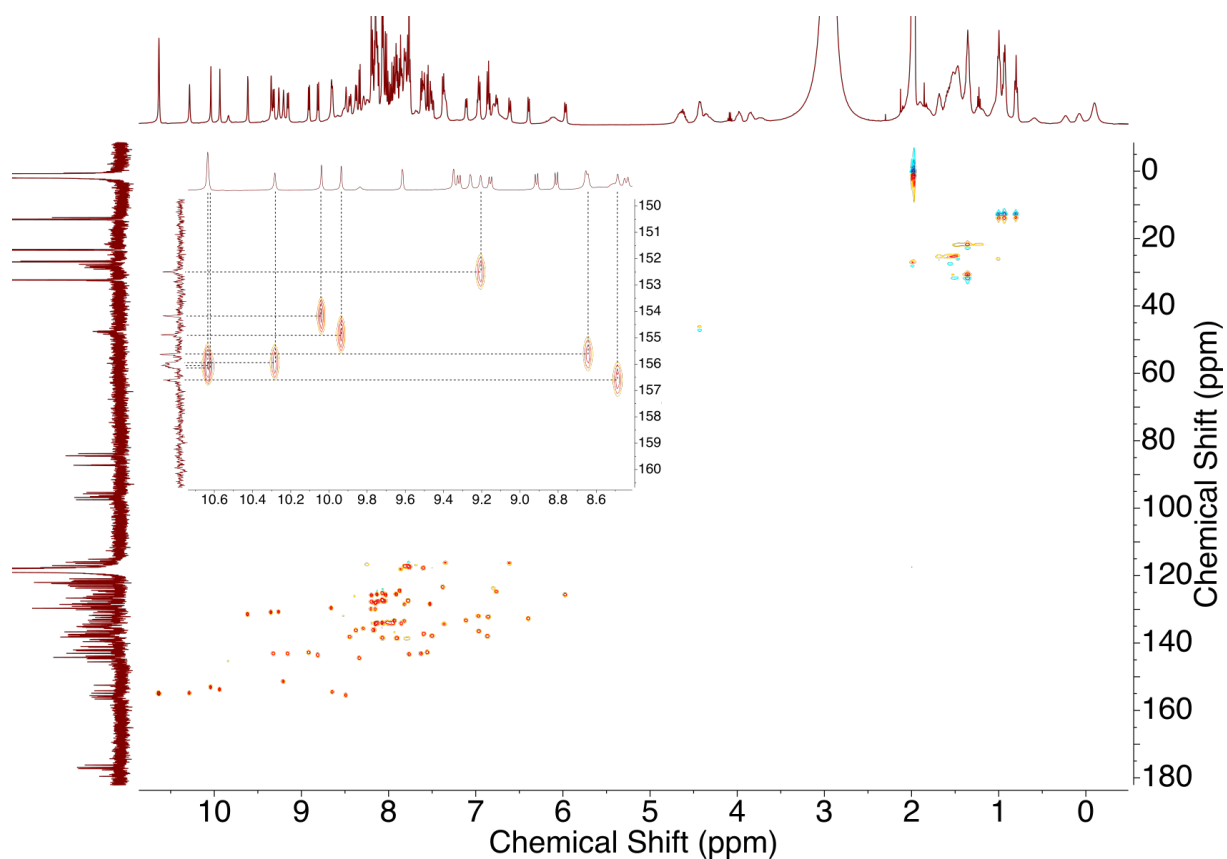


Figure ES14. ¹H-¹³C HSQC NMR (500 MHz, CD₃CN) spectrum of **[Pd₄(L9)₈](BF₄)₈**. The inset shows a zoom in the region 8.6 to 10.7 ppm and 149 to 161 ppm.

Screening experiment

An aliquot of a stock solution of LiBF₄ in CD₃CN was added to an NMR tube containing a solution of the respective Pd assembly (**C1** to **C13**, 1 equiv, [C_x] = 0.4–2.6 mM, Li:[C_x] = 50:1) in CD₃CN, and a ¹H NMR spectrum was recorded immediately after mixing. A second spectrum was recorded for **C8** after 20 h equilibration at room temperature (**Figure ES16**). Minor differences between the spectra were observed in several cases. In order to classify as a 'hit', differences of at least 0.05 ppm were observed for signals of protons pointing towards the cage interior. Changes of this magnitude were observed for **C1** and **C8**, and the interaction of these cages with LiBF₄ was investigated in more detail.

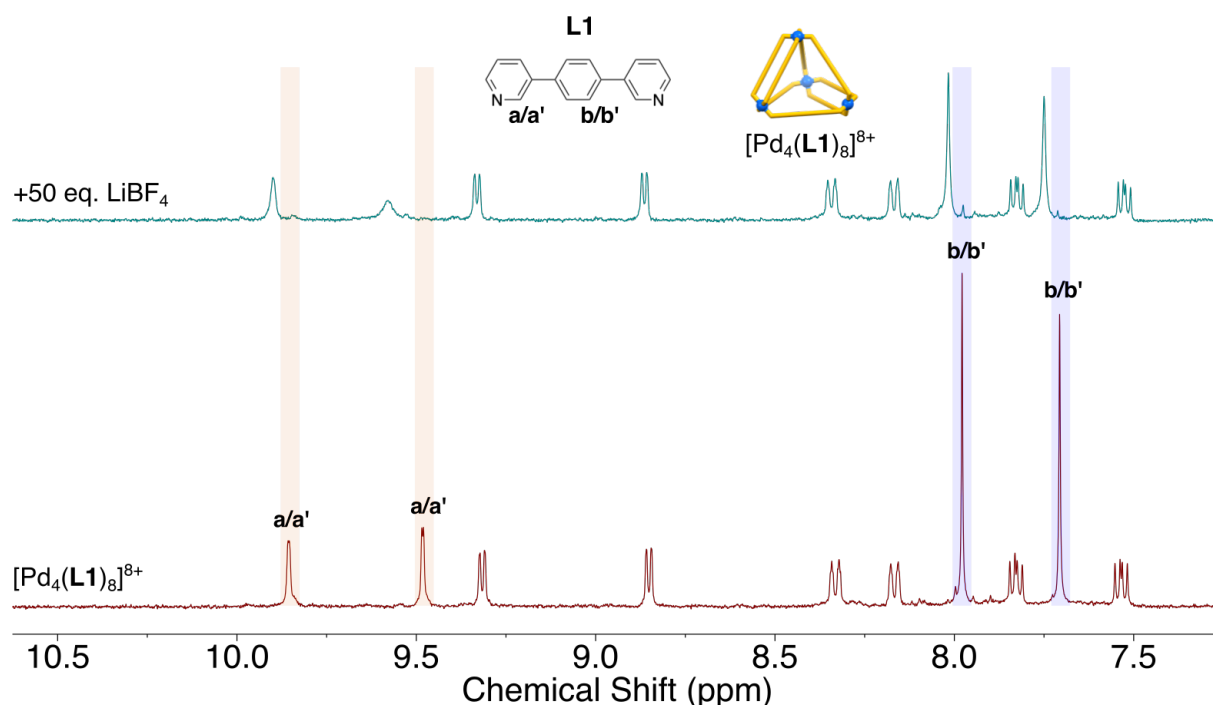


Figure ES15. ¹H NMR (400 MHz, CD₃CN) spectrum of [Pd₄(L1)₈](BF₄)₈ (**C1**) before (bottom) and after (top) addition of LiBF₄.

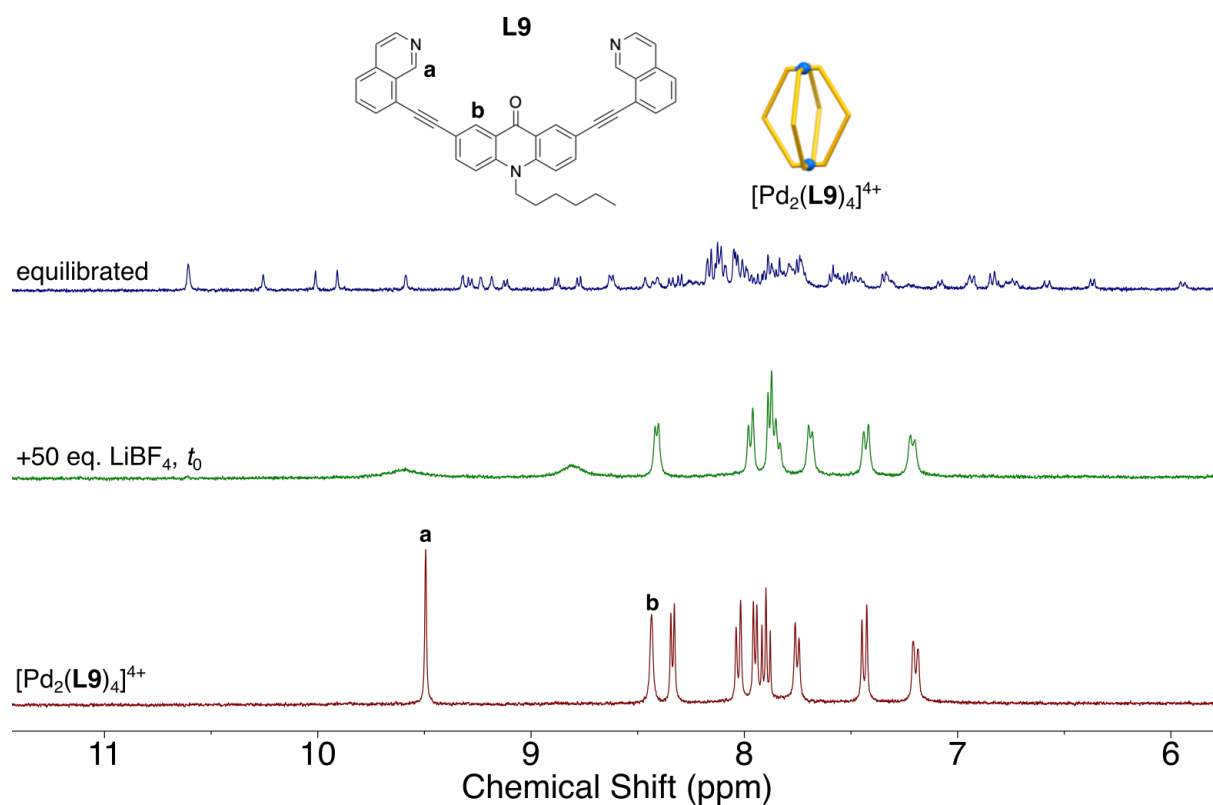


Figure ES16. ^1H NMR (400 MHz, CD_3CN) spectrum of $[\text{Pd}_2(\text{L2})_4](\text{BF}_4)_4$ (**C8**) before (bottom), directly after addition of LiBF_4 (middle), and after equilibration at room temperature for 20 h (top).

NMR titration

Aliquots (0.92 μL) of a 2.17 M stock solution of LiBF_4 in CD_3CN were added to a solution of $[\text{Pd}_4(\text{L1})_8](\text{BF}_4)_8$ (400 μL , 0.5 mM) in an NMR tube. ^1H NMR spectra were recorded directly after each addition (**Figure ES17**). The data were fitted to a 1:1 binding model using the online tool available at: <http://supramolecular.org>. Dilution effects were accounted for.

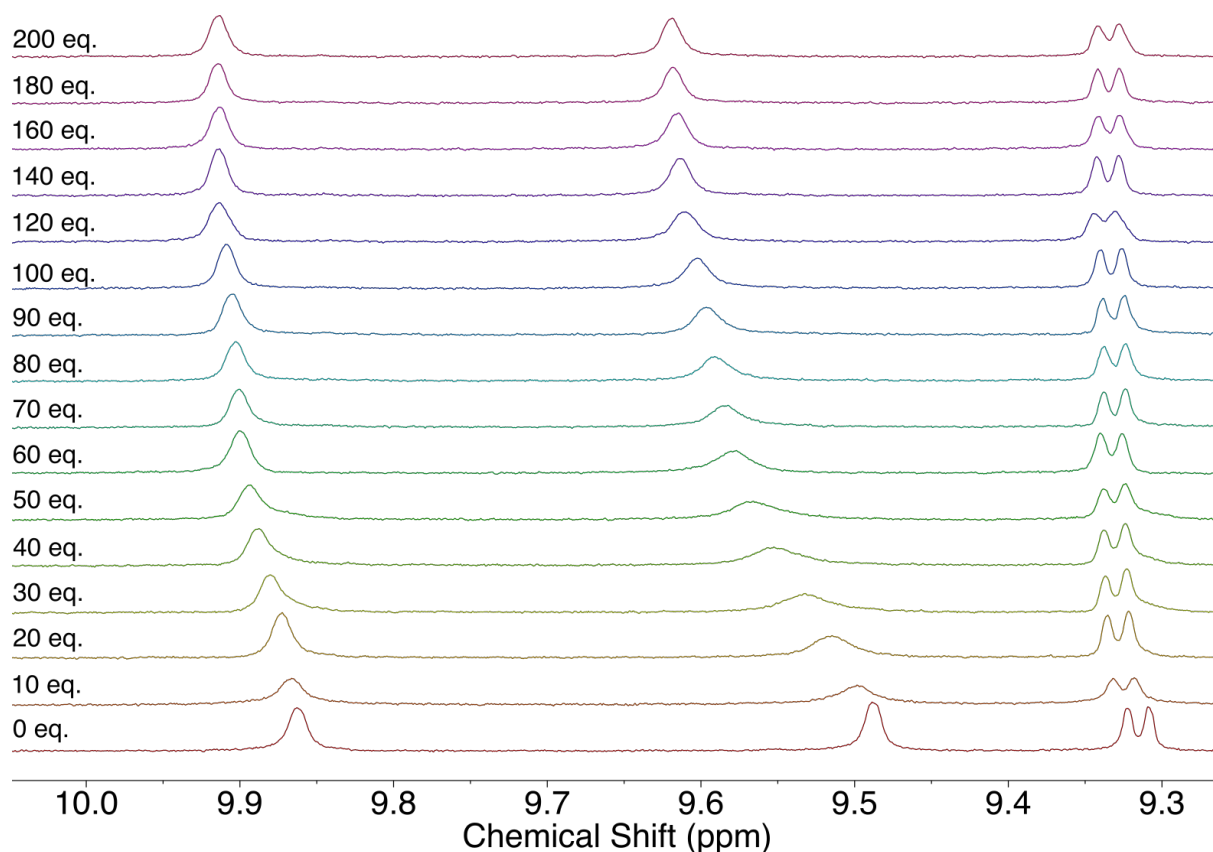


Figure ES17. ^1H NMR (400 MHz, CD_3CN) spectrum of $[\text{Pd}_4(\text{L1})_8](\text{BF}_4)_8$ in the presence of increasing amounts of LiBF_4 .

Time-dependence of the $[\text{Pd}_2(\text{L9})_4]$ to $[\text{Pd}_4(\text{L9})_8]$ transformation

An aliquot (35.9 μL , 50 eq.) of a 741.7 mM stock solution of LiBF_4 was added to 460 μL of a 1.16 mM solution (1 eq.) of $[\text{Pd}_2(\text{L9})_4](\text{BF}_4)_4$ in an NMR tube, and ^1H NMR spectra were recorded at different time intervals until complete conversion to $[\text{Pd}_4(\text{L9})_8](\text{BF}_4)_8$ was observed. The experiment was conducted at room temperature (**Figure ES18**).

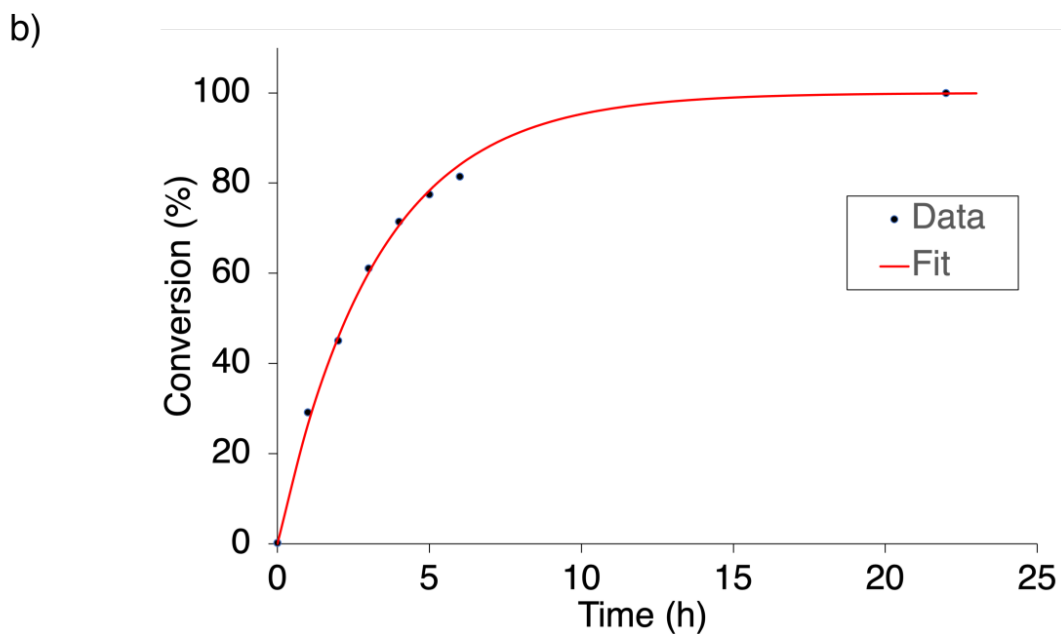
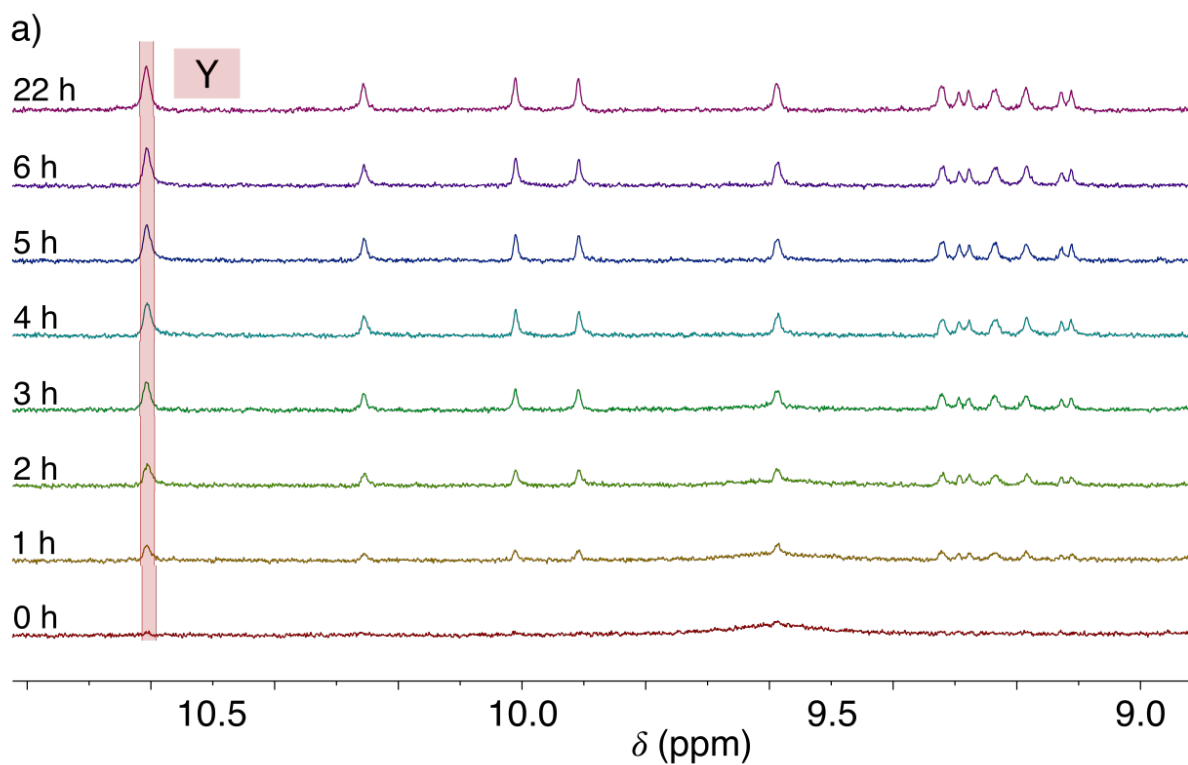


Figure ES18. (a) Aromatic region of the ^1H NMR spectra recorded at different time intervals after the addition of 50 eq. of LiBF_4 to a solution of $[\text{Pd}_2(\text{L9})_4](\text{BF}_4)_4$ at room temperature. (b) Conversion as a function of time as determined by integration of the signal at 10.7 ppm. The data were fitted to a first order kinetic model ($t_{1/2} = 135$ min).

Synthesis in the presence of water

[Pd(CH₃CN)₄](BF₄)₂ (1.36 μmol, 30.3 μL of a 44.8 mM stock solution in CD₃CN, 1 eq.) was added to a suspension of **L9** (2.72 μmol, 1.58 mg, 2 eq.) in CD₃CN (870 μL). Subsequently, D₂O (100 μL, 10 vol%) was added and the mixture was heated at 70 °C for 5 days to ensure equilibration. The resulting solution was analyzed by ¹H NMR spectroscopy and HRMS.

Addition of Na⁺, K⁺ and Cs⁺ salts

Aliquots of stock solutions of NaOTf (2.8 μL, 1.6 μmol, 5 eq.), KPF₆ (16.6 μL, 1.6 μmol, 5 eq.) and CsBPh₄ (131.6 μL, 1.6 μmol, 5 eq.) in CD₃CN were added to three separate NMR tubes containing a solution of [Pd₂(**L9**)₄](BF₄)₄ (450 μL, 0.32 μmol, 1 eq.). ¹H NMR spectra were recorded directly afterwards.

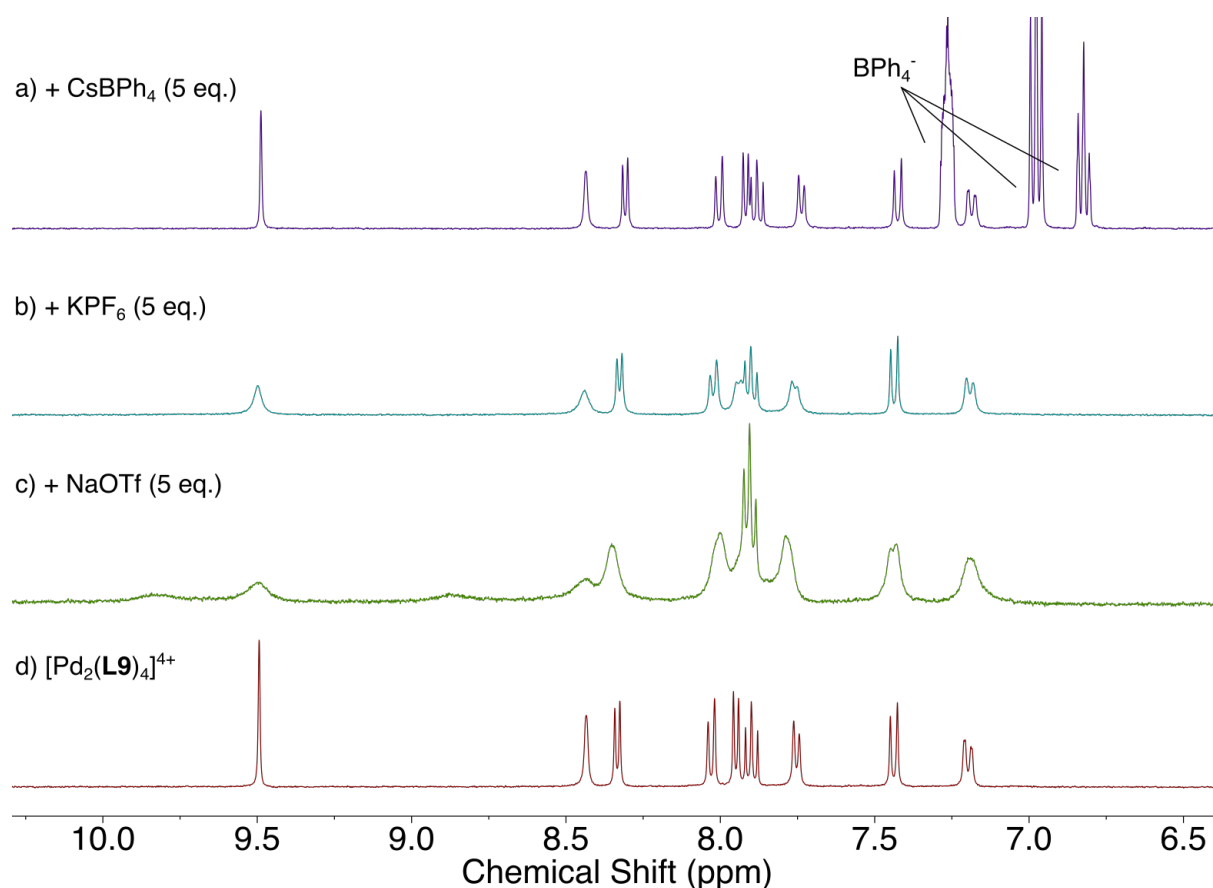


Figure ES19. Aromatic region of the ¹H NMR spectra (400 MHz, CD₃CN) of the equilibrated mixture of [Pd₂(**L9**)₄](BF₄)₄ with (a) CsBPh₄, (b) KPF₆, (c) NaOTf and (d) of [Pd₂(**L9**)₄](BF₄)₄ alone.

Mixture of LiOTf and NaOTf

Aliquots of stock solutions of LiOTf (18.3 μL , 18.2 μmol , 50 eq) and NaOTf (33.0 μL , 18.3 μmol , 50 eq.) in CD_3CN were added to a solution of $[\text{Pd}_2(\text{L9})_4](\text{BF}_4)_4$ (450 μL , 0.37 μmol , 1 eq.) in an NMR tube and the mixture was allowed to equilibrate for 72 h at RT.

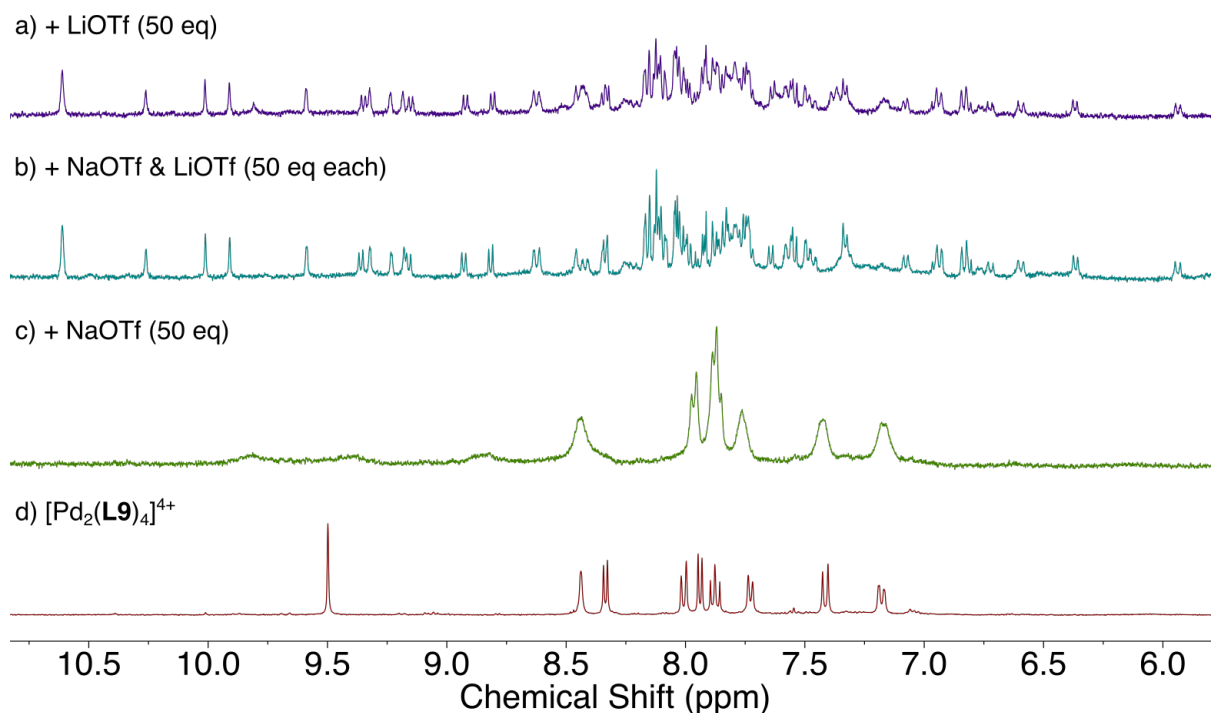


Figure ES20. Aromatic region of the ^1H NMR spectra (400 MHz, CD_3CN) of the equilibrated mixture of $[\text{Pd}_2(\text{L9})_4](\text{BF}_4)_4$ with (a) LiOTf, (b) NaOTf and LiOTf, (c) NaOTf and of (d) $[\text{Pd}_2(\text{L9})_4](\text{BF}_4)_4$ alone.

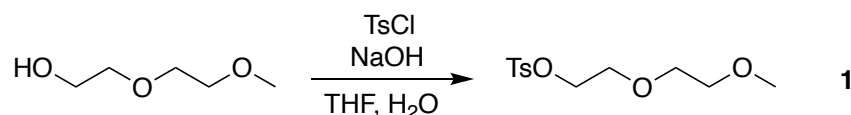
Addition of LiBF_4 under dry conditions

LiBF_4 was dried for 48 h at 70 $^\circ\text{C}$ under vacuum and stored under an N_2 atmosphere. $[\text{Pd}(\text{CH}_3\text{CN})_4](\text{BF}_4)_2$ (90.2 μL , 2.74 μmol , 1 eq.) was added to a suspension of ligand **L9** (2.9 mg, 4.98 μmol , 2 eq.) in CD_3CN (1.4 mL) under an atmosphere of N_2 and the mixture was stirred at RT for 48 h in the presence of 4 \AA molecular sieves. The formation of $[\text{Pd}_2(\text{L9})_4](\text{BF}_4)_4$ was confirmed by ^1H NMR spectroscopy. An aliquot of the $[\text{Pd}_4(\text{L9})_8](\text{BF}_4)_8$ stock solution (500 μL , 1 eq.) was then transferred to a vial containing dry LiBF_4 (3.2 mg, 83 eq.). A ^1H NMR spectrum was recorded after 72 h at room temperature. D_2O (0.5 μL) was then added to the tube and another ^1H NMR spectrum was recorded after equilibration for 72 h at room temperature.

8.4 Experimental details for Chapter 4

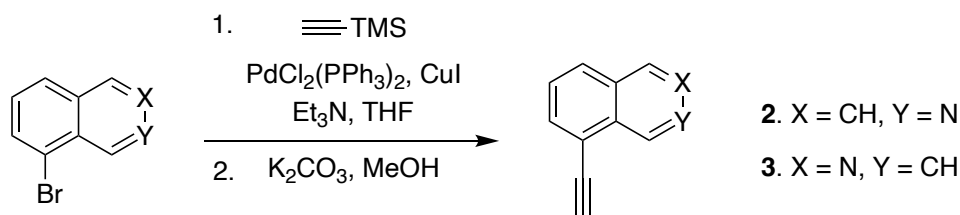
Compound **8** was synthesized following a reported procedure.^[246]

Synthesis and characterization



Scheme ES2. Synthesis of compound **1**.

2-(2-Methoxyethoxy)ethyl *p*-Toluenesulfonate (1). Compound **1** was synthesized according to a reported procedure.^[247] Diethylene glycol monomethyl ether (1.7 mL, 14 mmol, 1 eq.) in THF (3 mL) was added dropwise to a solution of NaOH (0.8 g, 20 mmol, 1.4 eq) in water (3 mL) and THF (3 mL) at 0 °C. The mixture was stirred for 30 min before a solution of *p*-toluenesulfonyl chloride (2.7 g, 14 mmol, 1 eq.) in THF (5 mL) was added dropwise. After stirring at room temperature for 2 h, the mixture was poured onto 20 mL of ice. The solution was extracted with dichloromethane (3x15 mL), the organic fractions collected, dried with MgSO₄, and the solvent removed by rotary evaporation to yield compound **1** as a colorless oil (3.5 g, 91 %). The product was used without further purification. ¹H NMR (400 MHz, CDCl₃) δ 7.80 (d, 2H), 7.34 (d, 2H), 4.17 (t, 2H), 3.69 (t, 2H), 3.60–3.55 (m, 2H), 3.51–3.44 (m, 2H), 3.35 (s, 3H), 2.45 (s, 3H).

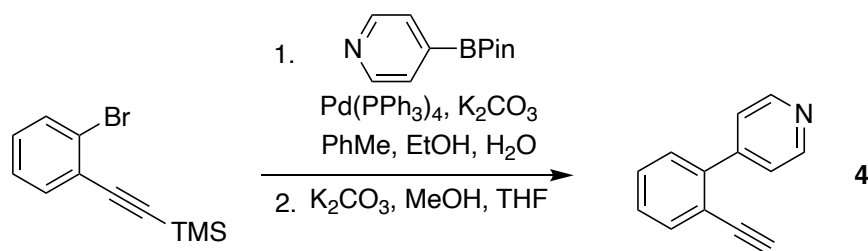


Scheme ES3. Synthesis of compound **2** and **3**.

Compounds **2** and **3** were synthesized based on a reported procedure.^[248]

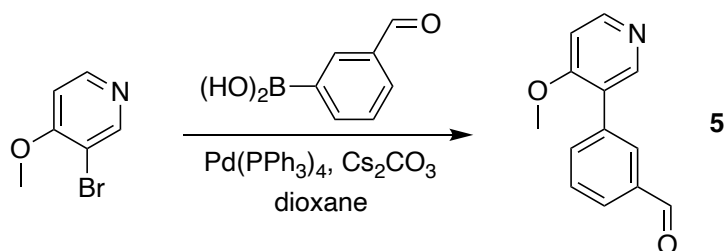
8-Ethynylisoquinoline (2). 8-Bromoisoquinoline (1.50 g, 7.2 mmol), $\text{PdCl}_2(\text{PPh}_3)_2$ (505 mg, 0.7 mmol, 0.1 eq.) and CuI (274 mg, 1.4 mmol, 0.2 eq.) were introduced in a schlenk flask and degassed via N_2 /vacuum cycles. Previously degassed (via freeze-thaw cycles) THF (15 mL) and triethylamine (15 mL) was added and trimethylsilylacetylene (1.55 mL, 11 mmol, 1.5 eq) was introduced. The mixture was stirred at 85 °C for 18 h. After cooling, EtOAc (20 mL) was added and the reaction mixture was filtered over Celite. The solvent was evaporated under reduced pressure and the residue was dissolved in MeOH (15 mL). K_2CO_3 (1.1 g, 8.0 mmol, 1.1 eq) was add and the mixture stirred for 2 h at room temperature. EtOAc (20 mL) was then added, the solids were filtered off and the solvent evaporated. The dark brown residue was purified by column chromatography (EtOAc/petroleum ether 4:6) to give the title compound as an off-white crystalline solid (695 mg, 63%). $^1\text{H NMR}$ (400 MHz, CDCl_3) δ 9.73 (t, 1H), 8.59 (d, 1H), 7.85–7.76 (m, 2H), 7.70–7.59 (m, 2H), 3.55 (s, 1H).

5-Ethynylisoquinoline (3). The same procedure as for the synthesis of **2** was used with 5-bromoisoquinoline (1.50 g, 7.2 mmol) as the starting material. After a column chromatography (DCM/MeOH 95:5), **3** was obtained as an off-white crystalline solid, (984 mg, 89%). $^1\text{H NMR}$ (400 MHz, CDCl_3) δ 9.2.7 (s, 1H), 8.63 (d, 1H), 8.11 (d, 1H), 7.99 (d, 1H), 7.92 (dd, 1H), 7.57 (t, 1H), 3.52 (s, 1H).



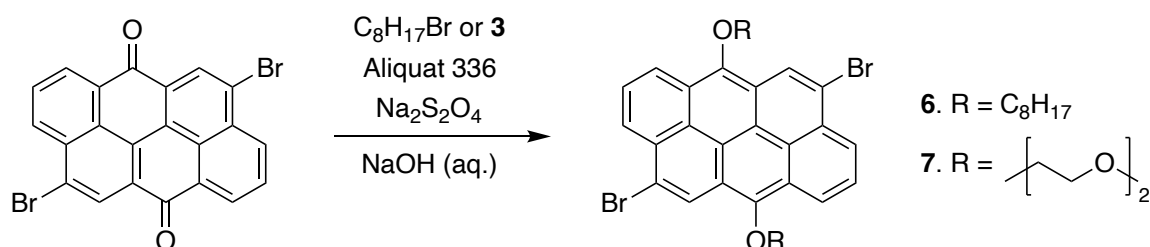
Scheme ES4. Synthesis of compound **4**.

4-(2-Ethynylphenyl)pyridine (4). 4-Pyridyl boronic pinacol ester (667 mg, 3.3 mmol, 1.1 eq), Pd(PPh₃)₄ (104 mg, 0.09 mmol, 0.03 eq.) and K₂CO₃ were introduced in a schlenk flask and degassed via N₂/vacuum cycles. 12 mL of a previously degassed toluene/EtOH/water mixture (8:2:2) and (2-bromo-phenylethynyl)trimethylsilane (0.64 mL, 3.0 mmol, 1 eq.) were added under N₂. The reaction mixture was stirred at 100 °C for 20 h. After cooling, the mixture was extracted with Et₂O, the organic phase collected and evaporated under reduced pressure. The residue was dissolved in THF (6 mL) and MeOH (6mL), and K₂CO₃ (0.5g, 0.54 mmol, 1.2 eq.) added. After stirring for 3 h at room temperature, water (15 mL) was added. The resulting mixture was extracted with EtOAc, and the combined organic phases washed with brine, dried over MgSO₄ and evaporated. The dark brown residue was purified by column chromatography (EtOAc/petroleum ether 2:8) to give the title compound as a red oil (96 mg, 18%). ¹H NMR (400 MHz, CDCl₃) δ 8.70–8.64 (m, 2H), 7.69–7.59 (m, 1H), 7.55–7.49 (m, 2H), 7.49–7.42 (m, 1H), 7.41–7.35 (m, 2H), 3.09 (s, 1H).



Scheme ES5. Synthesis of compound **5**.

3-(4-Methoxy-3-pyridine)benzaldehyde (5). 3-Formylphenyl boronic acid (0.87 g, 5.8 mmol, 1.1 eq), Pd(PPh₃)₄ (578 mg, 0.5 mmol, 5 %mol) and Cs₂CO₃ (2.65 g, 25 mmol, 2.5 eq) were introduced in a schlenk vessel under N₂. 10 mL of previously degassed (via N₂ bubling) dioxane was added and 3-bromo-4-methoxypyridine (0.67 mL, 5.3 mmol, 1.5 eq) was introduced. This mixture was stirred 3 days at 95 °C. The reaction was quenched with 10 mL of water, then 5 mL of brine was added and the crude was extracted with DCM. The solvent was evaporated and the resulting residue was purified by column chromatography (EtOAc/petroleum ether 9:1) to give the title compound as a brown solid, 919 mg, 94%. ¹H NMR (400 MHz, CDCl₃) δ 10.08 (s, 1H), 8.52 (d, 1H), 8.46 (s, 1H), 8.04 (t, 1H), 7.90 (dt, 1H), 7.78 (dt, 1H), 7.62 (t, 1H), 6.93 (d, 1H), 3.90 (s, 3H).

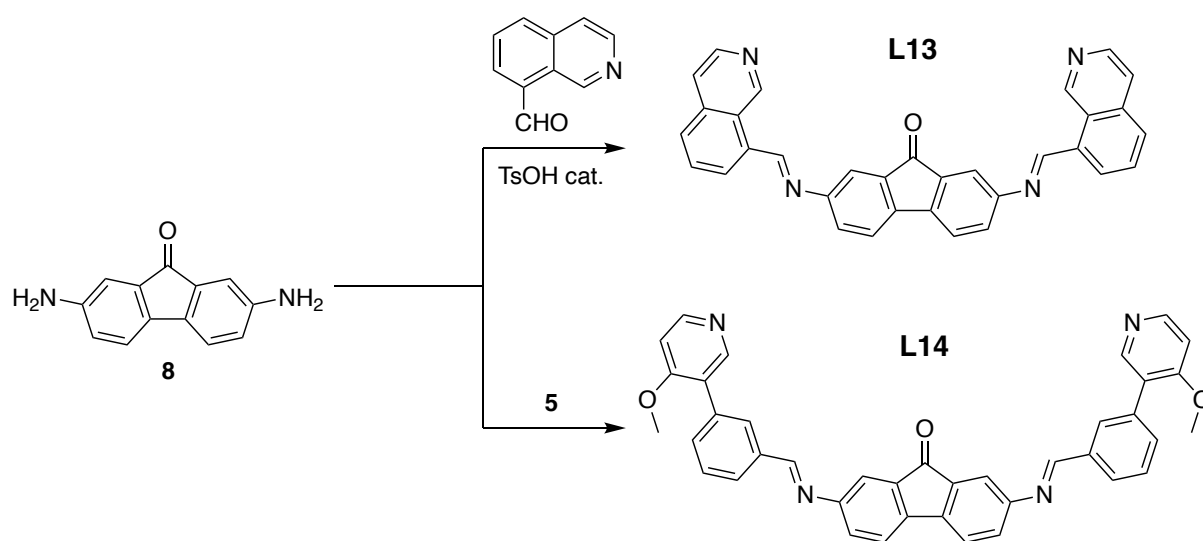


Scheme ES6. Synthesis of compounds **6** and **7**.

Compounds **6** and **7** were synthesized based on a reported procedure.^[249]

4,10-Dibromo-6,12-bis(octyloxy)anthanthrene (6). A flask under argon was charged with, VAT-orange 3 (4,10-dibromoanthanthrone, 500 mg, 1.08 mmol, 1.0 eq.), *n*-bromooctane (1.5 mL, 8.72 mmol, 8.0 eq), $Na_2S_2O_4$ (485 mg, 2.78 mmol, 2.5 eq), Aliquat 336 (0.6 mL, 1.3 mmol, 2.5 eq), aqueous NaOH (0.1 M, 50 mL, 5 mmol, 5.0 eq). The mixture was purged for 30 min with a flow of N₂ and then heated at 60 °C for 24 h until it turned colorless. After cooling down, the mixture was extracted with CHCl₃ (3 x 30 mL) and the combined organic phases dried over MgSO₄. The solvent was evaporated under reduced pressure and the residue was purified by column chromatography (DCM/petroleum ether 1:1) to yield **6** as a bright orange solid (516 mg, 69%). ¹H NMR (400 MHz, CDCl₃) δ 8.88–8.81 (m, 4H), 8.68 (d, 2H), 8.25 (t, 2H), 4.38 (t, 4H), 2.18 (p, 4H), 1.78 (p, 4H), 1.52–1.31 (m, 16H), 0.98–0.84 (m, 6H).

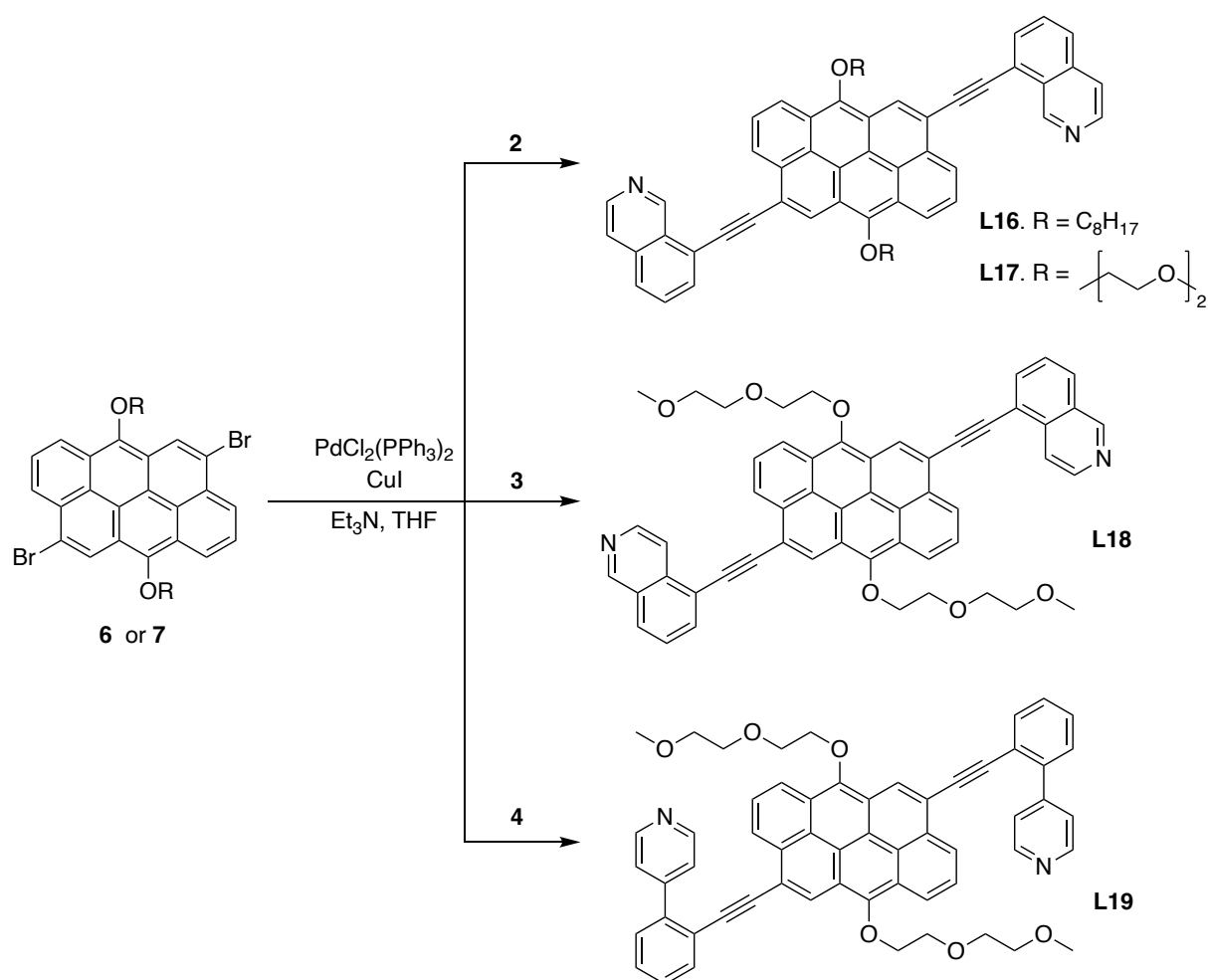
4,10-Dibromo-6,12-bis(2-(2-methoxyethoxy)ethoxy)anthanthrene (7). The same procedure as for the synthesis of **6** was followed using **1** (2.36 g, 8.62 mmol, 8 eq.) as the alkylating agent. Recrystallization in MeOH yielded **7** as a bright orange solid (510 mg, 70%). ¹H NMR (400 MHz, CDCl₃) δ 9.00 (s, 2H), 8.99–8.94 (m, 2H), 8.69 (d, 2H), 8.26 (t, 2H), 4.63–4.57 (m, 4H), 4.14–4.07 (m, 4H), 3.95–3.88 (m, 4H), 3.83–3.76 (m, 4H), 3.51 (s, 6H). ¹³C NMR (101 MHz, CDCl₃) δ 148.62, 130.53, 126.76, 126.33, 125.73, 125.32, 122.36, 107.55, 92.78, 75.77, 72.35, 71.26, 70.73, 59.45.



Scheme ES7. Synthesis of ligands **L13** and **L14**.

L13 was synthesized as follows: compound **8** (50 mg, 0.24mmol, 1.0 eq.), 8-formylisoquinoline (94 mg, 0.60 mmol, 2.5 eq) and TsOH (4 mg, 0.02 mmol, 0.1 eq.) were dissolved in EtOH (10 mL) and the mixture was refluxed for 2 h during which a red precipitate appeared. The precipitate was filtered, washed with cold EtOH and dried under vacuum to afford **L13** as a dark red-brown solid (98 mg, 84%). ¹H NMR (400 MHz, CDCl₃) δ 10.77 (s, 2H), 9.15 (s, 2H), 8.69 (d, 2H), 8.19–8.13 (m, 2H), 8.01 (d, 2H), 7.88 (t, 2H), 7.83 (d, 2H), 7.70–7.62 (m, 4H), 7.56 (dd, 2H). No ¹³C NMR spectrum could be recorded due to the low solubility of the product in usual solvents. HRMS (ESI/QTOF) *m/z*: [M+H]⁺ Calculated for C₃₃H₂₁N₄O⁺ 489.1710; Found 489.1706.

L14 was synthesized as follows Compound **8** (50 mg, 0.24 mmol) and compound **5** (110 mg, 0.60 mmol, 2.5 eq) were introduced in 10 mL of EtOH and the mixture was refluxed 3 days during which a red precipitate appeared. The precipitate was filtrated, washed with cold EtOH and dried under high vacuum to afford **L14** as a dark orange-brown solid (98 mg, 84%). ^1H NMR (400 MHz, CDCl_3) δ 8.60 (s, 2H), 8.52 (d, 2H), 8.50 (s, 2H), 8.07 (t, 2H), 7.94 (dt, 2H), 7.66 (dt, 2H), 7.61–7.50 (m, 6H), 7.39 (dd, 2H), 6.93 (d, 2H), 3.92 (s, 6H). ^{13}C NMR (101 MHz, CDCl_3) δ 162.59, 160.39, 152.65, 150.97, 150.79, 142.04, 135.98, 135.87, 135.64, 132.83, 130.5, 128.90, 128.62, 128.22, 125.74, 120.96, 116.18, 106.51, 55.52. HRMS m/z : $[\text{M}+2\text{H}]^{2+}$ Calculated for $\text{C}_{39}\text{H}_{30}\text{N}_4\text{O}_3^{2+}$ 301.1153; Found 301.1148.



Scheme ES8. Synthesis of ligands **L16** to **L19**.

L16 was synthesized as follows: compound **6** (83 mg, 0.12 mmol, 1.0 eq.), compound **2** (55 mg, 0.36 mmol, 3.0 eq.), PdCl₂(PPh₃)₂ (8 mg, 12 μmol, 0.1 eq.) and CuI (5 mg, 24 μmol, 0.2 eq.) were introduced in a schlenk tube and degassed via N₂/vacuum cycles. 6 mL of a previously degassed THF/triethylamine solution (1:1) were added and the mixture was stirred at 70 °C for 24 h. CHCl₃ (10 mL) was added, the mixture filtered and evaporated. The obtained residue was purified by column chromatography (CHCl₃/MeOH 8:2) to yield **L16** as a bright orange solid (60 mg, 60%). ¹H NMR (400 MHz, CDCl₃) δ 10.14 (s, 2H), 8.96–8.85 (m, 6H), 8.69, 8.31 (t, 2H), 8.10 (dd, 2H), 7.91 (d, 2H), 7.83–7.73 (m, 4H), 4.47 (t, 4H), 2.30–2.15 (m, 4H), 1.82 (q, 4H), 1.54–1.16 (m, 16H), 0.92–0.84 (m, 6H). ¹³C NMR (101 MHz, CDCl₃) δ 151.59, 144.08, 136.09, 132.22, 130.83, 130.05, 128.41, 128.26, 127.44, 126.57, 126.01, 124.78, 123.77, 121.95, 121.83, 121.59, 120.81, 120.53, 94.66, 90.55, 32.07, 31.00, 29.82, 29.57, 26.52, 22.85, 14.27. HRMS (ESI/QTOF) *m/z*: [M+H]⁺ Calculated for C₆₀H₅₅N₂O₂⁺ 835.4258; Found 835.4256.

L17 was synthesized as follows: compound **7** (80 mg, 0.12 mmol, 1.0 eq.) compound **2** (55 mg, 0.36 mmol, 3.0 eq.), PdCl₂(PPh₃)₂ (8 mg, 12 μmol, 0.1 eq.) and CuI (5 mg, 24 μmol, 0.2 eq.) were introduced in a schlenk tube and degassed via N₂/vacuum cycles. 6 mL of a previously degassed THF/triethylamine solution (1:1) were added and the mixture stirred at 70 °C for 24 h. CHCl₃ (10 mL) was added, the mixture filtered and evaporated. The obtained residue was purified by column chromatography (CHCl₃/MeOH 99:1) to yield **L17** as a bright orange solid (64 mg, 65%). ¹H NMR (400 MHz, CDCl₃) δ 10.10 (s, 2H), 9.02–8.96 (m, 4H), 8.88 (d, 2H), 8.67 (d, 2H), 8.28 (t, 2H), 8.06 (d, 2H), 7.86 (d, 2H), 7.78–7.67 (m, 4H), 4.70–4.64 (m, 4H), 4.20–4.13 (m, 4H), 3.98–3.91 (m, 4H), 3.80–3.73 (m, 4H), 3.42 (s, 5H). ¹³C NMR (101 MHz, CDCl₃) δ 151.51, 149.62, 144.00, 136.03, 132.16, 130.63, 130.02, 128.33, 128.19, 127.36, 126.61, 125.77, 124.58, 123.81, 122.08, 121.90, 121.66, 120.78, 120.60, 119.71, 94.68, 90.54, 75.79, 72.32, 71.24, 70.82, 59.34. HRMS (ESI/QTOF) *m/z*: [M+H]⁺ Calculated for C₅₄H₄₃N₂O⁶⁺ 815.3116; Found 815.3135.

L18 was synthesized as follows: compound **7** (80 mg, 0.12 mmol, 1.0 eq.), compound **3** (55 mg, 0.36 mmol, 3.0 eq), PdCl₂(PPh₃)₂ (8 mg, 12 μmol, 0.1 eq) and CuI (5 mg, 24 μmol, 0.2 eq.) were introduced in a schlenk tube and degassed via N₂/vacuum cycles. 6 mL of a previously degassed THF/triethylamine solution (1:1) were added and the mixture was stirred at 70 °C for 24 h. CHCl₃ (10 mL) was added, the mixture filtered and evaporated. The obtained residue was purified by column chromatography (CHCl₃/MeOH 97:3) to yield **L18** as a bright orange solid (62 mg, 63%). ¹H NMR (400 MHz, CDCl₃) δ 9.37 (s, 2H), 9.05 (s, 2H), 9.02 (dd, 1.0 Hz, 2H), 8.93 (dd, 2H), 8.77 (d, 2H), 8.47 (dt, 2H), 8.32 (d, 2H), 8.22 (dd, 2H), 8.08 (dt, 2H), 7.73 (dd, 2H), 4.72–4.66 (m, 4H), 4.20–4.13 (m, 4H), 3.97–3.90 (m, 4H), 3.79–3.72 (m, 4H), 3.40 (s, 6H). ¹³C NMR (101 MHz, CDCl₃) δ 153.10, 149.68, 144.46, 136.34, 134.76, 128.57, 128.24, 127.09, 126.65, 123.84, 122.07, 120.80, 119.21, 117.29, 94.27, 90.92, 87.46, 83.36, 75.83, 72.31, 71.26, 70.81, 59.34.

L19 was synthesized as follows: compound **7** (120 mg, 0.18 mmol, 1.0 eq.), compound **4** (96 mg, 0.54 mmol, 3.0 eq), PdCl₂(PPh₃)₂ (13 mg, 18 μmol, 0.1 eq.) and CuI (7 mg, 36 μmol, 0.2 eq.) were introduced in a schlenk tube and degassed via N₂/vacuum cycles. 9 mL of a previously degassed THF/triethylamine mixture (1:1) were added and the mixture stirred at 70 °C for 24 h. CHCl₃ (30 mL) was added, the mixture filtered and evaporated. The obtained residue was purified by column chromatography (CHCl₃/MeOH 97:3) to yield **L19** as a bright orange solid (81 mg, 52%). ¹H NMR (400 MHz, CDCl₃) δ 8.90 (dd, 2H), 8.84–8.78 (m, 4H), 8.74 (s, 2H), 8.16 (dd, 2H), 8.07 (d, 2H), 7.99–7.90 (m, 2H), 7.78–7.72 (m, 4H), 7.58–7.43 (m, 6H), 4.61–4.54 (m, 4H), 4.15–4.09 (m, 4H), 3.94–3.87 (m, 4H), 3.79–3.72 (m, 4H), 3.47 (s, 5H). ¹³C NMR (101 MHz, CDCl₃) δ 150.07, 149.41, 148.71, 141.47, 133.64, 130.59, 129.39, 129.15, 128.70, 127.66, 126.40, 125.70, 124.54, 123.62, 121.99, 121.83, 121.63, 120.83, 93.15, 92.24, 75.65, 72.31, 71.21, 70.76, 59.39. HRMS (ESI/QTOF) *m/z*: [M+H]⁺ Calculated for C₅₈H₄₇N₂O₆⁺ 867.3429; Found 867.3416.

[Pd₂(L16)₃]⁴⁺ and **[Pd₂(L17)₃]⁴⁺** were synthesized as follow: [Pd(CH₃CN)₄(BF₄)₂] (2 μmol, 2 eq.) from a stock solution was added to a suspension of **L16** or **L17** (3 μmol, 3 eq.) in CD₃CN (1.5 mL) and the mixture stirred for 12 h at 70 °C to give a clear red solution.

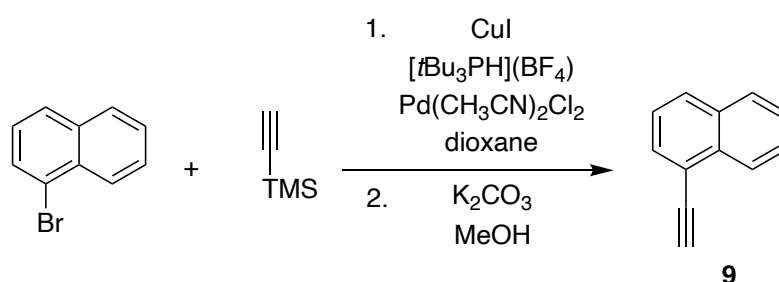
[Pd₂(L17)₃]⁴⁺ ¹H NMR (400 MHz, CD₃CN) δ 10.86 (s, 1H), 10.64 (s, 1H), 10.38 (s, 1H), 9.60 (d, 1H), 9.12 (d, 1H), 9.08–9.03 (m, 2H), 9.01 (d, 1H), 8.92–8.88 (m, 2H), 8.80 (d, 1H), 8.45 (d, 1H), 7.53 (s, 1H), 7.47 (t, 1H), 7.39 (d, 1H), 7.30 (d, 1H), 7.23 (s, 1H), 6.96 (t, 1H).

8.5 Experimental details for Chapter 5

The full experimental details can be found in the supplementary information of the related publication.^[250]

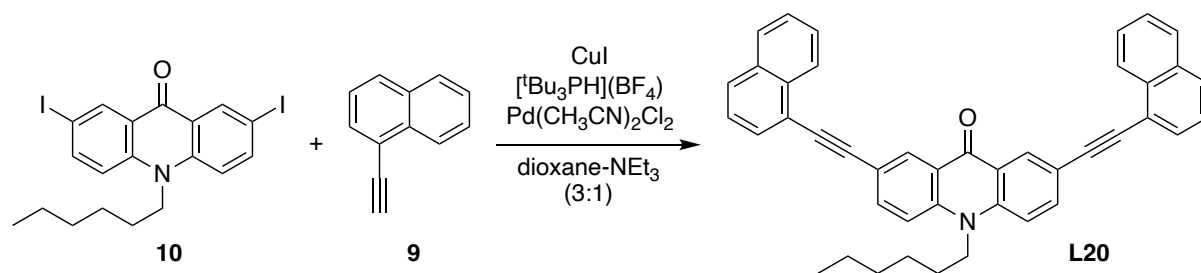
Synthesis and characterization

Compound **10** was synthesized following a reported procedure.^[251]



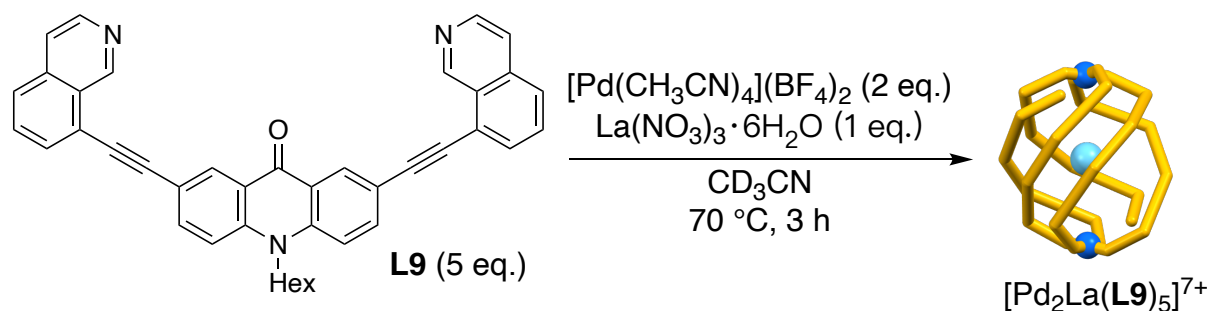
Scheme ES9. Synthesis of compound **9**.

1-Ethynynaphthalene (9). 1-Bromonaphthalene (1.43 g, 6.9 mmol, 1.0 eq) was degassed via vacuum/N₂ cycles. Trimethylsilylacetylene (1.25 mL, 9.0 mmol, 1.3 eq.), CuI (57 mg, 0.3 mmol, 0.04 eq.), [tBu₃PH](BF₄) (120 mg, 0.4 mmol, 0.06 eq), Pd(CH₃CN)₂Cl₂ (65 mg, 0.3 mmol, 0.04 eq.) and 30 mL of a previously degassed dioxane-NEt₃ mixture (3:1) were added under N₂ and the mixture was stirred at 70 °C for 20 h. After cooling-down to room temperature, the mixture was diluted with EtOAc (30 mL) and filtered through celite. The solvent was evaporated, replaced with DCM (5 mL), and passed through a silica plug. After evaporation under reduced pressure, the residue was redissolved in MeOH (40 mL) and K₂CO₃ (250 mg, excess) was added to the solution. After stirring overnight at room temperature, the suspension was filtered. The solvent was evaporated and the crude product was purified by column chromatography (100% hexane) to give **1** as a red oil (43 % yield). The chemical shifts observed in the ¹H NMR spectrum (400 MHz, CDCl₃) matched those reported in the literature.^[252] **1** was used directly in the next step without any further purification.



Scheme ES10. Synthesis of ligand **L20**.

L20 was synthesized as follow: a mixture of compound **10** (213 mg, 0.40 mmol, 1.0 eq.), **9** (183 mg, 1.20 mmol, 3.0 eq.) CuI (8 mg, 0.04 mmol, 0.1 eq), [tBu₃PH](BF₄) (18 mg, 0.06 mmol, 0.15 eq), and Pd(CH₃CN)₂Cl₂ (11 mg, 0.04 mmol, 0.1 eq.) was degassed via vacuum/N₂ cycles. 10 mL of a previously degassed dioxane-NEt₃ mixture (3:1) were added under N₂ and the solution was stirred at 80 °C for 24 h. After cooling-down to room temperature, the residue was diluted with CHCl₃ (10 mL) and filtered over celite. The solvent was removed under vacuum. The solid was redissolved in DCM (5 mL) and passed through a silica column. The yellow fluorescent fractions ($\lambda_{\text{exc}} = 366 \text{ nm}$) were collected and the solvent was evaporated under vacuum. The crude product was recrystallized from hot EtOAc to give **L2** as a yellow solid (68 mg, 29 % yield). ¹H NMR (500 MHz, CDCl₃, 298 K) δ 8.89 (d, 2H), 8.51 (d, 2H), 7.98 (dd, 2H), 7.88 (t, 4H), 7.81 (dd, 2H), 7.65 (ddd, 2H), 7.56 (m, 4H), 7.49 (dd, 2H), 4.41 (t, 2H), 1.99 (m, 2H), 1.65–1.39 (m, 6H), 0.97 (t, 3H). ¹³C NMR (125 MHz CDCl₃) δ 176.91, 141.28, 136.88, 133.40, 133.37, 131.75, 130.58, 128.99, 128.47, 127.08, 126.66, 126.46, 125.46, 122.71, 120.95, 117.03, 115.32, 93.61, 88.25, 46.73, 31.67, 27.43, 26.76, 22.82, 14.18. ESI-MS *m/z* calculated for C₄₃H₃₄NO⁺ [M+H]⁺ 580.264, found 580.264 .



Scheme ES11. Synthesis of $[\text{Pd}_2\text{La}(\text{L1})_5]^{7+}$.

$[\text{Pd}_2\text{La}(\text{L9})_5]^{7+}$ was synthesized as follow: $\text{La}(\text{NO}_3)_3 \cdot 6\text{H}_2\text{O}$ (0.7 μmol , 2.02 μL of a 133.9 mM stock solution in CD_3CN , 1.0 eq.) was added to a mixture of $[\text{Pd}(\text{CH}_3\text{CN})_4](\text{BF}_4)_2$ (1.4 μmol , 28.3 μL of a 49.3 mM stock solution in CD_3CN , 2.0 eq.) and **L9** (2.0 mg, 3.5 μmol , 5.0 eq.) in CD_3CN (1 mL). The mixture was heated at 70 $^\circ\text{C}$ for 3 h to give $[\text{Pd}_2\text{La}(\text{L9})_5]^{7+}$. ^1H NMR (800 MHz, CD_3CN , 298 K) δ 10.28 (s, 1H), 9.57 (s, 1H), 9.44 (s, 1H), 9.26 (s, 1H), 9.19 (s, 1H), 8.79 (d, 1H), 8.76 (s, 1H), 8.66 (s, 1H), 8.57–8.40 (m, 2H), 8.30 (d, 1H), 8.24 (s, 1H), 8.07 (d, 1H), 8.00 (t, 1H), 7.96 (d, 1H), 7.96–7.93 (m, 2H), 7.90 (d, 1H), 7.86 (t, 1H), 7.82 (d, 1H), 7.74–7.67 (m, 3H), 7.64 (d, 1H), 7.59–7.53 (m, 4H), 7.51 (m, 2H), 7.48–7.41 (m, 2H), 7.26 (t, 1H), 7.23 (d, 1H), 7.12 (d, 1H), 7.00–6.93 (m, 2H), 6.91–6.86 (m, 3H), 6.84–6.78 (m, 4H), 6.71 (d, 1H), 4.37–3.91 (m, 6H), 1.73–1.30 (m, 24H), 1.05, (t, 3H), 1.02 (t, 3H), 0.98 (t, 3H). ^{13}C NMR (200 MHz, CD_3CN , 298 K) δ 179.04, 177.70, 177.17, 157.35, 155.66, 154.26, 153.78, 150.51, 145.16, 145.00, 144.81, 144.59, 144.28, 142.49, 142.39, 141.81, 140.76, 140.53, 138.79, 138.09, 137.82, 137.49, 137.18, 137.09, 136.73, 136.41, 136.19, 136.15, 136.05, 135.32, 135.05, 134.88, 134.57, 134.38, 133.12, 132.46, 132.41, 132.34, 132.11, 131.48, 131.20, 130.48, 129.79, 129.63, 129.31, 128.69, 128.27, 128.25, 128.17, 127.99, 127.83, 126.49, 126.12, 126.10, 125.41, 124.89, 122.91, 122.24, 122.06, 121.27, 121.23, 120.95, 120.34, 119.19, 119.63, 119.35, 118.95, 117.82, 117.70, 117.47, 116.37, 116.03, 115.46, 96.43, 95.52, 95.28, 94.92, 93.46, 86.71, 86.49, 85.71, 83.93, 82.73, 48.35, 47.90, 47.59, 32.34, 32.21, 32.06, 28.73, 28.72, 28.25, 26.78, 26.77, 26.62, 23.49, 23.42, 23.33, 14.37, 14.34, 14.30.

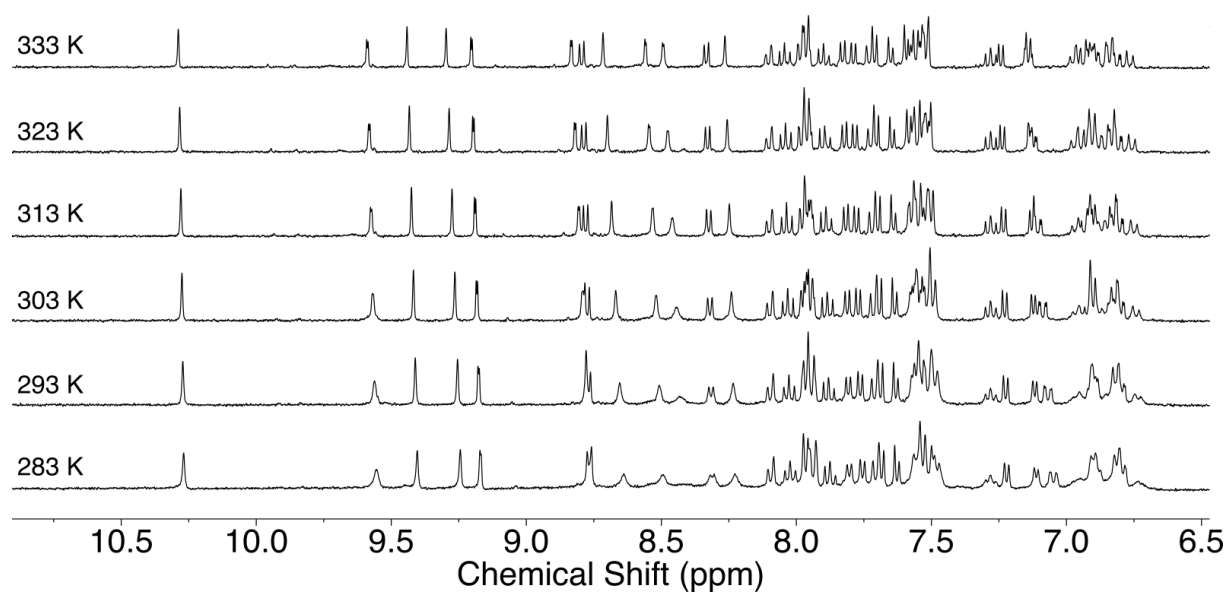


Figure ES 21. Variable temperature ^1H NMR (500 MHz) spectra of $[\text{Pd}_2\text{La}(\text{L9})_5]^{7+}$.

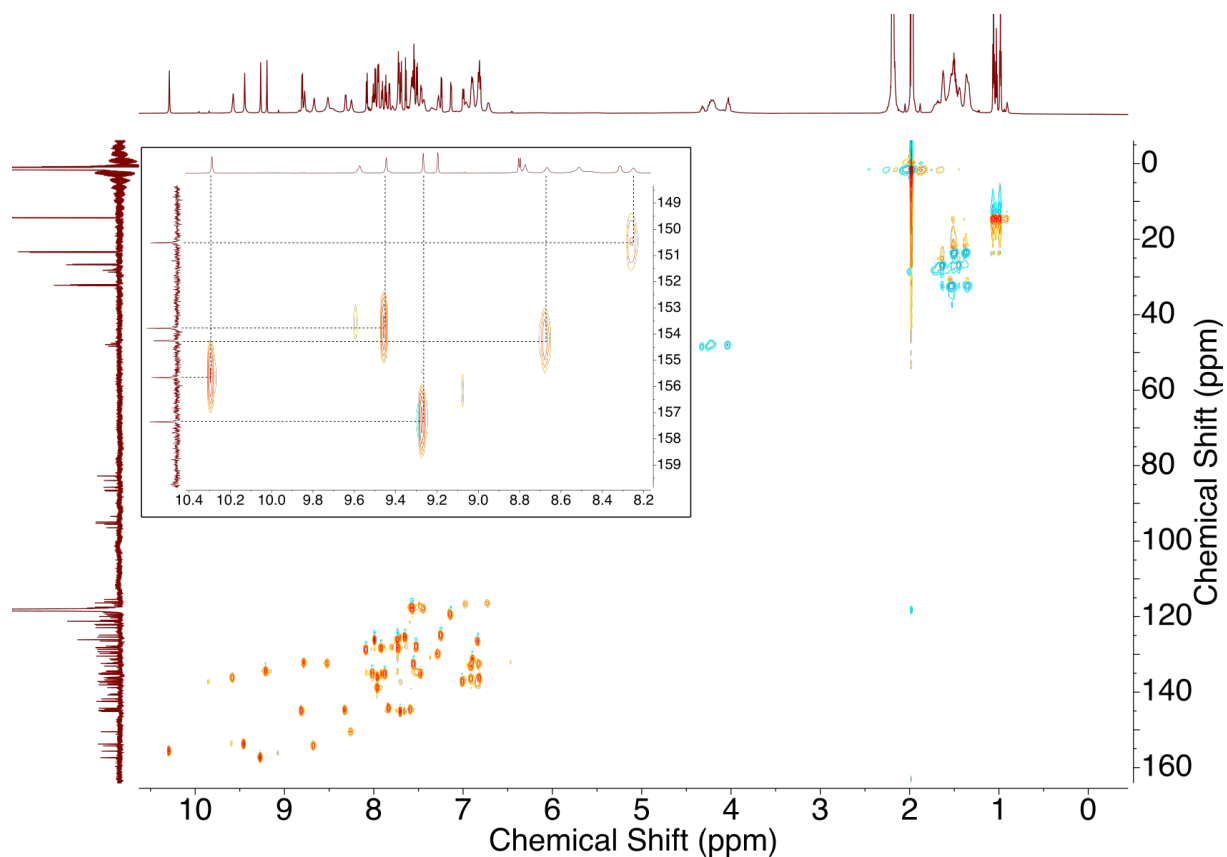
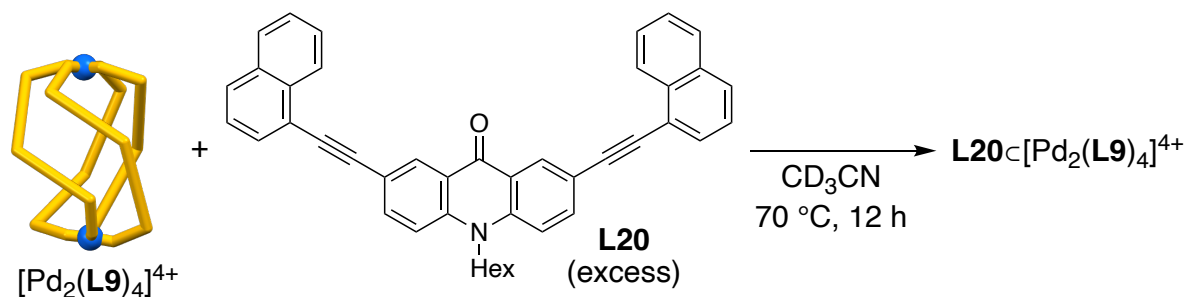


Figure ES 22. ^1H - ^{13}C HSQC NMR (500 MHz, CD_3CN) spectrum of $[\text{Pd}_2\text{La}(\text{L9})_5]^{7+}$. The inset shows a zoom in the region 8.2 to 10.4 ppm and 148 to 160 ppm.

Addition of L20 to $[\text{Pd}_2(\text{L9})_4]^{4+}$



Scheme ES12. Equilibration of a mixture of a mixture of $[\text{Pd}_2(\text{L9})_4]^{4+}$ and **L20**.

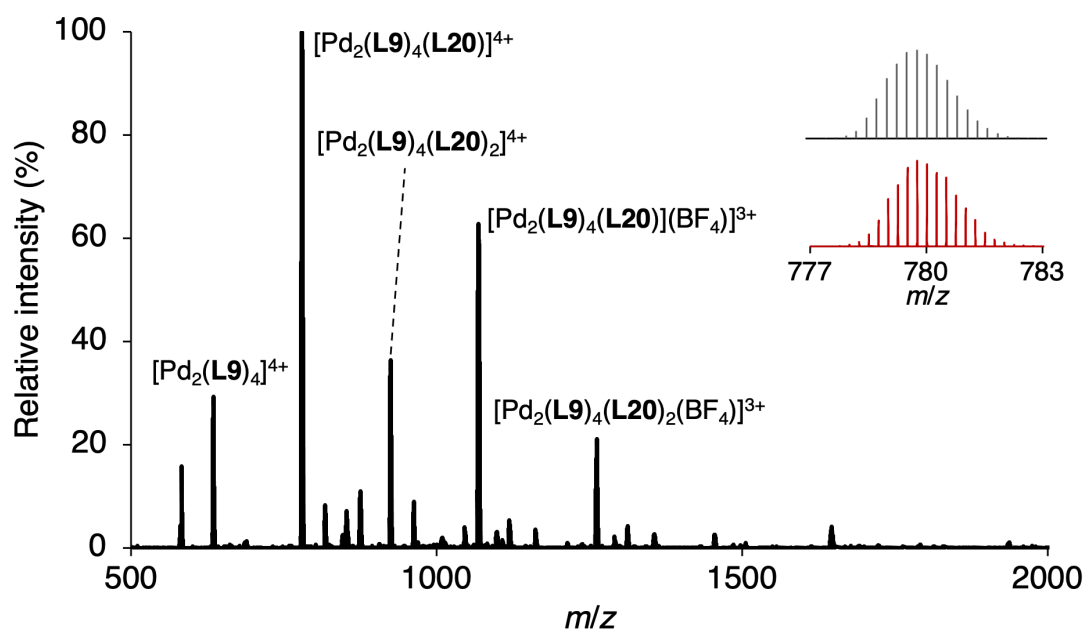
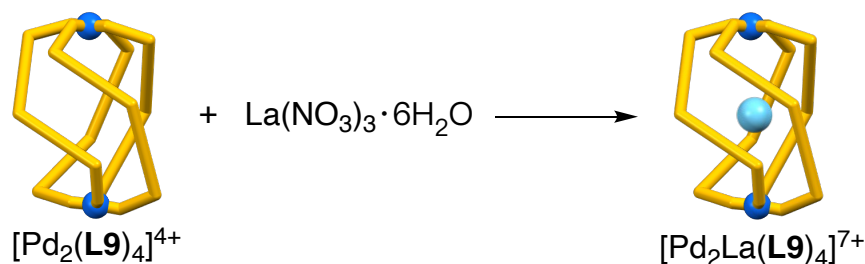


Figure ES23. HRMS of an equilibrated mixture of $[\text{Pd}_2(\text{L9})_4]^{4+}$ (1 eq.) and **L20** (4 eq.) in CD_3CN . The inset shows the comparison between the 777–783 m/z region (bottom) and the calculated mass spectrum for $[\text{Pd}_2(\text{L9})_4(\text{L20})]^{4+}$ (top).

Addition of La^{3+} to $[\text{Pd}_2(\text{L9})_4]^{4+}$



Scheme ES13. Addition of La^{3+} to $[\text{Pd}_2(\text{L9})_4]^{4+}$.

Aliquots (1.6 μL , 0.5 eq.) of a 97.5 mM $\text{La}(\text{NO}_3)_3 \cdot 6\text{H}_2\text{O}$ stock solution in CD_3CN were added to an NMR tube containing $[\text{Pd}_2(\text{L9})_4]^{4+}$ (400 μL of a 0.8 mM stock solution in CD_3CN , 1.0 eq), to give $[\text{Pd}_2\text{La}(\text{L9})_4]^{7+}$. ^1H NMR (400 MHz, CD_3CN , 298 K) δ 9.44 (s, 2H), 9.05 (s, 2H), 8.21 (d, 2H), 8.03 (d, 2H), 7.94 (t, 2H), 7.89 (d, 2H), 7.76 (d, 2H), 7.61 (d, 1H), 7.30 (d, 2H), 4.49 (dd, 2H), 1.66 (q, 2H), 1.48 (m, 4H), 0.99 (t, 3H). The ^1H NMR spectra recorded directly after the addition of 0.5 and 1.0 equivalent of La^{3+} are shown below.

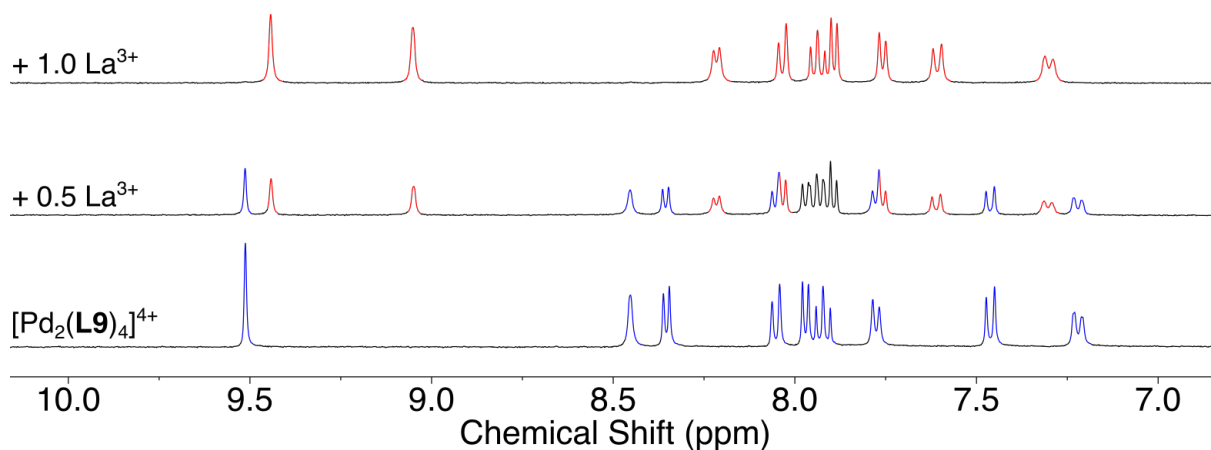


Figure ES24. ^1H NMR spectrum (400 MHz, CD_3CN , 298 K) of $[\text{Pd}_2(\text{L9})_4]^{4+}$ before (bottom) and after the addition of 0.5 (center) and 1.0 eq. (top) of $\text{La}(\text{NO}_3)_3 \cdot 6\text{H}_2\text{O}$. The peaks associated to $[\text{Pd}_2(\text{L9})_4]^{4+}$ and $[\text{Pd}_2\text{La}(\text{L9})_4]^{7+}$ are highlighted in blue and red, respectively.

[Pd₂La(L9)₄]⁷⁺ / [Pd₂La(L9)₅]⁷⁺ interconversion

[Pd₂(L9)₄]⁴⁺ to [Pd₂La(L9)₄]⁷⁺

La(NO₃)₃·6H₂O (1.0 μmol, 10.23 μL of a 97.5 mM stock solution in CD₃CN, 1.0 eq.) was added to [Pd₂(L9)₄]⁴⁺ (1.0 μmol, 1273.3 μL of a 0.78 mM stock solution in CD₃CN, 1.0 eq.) to give a 0.78 mM stock solution of [Pd₂La(L9)₄]⁷⁺ (I).

[Pd₂La(L9)₄]⁷⁺ to [Pd₂La(L9)₅]⁷⁺

[Pd₂La(L9)₄]⁷⁺ (0.8 μmol, 1022.4 μL of stock solution I, 1 eq.) was then added to L9 (0.46 mg, 0.8 μmol, 1.0 eq.) and the suspension heated at 70 °C for 1 h to give a 0.78 mM solution of [Pd₂La(L9)₅]⁷⁺ (II).

[Pd₂La(L9)₅]⁷⁺ to [Pd₂(L9)₄]⁴⁺

Finally, [Pd(CH₃CN)₄](BF₄)₂ (0.16 μmol, 5.43 μL of a 28.6 mM stock solution in CD₃CN, 0.5 eq.) and La(NO₃)₃·6H₂O (0.08 μmol, 0.80 μL of a 97.5 mM stock solution in CD₃CN, 0.25 eq.) were added to [Pd₂La(L9)₅]⁷⁺ (0.31 μmol, 400 μL of a 0.78 mM stock solution, 1.0 eq.) and the mixture heated at 70 °C for 1 h to give [Pd₂La(L9)₄]⁷⁺ (III).

^1H NMR spectra of the solutions, recorded at each step, are shown below.

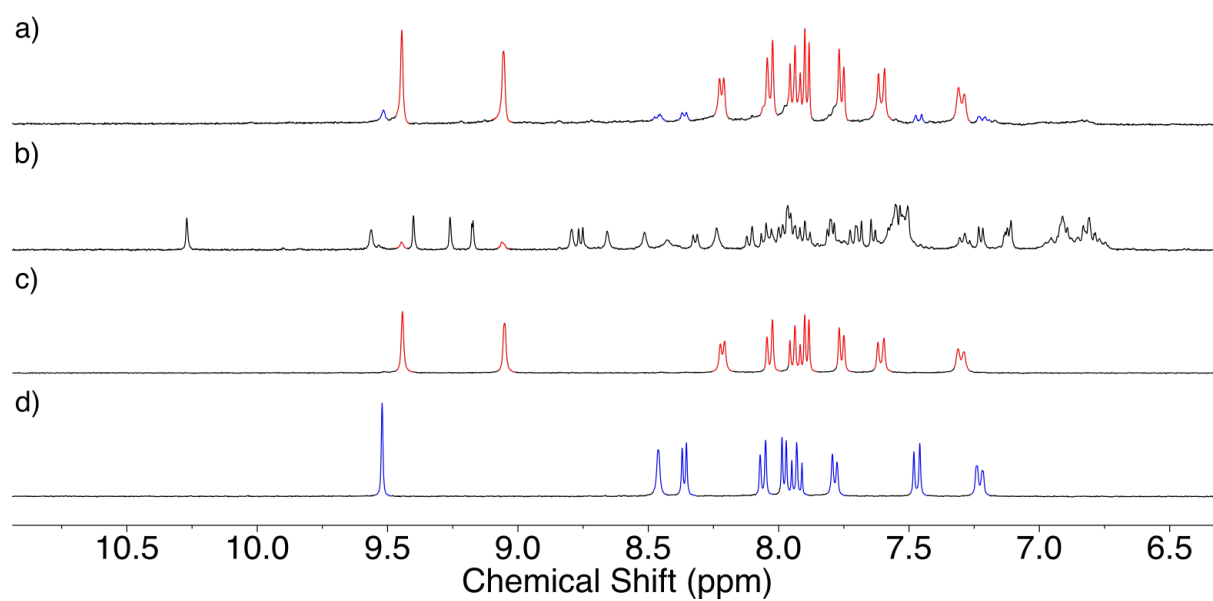


Figure ES25. ^1H NMR spectrum (400 MHz, CD_3CN , 298 K) of $[\text{Pd}_2(\text{L9})_4]^{4+}$ (1 eq.) (d) before and (c) after the subsequent addition of $\text{La}(\text{NO}_3)_3 \cdot 6\text{H}_2\text{O}$ (1 eq.), (b) **L9** (1 eq.), and (a) $[\text{Pd}(\text{CH}_3\text{CN})_4](\text{BF}_4)_2$ (0.5 eq.) and $\text{La}(\text{NO}_3)_3 \cdot 6\text{H}_2\text{O}$ (0.25 eq.).

8.6 Experimental details for Chapter 6

For the measurement of samples in mixtures of H₂O:D₂O, the NMR spectra were acquired on a Bruker Avance II spectrometer (¹H: 800 MHz) equipped with a 5 mm CPTCl_{xyz} cryoprobe with ATMA accessories. The pulse program employed for water suppression is *noesygppr1d*. The sequence is available in the default pulse program catalog of the spectrometer. Based on protocols available in literature, the sequence ensures the best compromise between quantitative and maximal solvent signal suppression.^[253–255] The optimal parameters found for the water-suppression NMR experiments were: *dummy scans*: 4, *mixing time*: 37.5 ms, *number of scans*: 16 and *recycle delay*: 5 s. Each sample was introduced in the spectrometer with the thermostat set at 298 K, the probe was tuned and matched automatically using the ‘*atma*’ command, the sample shimmed using the ‘*topshim*’ routine with additional care to optimize the x, y and z axes manually. The $\pi/2$ pulse duration was calculated using the automatic procedure ‘*pulsecal sn*’. The receiver gain was determined at the beginning of an experiment using the command ‘*rga*’. Prior to the acquisition, the deuterium lock signal was optimized for maximal stability by adjusting the *lock gain*, *lock power* parameters and using the ‘*loopadj*’ command for a final automatic optimization. The elaboration was carried out using MestreNova v. 14.2.1. An exponential apodization with $lb = 1.0$ Hz was applied to the raw FID, the phase of the spectrum was adjusted manually, and the baseline was automatically corrected using the ‘Whittaker smoother’ algorithm implemented in MestreNova.

Isothermal titration calorimetry (ITC) experiments were performed with a MicroCal “VP-ITC” instrument. The reference power was set to 10 $\mu\text{cal/s}$ for all measurements. The reference cell contained a 10 mM HEPES solution in miliQ water at pH 7.4. The raw thermograms were integrated using NITPIC^[256,257] and the data fitted to a 1:1 binding model using SEDPHAT.^[258]

The full experimental details can be found in the supplementary information of the related publication.^[80]

Synthesis and characterization

Compound **11**. was synthesized following reported literature procedures.^[259]

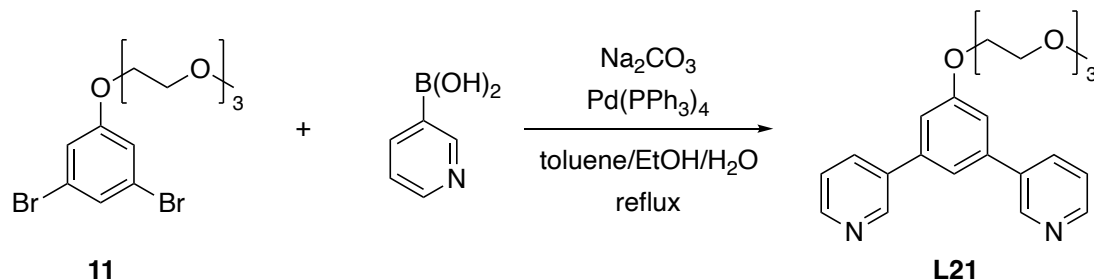


Figure ES26. Synthesis of ligand **L21**.

L21 was synthesized based on a reported literature procedure.^[260] Compound **11** (380 mg, 0.95 mmol, 1.0 eq.) was dissolved in a mixture of toluene (7 mL), ethanol (4 mL) and aqueous Na_2CO_3 (2 M, 7 mL). After degassing the solution by freeze-pump-thaw cycles, 3-Pyridylboronic acid (352 mg, 2.86 mmol, 3.0 eq.) and $\text{Pd}(\text{PPh}_3)_4$ (110 mg, 0.10 mmol, 0.1 eq.) were added under nitrogen. After heating at 100 °C for 3 days, ethyl acetate (20 mL) was added to the reaction mixture. The organic phase was washed three times with water, dried on MgSO_4 , and concentrated under vacuum. The residue was purified by column chromatography (SiO_2 , MeOH/DCM 0 to 5 %) to give **L2** as an off-white oil (240 mg, 64% yield). ^1H NMR (400 MHz, CD_3CN) δ 8.94 (d, 2H), 8.59 (dd, 2H), 8.08 (m, 2H), 7.54 (t, 1H), 7.44 (m, 2H), 7.27 (d, 2H), 4.28 (t, 2H), 3.83 (t, 2H), 3.65 (m, 2H), 3.52 – 3.60 (m, 4H), 3.45 (m, 2H), 3.27 (s, 2H). ^{13}C NMR (125 MHz, CD_3CN) δ 161.02, 149.90, 149.28, 141.06, 136.79, 135.53, 124.65, 119.52, 113.94, 72.59, 71.39, 71.15, 71.02, 70.30, 68.85, 58.86. ESI-MS: m/z calculated for $\text{C}_{23}\text{H}_{27}\text{N}_2\text{O}_4^+$ $[\text{M}+\text{H}]^+$ 395.20, found 395.20.

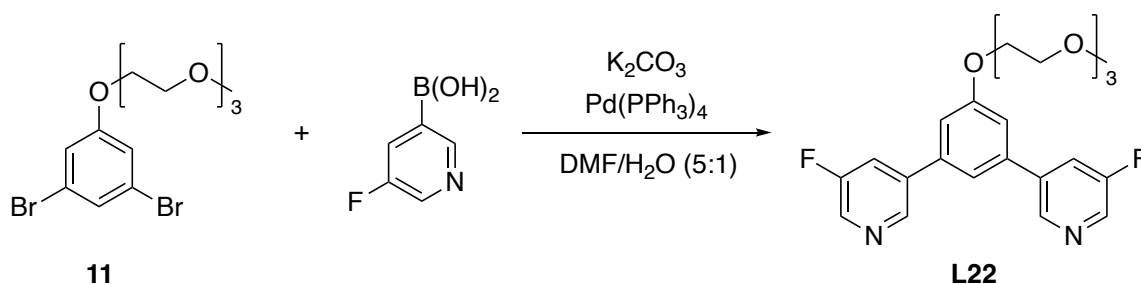


Figure ES27. Synthesis of ligand **L22**.

L22 was synthesized based on a reported literature procedure.^[261] Compound **11** (369.8 mg, 0.93 mmol, 1.0 eq.), 5-Fluoropyridine-3-boronic acid (399.3 mg, 2.83 mmol, 3.0 eq.) and K_2CO_3 (1.28 g, 9.24 mmol, 10.0 eq.) were dissolved in a mixture of DMF (15 mL) and H_2O (3 mL). After degassing the solution by vacuum-nitrogen cycles, $\text{Pd}(\text{PPh}_3)_4$ (55 mg, 0.05 mmol, 0.05 eq.) was added under nitrogen. After stirring the reaction mixture for 3 days at 100 °C, ethyl acetate (20 mL) was added to the yellow suspension. The organic phase was isolated, washed with brine, and dried over MgSO_4 . The solvent was removed under reduced pressure and the product was purified by flash-column chromatography (SiO_2 , pentane:EtOAc 6:4 to EtOAc:MeOH 92:8). After removing the solvent, the yellow solid was dissolved in EtOAc and extracted with HCl 0.1 M. After washing with diethyl ether (3 x 10 mL), NaOH (1 M) was added to the aqueous phase until pH = 11. The white precipitate was dissolved in EtOAc. The solvent was removed under vacuum to afford **L22** as a white solid (109 mg, 0.25 mmol, 27%). ^1H NMR (400 MHz, CD_3CN) δ 8.82 (t, 2H), 8.50 (d, 2H), 7.91 (ddd, 7.91), 7.58 (t, 1H), 7.32 (d, 2H), 4.29 (m, 2H), 3.84 (m, 2H), 3.65 (m, 2H), 3.58 (m, 2H), 3.55 (m, 2H), 2.45 (m, 2H), 3.27 (s, 3H). ^{13}C NMR (100 MHz, CD_3CN) δ 160.75 (d, $J = 252.86$ Hz), 161.09, 145.38, 139.63 (d, $J = 1.4$ Hz), 138.37 (d, $J = 4.01$), 137.90 (d, $J = 23.09$), 122.33 (d, $J = 18.95$), 119.83, 114.70, 72.58, 71.39, 71.14, 71.00, 70.26, 68.97, 58.86. ESI-MS: m/z calculated for $\text{C}_{23}\text{H}_{25}\text{F}_2\text{N}_2\text{O}_4^+$ $[\text{M}+\text{H}]^+$ 431.18, found 431.18.

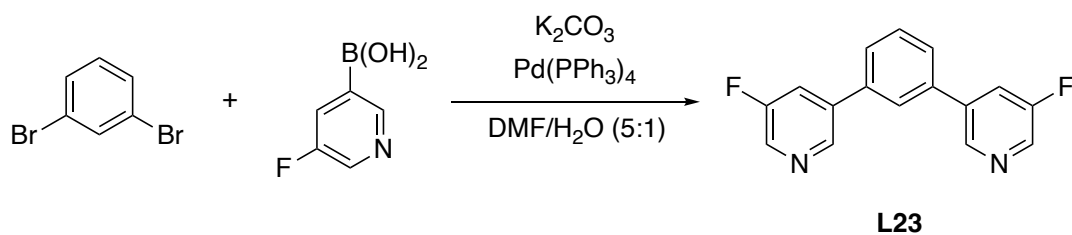


Figure ES28. Synthesis of ligand **L23**.

L23 was synthesized based on a reported literature procedure.^[243] 1,3-Dibromobenzene (358 mg, 1.51 mmol, 1.0 eq.), 5-Fluoropyridine-3-boronic acid (636 mg, 4.51 mmol, 3.0 eq.) and K_2CO_3 (2.1 g, 15.0 mmol, 10.0 eq.) were dissolved in a mixture of DMF (15 mL) and H_2O (3 mL). After degassing the solution by vacuum-nitrogen cycles, $Pd(PPh_3)_4$ (89 mg, 0.08 mmol, 0.05 eq.) was added under nitrogen. After stirring the reaction mixture for 3 days at 100 °C, ethyl acetate (30 mL) was added to the yellow suspension. The organic phase was isolated, washed with brine, and dried over $MgSO_4$. The solvent was removed under vacuum and the product was purified by flash-column chromatography (SiO_2 , pentane:EtOAc 7:3). The solvent was removed under vacuum to afford **L23** as an off-white solid (172 mg, 0.64 mmol, 43%). 1H NMR (400 MHz, CD_3CN) δ 8.82 (t, 2H), 8.51 (d, 2H), 8.01 (t, 1H), 7.91 (ddd, 2H), 7.78 (dd, 2H), 7.66 (m, 1H). ^{13}C NMR (125 MHz, CD_3CN) δ 160.78 (d, $J = 252.83$ Hz), 145.31 (d, 3.7 $J =$ Hz), 138.45 ($J = 4.13$ Hz), 138.27, 137.81 (d, $J = 23.03$), 131.07, 128.57, 127.31, 122.7 (d, $J = 18.75$). ESI-MS: m/z calculated for $C_{16}H_{11}F_2N_2^+$ $[M+H]^+$ 269.09, found 269.09.

[Pd₂(L21)₄(NO₃)](NO₃)₃ – Pd(NO₃)₂ · 2 H₂O (9.0 μ mol, 122.7 μ L of a 73.4 mM stock solution in CD_3CN , 1 eq.) was added to a solution of **L21** (18 μ mol, 7.10 mg, 2 eq.) in CD_3CN (4.0 mL) and the mixture was heated at 70 °C for 12 h to give **[Pd₂(L21)₄(NO₃)](NO₃)₃**. 1H NMR (400 MHz, CD_3CN) δ 10.24 (s, 8H), 9.39 (d, 8H), 8.78 (s, 4H), 8.28 (d, 8H), 7.66 (dd, 8H), 7.23 (s, 8H), 4.15 (t, 8H), 3.72 (t, 8H), 3.52 – 3.57 (m, 8H), 3.43–3.50 (m, 16H), 3.33–3.37 (m, 8H), 3.17 (s, 12H). ^{13}C NMR (100 MHz, CD_3CN) δ 161.54, 151.63, 151.24, 140.15, 139.49, 138.15, 128.24, 120.39, 115.00, 72.51, 71.33, 71.06, 70.93, 70.11, 69.05, 58.78.

[Pd₂(L22)₄(NO₃)](NO₃)₃ – Pd(NO₃)₂ · 2 H₂O (2.1 μmol, 210.3 μL of a 10 mM stock solution in CD₃CN, 1 eq.) was added to a solution of **L22** (4.2 μmol, 1.81 mg, 2 eq.) in CD₃CN (1 mL) and the mixture was heated at 70 °C for 12 h to give **[Pd₂(L3)₄(NO₃)](NO₃)₃**. ¹H NMR (400 MHz, CD₃CN) δ 10.05 (d, 2H), 9.50 (t, 2H), 8.75 (t, 1H), 8.19 (dt, 2H), 7.27 (d, 2H), 4.16 (m, 2H), 3.73 (m, 2H), 3.55 (m, 2H), 3.44 – 3.51 (m, 4H), 3.37 (m, 2H), 3.18 (s, 3H). ¹³C NMR (125 MHz, CD₃CN) δ 161.63, 161.38 (d, 252.64 Hz), 148.35 (d, 3.48 Hz), 141.38 (d, 6.55 Hz), 140.90 (d, 32.88), 137.08 (d, 1.55 Hz), 126.79 (d, 19.39 Hz), 120.59, 115.62, 72.50, 71.32, 71.05, 70.92, 70.03, 69.18, 58.78.

[Pd₂(L23)₄(NO₃)](NO₃)₃ – Pd(NO₃)₂ · 2 H₂O (2.3 μmol, 229.3 μL of a 10 mM stock solution in CD₃CN, 1 eq.) was added to a solution of **L23** (4.6 μmol, 1.23 mg, 2 eq.) in CD₃CN (1 mL) and the mixture was heated at 70 °C for 12 h to give **[Pd₂(L23)₄(NO₃)](NO₃)₃**. ¹H NMR (400 MHz, CD₃CN) δ 10.06 (d, 2H), 9.53 (t, 2H), 9.13 (t, 1H), 8.14 (dt, 2H), 7.71 (dd, 2H), 7.59 (m, 2H). ¹³C NMR (125 MHz, CD₃CN) δ 161.38 (d, *J* = 252.9 Hz), 148.34 (d, *J* = 3.53), 141.70 (*J* = 6.43), 140.68 (*J* = 32.7), 135.85, 131.77, 129.62, 128.36, 126.81 (*J* = 19.19).

Halides binding in CD₃CN

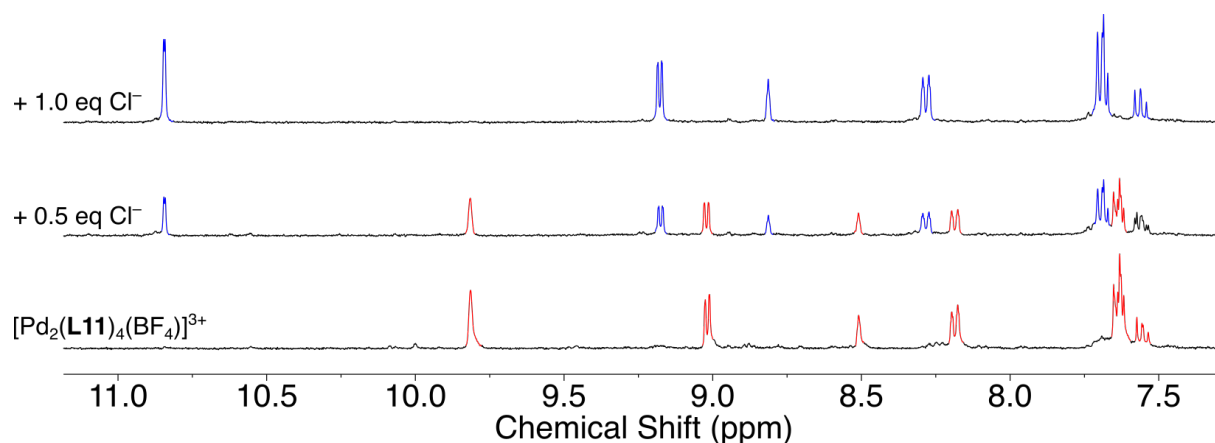
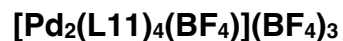


Figure ES29. Aromatic part of the ¹H NMR spectra (400 MHz, CD₃CN) of [Pd₂(L11)₄(BF₄)](BF₄)₃ before (bottom) and after the addition of 0.5 (middle) and 1.0 equivalent (top) of NBu₄Cl.

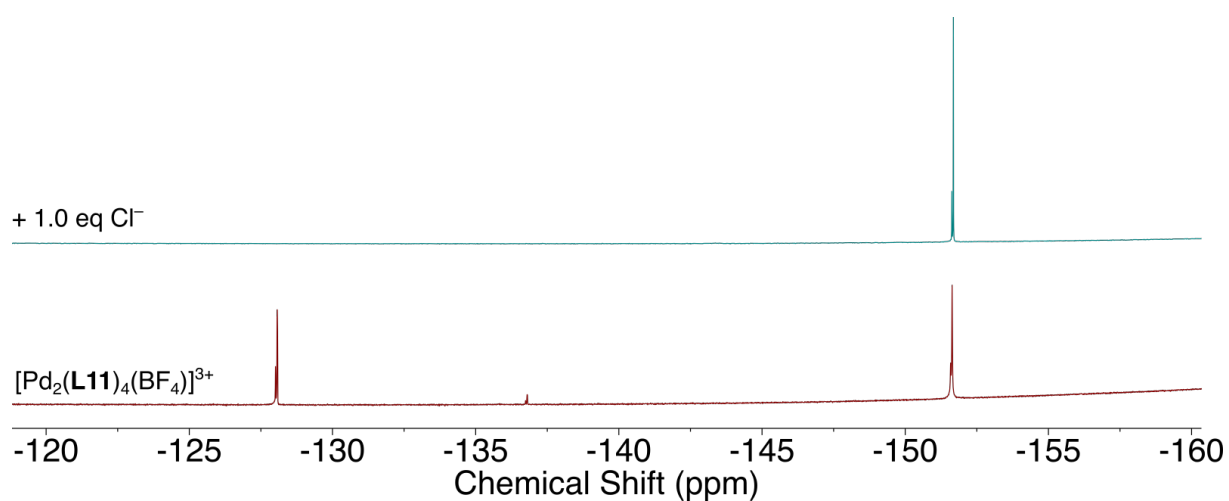


Figure ES30. -160 to -120 ppm region of the ¹⁹F NMR spectra (376 MHz, CD₃CN) of [Pd₂(L11)₄(BF₄)](BF₄)₃ before (bottom) and after the addition of 1.0 equivalent (top) of NBu₄Cl.

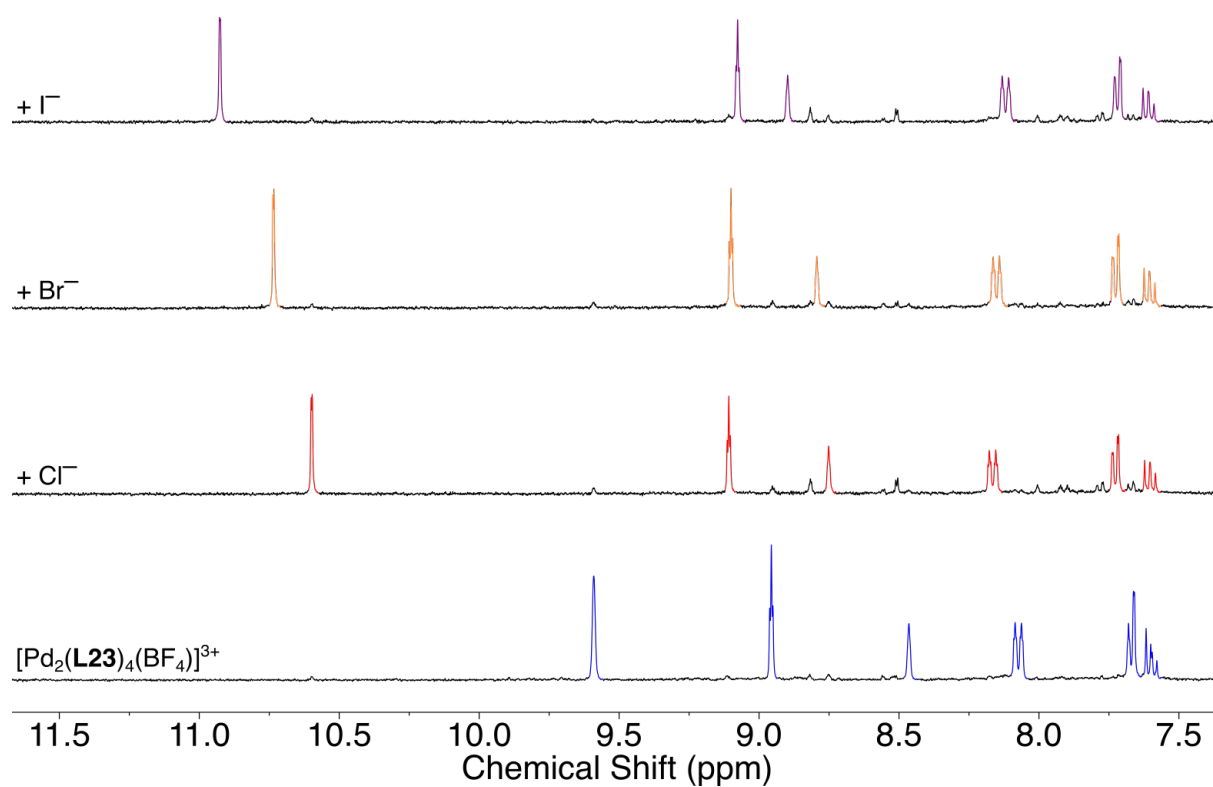
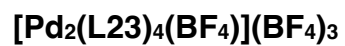


Figure ES31. Aromatic part of the ¹H NMR spectra (400 MHz, CD₃CN) of [Pd₂(L23)₄(BF₄)](BF₄)₃ and of solutions containing equimolar amounts of [Pd₂(L23)₄(BF₄)](BF₄)₃ and NBu₄X (X = Cl, Br, or I).

[Pd₂(L21)₄(NO₃)](NO₃)₃ chloride intake kinetics

An aliquot (3.12 μL, 1 eq.) of a 51.3 mM stock solution of NBu₄Cl was added to 400 μL of a 0.4 mM solution (1 eq.) of [Pd₂(L21)₄(NO₃)](NO₃)₃ in CD₃CN in an NMR tube and ¹H NMR spectra were recorded at different time intervals until equilibration. The experiment was conducted at 298 K.

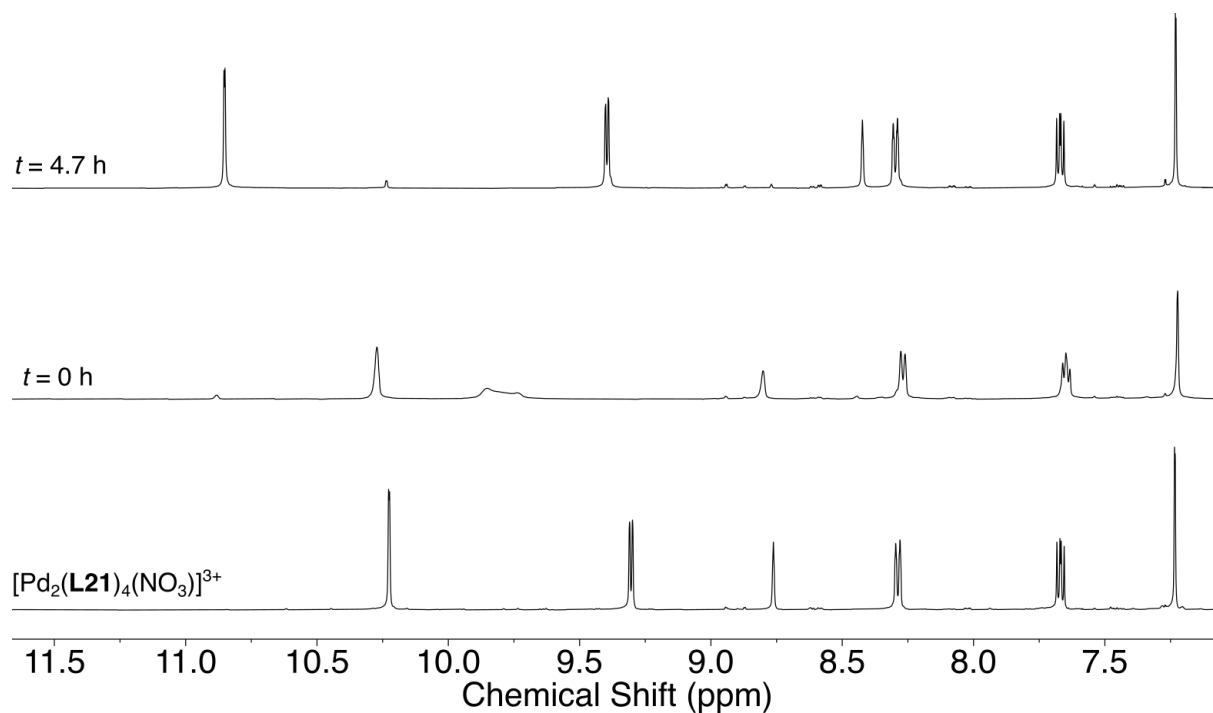


Figure ES32. Aromatic region of the ¹H NMR spectra (500 MHz, CD₃CN) at two different time intervals after addition of 1.0 equivalent of NBu₄Cl to a solution of [Pd₂(L21)₄(NO₃)](NO₃)₃.

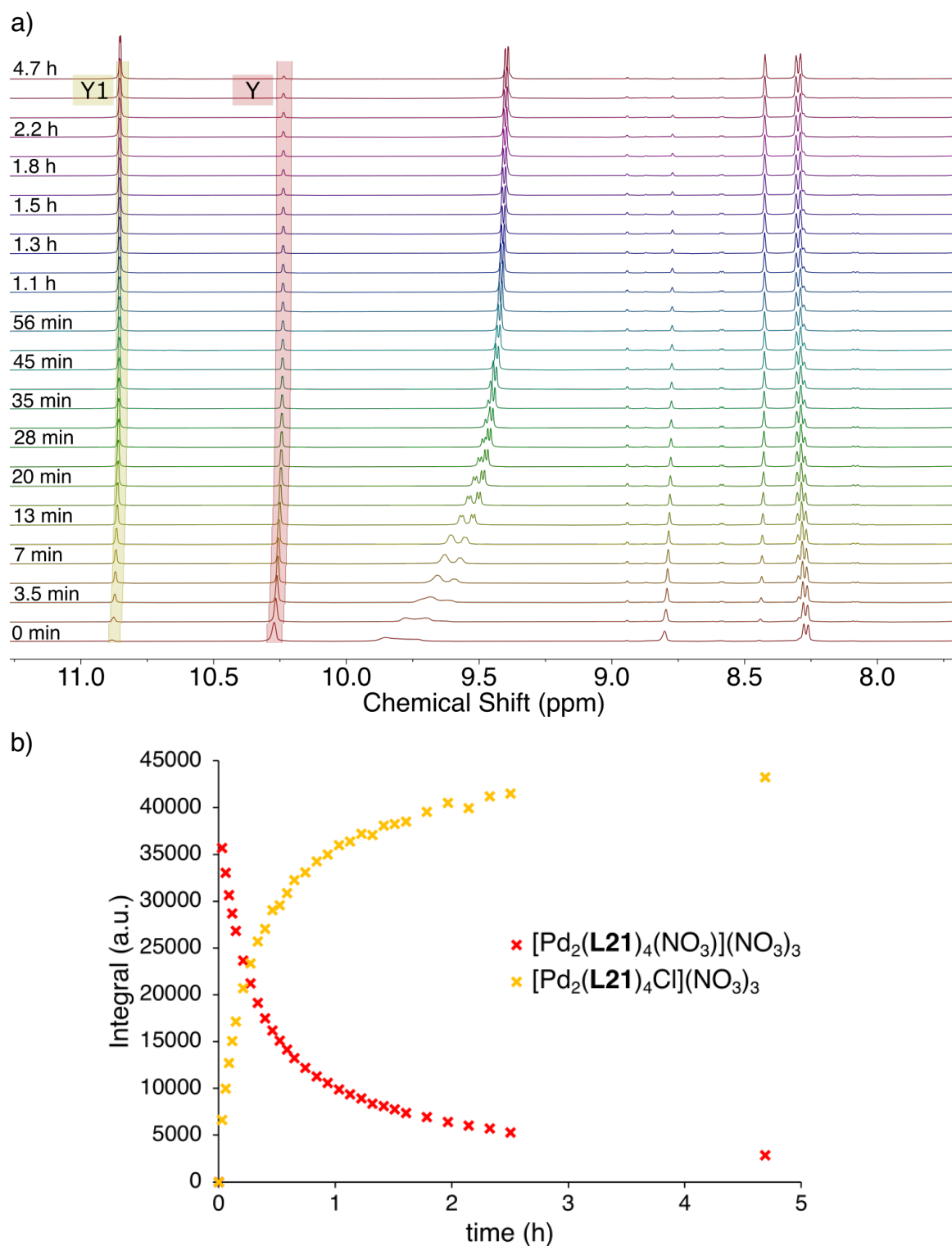


Figure ES33. (a) Aromatic region of the ^1H NMR spectra (500 MHz, CD_3CN) at different time intervals after addition of 1.0 equivalent of NBu_4Cl to a solution of $[\text{Pd}_2(\text{L21})_4(\text{NO}_3)](\text{NO}_3)_3$. (b) Integrals of the signals at 10.2 and 10.9 ppm associated to the H_a protons of $[\text{Pd}_2(\text{L21})_4(\text{NO}_3)](\text{NO}_3)_3$ and $[\text{Pd}_2(\text{L21})_4\text{Cl}](\text{NO}_3)_3$, respectively, as a function of time.

Halides binding in H₂O

¹H NMR

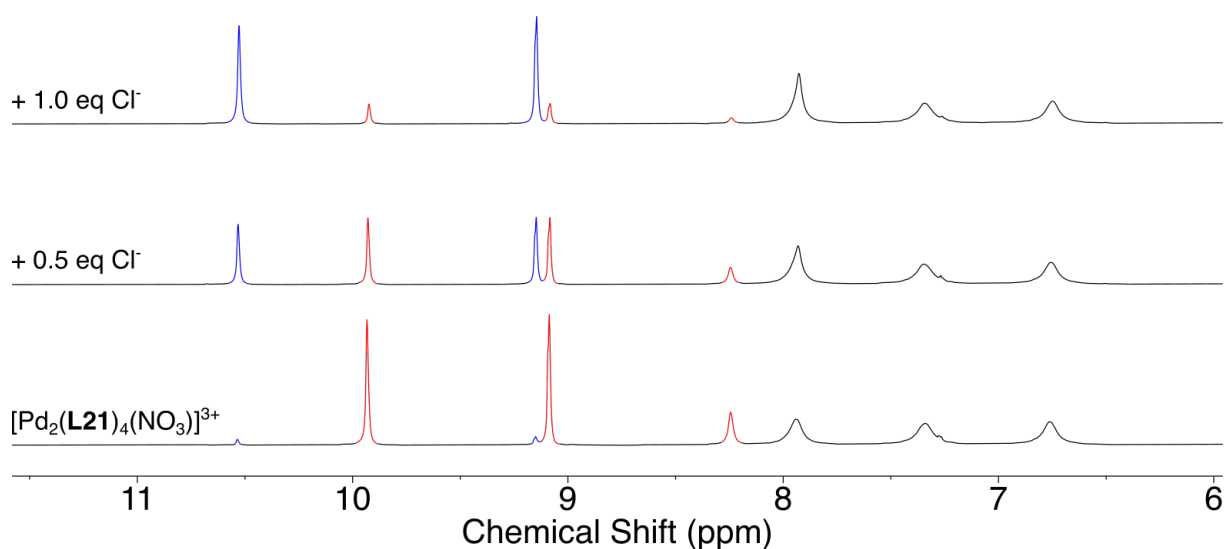


Figure ES34. Aromatic part of the ¹H NMR spectrum (800 MHz, H₂O/D₂O, 95:5) of $[\text{Pd}_2(\text{L2})_4(\text{NO}_3)](\text{NO}_3)_3$ before (bottom) and after the addition of 0.5 (center) and 1.0 (top) equivalent of NaCl.

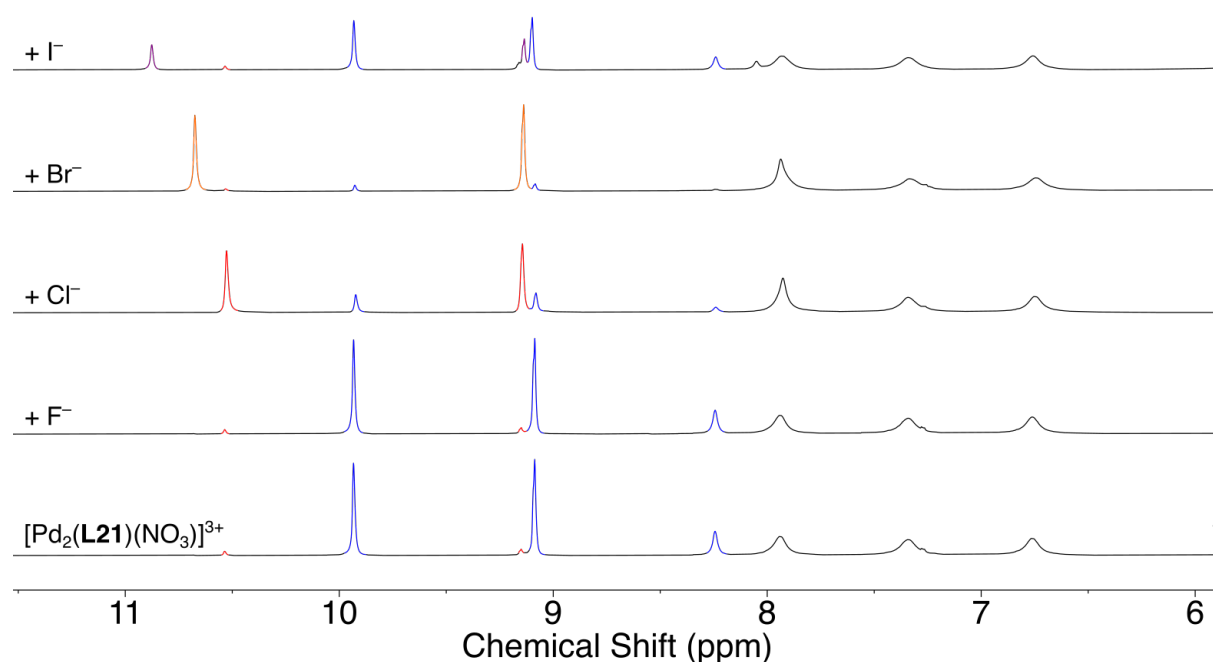


Figure ES35. Aromatic part of the ¹H NMR spectrum (800 MHz, H₂O/D₂O, 95:5) of $[\text{Pd}_2(\text{L21})(\text{NO}_3)](\text{NO}_3)_3$ before and after the addition of 1.0 equivalent of halide sodium salts. The reduced signal-to-noise ratio observed in the top spectrum is due to slow precipitation.

ITC measurements

Each experiment was repeated three times. The obtained parameters are summarized in **Tables ES6–ES10** and the final values were calculated as an average of the three independent measurements. $\text{Log}(K_a)$, N , and ΔH were obtained directly from the fitting while ΔG and $T\Delta S$ were calculated from the latter.

[Pd₂(L21)₄(NO₃)₃](NO₃)₃ – NaCl

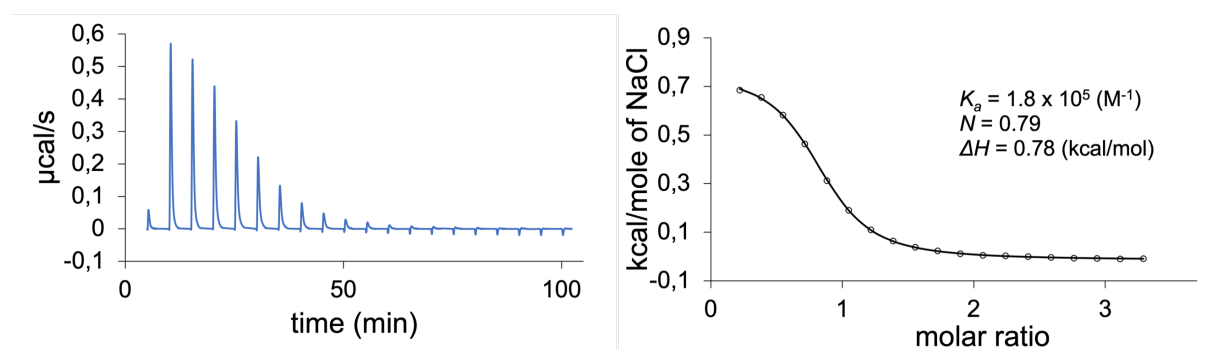


Figure ES36. ITC experiment **1a** (H_2O , HEPES 10 mM, pH 7.4, 298 K). Titration of $[\text{Pd}_2(\text{L21})_4(\text{NO}_3)](\text{NO}_3)_3$ (0.1 mM) with NaCl (4 mM). Corrected thermogram for 20 injections (6 μL per injection) (left) and the corresponding integrated heat of reaction as a function of the guest/host ratio (right). The solid black line represents the best-fitting curve obtained from a 1:1 binding model.

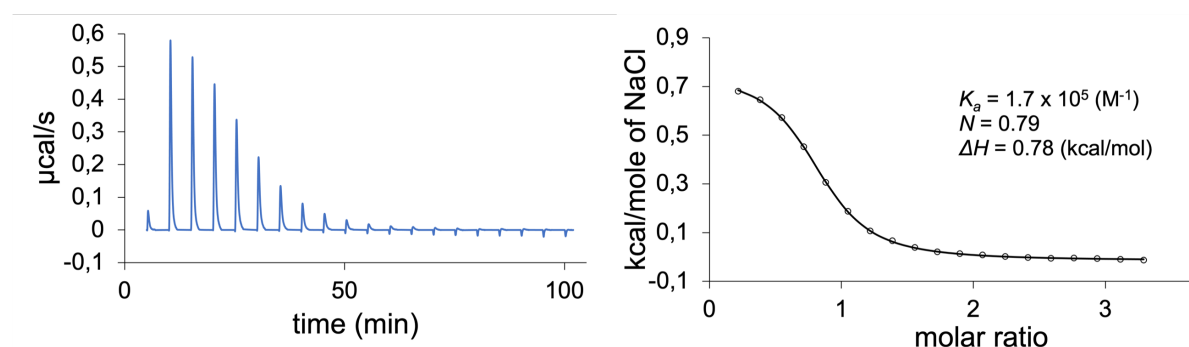


Figure ES37. ITC experiment **1b** (H_2O , HEPES 10 mM, pH 7.4, 298 K). Titration of $[\text{Pd}_2(\text{L21})_4(\text{NO}_3)](\text{NO}_3)_3$ (0.1 mM) with NaCl (4 mM). Corrected thermogram for 20 injections (6 μL per injection) (left) and the corresponding integrated heat of reaction as a function of the guest/host ratio (right). The solid black line represents the best-fitting curve obtained from a 1:1 binding model.

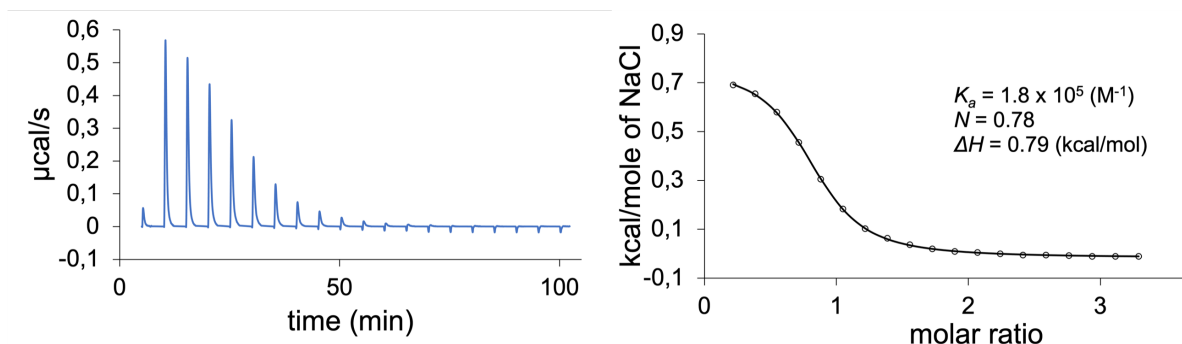


Figure ES38. ITC experiment **1c** (H₂O, HEPES 10 mM, pH 7.4, 298 K). Titration of [Pd₂(**L21**)₄(NO₃)](NO₃)₃ (0.1 mM) with NaCl (4 mM). Corrected thermogram for 20 injections (6 μL per injection) (left) and the corresponding integrated heat of reaction as a function of the guest/host ratio (right). The solid black line represents the best-fitting curve obtained from a 1:1 binding model.

Table ES6. Parameters obtained from the fitting of the data to a 1:1 binding model for the titration of NaCl into a solution of [Pd₂(**L2**)₄(NO₃)](NO₃)₃ (experiments **1a–c**).

Measurement	$\log(K_a)$	N	ΔH (kJ/mol)	ΔG (kJ/mol)	$T\Delta S$ (kJ/mol)
1a	5.26	0.79	3.3	-30.0	33.2
1b	5.23	0.79	3.2	-29.8	33.1
1c	5.25	0.78	3.3	-29.9	33.2
Average	5.24	0.79	3.3	-29.9	33.2

[Pd₂(L21)₄(NO₃)₃](NO₃)₃ – NaBr

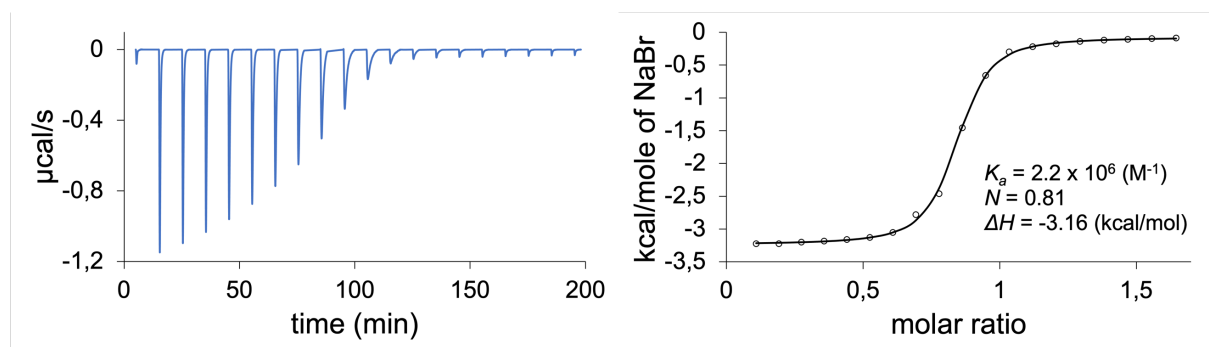


Figure ES39. ITC experiment **2a** (H₂O, HEPES 10 mM, pH 7.4, 298 K). Titration of [Pd₂(L21)₄(NO₃)₃](NO₃)₃ (0.1 mM) with NaBr (2 mM). Corrected thermogram for 20 injections (6 μL per injection) (left) and the corresponding integrated heat of reaction as a function of the guest/host ratio (right). The solid black line represents the best-fitting curve obtained from a 1:1 binding model.

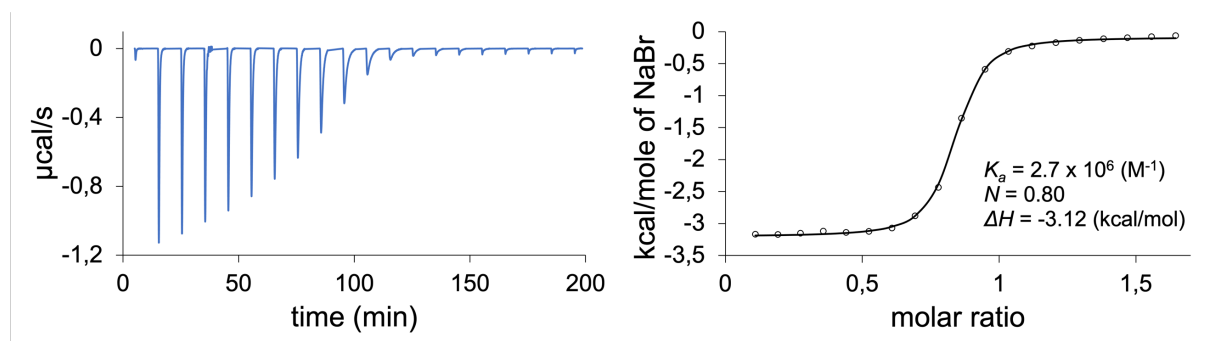


Figure ES40. ITC experiment **2b** (H₂O, HEPES 10 mM, pH 7.4, 298 K). Titration of [Pd₂(L21)₄(NO₃)₃](NO₃)₃ (0.1 mM) with NaBr (2 mM). Corrected thermogram for 20 injections (6 μL per injection) (left) and the corresponding integrated heat of reaction as a function of the guest/host ratio (right). The solid black line represents the best-fitting curve obtained from a 1:1 binding model.

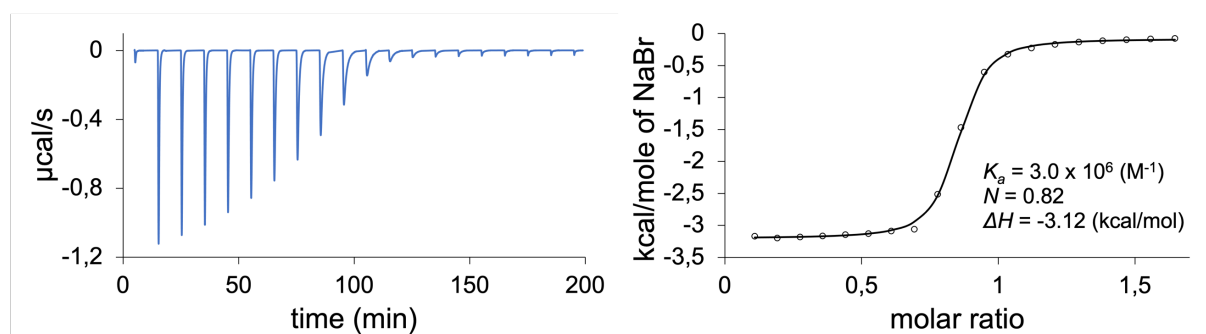


Figure ES41. ITC experiment **2c** (H₂O, HEPES 10 mM, pH 7.4, 298 K). Titration of [Pd₂(**L21**)₄(NO₃)](NO₃)₃ (0.1 mM) with NaBr (2 mM). Corrected thermogram for 20 injections (6 μL per injection) (left) and the corresponding integrated heat of reaction as a function of the guest/host ratio (right). The solid black line represents the best-fitting curve obtained from a 1:1 binding model.

Table ES7. Parameters obtained from the fitting of the data to a 1:1 binding model for the titration of NaBr into a solution of [Pd₂(**L2**)₄(NO₃)](NO₃)₃ (experiments **2a–c**).

Measurement	$\log(K_a)$	N	ΔH (kJ/mol)	ΔG (kJ/mol)	$T\Delta S$ (kJ/mol)
2a	6.34	0.81	-13.2	-36.2	23.0
2b	6.43	0.80	-13.0	-36.7	23.7
2c	6.48	0.82	-13.1	-37.0	23.9
Average	6.42	0.81	-13.1	-36.6	23.5

[Pd₂(L21)₄(NO₃)₂](NO₃)₃ + 4NaNO₃ – NaCl

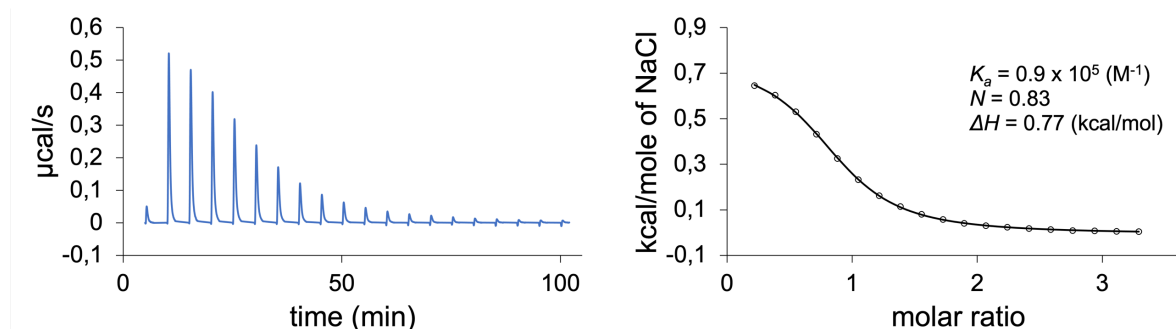


Figure ES42. ITC experiment **3a** (H₂O, HEPES 10 mM, pH 7.4, 298 K) Titration of [Pd₂(L21)₄(NO₃)₂](NO₃)₃ (0.1 mM) in presence of NaNO₃ (0.4 mM, [NO₃]_{tot} = 0.8 mM) with NaCl (4 mM). Corrected thermogram for 20 injections (6 μL per injection) (left) and the corresponding integrated heat of reaction as a function of the guest/host ratio (right). The solid black line represents the best-fitting curve obtained from a 1:1 binding model.

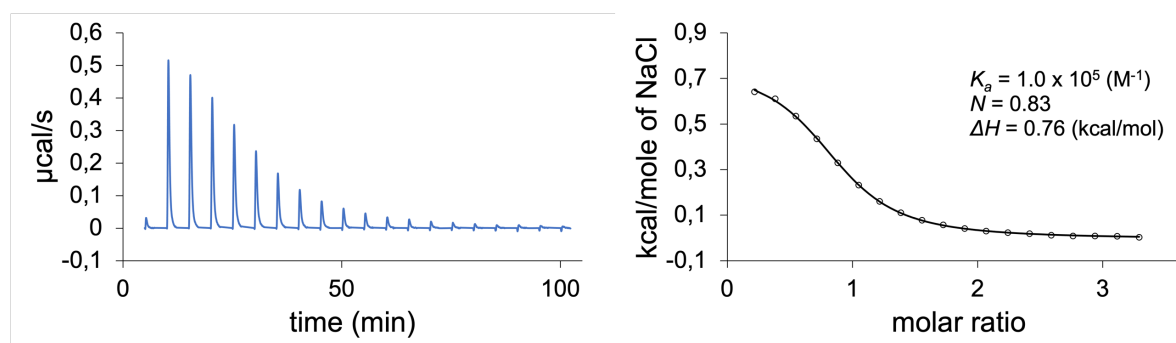


Figure ES43. ITC experiment **3b** (H₂O, HEPES 10 mM, pH 7.4, 298 K) Titration of [Pd₂(L21)₄(NO₃)₂](NO₃)₃ (0.1 mM) in presence of NaNO₃ (0.4 mM, [NO₃]_{tot} = 0.8 mM) with NaCl (4 mM). Corrected thermogram for 20 injections (6 μL per injection) (left) and the corresponding integrated heat of reaction as a function of the guest/host ratio (right). The solid black line represents the best-fitting curve obtained from a 1:1 binding model.

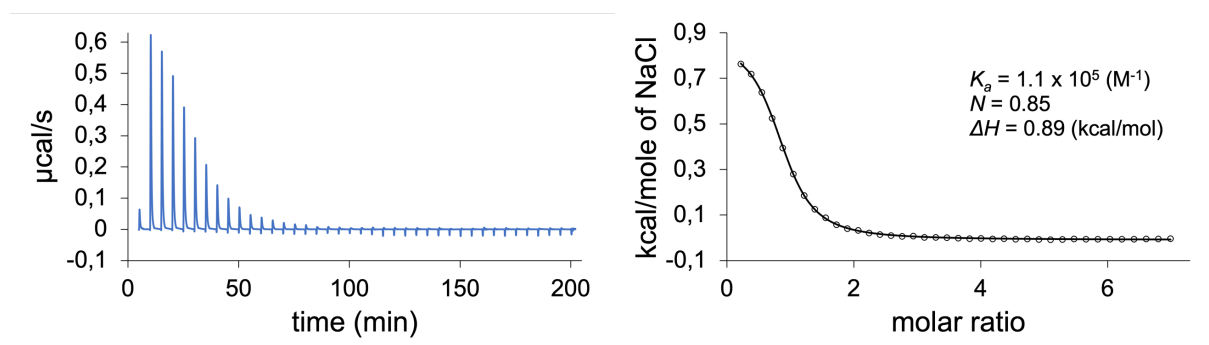


Figure ES44. ITC experiment **3c** (H_2O , HEPES 10 mM, pH 7.4, 298 K) Titration of $[\text{Pd}_2(\text{L21})_4(\text{NO}_3)](\text{NO}_3)_3$ (0.1 mM) in presence of NaNO_3 (0.4 mM, $[\text{NO}_3]_{\text{tot}} = 0.8$ mM) with NaCl (4 mM). Corrected thermogram for 40 injections (6 μL per injection) (left) and the corresponding integrated heat of reaction as a function of the guest/host ratio (right). The solid black line represents the best-fitting curve obtained from a 1:1 binding model.

Table ES8. Parameters obtained from the fitting of the data to a 1:1 binding model for the titration of NaCl into a mixture of $[\text{Pd}_2(\text{L21})_4(\text{NO}_3)](\text{NO}_3)_3$ (1 eq.) and NaNO_3 (4 eq.) (experiments **3a–c**).

Measurement	$\log(K_a)$	N	ΔH (kJ/mol)	ΔG (kJ/mol)	$T\Delta S$ (kJ/mol)
3a	4.97	0.83	3.2	-28.3	31.6
3b	5.00	0.83	3.2	-28.5	31.7
3c	5.04	0.85	3.7	-28.8	32.5
Average	5.00	0.84	3.4	-28.5	31.9

[Pd₂(L22)₄(NO₃)₃](NO₃)₃ – NaCl

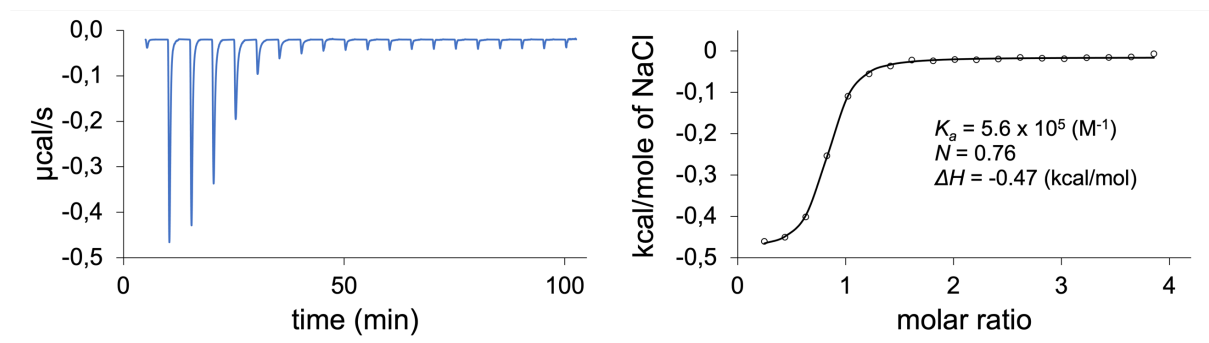


Figure ES45. ITC experiments **4a** (H₂O, HEPES 10 mM, pH 7.4, 298 K). Titration of [Pd₂(L22)₄(NO₃)₃](NO₃)₃ (0.1 mM) with NaCl (4 mM). Corrected thermogram for 20 injections (7 μL per injection) (left) and the corresponding integrated heat of reaction as a function of the guest/host ratio (right). The solid black line represents the best-fitting curve obtained from a 1:1 binding model.

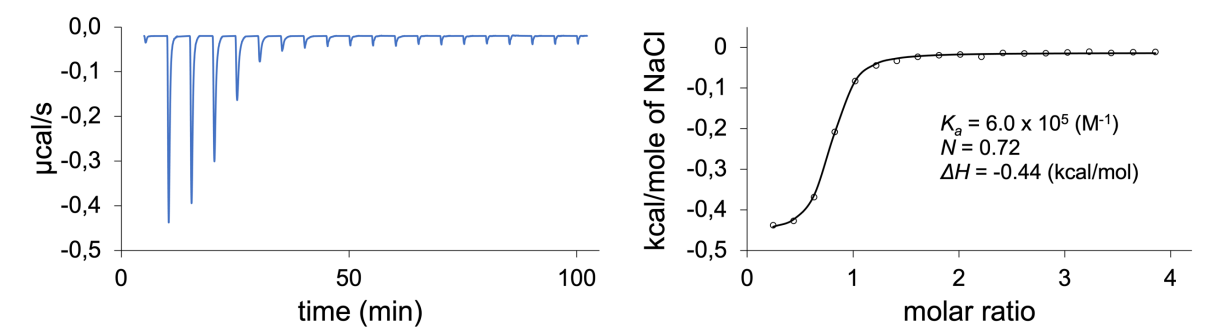


Figure ES46. ITC experiments **4b** (H₂O, HEPES 10 mM, pH 7.4, 298 K). Titration of [Pd₂(L22)₄(NO₃)₃](NO₃)₃ (0.1 mM) with NaCl (4 mM). Corrected thermogram for 20 injections (7 μL per injection) (left) and the corresponding integrated heat of reaction as a function of the guest/host ratio (right). The solid black line represents the best-fitting curve obtained from a 1:1 binding model.

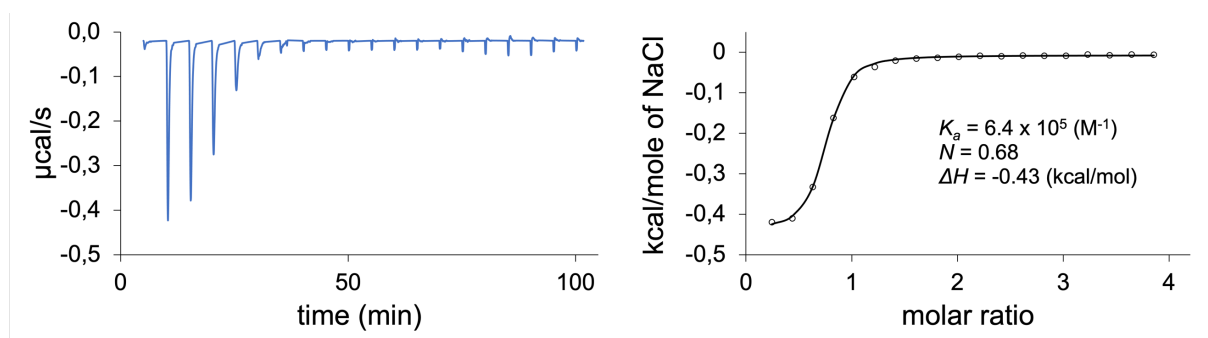


Figure ES47. ITC experiments **4c** (H₂O, HEPES 10 mM, pH 7.4, 298 K). Titration of [Pd₂(**L22**)₄(NO₃)](NO₃)₃ (0.1 mM) with NaCl (4 mM). Corrected thermogram for 20 injections (7 μL per injection) (left) and the corresponding integrated heat of reaction as a function of the guest/host ratio (right). The solid black line represents the best-fitting curve obtained from a 1:1 binding model.

Table ES9. Parameters obtained from the fitting of the data to a 1:1 binding model for the titration of NaCl into a solution of [Pd₂(**L22**)₄(NO₃)](NO₃)₃ (experiments **4a–c**)

Measurement	$\log(K_a)$	N	ΔH (kJ/mol)	ΔG (kJ/mol)	$T\Delta S$ (kJ/mol)
1	5.74	0.76	-2.0	-32.8	30.8
2	5.78	0.72	-1.9	-33.0	31.1
3	5.80	0.68	-1.8	-33.1	31.3
Average	5.77	0.72	-1.9	-33.0	31.1

[Pd₂(L22)₄(NO₃)₃](NO₃)₃ – NaBr

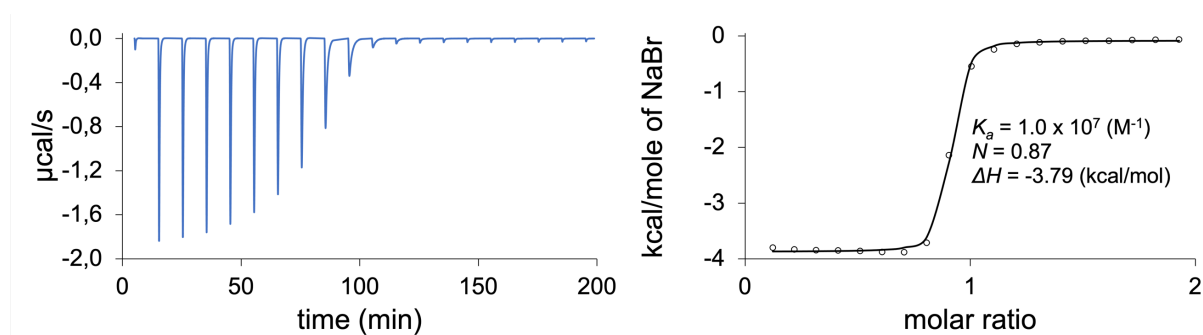


Figure ES48. ITC experiment **5a** (H₂O, HEPES 10 mM, pH 7.4, 298 K). Titration of [Pd₂(L22)₄(NO₃)₃](NO₃)₃ (0.1 mM) with NaBr (2 mM). Corrected thermogram for 20 injections (7 μL per injection) (left) and the corresponding integrated heat of reaction as a function of the guest/host ratio (right). The solid black line represents the best-fitting curve obtained from a 1:1 binding model.

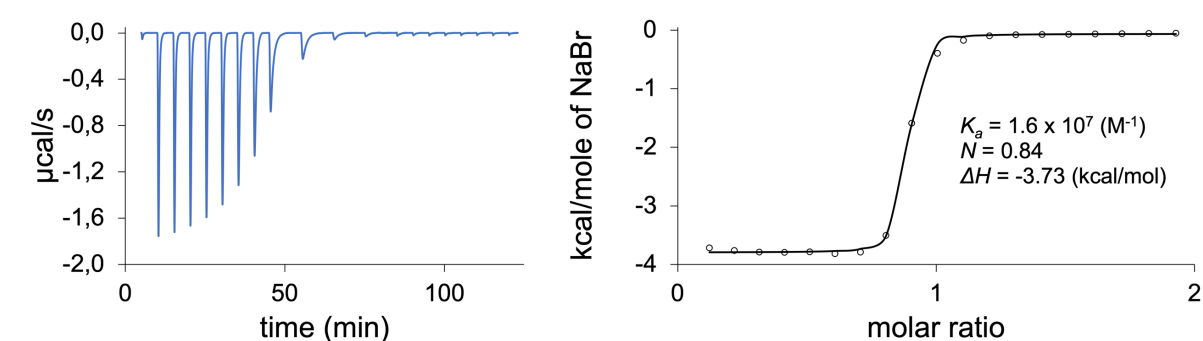


Figure ES49. ITC experiment **5b** (H₂O, HEPES 10 mM, pH 7.4, 298 K). Titration of [Pd₂(L22)₄(NO₃)₃](NO₃)₃ (0.1 mM) with NaBr (2 mM). Corrected thermogram for 20 injections (7 μL per injection) (left) and the corresponding integrated heat of reaction as a function of the guest/host ratio (right). The solid black line represents the best-fitting curve obtained from a 1:1 binding model.

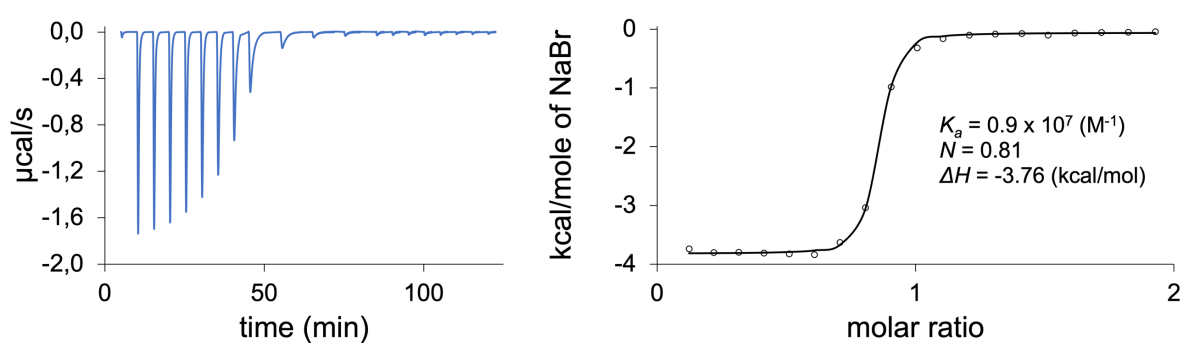


Figure ES50. ITC experiment **5c** (H₂O, HEPES 10 mM, pH 7.4, 298 K). Titration of [Pd₂(**L22**)₄(NO₃)](NO₃)₃ (0.1 mM) with NaBr (2 mM). Corrected thermogram for 20 injections (7 μL per injection) (left) and the corresponding integrated heat of reaction as a function of the guest/host ratio (right). The solid black line represents the best-fitting curve obtained from a 1:1 binding model.

Table ES10. Parameters obtained from the fitting of the data to a 1:1 binding model for the titration of NaBr into a solution of [Pd₂(**L22**)₄(NO₃)](NO₃)₃ (experiments **5a–c**).

Measurement	$\log(K_a)$	N	ΔH (kJ/mol)	ΔG (kJ/mol)	$T\Delta S$ (kJ/mol)
5a	7.00	0.87	-15.8	-40.0	24.1
5b	7.19	0.84	-15.6	-41.0	25.4
5c	6.94	0.81	-15.7	-39.6	23.9
Average	7.05	0.84	-15,7	-40.2	-24.5

UV/vis measurements

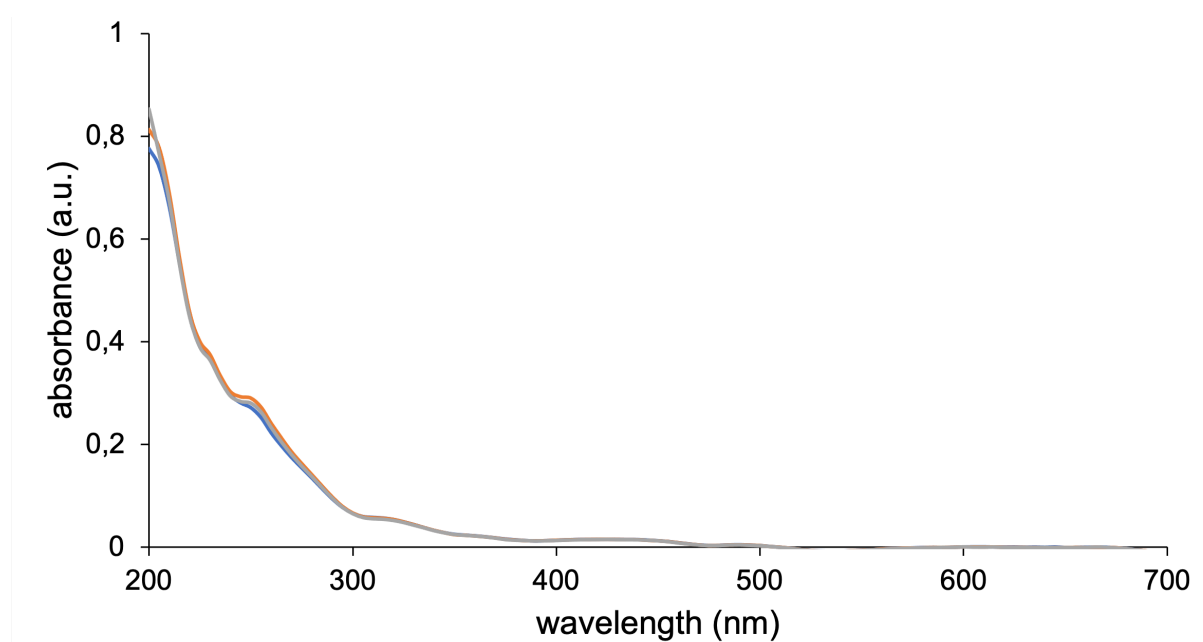


Figure ES51. UV/vis spectra of $[\text{Pd}_2(\text{L22})_4(\text{NO}_3)](\text{NO}_3)_3$ ($3 \mu\text{M}$, H_2O) before (blue), and after the addition of 100 (orange) and 1000 equivalents of NaCl (respective aliquots of 1.1 and 11 μL of a 259.2 mM stock solution in water).

Chloride extraction

400 μL of a 1.1 mM solution of NaCl in D_2O were added to a vial containing 400 μL of a 1.1 mM solution of $[\text{Pd}_2(\text{L11})_4(\text{BF}_4)](\text{BF}_4)_3$ in CD_3NO_2 . The vial was then vigorously shaken for 30 s, the organic phase separated and a ^1H NMR spectrum recorded. The organic phase was then poured back to the vial containing the aqueous NaCl solution and the procedure repeated two times until no more conversion from $[\text{Pd}_2(\text{L11})_4(\text{BF}_4)](\text{BF}_4)_3$ to $[\text{Pd}_2(\text{L11})_4(\text{Cl})](\text{BF}_4)_3$ was observed.

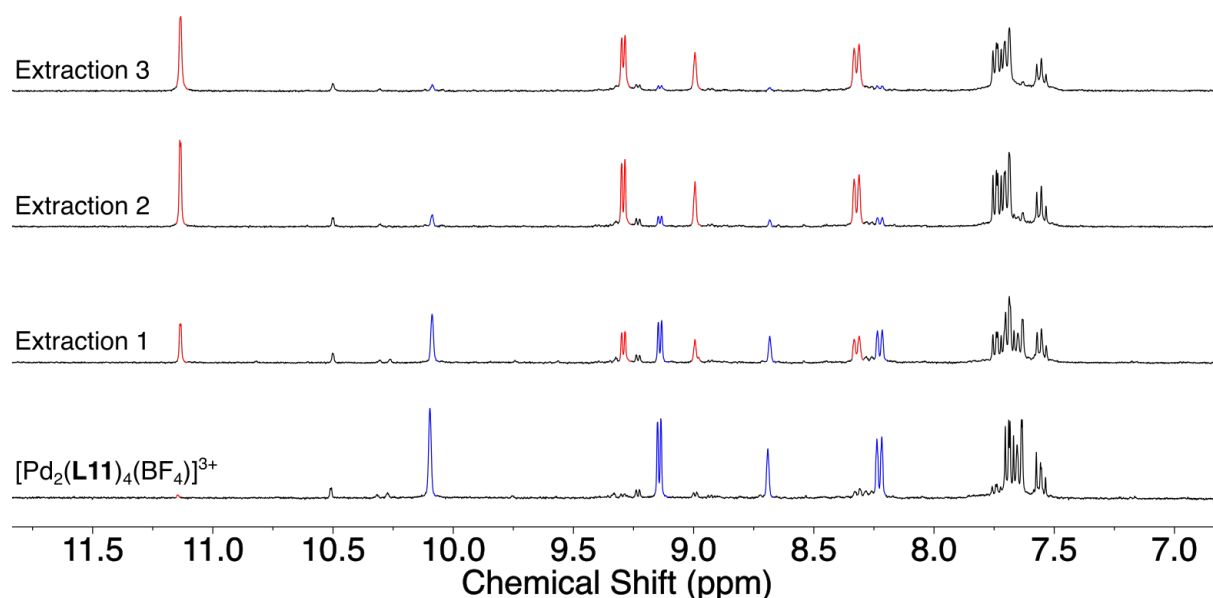


Figure ES52. ^1H NMR spectra (400 MHz, CD_3NO_2) of $[\text{Pd}_2(\text{L11})_4(\text{BF}_4)](\text{BF}_4)_3$ before (bottom) and after one to three extraction steps of the NaCl aqueous solution.

9. References

- [1] S. Saha, I. Regeni, G. H. Clever, *Coord. Chem. Rev.* **2018**, *374*, 1–14.
- [2] R. A. S. Vasdev, D. Preston, J. D. Crowley, *Chem. Asian J.* **2017**, *12*, 2513–2523.
- [3] G. H. Clever, P. Punt, *Acc. Chem. Res.* **2017**, *50*, 2233–2243.
- [4] M. Han, D. M. Engelhard, G. H. Clever, *Chem. Soc. Rev.* **2014**, *43*, 1848–1860.
- [5] S. Mukherjee, P. S. Mukherjee, *Chem. Commun.* **2014**, *50*, 2239–2248.
- [6] K. Harris, D. Fujita, M. Fujita, *Chem. Commun.* **2013**, *49*, 6703–6712.
- [7] R. Chakrabarty, P. S. Mukherjee, P. J. Stang, *Chem. Rev.* **2011**, *111*, 6810–6918.
- [8] S. Sharma, M. Sarkar, D. K. Chand, *Chem. Commun.* **2023**, *59*, 535–554.
- [9] A. E. Martín Díaz, J. E. M. Lewis, *Front. Chem.* **2021**, *9*.
- [10] D. A. McMorran, P. J. Steel, *Angew. Chem. Int. Ed.* **1998**, *37*, 3295–3297.
- [11] K. Suzuki, M. Tominaga, M. Kawano, M. Fujita, *Chem. Commun.* **2009**, 1638–1640.
- [12] M. Tominaga, K. Suzuki, M. Kawano, T. Kusukawa, T. Ozeki, S. Sakamoto, K. Yamaguchi, M. Fujita, *Angew. Chem. Int. Ed.* **2004**, *43*, 5621–5625.
- [13] D. Fujita, Y. Ueda, S. Sato, N. Mizuno, T. Kumasaka, M. Fujita, *Nature* **2016**, *540*, 563–566.
- [14] Q.-F. Sun, J. Iwasa, D. Ogawa, Y. Ishido, S. Sato, T. Ozeki, Y. Sei, K. Yamaguchi, M. Fujita, *Science* **2010**, *328*, 1144–1147.
- [15] J. Bunzen, J. Iwasa, P. Bonakdarzadeh, E. Numata, K. Rissanen, S. Sato, M. Fujita, *Angew. Chem. Int. Ed.* **2012**, *51*, 3161–3163.
- [16] D. Fujita, Y. Ueda, S. Sato, H. Yokoyama, N. Mizuno, T. Kumasaka, M. Fujita, *Chem* **2016**, *1*, 91–101.
- [17] W. M. Bloch, S. Horiuchi, J. J. Holstein, C. Drechsler, A. Wuttke, W. Hiller, R. A. Mata, G. H. Clever, *Chem. Sci.* **2023**, *14*, 1524–1531.
- [18] D. K. Chand, K. Biradha, M. Kawano, S. Sakamoto, K. Yamaguchi, M. Fujita, *Chem. Asian J.* **2006**, *1*, 82–90.
- [19] K. Suzuki, M. Kawano, M. Fujita, *Angew. Chem. Int. Ed.* **2007**, *46*, 2819–2822.

- [20] S. M. Jansze, G. Cecot, M. D. Wise, K. O. Zhurov, T. K. Ronson, A. M. Castilla, A. Finelli, P. Pattison, E. Solari, R. Scopelliti, G. E. Zelinskii, A. V. Vologzhanina, Y. Z. Voloshin, J. R. Nitschke, K. Severin, *J. Am. Chem. Soc.* **2016**, *138*, 2046–2054.
- [21] D. Bardhan, D. K. Chand, *Chem. Eur. J.* **2019**, *25*, 12241–12269.
- [22] S. Pullen, G. H. Clever, *Acc. Chem. Res.* **2018**, *51*, 3052–3064.
- [23] W. M. Bloch, G. H. Clever, *Chem. Commun.* **2017**, *53*, 8506–8516.
- [24] L. R. Holloway, P. M. Bogie, R. J. Hooley, *Dalton Trans.* **2017**, *46*, 14719–14723.
- [25] R. Zhu, W. M. Bloch, J. J. Holstein, S. Mandal, L. V. Schäfer, G. H. Clever, *Chem. Eur. J.* **2018**, *24*, 12976–12982.
- [26] W. M. Bloch, J. J. Holstein, W. Hiller, G. H. Clever, *Angew. Chem. Int. Ed.* **2017**, *56*, 8285–8289.
- [27] D. Preston, J. E. Barnsley, K. C. Gordon, J. D. Crowley, *J. Am. Chem. Soc.* **2016**, *138*, 10578–10585.
- [28] W. M. Bloch, Y. Abe, J. J. Holstein, C. M. Wandtke, B. Dittrich, G. H. Clever, *J. Am. Chem. Soc.* **2016**, *138*, 13750–13755.
- [29] M. Yamashina, T. Yuki, Y. Sei, M. Akita, M. Yoshizawa, *Chem. Eur. J.* **2015**, *21*, 4200–4204.
- [30] A. M. Johnson, R. J. Hooley, *Inorg. Chem.* **2011**, *50*, 4671–4673.
- [31] S. Prusty, K. Yazaki, M. Yoshizawa, D. K. Chand, *Chem. Eur. J.* **2017**, *23*, 12456–12461.
- [32] P. Howlader, P. Das, E. Zangrando, P. S. Mukherjee, *J. Am. Chem. Soc.* **2016**, *138*, 1668–1676.
- [33] Q.-F. Sun, S. Sato, M. Fujita, *Angew. Chem. Int. Ed.* **2014**, *53*, 13510–13513.
- [34] D. Fujita, K. Suzuki, S. Sato, M. Yagi-Utsumi, Y. Yamaguchi, N. Mizuno, T. Kumasaka, M. Takata, M. Noda, S. Uchiyama, K. Kato, M. Fujita, *Nat. Commun.* **2012**, *3*, 1093.
- [35] M. Frank, J. Ahrens, I. Bejenke, M. Krick, D. Schwarzer, G. H. Clever, *J. Am. Chem. Soc.* **2016**, *138*, 8279–8287.

- [36] R. Gramage-Doria, J. Hessels, S. H. A. M. Leenders, O. Tröppner, M. Dürr, I. Ivanović-Burmazović, J. N. H. Reek, *Angew. Chem. Int. Ed.* **2014**, *53*, 13380–13384.
- [37] M. Frank, L. Krause, R. Herbst-Irmer, D. Stalke, G. H. Clever, *Dalton Trans.* **2014**, *43*, 4587–4592.
- [38] K. Wu, B. Zhang, C. Drechsler, J. J. Holstein, G. H. Clever, *Angew. Chem. Int. Ed.* **2021**, *60*, 6403–6407.
- [39] S. Samantray, S. Krishnaswamy, D. K. Chand, *Nat. Commun.* **2020**, *11*, 1–11.
- [40] C.-B. Tian, Q.-F. Sun, *Chem. Eur. J.* **2023**, *29*, e202300195.
- [41] J. E. M. Lewis, *Chem. Commun.* **2022**, *58*, 13873–13886.
- [42] S. Pullen, J. Tessarolo, G. H. Clever, *Chem. Sci.* **2021**, *12*, 7269–7293.
- [43] K. Wu, J. Tessarolo, A. Baksi, G. H. Clever, *Angew. Chem. Int. Ed.* **2022**, *61*, e202205725.
- [44] J. Tessarolo, E. Benchimol, A. Jouaiti, M. W. Hosseini, G. H. Clever, *Chem. Commun.* **2023**, *59*, 3467–3470.
- [45] Y. Liu, S.-H. Liao, W.-T. Dai, Q. Bai, S. Lu, H. Wang, X. Li, Z. Zhang, P. Wang, W. Lu, Q. Zhang, *Angew. Chem. Int. Ed.* **2023**, *62*, e202217215.
- [46] K. Wu, E. Benchimol, A. Baksi, G. Clever, **2023**, DOI 10.26434/chemrxiv-2023-5gb4q.
- [47] R.-J. Li, F. Fadaei-Tirani, R. Scopelliti, K. Severin, *Chem. Eur. J.* **2021**, *27*, 9439–9445.
- [48] J. Tessarolo, H. Lee, E. Sakuda, K. Umakoshi, G. H. Clever, *J. Am. Chem. Soc.* **2021**, *143*, 6339–6344.
- [49] S. Sudan, R.-J. Li, S. M. Jansze, A. Platzek, R. Rudolf, G. H. Clever, F. Fadaei-Tirani, R. Scopelliti, K. Severin, *J. Am. Chem. Soc.* **2021**, *143*, 1773–1778.
- [50] C. Klein, C. Gütz, M. Bogner, F. Topić, K. Rissanen, A. Lützen, *Angew. Chem. Int. Ed.* **2014**, *53*, 3739–3742.
- [51] A. Walther, I. Regeni, J. J. Holstein, G. H. Clever, *J. Am. Chem. Soc.* **2023**, DOI 10.1021/jacs.3c09295.
- [52] M. Fukuda, R. Sekiya, R. Kuroda, *Angew. Chem. Int. Ed.* **2008**, *47*, 706–710.
- [53] S. Freye, J. Hey, A. Torras-Galán, D. Stalke, R. Herbst-Irmer, M. John, G. H. Clever, *Angew. Chem. Int. Ed.* **2012**, *51*, 2191–2194.

- [54] R. Zhu, J. Lübber, B. Dittrich, G. H. Clever, *Angew. Chem. Int. Ed.* **2015**, *54*, 2796–2800.
- [55] Y.-H. Li, J.-J. Jiang, Y.-Z. Fan, Z.-W. Wei, C.-X. Chen, H.-J. Yu, S.-P. Zheng, D. Fenske, C.-Y. Su, M. Barboiu, *Chem. Commun.* **2016**, *52*, 8745–8748.
- [56] D. Luo, B. Pan, J. Zhang, C. Ma, Y. Su, Q. Gan, *Chin. Chem. Lett.* **2021**, *32*, 1397–1399.
- [57] W. M. Bloch, J. J. Holstein, B. Dittrich, W. Hiller, G. H. Clever, *Angew. Chem. Int. Ed.* **2018**, *57*, 5534–5538.
- [58] T. R. Schulte, J. J. Holstein, L. Schneider, A. Adam, G. Haberhauer, G. H. Clever, *Angew. Chem. Int. Ed.* **2020**, *59*, 22489–22493.
- [59] M. Käseborn, J. J. Holstein, G. H. Clever, A. Lützen, *Angew. Chem. Int. Ed.* **2018**, *57*, 12171–12175.
- [60] S. K. Sen, R. Natarajan, *Inorg. Chem.* **2019**, *58*, 7180–7188.
- [61] J. E. M. Lewis, A. Tarzia, A. J. P. White, K. E. Jelfs, *Chem. Sci.* **2020**, *11*, 677–683.
- [62] D. Ogata, J. Yuasa, *Angew. Chem. Int. Ed.* **2019**, *58*, 18424–18428.
- [63] S. S. Mishra, S. V. K. Kompella, S. Krishnaswamy, S. Balasubramanian, D. K. Chand, *Inorg. Chem.* **2020**, *59*, 12884–12894.
- [64] J. E. M. Lewis, *Chem. Eur. J.* **2021**, *27*, 4454–4460.
- [65] A. Tarzia, J. E. M. Lewis, K. E. Jelfs, *Angew. Chem. Int. Ed.* **2021**, *60*, 20879–20887.
- [66] R.-J. Li, A. Marcus, F. Fadaei-Tirani, K. Severin, *Chem. Commun.* **2021**, *57*, 10023–10026.
- [67] H. Yu, J. Li, C. Shan, T. Lu, X. Jiang, J. Shi, L. Wojtas, H. Zhang, M. Wang, *Angew. Chem. Int. Ed.* **2021**, *60*, 26523–26527.
- [68] J. E. M. Lewis, *Angew. Chem. Int. Ed.* **2022**, *61*, e202212392.
- [69] R.-J. Li, A. Tarzia, V. Posligua, K. E. Jelfs, N. Sanchez, A. Marcus, A. Baksi, G. H. Clever, F. Fadaei-Tirani, K. Severin, *Chem. Sci.* **2022**, *13*, 11912–11917.
- [70] P. Molinska, A. Tarzia, L. Male, K. E. Jelfs, J. E. M. Lewis, *Angew. Chem. Int. Ed.* **2023**, *62*, e202315451.
- [71] J. de Montmollin, A. B. Solea, D. W. Chen, F. Fadaei-Tirani, K. Severin, *Inorg. Chem.* **2024**, DOI 10.1021/acs.inorgchem.3c04033.

- [72] P. J. Steel, D. A. McMorran, *Chem. Asian J.* **2019**, *14*, 1098–1101.
- [73] D. Preston, K. M. Patil, A. T. O’Neil, R. A. S. Vasdev, J. A. Kitchen, P. E. Kruger, *Inorg. Chem. Front.* **2020**, *7*, 2990–3001.
- [74] M. Frank, M. D. Johnstone, G. H. Clever, *Chem. Eur. J.* **2016**, *22*, 14104–14125.
- [75] R. Sekiya, M. Fukuda, R. Kuroda, *J. Am. Chem. Soc.* **2012**, *134*, 10987–10997.
- [76] J. M. Dieterich, G. H. Clever, R. A. Mata, *Phys. Chem. Chem. Phys.* **2012**, *14*, 12746–12749.
- [77] S. Freye, R. Michel, D. Stalke, M. Pawliczek, H. Frauendorf, G. H. Clever, *J. Am. Chem. Soc.* **2013**, *135*, 8476–8479.
- [78] S. Freye, D. M. Engelhard, M. John, G. H. Clever, *Chem. – Eur. J.* **2013**, *19*, 2114–2121.
- [79] A. P. Birvé, H. D. Patel, J. R. Price, W. M. Bloch, T. Fallon, *Angew. Chem. Int. Ed.* **2022**, *61*, e202115468.
- [80] S. Sudan, D. W. Chen, C. Berton, F. Fadaei-Tirani, K. Severin, *Angew. Chem. Int. Ed.* **2023**, *62*, e202218072.
- [81] V. Sivalingam, S. Krishnaswamy, D. K. Chand, *Chem. Eur. J.* **2023**, *29*, e202300891.
- [82] W.-L. Jiang, B. Huang, X.-L. Zhao, X. Shi, H.-B. Yang, *Chem* **2023**, *9*, 2655–2668.
- [83] V. V. Sivalingam, S. Krishnaswamy, D. K. Chand, **2023**, DOI 10.26434/chemrxiv-2023-07v16.
- [84] T. Murase, S. Sato, M. Fujita, *Angew. Chem. Int. Ed.* **2007**, *46*, 5133–5136.
- [85] K. Suzuki, K. Takao, S. Sato, M. Fujita, *J. Am. Chem. Soc.* **2010**, *132*, 2544–2545.
- [86] M. Yoshizawa, L. Catti, *Acc. Chem. Res.* **2019**, *52*, 2392–2404.
- [87] T. Tsutsui, S. Kusaba, M. Yamashina, M. Akita, M. Yoshizawa, *Chem. Eur. J.* **2019**, *25*, 4320–4324.
- [88] K. Matsumoto, S. Kusaba, Y. Tanaka, Y. Sei, M. Akita, K. Aritani, M. Haga, M. Yoshizawa, *Angew. Chem. Int. Ed.* **2019**, *58*, 8463–8467.
- [89] H. Dobashi, L. Catti, Y. Tanaka, M. Akita, M. Yoshizawa, *Angew. Chem. Int. Ed.* **2020**, *59*, 11881–11885.

- [90] R. Sumida, Y. Tanaka, K. Niki, Y. Sei, S. Toyota, M. Yoshizawa, *Chem. Sci.* **2021**, *12*, 9946–9951.
- [91] M. Yuasa, R. Sumida, Y. Tanaka, M. Yoshizawa, *Chem. Eur. J.* **2022**, *28*, e202104101.
- [92] M. Ueda, N. Kishida, L. Catti, M. Yoshizawa, *Chem. Sci.* **2022**, *13*, 8642–8648.
- [93] M. Shuto, R. Sumida, M. Yuasa, T. Sawada, M. Yoshizawa, *JACS Au* **2023**, *3*, 2905–2911.
- [94] P. Liao, B. W. Langloss, A. M. Johnson, E. R. Knudsen, F. S. Tham, R. R. Julian, R. J. Hooley, *Chem. Commun.* **2010**, *46*, 4932–4934.
- [95] J. E. M. Lewis, E. L. Gavey, S. A. Cameron, J. D. Crowley, *Chem. Sci.* **2012**, *3*, 778–784.
- [96] A. Schmidt, V. Molano, M. Hollering, A. Pöthig, A. Casini, F. E. Kühn, *Chem. Eur. J.* **2016**, *22*, 2253–2256.
- [97] P. J. Lusby, in *Supramol. Catal.*, John Wiley & Sons, Ltd, **2022**, pp. 229–240.
- [98] C. J. Bruns, D. Fujita, M. Hoshino, S. Sato, J. F. Stoddart, M. Fujita, *J. Am. Chem. Soc.* **2014**, *136*, 12027–12034.
- [99] X. Tang, H. Jiang, Y. Si, N. Rampal, W. Gong, C. Cheng, X. Kang, D. Fairen-Jimenez, Y. Cui, Y. Liu, *Chem* **2021**, *7*, 2771–2786.
- [100] I. F. Mansoor, K. G. Dutton, D. A. Rothschild, R. C. Remsing, M. C. Lipke, *J. Am. Chem. Soc.* **2021**, *143*, 16993–17003.
- [101] J.-P. Bourgeois, M. Fujita, M. Kawano, S. Sakamoto, K. Yamaguchi, *J. Am. Chem. Soc.* **2003**, *125*, 9260–9261.
- [102] G. H. Clever, W. Kawamura, S. Tashiro, M. Shiro, M. Shionoya, *Angew. Chem. Int. Ed.* **2012**, *51*, 2606–2609.
- [103] H. Takezawa, R. Tabuchi, H. Sunohara, M. Fujita, *J. Am. Chem. Soc.* **2020**, *142*, 17919–17922.
- [104] J.-M. Lehn, *Chem. Eur. J.* **1999**, *5*, 2455–2463.
- [105] I. Huc, J.-M. Lehn, *Proc. Natl. Acad. Sci.* **1997**, *94*, 2106–2110.
- [106] B. Hasenknopf, J.-M. Lehn, N. Boumediene, A. Dupont-Gervais, A. Van Dorsselaer, B. Kneisel, D. Fenske, *J. Am. Chem. Soc.* **1997**, *119*, 10956–10962.
- [107] B. Hasenknopf, J.-M. Lehn, B. O. Kneisel, G. Baum, D. Fenske, *Angew. Chem. Int. Ed. Engl.* **1996**, *35*, 1838–1840.

- [108] K. Severin, *Chem. Eur. J.* **2004**, *10*, 2565–2580.
- [109] Z. Grote, R. Scopelliti, K. Severin, *Angew. Chem. Int. Ed.* **2003**, *42*, 3821–3825.
- [110] H. S. Sahoo, D. K. Chand, *Dalton Trans.* **2010**, *39*, 7223–7225.
- [111] S. Löffler, J. Lübben, L. Krause, D. Stalke, B. Dittrich, G. H. Clever, *J. Am. Chem. Soc.* **2015**, *137*, 1060–1063.
- [112] S. M. Jansze, K. Severin, *J. Am. Chem. Soc.* **2019**, *141*, 815–819.
- [113] S. M. Jansze, K. Severin, *Acc. Chem. Res.* **2018**, *51*, 2139–2147.
- [114] M. D. Wise, J. J. Holstein, P. Pattison, C. Besnard, E. Solari, R. Scopelliti, G. Bricogne, K. Severin, *Chem. Sci.* **2015**, *6*, 1004–1010.
- [115] E. G. Percástegui, *Eur. J. Inorg. Chem.* **2021**, *2021*, 4425–4438.
- [116] T. K. Ronson, J. P. Carpenter, J. R. Nitschke, *Chem* **2022**, *8*, 557–568.
- [117] D.-N. Yan, L.-X. Cai, P.-M. Cheng, S.-J. Hu, L.-P. Zhou, Q.-F. Sun, *J. Am. Chem. Soc.* **2021**, *143*, 16087–16094.
- [118] K. Endo, H. Ube, M. Shionoya, *J. Am. Chem. Soc.* **2020**, *142*, 407–416.
- [119] P.-M. Cheng, L.-X. Cai, S.-C. Li, S.-J. Hu, D.-N. Yan, L.-P. Zhou, Q.-F. Sun, *Angew. Chem. Int. Ed.* **2020**, *59*, 23569–23573.
- [120] S. Wang, T. Sawada, K. Ohara, K. Yamaguchi, M. Fujita, *Angew. Chem. Int. Ed.* **2016**, *55*, 2063–2066.
- [121] H. Lee, P. Elumalai, N. Singh, H. Kim, S. U. Lee, K.-W. Chi, *J. Am. Chem. Soc.* **2015**, *137*, 4674–4677.
- [122] D. M. Wood, W. Meng, T. K. Ronson, A. R. Stefankiewicz, J. K. M. Sanders, J. R. Nitschke, *Angew. Chem. Int. Ed.* **2015**, *54*, 3988–3992.
- [123] T. Sawada, H. Hisada, M. Fujita, *J. Am. Chem. Soc.* **2014**, *136*, 4449–4451.
- [124] I. A. Riddell, M. M. J. Smulders, J. K. Clegg, Y. R. Hristova, B. Breiner, J. D. Thoburn, J. R. Nitschke, *Nat. Chem.* **2012**, *4*, 751–756.
- [125] M. Scherer, D. L. Caulder, D. W. Johnson, K. N. Raymond, *Angew. Chem. Int. Ed.* **1999**, *38*, 1587–1592.
- [126] S. Hiraoka, M. Fujita, *J. Am. Chem. Soc.* **1999**, *121*, 10239–10240.
- [127] S.-C. Li, T. Zhang, X.-P. Deng, X.-Q. Guo, L.-P. Zhou, F. Guo, Q.-F. Sun, *Inorg. Chem. Commun.* **2018**, *92*, 69–73.
- [128] S. Kai, T. Tateishi, T. Kojima, S. Takahashi, S. Hiraoka, *Inorg. Chem.* **2018**, *57*, 13083–13086.

- [129] C. Klein, C. Gütz, M. Bogner, F. Topić, K. Rissanen, A. Lützen, *Angew. Chem. Int. Ed.* **2014**, *53*, 3739–3742.
- [130] Z. Grote, M.-L. Lehaire, R. Scopelliti, K. Severin, *J. Am. Chem. Soc.* **2003**, *125*, 13638–13639.
- [131] H. Piotrowski, K. Severin, *Proc. Natl. Acad. Sci.* **2002**, *99*, 4997–5000.
- [132] H. Piotrowski, G. Hilt, A. Schulz, P. Mayer, K. Polborn, K. Severin, *Chem. Eur. J.* **2001**, *7*, 3196–3208.
- [133] H. Piotrowski, K. Polborn, G. Hilt, K. Severin, *J. Am. Chem. Soc.* **2001**, *123*, 2699–2700.
- [134] T. Nakamura, H. Ube, M. Shionoya, *Chem. Lett.* **2013**, *42*, 328–334.
- [135] *Foldamers: Structure, Properties, and Applications* (Eds.: S. Hecht, I. Huc), Wiley-VCH, Weinheim, **2007**
- [136] D. Preston, *Angew. Chem. Int. Ed.* **2021**, *60*, 20027–20035.
- [137] C. G. Pappas, P. K. Mandal, B. Liu, B. Kauffmann, X. Miao, D. Komáromy, W. Hoffmann, C. Manz, R. Chang, K. Liu, K. Pagel, I. Huc, S. Otto, *Nat. Chem.* **2020**, *12*, 1180–1186.
- [138] H. Song, M. Postings, P. Scott, N. J. Rogers, *Chem. Sci.* **2021**, *12*, 1620–1631.
- [139] M. Albrecht, *Eur. J. Inorg. Chem.* **2020**, *2020*, 2227–2237.
- [140] N. M. Tran, H. Yoo, *Dalton Trans.* **2020**, *49*, 11819–11827.
- [141] M. Albrecht, X. Chen, D. Van Craen, *Chem. Eur. J.* **2019**, *25*, 4265–4273.
- [142] A. P. Paneerselvam, S. S. Mishra, D. K. Chand, *J. Chem. Sci.* **2018**, *130*, 96.
- [143] M. Boiocchi, L. Fabbrizzi, *Chem. Soc. Rev.* **2014**, *43*, 1835–1847.
- [144] M. J. Hannon, L. J. Childs, *Supramol. Chem.* **2004**, *16*, 7–22.
- [145] M. Albrecht, *Chem. Rev.* **2001**, *101*, 3457–3498.
- [146] C. Piguet, G. Bernardinelli, G. Hopfgartner, *Chem. Rev.* **1997**, *97*, 2005–2062.
- [147] N. Capó, L. A. Barrios, J. Cardona, J. Ribas-Ariño, S. J. Teat, O. Roubeau, G. Aromí, *Chem. Commun.* **2022**, *58*, 10969–10972.
- [148] Y.-Q. Zou, D. Zhang, T. K. Ronson, A. Tarzia, Z. Lu, K. E. Jelfs, J. R. Nitschke, *J. Am. Chem. Soc.* **2021**, *143*, 9009–9015.
- [149] B. Shankar, S. Sahu, N. Deibel, D. Schweinfurth, B. Sarkar, P. Elumalai, D. Gupta, F. Hussain, G. Krishnamoorthy, M. Sathiyendiran, *Inorg. Chem.* **2014**, *53*, 922–930.

- [150] K. E. Allen, R. A. Faulkner, L. P. Harding, C. R. Rice, T. Riis-Johannessen, M. L. Voss, M. Whitehead, *Angew. Chem. Int. Ed.* **2010**, *49*, 6655–6658.
- [151] T. K. Ronson, H. Adams, T. Riis-Johannessen, J. C. Jeffery, M. D. Ward, *New J. Chem.* **2006**, *30*, 26–28.
- [152] B. Hasenknopf, J. M. Lehn, G. Baum, D. Fenske, *Proc. Natl. Acad. Sci.* **1996**, *93*, 1397–1400.
- [153] V. C. M. Smith, J.-M. Lehn, *Chem. Commun.* **1996**, 2733–2734.
- [154] A. Santoro, J. Holub, M. A. Fik-Jaskółka, G. Vantomme, J.-M. Lehn, *Chem. Eur. J.* **2020**, *26*, 15664–15671.
- [155] T. Riis-Johannessen, G. Bernardinelli, Y. Filinchuk, S. Clifford, N. D. Favera, C. Piguet, *Inorg. Chem.* **2009**, *48*, 5512–5525.
- [156] L. Aboshyan-Sorgho, H. Nozary, A. Aebischer, J.-C. G. Bünzli, P.-Y. Morgantini, K. R. Kittilstved, A. Hauser, S. V. Eliseeva, S. Petoud, C. Piguet, *J. Am. Chem. Soc.* **2012**, *134*, 12675–12684.
- [157] M. Cantuel, F. Gummy, J.-C. G. Bünzli, C. Piguet, *Dalton Trans.* **2006**, 2647–2660.
- [158] C. Piguet, J.-C. G. Bünzli, G. Bernardinelli, G. Hopfgartner, S. Petoud, O. Schaad, *J. Am. Chem. Soc.* **1996**, *118*, 6681–6697.
- [159] J. M. Lehn, A. Rigault, J. Siegel, J. Harrowfield, B. Chevrier, D. Moras, *Proc. Natl. Acad. Sci.* **1987**, *84*, 2565–2569.
- [160] C. M. Harris, E. D. McKenzie, *J. Chem. Soc. Inorg. Phys. Theor.* **1969**, 746–753.
- [161] R. C. Scarrow, D. L. White, K. N. Raymond, *J. Am. Chem. Soc.* **1985**, *107*, 6540–6546.
- [162] S.-J. Shieh, C.-C. Chou, G.-H. Lee, C.-C. Wang, S.-M. Peng, *Angew. Chem. Int. Ed. Engl.* **1997**, *36*, 56–59.
- [163] M. Albrecht, K. Witt, H. Röttele, R. Fröhlich, *Chem. Commun.* **2001**, 1330–1331.
- [164] C. T. McTernan, T. K. Ronson, J. R. Nitschke, *J. Am. Chem. Soc.* **2021**, *143*, 664–670.
- [165] Q. Lin, L. Gao, B. Kauffmann, J. Zhang, C. Ma, D. Luo, Q. Gan, *Chem. Commun.* **2018**, *54*, 13447–13450.

- [166] S. M. McNeill, D. Preston, J. E. M. Lewis, A. Robert, K. Knerr-Rupp, D. O. Graham, J. R. Wright, G. I. Giles, J. D. Crowley, *Dalton Trans.* **2015**, *44*, 11129–11136.
- [167] L.-P. Zhou, Q.-F. Sun, *Chem. Commun.* **2015**, *51*, 16767–16770.
- [168] D. Tripathy, A. K. Pal, G. S. Hanan, D. K. Chand, *Dalton Trans.* **2012**, *41*, 11273–11275.
- [169] S. Ø. Scott, E. L. Gavey, S. J. Lind, K. C. Gordon, J. D. Crowley, *Dalton Trans.* **2011**, *40*, 12117–12124.
- [170] S. Sudan, F. Fadaei-Tirani, R. Scopelliti, K. E. Ebbert, G. H. Clever, K. Severin, *Angew. Chem. Int. Ed.* **2022**, *61*, e202201823.
- [171] C. T. McTernan, J. A. Davies, J. R. Nitschke, *Chem. Rev.* **2022**, *122*, 10393–10437.
- [172] J. E. M. Lewis, James. D. Crowley, *ChemPlusChem* **2020**, *85*, 815–827.
- [173] D. Komáromy, T. Tiemersma-Wegman, J. Kemmink, G. Portale, P. R. Adamski, A. Blokhuis, F. S. Aalbers, I. Marić, G. M. Santiago, J. Ottelé, A. Sood, V. Saggiomo, B. Liu, P. Van Der Meulen, S. Otto, *Chem* **2021**, *7*, 1933–1951.
- [174] L. K. Macreadie, A. M. Gilchrist, D. A. McNaughton, W. G. Ryder, M. Fares, P. A. Gale, *Chem* **2022**, *8*, 46–118.
- [175] S. Kubik, *Acc. Chem. Res.* **2017**, *50*, 2870–2878.
- [176] M. J. Langton, C. J. Serpell, P. D. Beer, *Angew. Chem. Int. Ed.* **2016**, *55*, 1974–1987.
- [177] S. Kubik, *Chem. Soc. Rev.* **2010**, *39*, 3648–3663.
- [178] S. Kubik, C. Reyheller, S. Stüwe, *J. Incl. Phenom. Macrocycl. Chem.* **2005**, *52*, 137–187.
- [179] Y. Liu, W. Zhao, C.-H. Chen, A. H. Flood, *Science* **2019**, *365*, 159–161.
- [180] H. Valkenier, O. Akrawi, P. Jurček, K. Sleziaková, T. Lízal, K. Bartik, V. Šindelář, *Chem* **2019**, *5*, 429–444.
- [181] A. B. Aletti, A. Miljkovic, L. Toma, R. Bruno, D. Armentano, T. Gunnlaugsson, G. Bergamaschi, V. Amendola, *J. Org. Chem.* **2019**, *84*, 4221–4228.
- [182] S. J. Edwards, H. Valkenier, N. Busschaert, P. A. Gale, A. P. Davis, *Angew. Chem. Int. Ed.* **2015**, *54*, 4592–4596.
- [183] Y. Haketa, H. Maeda, *Chem. Eur. J.* **2011**, *17*, 1485–1492.

- [184] Y. Li, A. H. Flood, *Angew. Chem. Int. Ed.* **2008**, *47*, 2649–2652.
- [185] K.-J. Chang, D. Moon, M. S. Lah, K.-S. Jeong, *Angew. Chem. Int. Ed.* **2005**, *44*, 7926–7929.
- [186] A. J. Ayling, M. N. Pérez-Payán, A. P. Davis, *J. Am. Chem. Soc.* **2001**, *123*, 12716–12717.
- [187] T. Bunchuay, K. Boonpalit, A. Docker, A. Ruengsuk, J. Tantirungrotechai, M. Sukwattanasinitt, P. Surawatanawong, P. D. Beer, *Chem. Commun.* **2021**, *57*, 11976–11979.
- [188] X. Wu, P. Wang, P. Turner, W. Lewis, O. Catal, D. S. Thomas, P. A. Gale, *Chem* **2019**, *5*, 1210–1222.
- [189] Y. Liu, A. Sengupta, K. Raghavachari, A. H. Flood, *Chem* **2017**, *3*, 411–427.
- [190] Y. Hua, Y. Liu, C.-H. Chen, A. H. Flood, *J. Am. Chem. Soc.* **2013**, *135*, 14401–14412.
- [191] W. W. H. Wong, M. S. Vickers, A. R. Cowley, R. L. Paul, P. D. Beer, *Org. Biomol. Chem.* **2005**, *3*, 4201–4208.
- [192] S. Kubik, R. Kirchner, D. Nolting, J. Seidel, *J. Am. Chem. Soc.* **2002**, *124*, 12752–12760.
- [193] S. Kubik, R. Goddard, R. Kirchner, D. Nolting, J. Seidel, *Angew. Chem. Int. Ed.* **2001**, *40*, 2648–2651.
- [194] T. Lizal, V. Sindelar, *Isr. J. Chem.* **2018**, *58*, 326–333.
- [195] T. Fiala, K. Sleziakova, K. Marsalek, K. Salvadori, V. Sindelar, *J. Org. Chem.* **2018**, *83*, 1903–1912.
- [196] M. A. Yawer, V. Havel, V. Sindelar, *Angew. Chem. Int. Ed.* **2015**, *54*, 276–279.
- [197] M. Lisbjerg, B. E. Nielsen, B. O. Milhøj, S. P. A. Sauer, M. Pittelkow, *Org. Biomol. Chem.* **2014**, *13*, 369–373.
- [198] Y. Chen, G. Wu, L. Chen, L. Tong, Y. Lei, L. Shen, T. Jiao, H. Li, *Org. Lett.* **2020**, *22*, 4878–4882.
- [199] F. Sommer, Y. Marcus, S. Kubik, *ACS Omega* **2017**, *2*, 3669–3680.
- [200] A. Brown, P. D. Beer, *Chem. Commun.* **2016**, *52*, 8645–8658.
- [201] M. J. Langton, S. W. Robinson, I. Marques, V. Félix, P. D. Beer, *Nat. Chem.* **2014**, *6*, 1039–1043.

- [202] A. Borissov, I. Marques, J. Y. C. Lim, V. Félix, M. D. Smith, P. D. Beer, *J. Am. Chem. Soc.* **2019**, *141*, 4119–4129.
- [203] C. H. Park, H. E. Simmons, *J. Am. Chem. Soc.* **1968**, *90*, 2431–2432.
- [204] E. Graf, J. M. Lehn, *J. Am. Chem. Soc.* **1976**, *98*, 6403–6405.
- [205] E. García-España, P. Díaz, J. M. Llinares, A. Bianchi, *Coord. Chem. Rev.* **2006**, *250*, 2952–2986.
- [206] J. M. Llinares, D. Powell, K. Bowman-James, *Coord. Chem. Rev.* **2003**, *240*, 57–75.
- [207] P. Ballester, *Chem. Soc. Rev.* **2010**, *39*, 3810–3830.
- [208] F. P. Schmidtchen, M. Berger, *Chem. Rev.* **1997**, *97*, 1609–1646.
- [209] K. Worm, F. P. Schmidtchen, *Angew. Chem. Int. Ed. Engl.* **1995**, *34*, 65–66.
- [210] M. Lisbjerg, B. M. Jessen, B. Rasmussen, B. E. Nielsen, A. Ø. Madsen, M. Pittelkow, *Chem. Sci.* **2014**, *5*, 2647–2650.
- [211] R.-J. Li, C. Pezzato, C. Berton, K. Severin, *Chem. Sci.* **2021**, *12*, 4981–4984.
- [212] L. M. Eytel, H. A. Fargher, M. M. Haley, D. W. Johnson, *Chem. Commun.* **2019**, *55*, 5195–5206.
- [213] K. Dabrowa, F. Ulatowski, D. Lichosyt, J. Jurczak, *Org. Biomol. Chem.* **2017**, *15*, 5927–5943.
- [214] T. Riis-Johannessen, K. Severin, *Chem. Eur. J.* **2010**, *16*, 8291–8295.
- [215] T. Riis-Johannessen, K. Schenk, K. Severin, *Inorg. Chem.* **2010**, *49*, 9546–9553.
- [216] F. Wang, H. Chen, S. Parsons, I. D. H. Oswald, J. E. Davidson, P. J. Sadler, *Chem. Eur. J.* **2003**, *9*, 5810–5820.
- [217] M. Robitzer, C. Sirlin, N. Kyritsakas, M. Pfeffer, *Eur. J. Inorg. Chem.* **2002**, *2002*, 2312–2319.
- [218] V. Amendola, E. Bastianello, L. Fabbrizzi, C. Mangano, P. Pallavicini, A. Perotti, A. Manotti Lanfredi, F. Ugozzoli, *Angew. Chem. Int. Ed.* **2000**, *39*, 2917–2920.
- [219] D. Parker, K. Senanayake, J. A. G. Williams, *Chem. Commun.* **1997**, 1777–1778.
- [220] R. J. Motekaitis, A. E. Martell, B. Dietrich, J. M. Lehn, *Inorg. Chem.* **1984**, *23*, 1588–1591.
- [221] B. J. J. Timmer, T. J. Mooibroek, *Chem. Commun.* **2021**, *57*, 7184–7187.

- [222] J. Zhang, D. Luo, C. Ma, L. Huang, Q. Gan, *Nat. Commun.* **2021**, *12*, 2659.
- [223] M. Frank, J. M. Dieterich, S. Freye, R. A. Mata, G. H. Clever, *Dalton Trans.* **2013**, *42*, 15906–15910.
- [224] N. L. S. Yue, D. J. Eisler, M. C. Jennings, R. J. Puddephatt, *Inorg. Chem. Commun.* **2005**, *8*, 31–33.
- [225] X. Schaapkens, J. N. H. Reek, T. J. Mooibroek, *Inorg. Chem. Commun.* **2022**, 109284.
- [226] S. Bandi, S. Samantray, R. D. Chakravarthy, A. K. Pal, G. S. Hanan, D. K. Chand, *Eur. J. Inorg. Chem.* **2016**, *2016*, 2816–2827.
- [227] J. Pitarch-Jarque, H. R. Jiménez, E. Kalenius, S. Blasco, A. Lopera, M. P. Clares, K. Rissanen, E. García-España, *Dalton Trans.* **2021**, *50*, 9010–9015.
- [228] J.-F. Ayme, J. E. Beves, C. J. Campbell, D. A. Leigh, *J. Am. Chem. Soc.* **2019**, *141*, 3605–3612.
- [229] W. J. Ramsay, F. J. Rizzuto, T. K. Ronson, K. Caprice, J. R. Nitschke, *J. Am. Chem. Soc.* **2016**, *138*, 7264–7267.
- [230] J.-F. Ayme, J. E. Beves, D. A. Leigh, R. T. McBurney, K. Rissanen, D. Schultz, *Nat. Chem.* **2012**, *4*, 15–20.
- [231] J.-F. Ayme, J. E. Beves, D. A. Leigh, R. T. McBurney, K. Rissanen, D. Schultz, *J. Am. Chem. Soc.* **2012**, *134*, 9488–9497.
- [232] B. Hasenknopf, J.-M. Lehn, N. Boumediene, E. Leize, A. Van Dorsselaer, *Angew. Chem. Int. Ed.* **1998**, *37*, 3265–3268.
- [233] R. Vilar, D. M. P. Mingos, A. J. P. White, D. J. Williams, *Angew. Chem. Int. Ed.* **1998**, *37*, 1258–1261.
- [234] R. Custelcean, *Chem. Soc. Rev.* **2014**, *43*, 1813–1824.
- [235] M. D. Ludden, M. D. Ward, *Dalton Trans.* **2021**, *50*, 2782–2791.
- [236] E. G. Percástegui, T. K. Ronson, J. R. Nitschke, *Chem. Rev.* **2020**, *120*, 13480–13544.
- [237] O. Jurček, P. Bonakdarzadeh, E. Kalenius, J. M. Linnanto, M. Groessl, R. Knochenmuss, J. A. Ihalainen, K. Rissanen, *Angew. Chem. Int. Ed.* **2015**, *54*, 15462–15467.
- [238] C. A. Schalley, *Analytical Methods in Supramolecular Chemistry*, John Wiley & Sons, **2012**.

- [239] R. Dutta, P. Ghosh, *Chem. Commun.* **2015**, *51*, 9070–9084.
- [240] O. A. Okunola, P. V. Santacroce, J. T. Davis, *Supramol. Chem.* **2008**, *20*, 169–190.
- [241] B. W. Tresca, R. J. Hansen, C. V. Chau, B. P. Hay, L. N. Zakharov, M. M. Haley, D. W. Johnson, *J. Am. Chem. Soc.* **2015**, *137*, 14959–14967.
- [242] M. Schulze, V. Kunz, P. D. Frischmann, F. Würthner, *Nat. Chem.* **2016**, *8*, 576–583.
- [243] L. Zeng, Y. Xiao, J. Jiang, H. Fang, Z. Ke, L. Chen, J. Zhang, *Inorg. Chem.* **2019**, *58*, 10019–10027.
- [244] S. M. Jansze, M. D. Wise, A. V. Vologzhanina, R. Scopelliti, K. Severin, *Chem. Sci.* **2017**, *8*, 1901–1908.
- [245] B. Avitia, E. MacIntosh, S. Muhia, E. Kelson, *Tetrahedron Lett.* **2011**, *52*, 1631–1634.
- [246] I. H. Bae, H. S. Kim, Y. You, C. Chough, W. Choe, M. K. Seon, S. G. Lee, G. Keum, S. K. Jang, B. Moon Kim, *Eur. J. Med. Chem.* **2015**, *101*, 163–178.
- [247] R. Hooper, L. J. Lyons, M. K. Mapes, D. Schumacher, D. A. Moline, R. West, *Macromolecules* **2001**, *34*, 931–936.
- [248] V. D. Cao, D. G. Jo, H. Kim, C. Kim, S. Yun, S. Joung, *Synthesis* **2021**, *53*, 754–764.
- [249] J.-B. Giguère, Q. Verolet, J.-F. Morin, *Chem. Eur. J.* **2013**, *19*, 372–381.
- [250] S. Sudan, F. Fadaei-Tirani, K. Severin, *Chem. Commun.* **2023**, *59*, 8258–8261.
- [251] M. Krick, J. Holstein, C. Würtele, G. H. Clever, *Chem. Commun.* **2016**, *52*, 10411–10414.
- [252] D. Sharma, Y. Hussain, M. Sharma, P. Chauhan, *Green Chem.* **2022**, *24*, 4783–4788.
- [253] P. Giraudeau, V. Silvestre, S. Akoka, *Metabolomics* **2015**, *11*, 1041–1055.
- [254] C. Berton, D. M. Busiello, S. Zamuner, E. Solari, R. Scopelliti, F. Fadaei-Tirani, K. Severin, C. Pezzato, *Chem. Sci.* **2020**, *11*, 8457–8468.
- [255] C. Berton, D. M. Busiello, S. Zamuner, R. Scopelliti, F. Fadaei-Tirani, K. Severin, C. Pezzato, *Angew. Chem. Int. Ed.* **2021**, *60*, 21737–21740.
- [256] S. Keller, C. Vargas, H. Zhao, G. Piszczek, C. A. Brautigam, P. Schuck, *Anal. Chem.* **2012**, *84*, 5066–5073.

- [257] T. H. Scheuermann, C. A. Brautigam, *Methods* **2015**, *76*, 87–98.
- [258] H. Zhao, G. Piszczek, P. Schuck, *Methods* **2015**, *76*, 137–148.
- [259] S. Chen, S. Zhang, C. Bao, C. Wang, Q. Lin, L. Zhu, *Chem. Commun.* **2016**, *52*, 13132–13135.
- [260] D. Schindler, A.-L. Meza-Chincha, M. Roth, F. Würthner, *Chem. Eur. J.* **2021**, *27*, 16938–16946.
- [261] L. Zeng, Y. Xiao, J. Jiang, H. Fang, Z. Ke, L. Chen, J. Zhang, *Inorg. Chem.* **2019**, *58*, 10019–10027.

10. Curriculum vitae

Sylvain SUDAN

Route de Blonay 122
1814 La Tour-de-Peilz
+41 79 103 50 40
✉ sylvain.sudan@epfl.ch

Born 09.03.1992
Switzerland

ORCID: 0000-0002-3572-6122



Experience

2020 - present

PhD student, group of Prof. Kay Severin, EPFL

- My research focused on increasing the structural complexity of palladium-based supramolecular and the study of their host-guest properties. The key results of my work include the development of a screening method to facilitate the identification of such structures, the discovery of two specific cation receptors and the development of a water-soluble anion receptor that showed an unprecedented affinity for chloride. The four projects were completed and published.
- Supervision of students at both bachelor's and master's levels for a semester-long research project.
- Presentation of research projects at international conferences:
International Symposium on Macrocyclic and Supramolecular Chemistry (Reykjavik, 2023)
International Conference on Coordination Chemistry (Rimini, 2022)

Safety correspondent, group of Prof. Kay Severin, EPFL

- Lab safety and compliance: ensured conformity to safety regulations and best laboratory practices. Took part in the regular safety inspections and implemented corrective measures to maintain a safe working environment.
- Diverse problem solving: collaborated with various parties including faculty, staff and external stakeholders to address lab safety, infrastructure and equipment-related issues.
- Lab design and relocation: actively participated in designing plans for a new laboratory, ensuring functionality and safety. Oversaw the organization and coordination of the lab's relocation.

2018 - 2019

Internship and master's project, group of Prof. Berend Smit, EPFL

Supervised by Dr. Kyriakos Stylianou. The project aimed at optimizing the synthesis of a metal-organic framework. The material was further applied for the capture of volatile organic compounds under humid conditions. The project was completed and published.

Education

2020 - present	Ecole Polytechnique Fédérale de Lausanne (EPFL) PhD student under the supervision of Prof. Kay Severin Expected graduation: spring 2024
2017 - 2019	Ecole Polytechnique Fédérale de Lausanne (EPFL) Master's degree in molecular and biological chemistry
2014 - 2017	Ecole Polytechnique Fédérale de Lausanne (EPFL) Bachelor's degree in chemistry and chemical engineering

BA Projects at EPFL

Spring 2017	Semester project under the direction of Prof. Marinella Mazzanti (GCC group). Name of the project: " <i>Reactivity of a Uranium (III) bridging oxo complex</i> ".
Fall 2017	Semester project under the direction of Prof. Jérôme Waser (LCSO group). Name of the project: " <i>Palladium Catalyzed Oxazolidinone Formation by CO₂ incorporation</i> ".

Publications & Awards

- [S. Sudan](#), F. Fadaei-Tirani and K. Severin, *Chem. Commun.*, **2023**, 8258-8261
- [S. Sudan](#), D. W. Chen, C. Berton, F. Fadaei-Tirani and K. Severin, *Angew. Chem. Int. Ed.*, **2023**, e202218072.
- [S. Sudan](#), F. Fadaei-Tirani, R. Scopelliti, K. E. Ebbert, G. H. Clever and K. Severin, *Angew. Chem. Int. Ed.*, **2022**, e202201823.
- [S. Sudan](#), R.-J. Li, S. M. Jansze, A. Platzek, R. Rudolf, G. H. Clever, F. Fadaei-Tirani, R. Scopelliti and K. Severin, *J. Am. Chem. Soc.*, **2021**, 1773-1778.
- [S. Sudan](#), A. Gładysiak, B. Valizadeh, J.-H. Lee and K. C. Stylianou, *Inorg. Chem.*, **2020**, 9029-9036.
- 2023 SCNAT / SCS Chemistry Travel Award
- EPFL School of Basic Sciences Dean's Award for Excellence in Teaching 2021-2022

Languages

- French Mother tongue
- English Fluent (PhD and master's studies main language)
- German B2 level (high school)
- Spanish B2 level (high school)